A Landform Based 3D Reconstruction of Glacier Ice at the Last Glacial Maximum in the Southern Alps, New Zealand

William Henry Meurig James

Submitted in accordance with the requirements for the degree of

Doctor of Philosophy

The University of Leeds

School of Geography

September 2016

The candidate confirms that the work submitted is his own, except where work which has formed part of jointly-authored publications has been included. The contribution of the candidate and the other authors to this work has been explicitly indicated below. The candidate confirms that appropriate credit has been given within the thesis where reference has been made to the work of others.

The work in Chapter 2 of the thesis has appeared in publication as follows:

James, W. H. M. and J. L. Carrivck. 2016. Automated modelling of distributed glacier ice thickness and volume. *Computers & Geosciences,* **92**, pp.90 - 103.

William H.M. James conceived the project, carried out the analysis and was the primary writer of the paper. Jonathan L. Carrivick co-authored; advising, commenting and editing.

Carrivick, J., B. Davies, W.H.M. James et al. IN REVIEW-a. Spatial distribution of potential sea-level rise contributions from the Antarctic Peninsula and outlying islands. *Scientific Reports*.

William H.M. James designed, coded, ran and generated the ice thickness model and produced the outputs. Jonathan L. Carrivick and B. Davies conceived of the paper, obtained the raw data and wrote the paper.

Carrivick, J., B. Davies, W.H.M. James et al. IN REVIEW-b. Distributed ice thickness and glacier volume in southern South America. *Global and Planetary Change*.

William H.M. James designed, coded, ran and generated the ice thickness model and produced the outputs. Jonathan L. Carrivick and B. Davies conceived of the paper, obtained the raw data and wrote the paper.

The work in Chapter 4 of the thesis has appeared in publication as follows:

Carrivick, J. L., W.H.M James et al. 2015. Decadal Scale Changes Of The Ödenwinkelkees, Central Austria, Suggest Increasing Control of Topography and Evolution Towards Steady State. *Geografiska Annaler: Series A, Physical Geography*.

William H.M. James coded, ran and analysed the ice thickness model (Figure 5). Jonathan L. Carrivick conceived of the paper, obtained the raw data, supervised Katie and Will, and wrote the paper. Katie Berry did all the rest of the analysis and wrote a version of the analysis for her dissertation.

Acknowledgements

I owe much to all of those special and dedicated people who have helped bring this challenging project to fruition.

Firstly, a large thank-you to my supervisors Dr Jonathan Carrivick and Dr Duncan Quincey who saw the potential value of this project in the first place, and showed unwavering support for me throughout. Professor Neil Glasser is also thanked for his support and encouragement during the project. A special thanks is given to those who supported my research on the other side of the world, especially Professor James Shulmeister for his insights into cosmogenic dating, Dr Stefan Winkler for his advice on field locations and Dr Trevor Chinn for his unrivalled knowledge of glaciers in New Zealand. Thanks also to Joseph Mallalieu, Mark Smith and Megan Klarr for helping to make my time in New Zealand so enjoyable.

This project could not have proceeded without a number of existing datasets which were not always publically available. Professor Peter Jansson is thanked for provision of bed topography GIS files of Storglaciären and Nick Golledge is thanked for his ice thickness dataset of the New Zealand Southern Alps. The generosity of Dr Matthias Huss is greatly acknowledged for his supply of ice thickness data whilst GNS and NIWA are also thanked for their kind response to my requests for lake bathymetry and glacial geomorphology datasets. The mountains of data required for this project also presented significant challenges, with the University of Leeds IT department thanked for their patience and Rachel Homer thanked for her statistical support.

The project could not have proceeded without financial support. Academic study was gratefully supported by NERC PhD studentship (grant number NE/K500847/1) and the bank of Mum and Dad. Finally a large thank-you to all of my friends, family and colleagues who have made this a genuinely enjoyable time. A special thanks to Mum (Carolyn James) and Dad (Alan James) for their unwavering support for whatever I choose to do.

Abstract

New Zealand fills a large geographic gap in the global glacial record, with landforms and near-surface deposits preserving a remarkable footprint of Quaternary glaciation. As one of the few land masses in the Southern Hemisphere, the record of glacial geomorphology is of great importance for research into the natural behaviour of the Earth's climate system.

This thesis presents a 3D simulation of the New Zealand Southern Alps glaciers at the Last Glacial Maximum (LGM, c. 30 to 18 ka) in an attempt to constrain glacial geometry of that period. To achieve this, the REVOLTA (Reconstruction of Volume and Topography Automation) model was developed, a Python script tool for ArcGIS™ that requires just a DEM of glacier bed conditions and the down-valley extent of glaciation as initial inputs. Ice thickness is initially estimated at points along an automatically generated centreline network based on the perfect-plasticity rheology assumption, taking into account a valley side drag component of the force balance equation. Distributed ice thickness is subsequently interpolated using a glaciologically correct algorithm. Results indicate a total LGM ice volume of 6771.9 km^3, in good correspondence of previous studies using a climate-driven ice dynamics approach. Combined with an estimate of contemporary ice volume (50.67 km^3), this result reinforces the notion that New Zealand has lost almost the entirety (99.25 %) of its glacial ice since the LGM, although this volume has contributed to just 17.02 mm of global sea level rise. Analysis of the LGM distributed ice thickness output shows a large number of nunataks and exposed ridges in the central Mt. Cook and northern regions, with a localised icefield in the Fiordland area.

LGM Equilibrium Line Altitudes (ELAs) automatically calculated using the Accumulation Area Ratio (AAR) method reveals an average lowering of 1074 m from present, with those to the west of main divide 461m lower than those to the east on average. LGM climatic conditions were estimated using the ELAs and scaled versions of contemporary temperature and precipitation distributions, suggesting a temperature reduction of between 5.6°C to 10.3°C and precipitation change of +4.3 % to +100.4% from present. When considering these new estimates in conjunction

with critically evaluated previous evidence, an average LGM cooling of 6.5 °C to 8°C is proposed, a refinement on the wide range of previously published values.

Importantly, there is large spatial variability between catchments, with eastern regions experiencing significantly greater cooling and greater precipitation increases (or less decrease) than their western counterparts. Increased westerly circulation and reduced sea level altering the relative position of the orographic barrier is a suggested potential mechanism for the predicted precipitation pattern changes, whilst increased southerly flow bringing cool air up the east coast is a possible cause of the temperature change differential predicted. The proportion of precipitation falling as snow or rain was also found to be an important factor when considering New Zealand LGM conditions, with up to 50% estimated to be falling as rain at the LGM ELA, with a strong east-west differential.

Input dataset generation for REVOLTA resulted in several important research outcomes. A DEM approximating LGM bed conditions was created, using a variety of novel techniques to modify the existing DEM. These included the estimation of contemporary ice thickness distribution using the VOLTA (Volume and Topography Automation) model for removal from the DEM, merging offshore and lake bathymetry and considering Holocene in-fill sediments. Furthermore, an in-depth review of the most up to date literature and datasets regarding the lateral extent of LGM glaciation was also carried out, generating an updated 'outline' of LGM glaciation.

Table of Contents

List of Tables

List of Figures

List of Abbreviations

ACC	Antarctic Circumpolar Current
ANUDEM	Australian National University Digital Elevation Model
ASTER	Advanced Spaceborne Thermal Emission and Reflection Radiometer
DEM	Digital Elevation Model
ELA	Equilibrium Line Altitude
EOSS	End of Summer Snowline
GLIMS	Global Land Ice Measurements from Space
GUI	Graphical User Interface
IQR	Interquartile Range
IRSL	Infrared stimulated luminescence
LGM	Last Glacial Maximum
LIA	Little Ice Age
MBG	Minimum Bounding Geometry
MIS	Marine Isotope Stage
OIS	Oxygen Isotope Stage
PAEK	Polynomial Approximation with Exponential Kernel
PISM	Parallel Ice Sheet Model
QMAP	Quarter Million Scale Mapping
REVOLTA	Reconstruction of Volume and Topography Automation
RGI	Randolph glacier inventory
SED	Surface Exposure Dating
TCN	Terrestrial Cosmogenic Nuclide
TIR	Thermal Infrared
UMISM	University of Maine Ice Sheet Model
VNIR	Visible and Near-Infrared
VOLTA	Volume and Topography Automation

Chapter 1. Introduction

1.1 General introduction

New Zealand is an archipelago spanning the mid latitudes of the Southern Hemisphere (Figure 1.1). At approximately 1500 km in length and typically 200 to 300 km wide, it consists of the North Island, South Island and over 600 smaller islands. From a glaciological perspective, it is the South Island which is of most interest, dominated by the Southern Alps mountain chain, approximately 500 km long and reaching a maximum elevation of 3724 m. Over 3000 glaciers persist today (Chinn *et al.*, 2014) with surrounding landforms and near-surface deposits preserving a remarkable footprint of Quaternary glaciation (Barrell, 2011).

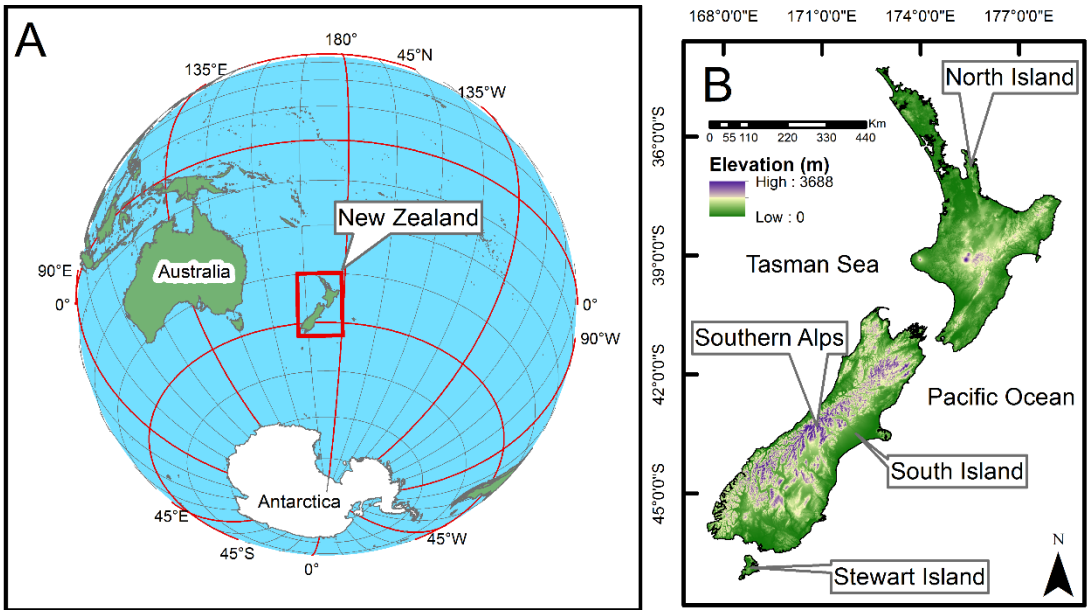

Figure 1.1 Location map of New Zealand in global context (a) and local topography (b)

New Zealand's unique location and natural environment means its climate and glacial record are of global importance. Due to its remote position in the Southwest Pacific, its climate directly reflects changes in the atmospheric-ocean system without the complexities related to large continental land masses as found in the Northern Hemisphere. Furthermore, with New Zealand remaining at least partially ice-free during the Last Glacial Maximum (LGM) (Suggate, 2004), a range of biotic environments persisted throughout and were able to respond rapidly to ensuing climatic change (McGlone *et al.*, 1993), thus providing a valuable terrestrial record in the ocean dominated Southern Hemisphere.

Mountain valley glaciers such as those found in the Southern Alps are a sensitive barometer of climate change, with the reconstruction of former extents and ice configurations allowing a valuable insight into former conditions. With glacier volume loss contributing directly to global sea-level rise, reconstructing former glaciers allows the influence of individual regions to be readily assessed (e.g. Glasser *et al.*, 2011). Glacier reconstructions can also be used in palaeoclimatic studies, with resultant Equilibrium Line Altitudes (ELAs) providing an important method for estimating palaeo-precipitation or temperature (Hughes & Braithwaite, 2008). With glaciers of the Southern Hemisphere amongst the least studied in the world (Grove, 1988), the Southern Alps represents a key site for improving our understanding of glacial and climatic conditions.

1.2 Definitions of glaciers

It may seem surprising that the New Zealand Southern Alps currently supports over 3000 individual glaciers (Chinn *et al.*, 2014). To understand this figure and to place many of the examples in this thesis into context, it is important to define what is meant by the term glacier and how it is defined.

This thesis follows the convention of Chinn (2001, p.147), stating that a glacier must be of at least 0.01 km^2 in area and is defined as:

"The accumulation of many years of snow surplus remaining above the snowline at the end of summer, which, metamorphosed into ice, flows slowly down slope until melt at lower altitude equals the supply".

There are a vast array of glacier morphologies both with New Zealand and worldwide, which can be classified accordingly. The characteristics of an individual glacier are the product of climate and topography, resulting in a broad continuum from small niche glaciers to the massive ice sheets of Greenland and Antarctica. For convenience, this continuum is often sub-divided into different glacier types based on size, morphology and topographic setting. Table 1.1 summarises the major classifications of glaciers, providing an example of each. It should be noted that these

distinctions are not strict and transitions exist between classifications (Hambrey & A, 2004).

Table 1.1 Classification scheme for glacier morphology. Adapted from Benn and Evans (2010)

First-order classification	Sub category	Description	Example
Ice sheet and ice cap (topographically unconstrained)	Ice domes	Broad, upstanding area of an ice sheet/cap. Thickness can exceed 3000 m.	East Antarctica
	Ice streams	Fast moving, channelized ice flanked by regions of slower moving ice. Radiating from interior ice sheet/cap.	Rutford Ice Steam, Antarctica
	Outlet glaciers	Fast moving, channelized ice occupying troughs or valleys. Radiating from interior ice sheet/cap.	Jakobshavn, Greenland
Topographically constrained	Ice fields	Form in regions of generally gentle but locally fretted topography. Flow influenced by underlying topography.	Columbia Ice Fields, Canadian Rocky Mountains
	Valley Glaciers	Form where ice is discharged into a deep bedrock valley. Form influenced by bedrock structure and lithology	Tasman Glacier, New Zealand
	Transection Glaciers	Interconnected systems of valley glaciers. Found in deeply dissected mountain regions.	King Christian iX Land, Greenland
	Cirque Glaciers	Form in bedrock hollow acting as an accumulation basin	Dana Glacier, Yosemite
	Piedmont Glacier	Lobe formation occurs when valley glaciers reach lowland plains.	Elephant Foot Glacier, Greenland
Ice Shelves		Low gradient, floating glacier tongues formed where glaciers flow offshore	Coast of continental Antarctica

Contemporary glaciers of the Southern Alps are mainly of the topographically constrained types, with a detailed discussion of current and former glacier morphology discussed in subsequent chapters.

1.3 Causes and distribution of glaciation

To understand the presence and distribution of glacial ice in New Zealand (both contemporary and former), it is important to appreciate global patterns and processes of glaciation, placing New Zealand in context. Whilst it is beyond the scope of this thesis to review all aspects controlling the magnitude and timing of glaciation, the following section is intended to provide a brief overview of the major processes pertaining to the evolution and morphology of glaciers of New Zealand.

The glaciers of the Southern Alps form part of the global ice mass, currently occupying approximately 16 million km^3 with a total volume of 0.35 ± 0.07 m sea level equivalent (Grinsted, 2013b). This ice mass fluctuates on timescales of less than a day to hundreds of millions of years, with Earth undergoing several major

transitions between periods of high glacier cover ('icehouse' phases) and periods of much reduced or absent cover ('greenhouse' phases), upon which shorter term cycles are superimposed (Deynoux *et al.*, 2004). There are a variety of factors important for controlling the long-term switches between icehouse and greenhouse climates, including a gradual increase in solar luminosity over billions of years (Beer *et al.*, 2000), changes in atmospheric CO_2 concentration due to tectonic processes (Donnadieu *et al.*, 2004) and large scale changes in the distribution of continents and mountain chains altering circulation patterns (Pearson & Palmer, 2000).

Superimposed upon this icehouse-greenhouse trend are shorter-term oscillations of cooler (glacial) and warmer (interglacial) conditions. Over the past 2 million years, the sequence of glacial and interglacial periods is strongly linked to cyclical changes in the Earth's orbit around the sun causing variations in the amount and pattern of solar radiation received at Earth's surface (Imbrie *et al.*, 1992). Specifically, variations in the eccentricity (elliptical nature of Earth's orbit), obliquity (tilt of Earth's axis in relation to the orbital plane) and precession (direction of tilt) combine to alter the radiation receipt, thus initiating a range of changes and feedbacks in the atmospheric, ocean, hydrological, vegetation cover and glacial systems (Clark *et al.*, 1999).

At a global scale, glaciation is concentrated towards the poles in the form of the Arctic and Antarctic ice sheets where the low solar angle results in reduced energy to melt ice and snow. Glaciers are also more prevalent at increased altitude as average temperatures decrease with air density (Benn & Evans, 2010). A combination of these two gradients broadly describe the current global pattern of global glaciation, with glaciers only existing in equatorial regions at high altitude (e.g. Ecuador, Central Africa), and forming at progressively lower altitudes towards the poles (e.g. Antarctic and Arctic ice sheets). This also partly explains the presence and distribution of glacial ice within New Zealand itself, with the most extensive glaciation occurring around the highest peaks of the Mt. Cook region whilst ice cover is rapidly diminished in lower relief regions nearby (e.g. Canterbury Plains and in the North Island) (Chinn, 2001).

On an individual catchment scale, the degree of glaciation is also influenced by local topography and climatic conditions. In the Southern Alps, there is a clear aspect control, with Chinn and Whitehouse (1980) calculating a 310 m difference in mean Equilibrium Line Altitude (ELA) between North and South facing glaciers due to south facing slopes receiving the least solar radiation (opposite to the Northern Hemisphere). Wind direction is also a control on glaciation, with those in the lee of the prevailing direction enhanced due to a 'snow trap' effect. Furthermore, relief and topography directly control glaciation, with narrow, steep sided summits unable to support snow accumulation whilst highland plateaux areas encourage ice fields and ice caps (Benn & Evans, 2010). This effect is evident in the Southern Alps where the steep topography favours a large number of individual glaciers on separate peaks (Chinn, 2001).

Even though a location may be cold enough to support glaciation, if insufficient precipitation is available it may not be able to maintain ice cover. The Canadian Arctic provides a good example of moisture control, where large ice fields on South-east Ellesmere and Devon Island are supported by precipitation from the 'North Water' of Baffin Bay whilst glacier cover is diminished to the west due to moisture starvation (Koerner, 1977). Precipitation control is also highly evident in the Southern Alps, where there is a dramatic precipitation gradient, rising from approximately 3000 mm yr^{-1} along the western coastal plains to a maximum of over 10000 mm yr^{-1} near the main divide before dropping again to approximately 1000 mm yr^{-1} in the eastern ranges (Henderson & Thompson, 1999). This results in a strong east-west differential in ice coverage, with mean glacier elevations rising from 1500 m in the west to over 2000 m in the moisture deprived eastern catchments (Chinn, 2001).

Under the mechanisms described above, New Zealand has undergone multiple glacial and interglacial phases. Whilst the exact number of glacial cycles is unknown, there is evidence of at least five major Quaternary glaciations in addition to the earlier Ross (2.4 to 2.6 Ma) and Porika glaciations (2.2. to 2.1 Ma) (Barrell, 2011). An in-depth review of the glacial history of the New Zealand Southern Alps is provided in section 3.2.

1.4 Aims and objectives

The primary aim of this thesis is to refine our understanding of distributed ice thickness and paleoclimate (specifically temperature and precipitation) of the New Zealand Southern Alps during the Last Glacial Maximum (LGM).

To achieve the primary aim, four specific objectives are addressed. These are to:

1. Develop a new method for the refined estimate of contemporary ice volume and distributed bed topography of the New Zealand Southern Alps.
2. Produce a refined consideration of ice extent during the LGM for the New Zealand Southern Alps.
3. Develop a new landform based method for the reconstruction of LGM ice surface profiles and distributed thickness of the New Zealand Southern Alps.
4. Use the resultant ice configurations and equilibrium line altitudes (ELAs) to establish the likely range and spatial variability of climatic conditions at the Last Glacial Maximum (LGM).

1.5 Thesis structure

Whilst this thesis is presented largely in a 'traditional' format, individual chapters are written in the form of extended journal publications where appropriate. Chapter 2 forms the basis of the published article *Automated modelling of distributed glacier ice thickness and volume* in the Computers & Geosciences journal (James & Carrivick, 2016) whilst it is envisaged that Chapters 3 and 4 will subsequently form individual research papers. As such, each chapter contains a standalone review of the relevant literature rather than the thesis incorporating a dedicated 'literature review' chapter.

To meet the overall aim of the project (section 1.4), each chapter addresses the specific objective(s) as shown in Figure 1.2. Whilst producing important and novel research outcomes in their own right, Chapters 2 and 3 are effectively model precursors/data preparation components of the REVOLTA (**Re**construction of

Volume and **T**opography **A**utomation) model developed and implemented in Chapter 4.

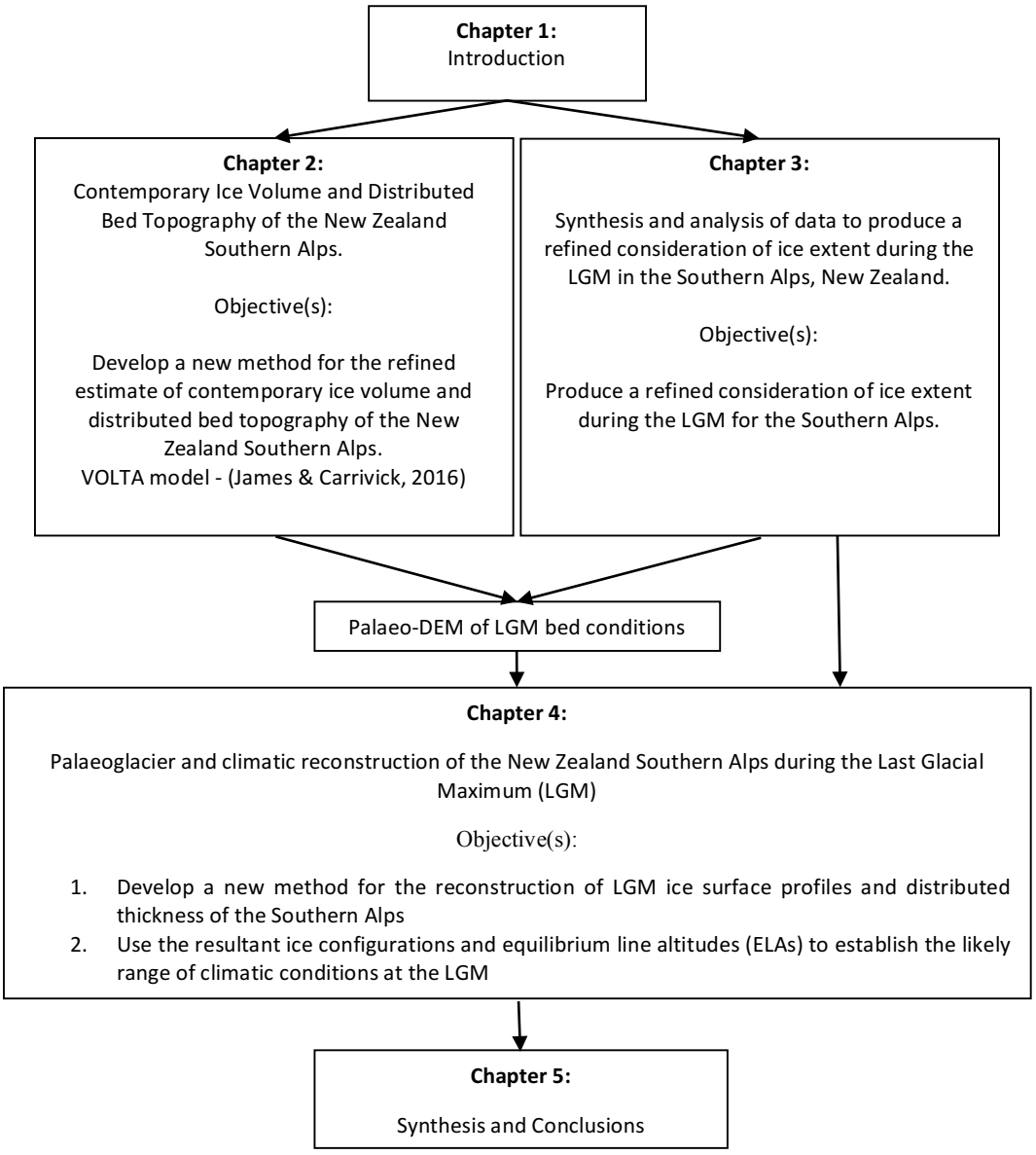

Figure 1.2 Schematic diagram showing thesis structure and specific objective(s) of each chapter

Chapter 2. Contemporary Ice Volume and Distributed Bed Topography of the New Zealand Southern Alps

2.1 Introduction

Outside Antarctica and the Andes, the glaciers and snowfields of New Zealand are the most significant in the Southern Hemisphere, with over 3,000 glaciers exceeding 0.01 km^2 in area (Chinn, 1989). The glaciers of New Zealand are also extremely isolated, with the next nearest glacial ice situated 2,300 km away on Balleny Island, which is a glaciated Antarctic Island. Indeed considering the whole World, only the glaciers of East Africa are situated further from their next nearest neighbour, demonstrating how the glaciers of New Zealand fill a huge geographic gap in the global distribution (Chinn *et al.*, 2014). Therefore, whilst the glaciers of New Zealand represent only a minor portion of the contemporary glacier ice on Earth and would contribute to just 0.15 mm of sea level rise if they disappeared completely (Huss & Hock, 2015), their unique location has considerable potential to offer an invaluable insight into worldwide glacier-climate interactions, especially since the New Zealand Southern Alps holds exceptionally well-preserved geological evidence of former glacier fluctuations (Barrell, 2011). Locally, within New Zealand, contemporary glacier ice distribution and volume is of great importance for hydrology, ecology and the economy (Fitzharris *et al.*, 1999), resulting in a considerable research interest.

Despite the importance of knowledge regarding the ice thickness distribution of the Southern Alps it is very poorly understood. Field measurements are impractical and thus extremely sparse and consequently the typical data requirements for modelling studies are virtually absent. The limited field measurements which do exist and estimates that go into models will both be explained in subsequent sections of this chapter.

Development of methods for assessing regional ice thickness distribution is essential for improving our understanding of many glaciological, hydrological and climatological issues. In the context of ongoing climate change, large-scale assessments are important because a climate signal extracted from an individual glacier may not be representative of the entire region (Hoelzle *et al.*, 2007). Furthermore, it is total regional ice volume that is essential for exploring the response of glaciers to climate change (Chinn *et al.*, 2012) and for the projection of

meltwater availability (Kaser *et al.*, 2010). Ice thickness distribution is required for glacier dynamics models (e.g. Oerlemans *et al.*, 1998) and for assessing the impact of climate change on the hydrology of glaciated catchments (e.g. Huss *et al.*, 2008). Glacier bed topography derived via distributed ice thickness estimations can be used to reconstruct palaeoglaciers (e.g. Benn & Hulton, 2010), and the resultant equilibrium-line altitudes are a widely-used source of palaeoclimatic information (e.g. Benn & Ballantyne, 2005). Bed topography is also of great assistance in understanding glaciological hazards, such as jökulhlaups (e.g. Carrivick, 2007; Staines & Carrivick, 2015), and for understanding subglacial lake formation (e.g. Frey *et al.*, 2010).

2.2 Contemporary glaciation in New Zealand

The occurrence, distribution and morphology of glaciers in New Zealand is primarily due to the Southern Alps mountain chain, created by the interaction between the Pacific and Australian plates (Figure 2.1a). This 500 km long mountain chain rises rapidly from the coastline and contains a number of peaks over 3,000 m, including Mt. Cook, 3,724 m just 35 km from the West coast. The main watershed of the Southern Alps is known as the 'main divide', separating catchments draining east and west (Figure 2.1b). The vast majority of glacial ice in New Zealand resides along the Southern Alps between 42° 08′ S to 45° 56′ S and 167 ° 11′ E to 173° 38′ E and can be broadly divided into four regions containing groups of larger glaciers (Chinn, 1989). Whilst there a few small glaciers and permanent snow patches north of Arthurs Pass, substantial glaciation begins to occur South of Mount Whitcombe Figure 2.1b) where the Lyell and Ramsay glaciers are located, along with the snowfields of the Garden of Allah and the Garden of Eden. Central to the Southern Alps is the Mount Cook region, containing New Zealand's largest glaciers, with the Tasman Glacier flowing to the east of the main divide and the Fox Glacier and Franz Josef Glacier to the west. Further South is the Mount Aspiring region containing the Bonar and Volta glaciers and the Olivine Ice Plateau, whilst the Mount Tutoko region encompasses the Southernmost Fiordland glaciers. This wide distribution of glaciers is in contrast to a common perception of a limited distribution of a small number of glaciers centred around Mount Cook and Franz Josef (Chinn, 2001).

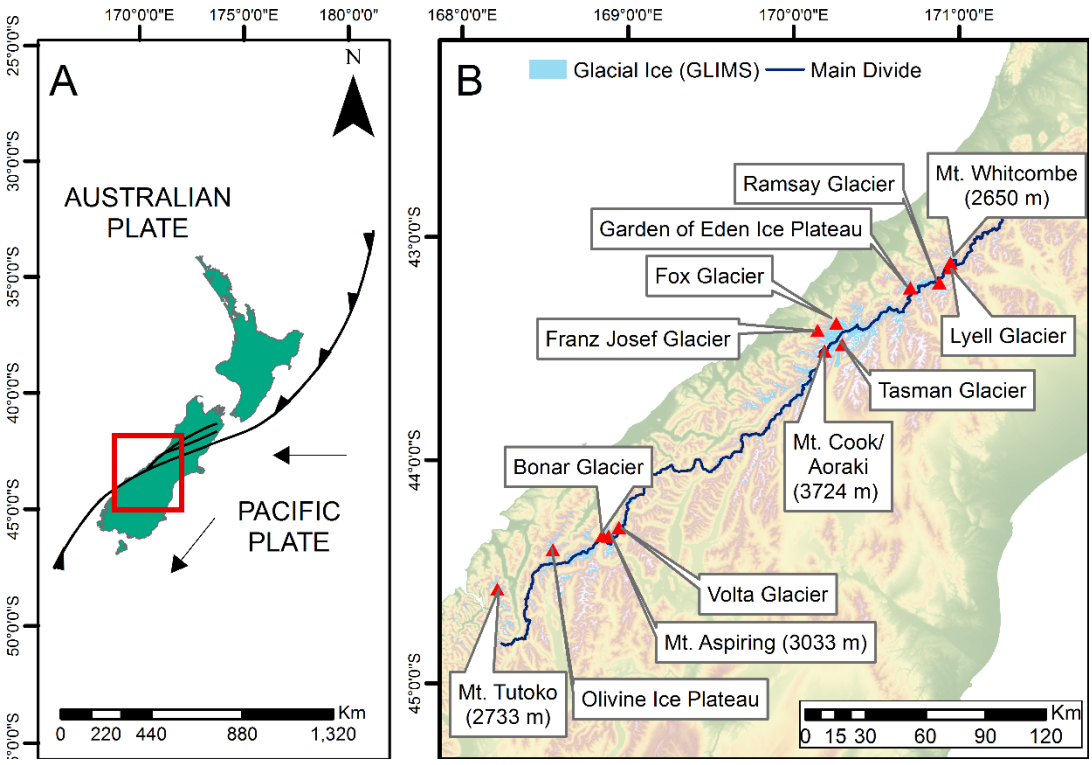

Figure 2.1 Position and interaction between the Australian and Pacific plates (adapted from (Coates, 2002) (a). Present day distribution of glacial ice in the Southern Alps and key locations mentioned in the text (b).

In the North Island, tectonic activity is evident from volcanic cones, with Mount Ruapehu (2,752 m) the only peak high enough to support glaciers today (Chinn, 1989). Indeed, of the 3,144 glaciers mapped in New Zealand, only 21 are situated in the North Island (Arendt *et al.*, 2015), covering an area of 5.9 km^2, just 0.47 % of the total (1250.2 km^2). Being situated on an isolated volcanic cone over 380 km from the next nearest glacial ice, these glaciers are not strictly part of the Southern Alps and are therefore excluded from further analysis in this thesis. It should be noted that some of the literature includes these glaciers in analysis, although they are not significant to influence any comparisons between such studies.

2.3 Inventory of glaciers and glaciological data of the New Zealand Southern Alps

Although glacier volume is difficult to quantify (Farinotti *et al.*, 2009), glaciated area is much easier to measure. Furthermore, if a scaling relationship is defined, area can be used to estimate associated volume via a volume-area scaling approach, discussed further in sections 2.4.9 and 2.6.1.1. The planform area of almost all

glaciers in the world has been inventoried, with data repositories such as the Randolph glacier inventory (RGI) and Global Land Ice Measurements from Space (GLIMS) providing free access to the datasets. These inventories are constructed from composite sources, with glaciers mapped by different techniques and at different time intervals depending on the region.

For New Zealand, a full glacier inventory of planform area was produced in 1978 by Trevor Chinn, derived from aerial imagery (Chinn, 1978). This inventory identified 3,144 glaciers over 0.01 km^2, covering a total area of 1,158 km^2 (Chinn, 2001). To date this remains the only complete, continuous inventory for the Southern Alps and is therefore commonly used for regional modelling and assessment (e.g. Huss & Hock, 2015; Huss & Farinotti, 2012). The glacier outlines from this inventory are also used as the basis for local topographic mapping (NZ Topo50 map series) and in global glacier inventories (GLIMS, RGI). The same glacier outlines have been used throughout all RGI versions, including the latest release, version 5.0 released July 2015, although individual glaciers were distinguished from glacier complexes between for version 3.0 onwards (Arendt *et al.*, 2015). In detail, the GLIMS database not only contains the same full set of original 1978 glacier outlines, but additionally includes updated (2009) glacier outlines for the Mt Cook region (Sirguey, 2010). These new outlines were obtained primarily from an object-oriented classification (Definiens eCognition v5) using VNIR (Visible and Near-Infrared) and (TIR) (Thermal Infrared) bands of an orthorectified ASTER (Advanced Spaceborne Thermal Emission and Reflection Radiometer) image (RMS < 15m) along with topographic layers obtained from the DEM (Sirguey, 2010). Additionally, Gjermundsen *et al.* (2011) compiled glacier outlines for the central portion of the Southern Alps in 2002 derived from ASTER imagery, although these do not form part of the GLIMS or RGI databases.

In addition to inventories of planform glaciated area, various other parameters have been measured for glaciers in New Zealand which can help to assess changes in glaciation limits and response to changing climate. The End of Summer Snowline (EOSS) has been monitored annually since 1977 for 50 selected index glaciers (see Willsman *et al.* (2014) for the most recently published results), forming the most complete such dataset in the world, giving an exceptional insight into decadal scale

changes in the Southern Alps. This dataset has been used as a proxy for mass balance change (Chinn *et al.*, 2012); with its application for estimating changes in volume discussed in section 2.3.3. Associated ELAs are also used extensively in Chapter 4 as a baseline condition.

Alongside regional datasets, various glaciological parameters have also been measured for individual glaciers. Whilst these are therefore not suitable for modelling the entire Southern Alps, they are useful for calibrating, parameterising and validating regional models. Field based ice thickness measurements are crucial for validating models of distributed ice thickness, with available measurements discussed in section 2.3.2. Ice velocity can be used as an input for distributed ice thickness models (e.g. Farinotti *et al.*, 2013) although measurements in New Zealand are only available for a select number of individual glaciers (e.g. Kirkbride, 1995). Direct mass balance measurements are also an established method of determining changes in ice volume (Paterson, 1994) and is a required input for some ice volume estimation models (e.g. Michel *et al.*, 2013; Farinotti *et al.*, 2009). However, direct measurement of mass balance is laborious and costly, requiring the installation of an array of stakes throughout the glacier, with repeated visits required to monitor gains/loss. Consequently there are very few glaciers with series of mass balance measurements in New Zealand with the longest study from the Ivory glacier between 1969 and 1975 (Anderton & Chinn, 1978). Mass balance was also measured on the Tasman glacier between 1971 – 1973 (Anderton, 1975) and more recently on the Brewster glacier (Anderson *et al.*, 2010).

2.3.1 Recent trends in New Zealand glaciation

The late 20th and early 21st Century has seen dramatic changes in glacier extent in New Zealand, with a general trend of retreat punctuated by smaller re-advances. Modelling by Chinn *et al.* (2012) found a reduction in volume (water equivalent) from 54.5 km^3 in 1976 to 46.1 km^3 in 2008. However, substantial re-advances of individual glaciers have also been recorded during this period with the Franz Josef Glacier advancing 1420 m between 1983 and 1999 (Purdie *et al.*, 2014). The recent development of large proglacial lakes is another important feature of the contemporary glacial system of the Southern Alps, effectively 'decoupling' the rate

of retreat of certain glaciers from changes in climate, with the switch to calving termini overriding climatic inputs (Warren & Kirkbride, 2003). The nature and influence of such proglacial lakes is discussed in detail in 3.2.5.1. These rapid changes require careful monitoring, with the accurate and quick methods for assessing glacier extent and volume of paramount importance.

2.3.2 Field measurements of ice thickness in New Zealand

Measurement of ice thickness is the only direct method to determine distributed thickness, bed topography and volume. Thickness can be measured via boreholes (e.g. Hochstein *et al.*, 1998) or by reflection techniques such as seismics (e.g. Shean *et al.*, 2007) or radar (e.g Singh *et al.*, 2012). If these field measurements are sufficiently numerous and well distributed, it is possible to build a detailed bed topography map and constrain volume (e.g. Björnsson, 1981), However, to date there has been no attempts to do this for any glacier(s) in New Zealand.

There are very few direct measurements of ice thickness in New Zealand as the process is laborious, expensive and logistically difficult (Farinotti *et al.*, 2009), with Table 2.1 summarising those that are available in the literature. The steep topography of New Zealand favours a large number of cirque glaciers and glacierettes on separate peaks (Chinn, 2001), making thickness measurements perhaps more difficult than in other glaciated regions. For measurements which do exist, many early studies were initiated by government bodies, motivated by the importance of glaciers in relation to hydroelectric power generation (e.g. Anderton, 1975). More recently, ice thickness measurements in New Zealand have been carried out with regards to awareness of climatic change.

Table 2.1 Published ice thickness measurements for the New Zealand Southern Alps

Study	Glacier	Survey Method	Results
Anderton (1975), provisional interpretation by Broadbent (1974)	Tasman	Seismic reflection	Thickness of ~150 m at 1.5 km from terminus, increasing to 400 – 600 m at confluence with Ball glacier.
Claridge (1983)	Tasman	Gravity and resistivity surveys	Thickness of 600 m (± 90m) at 10 km from terminus, thinning to 200 m at 2 km from terminus
	Murchison	Gravity and resistivity surveys	Thickness of 230 m 3-4 km upstream of terminus
	Hooker	Gravity and resistivity surveys	Thickness of 150 m at 1.5 km from terminus
Hochstein *et al.* (1995)	Hooker	Radar	Thickness of 165 m and 260 m at 1.7 km and 3 km from terminus respectively
Hart (2014)	Tasman	Gravity and seismic refraction	12 transects in lower 5km, maximum thickness of 722 m

2.3.3 Previous volume estimates of the New Zealand Southern Alps

Estimates of the volume of the Southern Alps are available in the literature using a variety of methods (Table 2.2). Volume estimates range from 53.29 km^3 (Chinn, 2001) to 83 km^3 (Radić & Hock, 2010); the range in these estimates reflects the level of uncertainty involved with ice volume estimation. Even within studies, there is substantial uncertainty in the estimated volume. For example, Huss and Farinotti (2012) quantified this uncertainty in their study as ± 5 km^3, being affected by uncertainty in the glacier outlines used, the DEM used and of the model in general. Furthermore, in their assessment of ice volume globally, Huss and Farinotti (2012) report a relative difference of -49 % between their New Zealand calculations and the New Zealand estimate of (Radić & Hock, 2010), who used the same input data!

Table 2.2 Published volume estimates for the New Zealand Southern Alps. Expressed as total ice volume, converted from water equivalent assuming an ice density of 900 kg m^{-3} where required.

Study	Volume (km^3)		Method and data
Anderton (1973)	63 ± 4 km^3		Volume area scaling (derived from non-NZ glaciers). 527 glacier outlines mapped.
Chinn (2001)	53.29 km^3		Volume area scaling (WGMS relationship derived from non-NZ glaciers). 3,144 glaciers mapped, based on 1978 aerial photograph survey.
Hoelzle *et al.* (2007)	67 km^3		Basic perfect plasticity assumption with theoretical values. Volume calculated for 702 glaciers over 0.2 km^2 from WGI inventory (1978)
(Radić & Hock, 2010)	83 ± 11 km^3		Volume area scaling, modified from (Chen & Ohmura, 1990). WGI-XF glacier outline dataset
Huss and Farinotti (2012)	70 ± 5 km^3		Ice flow mechanics (Farinotti *et al.*, 2009). RGI V2 outlines and SRTM DEM
Grinsted (2013a)	80.4 km^3		Volume area scaling with adjustments for continentally and elevation range. Calculated for WGI/GLIMS glacier outlines. Based on a figure of 0.2 mm SLE assuming an ice density of 900 kg m^3 and an ocean area of 362 x 10^6 km^2
(Huss & Hock, 2015)	59.5 km^3	North 0.19 km^3 South 59.31 km^3	Ice flow mechanics (Farinotti *et al.*, 2009).Calculated for RGI 4.0 outlines and SRTM DEM

Most attempts to estimate volume of the Southern Alps utilise a 'volume-area' scaling approach, relying on an empirical relationship between the surface area and volume of measured glaciers. Whilst this allows the rapid estimation of regional ice volume, a major drawback is that no information on distributed thickness can be obtained. This method is conventionally used to derive a total volume (e.g. Anderton, 1973) whilst Chinn *et al.* (2012) used it as part of a hybrid approach to estimate volume change between 1976 and 2008 for the Southern Alps. In their study, volume area scaling was used to estimate an initial (1976) volume of 54.5 km^3, with mass balance changes (inferred from the end of summer snowline dataset, see section 2.3) used to estimate ice loss, finding an overall volume decrease of 8.41 km^3 to 2008, a reduction of 15 %. Despite its widespread use, a range of scaling relationships exist and there is considerable debate and confusion in the literature surrounding volume-area scaling, with its theory and application discussed further in sections 2.4.9 and 2.6.1.1.

Recently, the volume of the Southern Alps has been estimated as part of worldwide assessments (Huss & Farinotti, 2012; Huss & Hock, 2015), with estimates of 70 km^3 and 59.5 km^3 respectively (Table 2.2). These studies both utilised the approach presented by Farinotti *et al.* (2009), based on glacier mass turnover and ice flow mechanics and are discussed in section 2.6.1.2.

2.4 Methods

2.4.1 VOLTA: A new tool for estimating ice volume and distributed thickness

There is clearly uncertainty surrounding the total ice volume of the Southern Alps, with section 2.3.3 reviewing the wide range of previous estimates in the literature. Furthermore, the majority of existing estimates do not calculate distributed ice thickness, an important parameter for many glaciological, hydrological and climatological applications. Whilst distributed ice thickness of the Southern Alps has been modelled using ice mechanics methods, to date this has only been achieved as part of worldwide assessments (Huss & Farinotti, 2012; Huss & Hock, 2015), using models not specifically designed for New Zealand, whilst also appearing to be sensitive to the format of input datasets (discussed in section 2.6.1.2). With the climate and steep topography of the Southern Alps creating an alpine style of glaciation (Chinn, 2001), a new model; VOLTA (Volume and Topography Automation) has been developed to model ice thickness under such circumstances. VOLTA is designed to take advantage of the data sources available for New Zealand (high resolution DEMs and glacier outlines), with the ability to run rapidly and from a user friendly interface. This is achieved by estimating ice thickness along automatically derived centrelines following the perfect plasticity assumption (Nye, 1952), before interpolating fully distributed ice thickness. VOLTA is written in the Python scripting language and executed via ArcGIS™ as a geoprocessing tool. VOLTA, installation instructions and manual are available for download at: https://github.com/williamjames/volta. A schematic flowchart of the VOLTA workflow is presented in Figure 2.2.

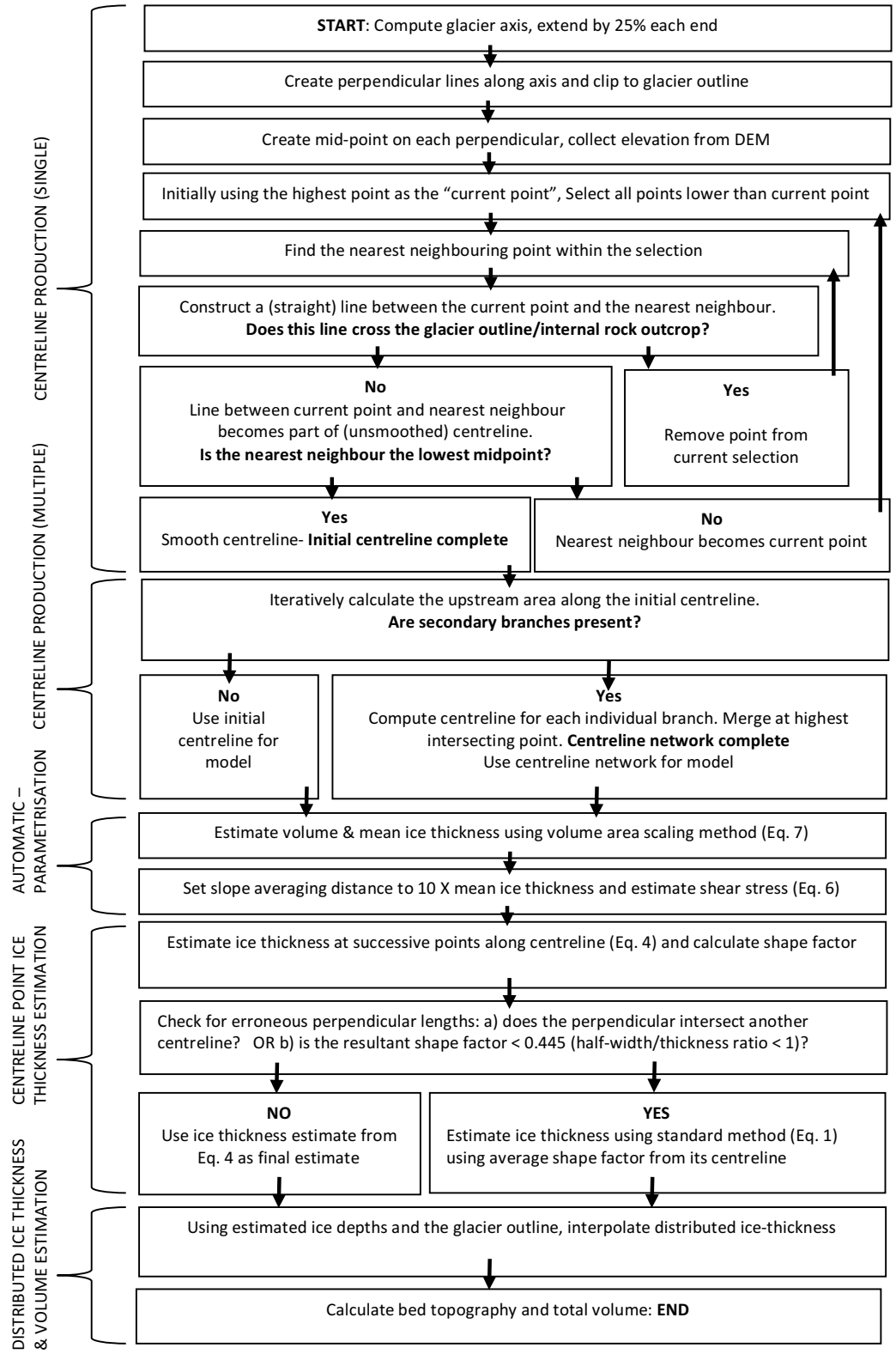

Figure 2.2 Flowchart conceptually illustrating the automatic generation of glacier centrelines and estimation of distributed ice thickness and volume with VOLTA.

2.4.2 Automating centreline production

VOLTA initially estimates ice thickness along automatically derived centrelines. Whilst it would be desirable to derive centrelines which represent actual flowlines (i.e. ice trajectories), this would require fully distributed velocity fields, which are not available for New Zealand and many other areas of the world, making regional scale applications unachievable (Kienholz *et al.*, 2014). Whilst centrelines will usually coincide with the location of maximum ice thickness along a transverse profile, they may be offset in some circumstances, such as in the vicinity of sharp bends.

Traditionally, centreline production required manual digitisation, a time consuming and subjective process. Recently, automated techniques using GIS hydrology tools (Schiefer *et al.*, 2008; Machguth & Huss, 2014), cost-distance analysis (Kienholz *et al.*, 2014) and geometric analysis (Le Bris & Paul, 2013) have been developed, although to date only appearing in the literature with regards to method development. To overcome the constraints of manually digitising centrelines, VOLTA generates centreline(s) using the glacier axis concept (Le Bris & Paul, 2013). VOLTA develops the algorithm of Le Bris and Paul (2013) by:

- Improving the axis creation technique
- Automatically adjusting the smoothing parameter
- Automatically creating separate centrelines for multiple tributaries
- Incorporating the algorithm of Le Bris and Paul (2013) with VOLTA

Firstly, a glacier axis is created to define the main direction of the glacier. Whereas Le Bris and Paul (2013) determined the axis by joining the highest and lowest points of the glacier, VOLTA uses a Minimum Bounding Geometry (MBG) technique, followed by connecting the two farthest points (Figure 2.3a). This creates an axis not influenced by individual high and low DEM cells, which may otherwise create an unrealistic axis. Perpendicular traverses are then created along the axis at the resolution of the DEM, which are subsequently clipped to the glacier outline and midpoints placed on each traverse segment (Figure 2.3b).

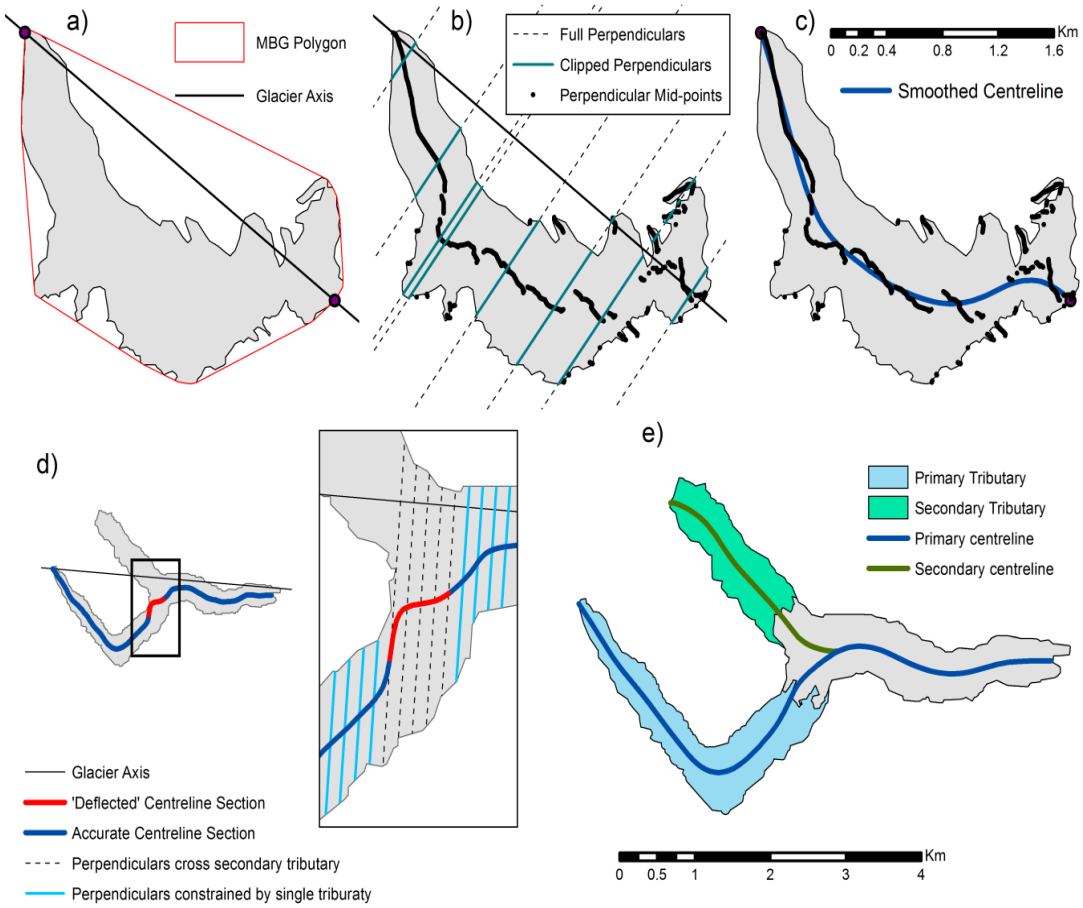

Figure 2.3 VOLTA centreline production: a) definition of glacier axis, b) midpoints on perpendicular traverses, c) smoothed single centreline, d) example of deflected centreline, e) multi-centrelines

An initial centreline is constructed by iteratively joining traverse midpoints (starting at the highest midpoint) in a similar manner to that described by Le Bris and Paul (2013). The line is then smoothed using the Polynomial Approximation with Exponential Kernel (PAEK) algorithm to remove irregularities caused by small scale variations in glacier shape. Larger glaciers require greater smoothing as wide tributaries result in a smooth course of the centreline (Kienholz *et al.*, 2014). The amount of smoothing is controlled by glacier area in an approach similar to that of Kienholz *et al.* (2014):

$$l = \begin{cases} 2 \cdot 10^{-6} \cdot A + 200 & : l \leq l\,max \\ l\,max & : l > l\,max \end{cases}$$

Equation 1

Where l is smoothing length, A is glacier area (m^2) and $l\,max$ is 1000 m

2.4.3 Glaciers of complex geometry

A single centreline may not be suitable if the glacier is of complex geometry due to multiple tributaries or cirques (e.g. Figure 2.3e), a common feature of many glaciers in the New Zealand Southern Alps. Whilst the lack of a secondary tributary centreline is the main issue, the initial centreline is also laterally deflected where the perpendicular traverses are elongated as they continue into the secondary tributary (Figure 2.3d. To overcome these issues, VOLTA utilises a novel 'upstream area' approach to delineate separate tributaries, allowing multiple centrelines to be generated (Figure 2.3e). Iteratively working down the initial centreline, upstream area is calculated. Total area will steadily increase down-centreline, but a marked increase occurs when a new tributary enters (Figure 2.4). VOLTA calculates area at an interval equal to 1 % of centreline length with a new tributary identified if area increases by more than 20 % between successive points. Furthermore, any new tributary must also have an area of at least 5 % of the total. Whilst these thresholds may be altered via the Graphical User Interface (GUI), testing against manually identified tributaries for 25 glaciers found these values were able to correctly delineate tributaries where appropriate, whilst not adding 'extra' tributaries due to small areas of ice adjoining. If secondary tributaries are identified, new tributary outlines are created from a subset of the original (Figure 2.3e) and secondary centrelines are created in the standard manner, ignoring any midpoints of which the corresponding perpendicular crosses into another tributary. Branch order is managed in the same manner as Kienholz *et al.* (2014), with the initial centreline classed as the primary centreline. Further centrelines are clipped so they reach from their head to the next, larger centreline.

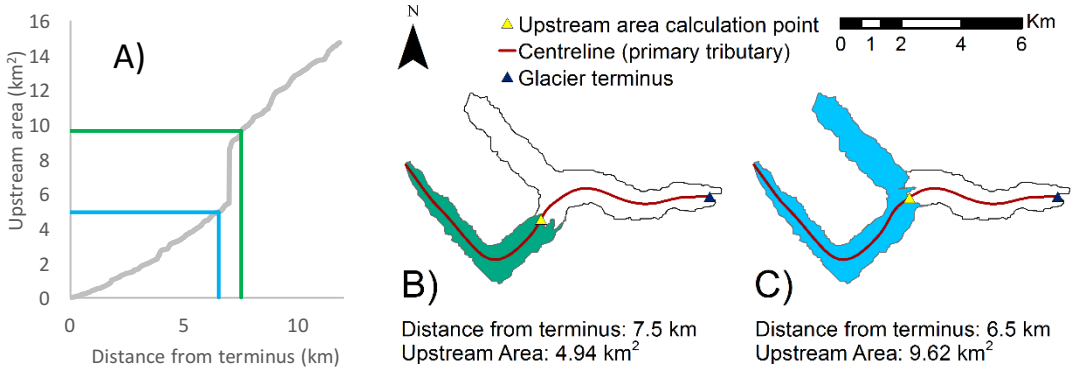

Figure 2.4 a) Glacier upstream area as moving along centreline (for Unteraargletscher). Note the large 'step' at 7km when secondary branch becomes connected. b) Upstream area calculated 7.5 km along centreline (after secondary branch confluence). c) Upstream area calculated 6.5 km along centreline (before secondary branch confluence).

2.4.4 Calculating ice thickness at points along the centreline

VOLTA estimates thickness along the centreline(s) using the perfect plasticity approach first developed by Nye (1951) and later refined for mountain valley glaciers (Nye, 1965):

$$T_b = fpgh\ sin\ \alpha$$

Equation 2

Where T_b is the basal shear stress, p is the ice density, g is gravitational acceleration, h is ice thickness and α is the ice surface slope. For mountain valley glaciers, a shape factor (f) is required because valley sides support part of the weight of the glacier, resulting in T_b on the centreline being lower than for an infinitely wide basin. f can be incorporated as a constant (usually 0.8: Nye, 1965), a form which has been used previously in the literature (e.g. Linsbauer *et al.*, 2012).

Li *et al.* (2012) developed a more physically realistic method which dynamically adjusts f depending on the local width of the glacier (see Li *et al.* (2012) for a full-derivation):

$$h = \frac{0.9\ w(\frac{T_b}{pg\ sin\ \alpha})}{0.9\ w - (\frac{T_b}{pg\ sin\ \alpha})}$$

Equation 3

Where w is half the glacier width at the specified point.

Whilst Equation 3 estimates ice thickness perpendicular to the ice surface Figure 2.5a, VOLTA estimates 'vertical' ice thickness, perpendicular to a horizontal x-axis Figure 2.5b form appropriate for GIS geometry (Equation 4):

$$h = \frac{0.9\ w(\frac{\tau_B}{pg\ tan\ \alpha})}{0.9\ w - (\frac{\tau_B}{pg\ tan\ \alpha})}$$

Equation 4

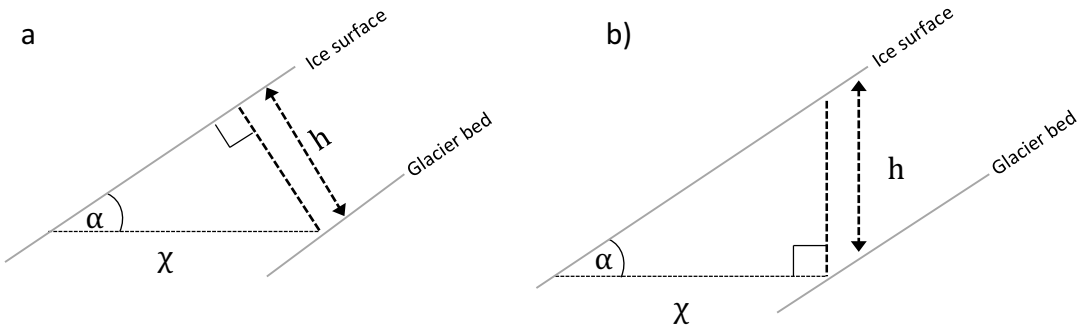

Figure 2.5 a) Surface-perpendicular ice thickness calculated using the (original) sin function (Equation 3) and b) vertical ice thickness calculated using the tan function (Equation 4), as used by VOLTA.

For some glacier geometries (e.g. where nunataks are present or where tributaries converge), width calculation may be inaccurate, with Li *et al.* (2012) cautioning against its use without cross-checking. VOLTA automatically checks for erroneous values by: (i) checking if the perpendicular line intersects another centreline (Figure 2.6a) and (ii) cross checking if the resulting *f* value is realistic (> 0.445, equal to a half width to centreline thickness ratio of 1: Nye 1965) (Figure 2.6b). At points where either of these conditions is met, VOLTA calculates thickness using the original Equation 2 rearranged to solve for thickness, with *f* set to that of the average for the tributary (calculated from points on the same tributary with accurate width calculations). The '*f_type*' field in the output point file indicates which method is used, with 'W' denoting the independent width has been used and 'A' denoting the tributary average value has been used.

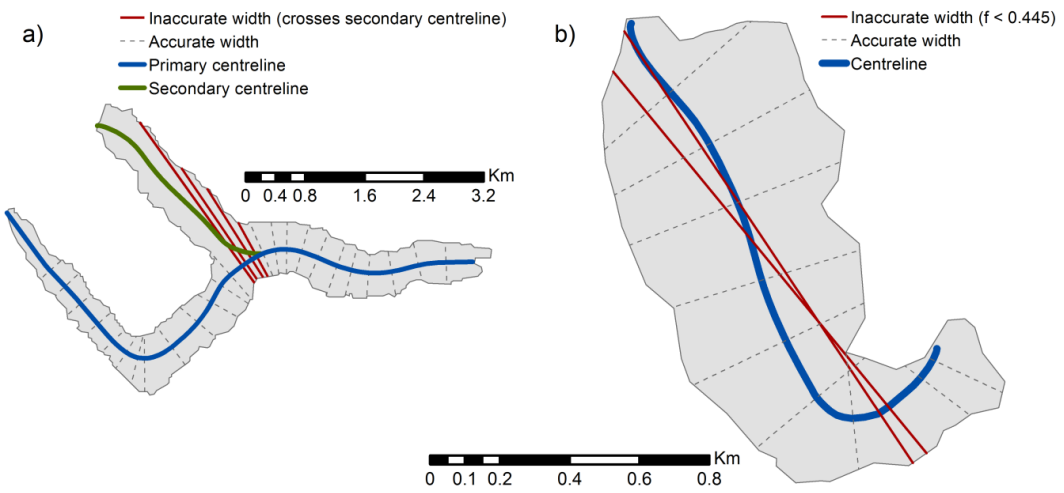

Figure 2.6 Inaccurate glacier width calculations identified where: (a) the perpendicular crosses an alternative centreline or (b) the resultant f value is < 0.445

2.4.5 Interpolating distributed ice thickness and bed topography

VOLTA interpolates distributed ice thickness using the ANUDEM (Australian National University Digital Elevation Model) 5.3 interpolation routine, which is an iterative finite difference technique designed for the creation of hydrologically correct DEMs (Hutchinson, 1989). ANUDEM is implemented via the 'TopoToRaster' tool in ArcGIS, using ice thickness points as 'spot elevation' inputs and the glacier outline as a contour input (assumed to represent zero ice thickness). This process generates preferably concave shaped landforms, mimicking the typical parabolic shape of (idealised) glacier beds (Linsbauer *et al.*, 2009) and is the method of choice for interpolating both mountain valley glaciers (e.g. Fischer & Kuhn, 2013) and ice sheets, such as the Bedmap2 Antarctica dataset (e.g. Fretwell *et al.*, 2013). Interpolation of this manner is an accepted method for bed topography estimation (Farinotti *et al.*, 2009; Li *et al.*, 2012; Linsbauer *et al.*, 2012), although sediment infill or the compound incision effects of multiple glaciation phases may result in modified cross sections under some circumstances (Schrott *et al.*, 2003). VOLTA additionally outputs the raw centreline ice thickness points, allowing bespoke interpolation by the user if required.

Once ice thickness (h) for each cell has been interpolated, total volume, V can be calculated:

$$\boldsymbol{V} = \sum (\boldsymbol{c^2 h})$$

Equation 5

Where c is the cell size.

2.4.6 VOLTA parameters

The parameters of basal shear stress (T_b), slope averaging distance (α_d), 'effective width' slope threshold (α_{lim}) and 'minimum slope' threshold(α_0) are used by VOLTA for effective ice thickness estimation. By default, VOLTA does not require any user specification of these parameters, using the DEM and glacier outline(s) to derive glacier specific values. However, some parameters may be altered via the GUI if required (e.g. if independent ice thickness measurements exist).

2.4.6.1 Basal shear stress

Basal shear stress (T_b) is variable between individual glaciers due to many factors (e.g. basal water pressure, ice viscosity, subglacial sediment deformation), meaning no universal value should be used between glaciers. For modelling, T_b does not have to be varied longitudinally for an individual glacier as a constant value can reproduce accurate thickness estimates along the length of a centreline (Li *et al.*, 2012).

Whilst T_b can be "*constrained reasonably from just a few ice-thickness measurements*" (Li *et al.*, 2012 p.7), in the majority of cases there are no independent measurements, requiring T_b to be estimated. An empirical relationship between altitudinal extent and T_b developed by Haeberli and Hoelzle (1995) is often used in the literature, although the spread of data points is large (r^2 = 0.44), with Linsbauer *et al.* (2012) estimating an uncertainty of up to ± 45 %. A more robust relationship was developed by Driedger and Kennard (1986a), using area and slope in an elevation band approach:

Equation 6

$$T_b = 2.7 \cdot 10^4 \sum_{i=1}^{n} \left(\frac{A_i}{\cos \alpha_i} \right)^{0.106}$$

Where the elevation band area (A_i) is in m^2 and shear stress (T_b) is in Pa. This method was tested by Driedger and Kennard (1986b) as part of a volume estimation study, finding a standard deviation of error of 5 % when comparing with measured volumes. This is the default method used by VOLTA, with A_i and $\cos \alpha_i$ calculated over 200 m elevation bands. The result is a glacier specific mean T_b value which is applied to each centreline point. Optionally, T_b may be defined via the GUI by the user.

2.4.6.2 Slope averaging distance

Analysing the centreline gradient over an appropriate distance (α_d) is required for producing reliable thickness estimates. If α_d is too low, small-scale variations in the surface topography will be reproduced in the bed profile. Conversely, if α_d is too large, variations in the surface topography may be smoothed or omitted. α_d should be 'several times' the local ice thickness (Paterson, 1994). As such, it is initially set to 10 times the average glacier thickness ($\bar{h}$), with $\bar{h}$ derived from a volume area scaling approach, using the relationship developed by Bahr *et al.* (1997):

Equation 7

$$\bar{h} = \frac{0.034\, A^{1.375}}{A}$$

Where A is the glacier area and $\bar{h}$ is average ice thickness. For further discussion of the volume-area approach, see sections 2.5.2 and 2.6.1.1.

2.4.6.3 Minimum slope threshold

Using Equation 4, ice thickness will tend to infinity as surface slope tends to zero, meaning thickness may be overestimated in flat regions (Li *et al.*, 2012; Farinotti *et al.*, 2009), To overcome this, a 'minimum slope threshold' (α_0) is used in the same

manner as Farinotti *et al.* (2009) and Li *et al.* (2012), setting any lower slope values to it. The threshold was determined empirically at 5° by Farinotti *et al.* (2009) and 4° by (Li *et al.*, 2012). In VOLTA, α_0 is initially set to 4°, although this may be altered via the GUI if required.

2.4.6.4 'Effective width' slope threshold

VOLTA accounts for valley side drag by incorporating glacier width (Equation 4). However, thin ice on higher parts of the valley wall will contribute negligible support and thus should not be included in the width calculation. An 'effective width' slope threshold (α_{lim}) is used to help exclude those areas as described by Li *et al.* (2012). In VOLTA, α_{lim} is set by default to 30° , which is the optimal value found during analysis by Li *et al.* (2012), although this value may be altered via the GUI if required. Under the original perfect plasticity assumption (Nye, 1965), a slope angle of 30° represents an ice thickness of 27 and 37 m when using shear stress values parameterised by Hoelzle et al. 2007 for the European Alps (130 kPa) and for the New Zealand Alps (180 kPa). These thickness values are consistent with Driedger and Kennard (1986a) who found a threshold of average glacier thickness at 36 m where the perfect plasticity assumption becomes valid.

2.4.7 VOLTA testing: application to glaciers with different geometry

For comparison and to evaluate performance, VOLTA was initially applied to 5 separate glaciers with 'known' bed topography. Glaciers were selected for: (i) ice thickness distribution that has been well constrained from field measurements; (ii) comprising a range of different spatial scales and geometries (single, multi-tributary); and (iii) occupying different regional settings and thus different thermal and dynamic characteristics. Datasets used to produce the 'field based' ice distributions are summarized in Table 2.3.

Table 2.3 Location of each glacier and details of the datasets used for determining the 'field derived' volume and VOLTA inputs.

Glacier	Location	Surface DEM	Outline	Bed topography
South Cascade	48.36° -121.05°	ASTER, 30m (USGS, 2014)	Fountain and Jacobel (1997)	Interpolated from 50m bed contours (derived from 5000+ measurements from multiple GPR transects) (Fountain & Jacobel, 1997)
Ödenwinkelkees	47.11° 12.64°	LIDAR, 2m (Carrivick *et al.*, 2013)	GLIMS (GLIMS, 2014)	Interpolated from 77 GPR measurements (Span *et al.*, 2005)
Storglaciären	67.90° 18.56°	10m, Composite dataset (e.g Björnsson, 1981)	Composite dataset (e.g Björnsson, 1981)	Composite dataset (e.g. Björnsson, 1981). Interpolation provided by Peter Jansson
Tasman	43.616° 170.20°	(Geographix, 2012)	GLIMS (GLIMS, 2014)	Interpolated from 14 transects (seismics) (Hart, 2014) & (Broadbent, 1974)
Unteraargletscher	46.566° 8.216°	ASTER, 30m (USGS, 2014)	Bauder *et al.* (2003)	Interpolated from 50m bed contours (derived from radar transects and 27 boreholes) (Bauder *et al.*, 2003)

The Ödenwinkelkees glacier, Austrian Alps (Figure 2.7a) is the smallest glacier (1.9 km^2) and is of a relatively simple geometry. South Cascade glacier (Figure 2.7b) was chosen due to its exceptionally well-constrained bed topography, providing an example of a simple geometry glacier in North America. Storglaciären (Sweden) is more complex, characterised by a branched accumulation area (Figure 2.7c), whilst the Tasman glacier, (New Zealand) and its tributaries form the largest and most complex system, covering 90 km^2 (Figure 2.7d). Finally, Unteraargletscher (Swiss Alps) provides an example of a larger multi-tributary glacier in the Northern Hemisphere (Figure 2.7e).

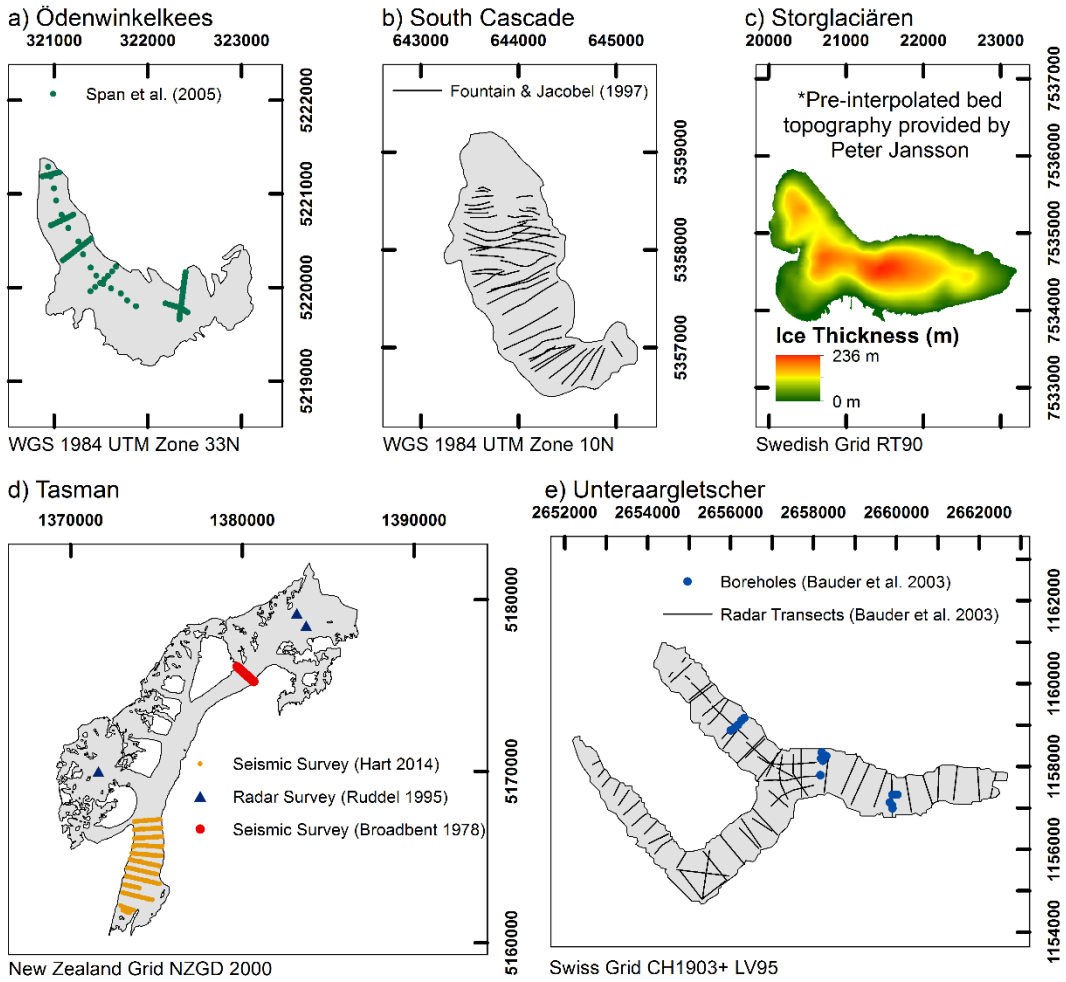

Figure 2.7 Distribution of field measurements used to create bed topography datasets.

Glacier outlines and field observations of ice thickness were digitized, georeferenced and projected in a Cartesian co-ordinate system. To account for ice surface topography changes between thickness measurement and DEM capture (surface lowering, retreat etc.), ice thickness was standardised to the surface DEM by subtracting the bed elevation from the surface DEM. The following analysis is therefore correct for the time of DEM capture. Ice thickness was interpolated using the ANUDEM algorithm (Hutchinson, 1989). Due to interpolation and also original error in the ice thickness measurements, the interpolated bed cannot be regarded as a truly accurate representation of the subglacial topography. Whilst the datasets used have no error analysis available, it is assumed to be ± 10 m to account for errors in the raw data collection (Pellikka & Rees, 2009) and in digitization. For the Tasman glacier, error is estimated to be ± 20 m due to the small scale of diagrams from which measurements were digitized (e.g. Hart, 2014).

2.4.7.1 Centreline generation

VOLTA generated a single centerline for the Ödenwinkelkees and South Cascade glaciers and multiple centerlines for Storglaciären, Unteraargletscher and the Tasman glacier (Figure 2.8). Due to the complex nature of the Tasman glacier system and the format of the outline, additional ice divides were digitized between nunataks and the main outline to ensure that individual branches were defined correctly. An initial GIS generated ridgeline network was used to inform the location of potential ice divides (Figure 2.9), whilst velocity fields may also be used if available. The main advantages compared to manual centreline production come with the reproducible and fast computation. Application to the Southern Alps of New Zealand resulted in 18 of the 196 (i.e. 9 %) of the centrelines (and one outline polygon) requiring manual adjustment, which is comparable to the original centreline algorithm developed by Le Bris and Paul (2013), which required adjustment in 13 % of cases.

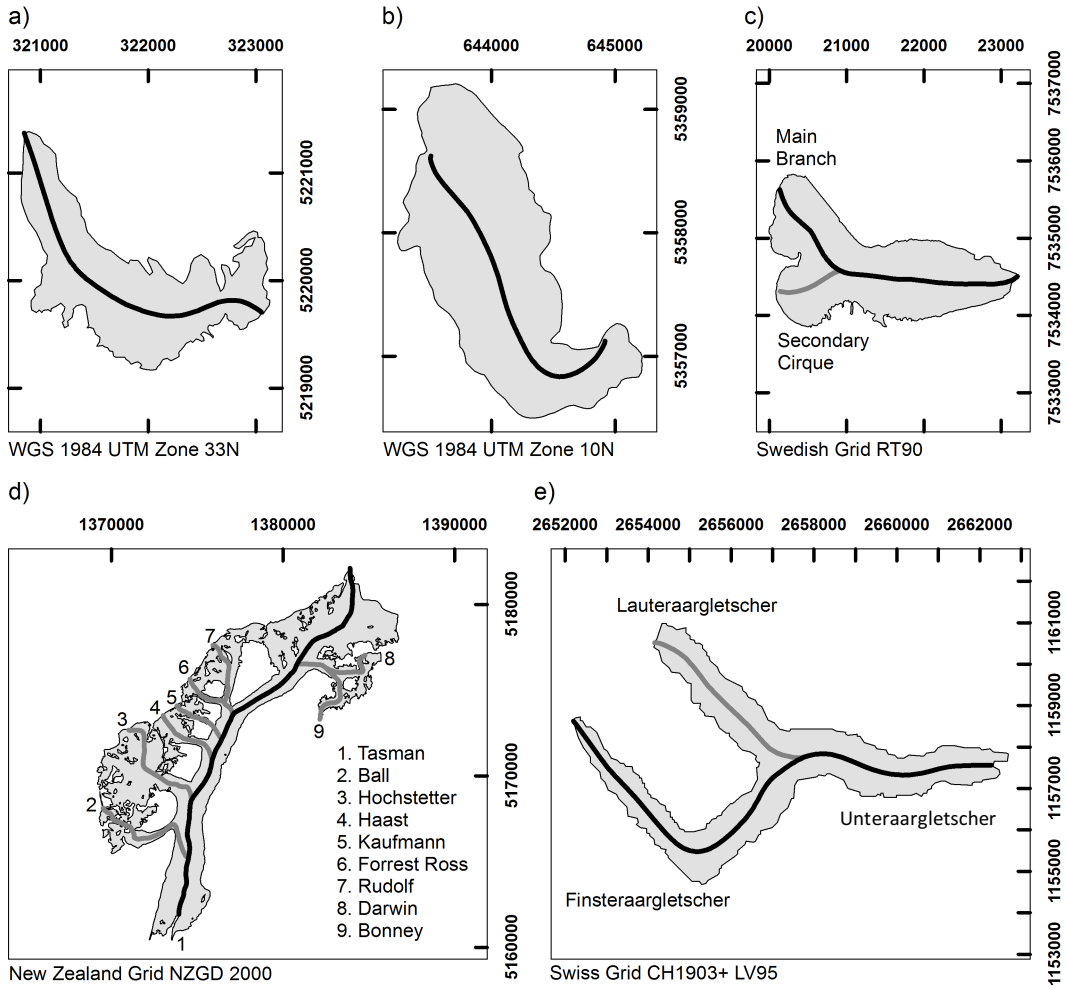

Figure 2.8 Centrelines generated by VOLTA for sample glaciers. a) Ödenwinkelkees, b) South Cascade glacier, c) Storglaciären, d) Tasman glacier, e) Unteraargletscher (including Lauteraar- and Finsteraargletscher).

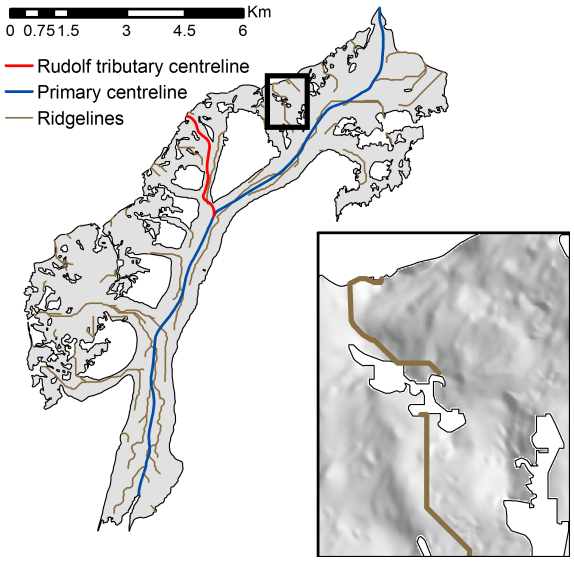

Figure 2.9 GIS ridgeline network generated to indicate potential ice divide locations

2.4.7.2 Distributed ice thickness and volume

Distributed ice thickness was estimated as described in section 2.4.5, with results shown in Table 2.4 and Figure 2.10. Overall volume was estimated to between 26.5 % (underestimate) and 16.6 % (overestimate) of that derived from field measurements. For comparison, approximate errors for scaling approaches range from 30 % for large samples to 40 % when considering smaller (approximately 200 glaciers) samples (Farinotti & Huss, 2013). The model presented by Farinotti *et al.* (2009) had an accuracy of ~25 % inferred from point-to-point comparison of measured and modelled thickness values whilst Li *et al.* (2012) reproduced measured thicknesses (radar transects) with a mean absolute error of 11.8 %. Histograms in Figure 2.10 graphically display the distribution of deviation between VOLTA and field measurements, with the positive skews in Figure 2.10a (Unteraargletscher) and Figure 2.10d (Ödenwinkelkees) representing an overestimate by VOLTA and the negative skews in Figure 2.10c (South Cascade), Figure 2.10e (Storglaciären) and Figure 2.10b (Tasman Glacier) representing an underestimate.

Table 2.4 Comparison between volumes calculated from field based observations and modelled by VOLTA. Parameters derived and summary statistics are also shown. Deviation is defined as the modelled (VOLTA) ice thickness subtracted from field measured value for each cell. *IQR = Interquartile Range

Glacier	Volume (field), km^3	Volume VOLTA, km^3	Volume Difference, %	Shear stress, kPa	Slope window, m	Median deviation, m	Deviation IQR*, m
Unteraargletscher	2.983	3.279	9.9	155	800	-11.2	112.6
Tasman	12.040	10.062	-16.4	187	1000	13.6	46.7
South Cascade	0.200	0.147	-26.5	115	500	25.8	59.0
Ödenwinkelkees	0.078	0.091	16.6	124	450	-2.7	22.3
Storglaciären	0.292	0.282	-3.4	127	550	7.7	42.4

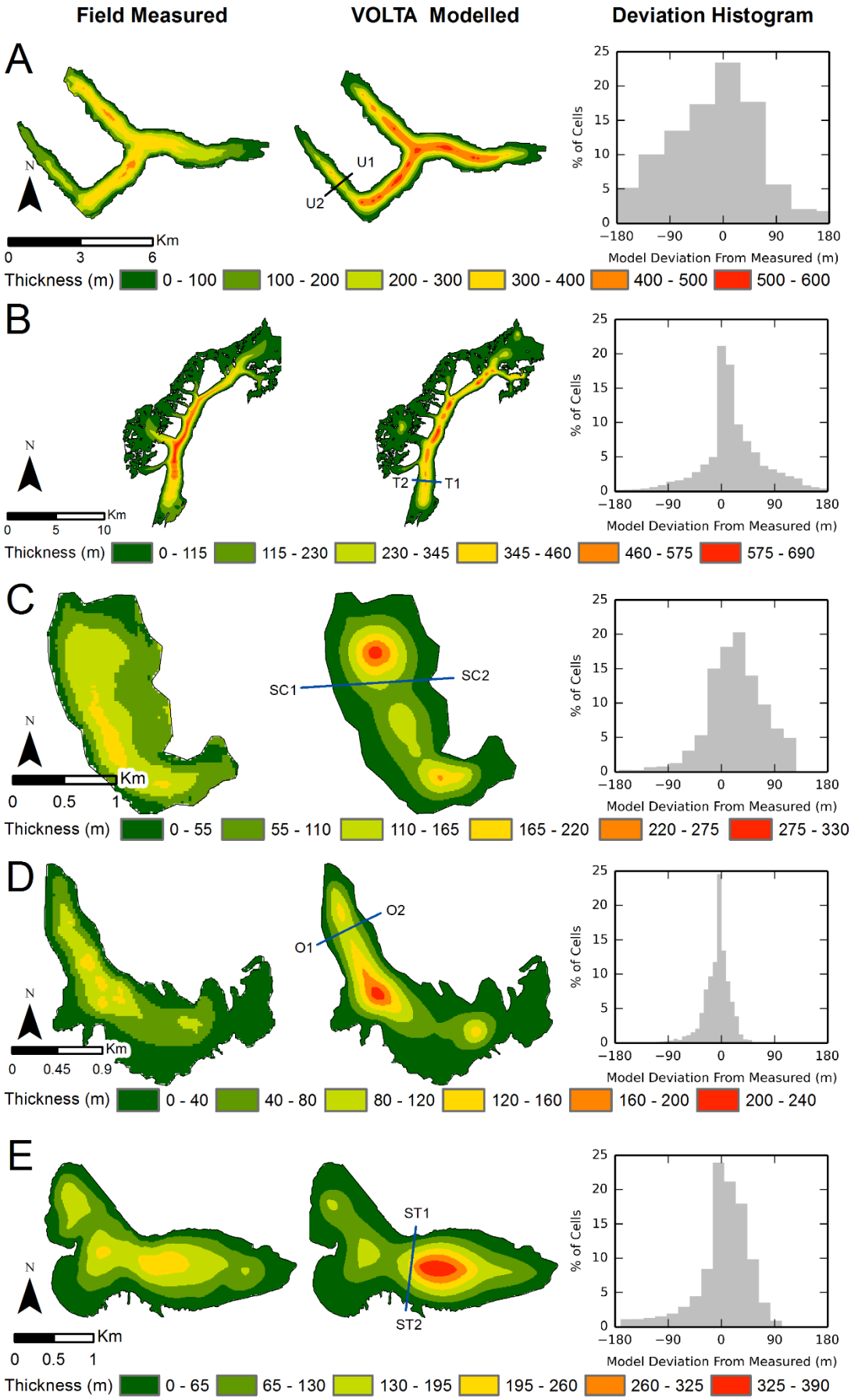

Figure 2.10 Field derived and VOLTA modelled ice thickness maps with accompanying deviation histograms. a) Unteraargletscher, b) Tasman Glacier, c) South Cascade Glacier, d) Ödenwinkelkees, e) Storglaciären

For Unteraargletscher (Figure 2.10a), both the field measured and modelled ice thickness show a parabolic cross section with the maximum ice thickness situated close to the centreline (Figure 2.11a). For the Tasman system, field measurements on the main branch suggest a bed cross section with a relatively flat base (Figure 2.11b), whilst VOLTA predicts a parabolic shape. Despite this, VOLTA is still able to accurately predict maximum ice thickness on the centerline and total volume (Table 2.4). South Cascade glacier field data reveals an asymmetrical bed cross section (Figure 2.10c and Figure 2.11c), which is not particularly well defined by VOLTA, resulting in a relatively large difference between volume estimated from field data and by VOLTA (Table 2.4). The parabolic bed profile of Storglaciären shown by field measurements (Figure 2.11e) are well reproduced by VOLTA, with longitudinal variations (including a potential overdeepening) also defined (Figure 2.10e). The good agreement between field data and VOLTA is shown by similar final volume calculations (Table 2.4). This is also the case of the Ödenwinkelkees, where an overdeepening evident in the field measurements (Figure 2.10d) is also predicted by VOLTA.

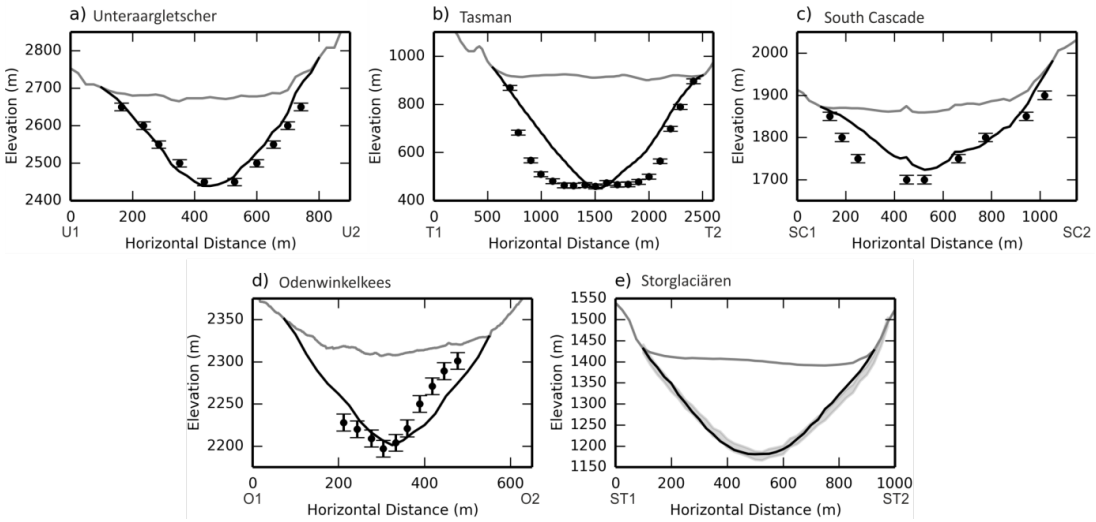

Figure 2.11 Comparison of transverse glacier-bed profiles generated by VOLTA (black lines) from field measurements (black dots). Panel e) shows field measurements as a grey band as it was provided as a pre-interpolated raster by Peter Jansson. Transect locations in Figure 2.10.

The Tasman glacier is an example of a contemporary glacier overriding previously deposited sediments, resulting in the near-horizontal bed profile visible in the field measurements (Figure 2.11b). VOLTA is able to predict the maximum thickness well (VOLTA modelled 496 m versus measured 510 m) because the perfect plasticity

assumption accounts for the corresponding low bed gradient along the centreline. However, the parabolic profile generated by ANUDEM underestimates ice thickness towards the valley sides, contributing to the 16.4 % overall volume deficit for the Tasman glacier.

Whilst the centreline will usually approximate the line of maximum thickness, in some cases this may be offset due to bends in the glacier (e.g. Ödenwinkelkees and South Cascade glacier). Whilst VOLTA can still accurately estimate the maximum thickness under such circumstances, this may be offset from the centre, resulting in 'skewed' bed topography such as for South Cascade glacier Figure 2.11c. This may be overcome by using actual flowlines (i.e. ice trajectories), rather than centrelines, although there is currently no feasible method to generate such inputs on a regional scale.

Considering the uncertainty in the field based glacier volume estimates used for benchmarking, VOLTA can be seen to perform at a similar level to other approaches. Crucially, the fully automated and user friendly approach offers advantages over previous models, offering the potential to rapidly model regions which would otherwise be prohibitively laborious. In general, VOLTA is able to predict maximum ice thickness values well, even if infilling or multiple past glaciations have occurred. Whilst the ANUDEM interpolation routine generally works well for linear glaciers with a bedrock base (parabolic profile), the user should be aware of potential issues when considering in-filled valleys or glaciers with sharp bends in their centreline. VOLTA outputs the original point ice thickness estimations if the user wishes to use an alternative interpolation routine.

2.4.8 Sensitivity testing

To assertain to what extent uncertainties in VOLTA parameters influence volume estimates, sensitivity tests were performed (Figure 2.12). Parameters T_b, α_d, α_0 and α_{lim} were tested independantly by altering their value whilst keeping others constant. Parameters were varied within bounds that could be reasonably expected, with the baseline set to that used for initial volume estimation. For each parameter, a range of 12 values was used, so Figure 2.12 reports a total of 240 model runs.

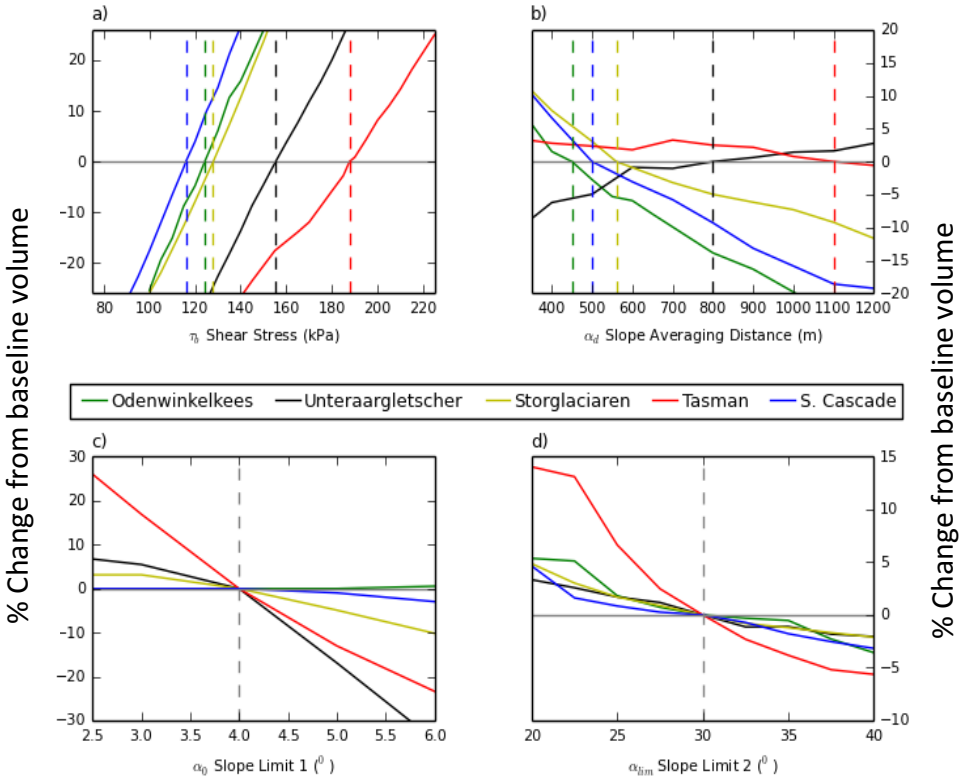

Figure 2.12 Sensitivity of volume estimate to parameters: a) shear stress, b) slope averaging distance, c) slope limit 1 and d) slope limit 2. The solid grey horizontal lines represent a zero change in volume and the vertical dashed grey lines indicate the baseline value.

T_b is the most sensitive parameter, showing a similar positive linear relationship for all glaciers (Figure 2.12a). For example, a 10 % increase in T_b results in a 12.2 % increase in volume for the Ödenwinkelkees. This is expected as the critical thickness at which deformation occurs will be greater as T_b is increased (Paterson, 1994). Volume is also sensitive to α_d, with smaller glaciers (Ödenwinkelkees, South Cascade, Storglaciären) showing a negative relationship (Figure 2.12b). An increase in α_d results in fewer thickness estimation points as no values can be determined at each end of the centreline (to a distance equal to half of α_d). Interpolations therefore trend to zero sooner, a potential mechanism for the negative relationship observed for smaller glaciers. Sensitivity to α_0 is variable (Figure 2.12c), with glaciers dominated by large regions of low gradient ice (e.g. Unteraargletscher) showing a negative relationship whilst steep glaciers (e.g. Ödenwinkelkees) are not sensitive to α_0. Likewise the sensitivity of VOLTA-derived volumes to α_{lim} is variable depending on glacier surface topography; glaciers with large steep accumulation zones (e.g. Tasman) are most sensitive. Overall, it is the volume of small glaciers with areas of

extreme gradient (either high or low) that are likely to be most sensitive to VOLTA input parameters. In contrast, the modelled volume of larger glaciers comprising moderate gradient surfaces will be least sensitive to VOLTA input parameters. These factors influencing the sensitivity of VOLTA should inform the choice of glaciers and regions to apply the model to, and should be taken into account when interpreting results.

2.4.9 Small Glaciers: Volume Area Scaling

The perfect plasticity assumption (and consequently VOLTA) will not hold true for small glaciers which do not reach a sufficient thickness to obtain a critical shear stress and associated deformation (see Driedger and Kennard (1986a)). This was demonstrated empirically by Driedger and Kennard (1986a) who found that for glaciers of less than approximately 2.6 km in length, volume was best estimated using a scaling approach, whilst for larger glaciers, the perfect plasticity assumption was appropriate. For this reason and for efficient computing, volume-area scaling is used to estimate the volume of small (< 1 km^2) glaciers. Whilst a distributed bed topography will therefore not be created for these smaller glaciers, they are likely to be thin (using the volume area relationship of Bahr *et al.* (1997), a 1 km^2 glacier is estimated to have an average thickness of just 37 m) with the average thickness used to approximate the bed.

For this thesis, volume is calculated using the relationship developed by Bahr *et al.* (1997), stating that for a glacier of given surface area S, volume, V, can be estimated as:

$$\boldsymbol{V = 0.034\, S^{1.375}}$$

Equation 8

A discussion of other relationships available in the literature and the reasons for utilising that of Bahr *et al.* (1997) is provided in section 2.6.1.1 with comparative results for alternative relationships explored in section 2.5.2.

2.4.10 Modelling of the Southern Alps: Input datasets

For modelling of the Southern Alps, appropriate input datasets (DEM and glacier outlines) for the region had to be sourced. The DEM is one of the major inputs for VOLTA, providing information on surface topography, slope and altitudinal extent of glaciers. Subsequently, the quality and acquisition date of the DEM will influence the results of VOLTA. For the regional modelling of New Zealand presented in this thesis, two DEMs were used: (i) the 8 m resolution Geographix New Zealand Digital Elevation Model version 2.1 downloaded from https://data.linz.govt.nz/layer/1768-nz-8m-digital-elevation-model-2012 and (ii) the 90 m resolution SRTM DEM version 4 (Jarvis *et al.*, 2008). The Geographix DEM is a composite product, primarily derived from LINZ 1:50,000 1984 topographic data. Spatial accuracy is nominally the same as the LINZ source data: 90% of well-defined points are within ± 10 m vertically and ± 22 m horizontally (Geographix, 2012). The SRTM DEM is of a lower spatial resolution (90 m), based on elevation data gathered from the shuttle mission in February 2000 and has previously been used for regional ice thickness modelling in New Zealand (Huss & Hock, 2015).

As discussed in section 2.3, the only complete coverage of glacier outlines for the Southern Alps is for 1978 (Chinn, 1978) although updated outlines (for the year 2009) are available for the Mt Cook region (Sirguey, 2010). VOLTA was therefore ran on both sets of outlines; the former providing regional analysis and the later providing the most up-to date analysis for the heavily glaciated Mt. Cook region. Glaciers were initially grouped into those over 1 km^2 (for VOLTA analysis) and those under 1 km^2 (for volume-area analysis). Table 2.5 shows the number and surface area of glaciers in each category for both datasets. Whilst glaciers over 1 km^2 (i.e. those analysed by VOLTA) make up a small proportion of the total number, they represent the majority of the total area, contributing to 59.9 % of the RGI 5.0 dataset area (Chinn, 1978) and 82.4 % of the GLIMS dataset area for 2009 (Sirguey, 2010).

Table 2.5 Number of glacier outlines and associated surface area for the entire Southern Alps and Mt. Cook region.

	TOTAL		VOLTA (> 1km^2)		Volume-Area Scaling (< 1 km^2)	
	Number of glaciers	**Area (km^2)**	**Number of glaciers**	**Area (km^2)**	**Number of glaciers**	**Area (km^2)**
RGI 5.0 Entire Southern Alps (Chinn, 1978)	3537	1157.06	158	692.54 (59.9%)	3379	464.52 (40.1%)
Mt. Cook Region only: (Sirguey, 2010)	467	351.38	37	289.51 (82.4 %)	430	61.87 (17.6%)
Mt. Cook Region only: RGI 5.0 (clipped to (Sirguey, 2010) extent)	486	400.27	35	327.67 (81.7%)	451	72.60 (18.3%)

2.5 Results

2.5.1 Glaciers > 1 km^2: VOLTA

For glaciers over 1 km^2 in area, VOLTA was run on a range of input datasets and with different parameters (Table 2.6). Model V1 utilised the high resolution (8m) Geographix DEM and the full set of outlines (RGI v5) (Chinn, 1978). The calculated volume was 40.68 km^3, with Figure 2.13 showing an example of the distributed ice thickness output. As previous research (e.g. Li *et al.*, 2012) and sensitivity testing (section 2.4.8) suggest that perfect plasticity are sensitive to the shear stress value used, model V2 was designed to test the performance of VOLTA using an alternative shear stress value. Rather than calculating a glacier-specific shear stress value in the standard manner (section 2.4.6.1), glaciers were assigned a shear stress value based on those calculated by Hoelzle *et al.* (2007): 180 kPa for those to the West of the main divide and 120 kPa for those to the East, with the differential driven by different mass balance gradients. This alternative approach resulted in a total volume calculation of 39.99 km^3, 1.7 % lower than model V1.

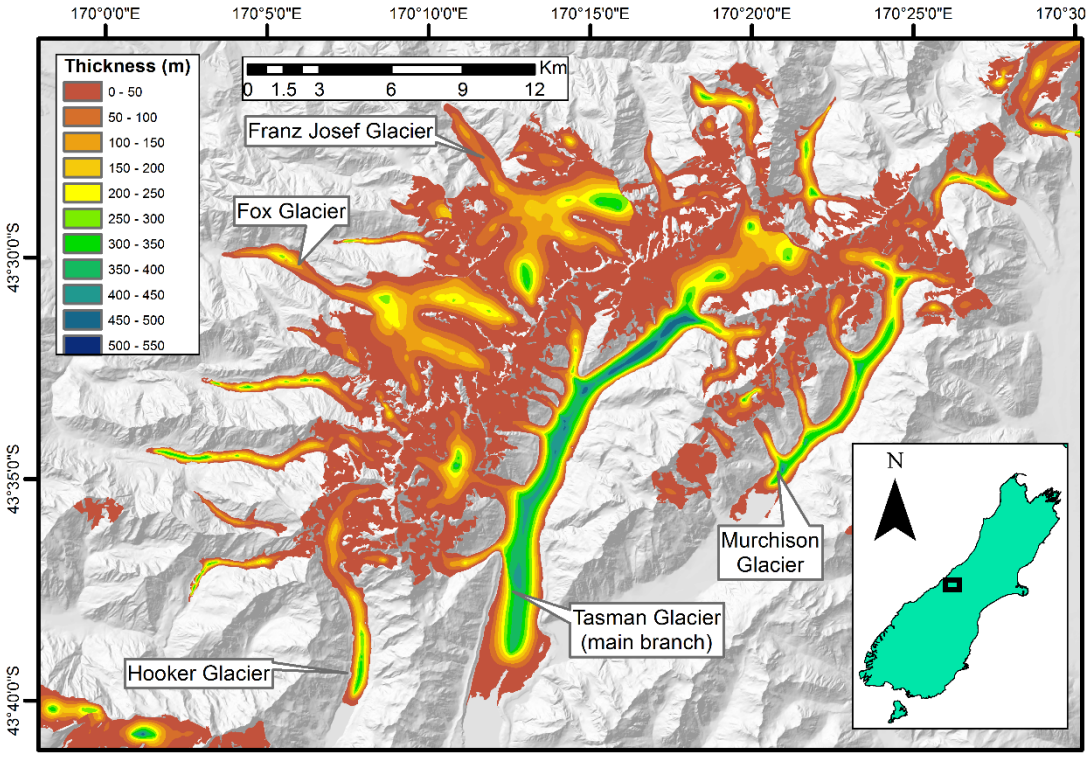

Figure 2.13 Extract of VOLTA estimated distributed ice thickness using model V1 parameters (Table 2.6)

Table 2.6 VOLTA derived volume estimates for all glaciers with a surface area > 1km^2, using a range of input datasets.

ID	Description	DEM		Outlines	Shear stress parameterisation	Volume Estimate (km^3)
V1	Full Southern Alps	Geographix DEM	8m	RGI V5 (n = 158)	Driedger and Kennard (1986a)	**40.68**
V2	Full Southern Alps – Alternative Shear Stress Calculation	Geographix DEM	8m	RGI V5 (n = 158)	West = 180 kPa, East = 120 kPa (Hoelzle *et al.*, 2007)	**39.99**
V3	Full Southern Alps - Comparison to Huss and Hock (2015)	SRTM v4		RGI V4 (identical to RGI V5) (n = 158)	Driedger and Kennard (1986a)	**40.12**
V4	Mt Cook Region, updated outlines	Geographix DEM	8m	GLIMS 2009 Outlines (n = 37)	Driedger and Kennard (1986a)	**22.70**
V5	Mt Cook Region, original outlines	Geographix DEM	8m	RGI v5 (n= 35)	Driedger and Kennard (1986a)	**24.16**
HH	Full Southern Alps (Huss & Hock, 2015)	SRTM v4		RGI V4 (identical to RGI V5) n = 158	n/a	**49.02**

To compare VOLTA with an alternative (non perfect-plasticity based) approach published in the literature, model V3 was ran on exactly the same input datasets as Huss and Hock (2015) (SRTM DEM and RGI v4 outlines), with a resulting calculated volume of 40.12 km^3. This is 18 % lower than the volume of 49.02 km^3 estimated by Huss and Hock (2015) (model HH in Table 2.6) for the same domain (all glaciers > 1 km^2 in the South Island). Furthermore, as the outlines used for model V3 are identical to those used in V1 (there were no changes between RGI v4 and RGI v5 for New Zealand (Arendt *et al.*, 2015), comparison between model V3 and model V1 shows the impact of using an alternative DEM. Using the Geographix DEM (model V1) results in a volume of 40.68 km^3 whilst the SRTM DEM (model V3) results in a volume of 40.12 km^3, 1.4% less.

VOLTA was also run on the Mount Cook region alone, as this area has updated outlines for 2009 (Sirguey, 2010). Model V4 utilises the new outlines, with a volume estimate of 22.7 km^3 when using the Geographix DEM. By clipping the original (1978) outlines to the same extent as covered by the updated (2009) outlines, a comparison between datasets was made, with VOLTA estimating a volume of 24.16 km^3 when using the original outlines for this area (model V5). This represents a volume reduction of 6.04 % between 1978 and 2009 for the Mt. Cook region.

2.5.2 Glaciers < 1 km^2: volume area scaling

For glaciers below 1 km^2, volume was estimated using the volume-area relationship developed by Bahr *et al.* (1997), with analysis carried out for the entire Southern Alps (RGI 5 outlines) and for the Mt. Cook area outlines (Sirguey, 2010). For comparison, a variety of other scaling relationships were tested on the same outlines whilst the results of a non-volume-area method (Huss & Hock, 2015) is also included in Table 2.7.

For the entire Southern Alps (glaciers < 1 km^2), the relationship of Bahr *et al.* (1997) yielded a volume estimate of 9.99 km^3, with alternative relationships estimating between 6.4 km^3 – 14.66 km^3 (Table 2.7). For the same domain, the non-volume-area approach of Huss and Hock (2015) estimated a volume of 9.41 km^3. The pattern of results for the Mt. Cook outlines is similar, ranging between 0.87 km^3 – 1.93 km^3, with the preferred method of Bahr *et al.* (1997) predicting 1.37 km^3.

Table 2.7 Comparison between volume estimates using the preferred method (Bahr *et al.*, 1997) and a variety of other scaling schemes V = Volume, A = Area, R = Altitudinal Extent (calculated from Geographix DEM).

Scaling Scheme	Entire S. Alps, < 1 km^2, RGI 5	Mt Cook Region, < 1 km^2, GLIMS 2009
	Volume (km3)	
V = 0.034 A$^{1.375}$ (Bahr *et al.*, 1997)	**9.99**	**1.37**
V = 0.0385 R$^{-0.2}$ A$^{1.29}$ (Grinsted, 2013a)	14.66	1.93
V = 0.2055 A$^{1.375}$ (Radić & Hock, 2010)	10.74	1.48
V = 5.2 + 15.4 √A (Chinn, 2001)	6.40	0.87
Huss and Hock (2015)	9.41	

2.5.3 Total volume of the New Zealand Southern Alps

By combining the volume estimate of glaciers less than 1 km^2 (using volume area scaling) and those over 1 km^2 (using VOLTA), a total volume for the New Zealand Southern Alps is calculated at **50.67 km^3**. This is comprised of 9.9 km^3 (19.5% of the total volume) for glaciers < 1 km^2 using the preferred volume-area scaling relationship (Bahr *et al.*, 1997) and 40.68 km3 (80.5%) for larger glaciers using VOLTA with the Geographix DEM and RGI 5.0 outlines as inputs (model V1, Table 2.6).

2.6 Discussion

2.6.1 Methods for estimating ice volume and distributed thickness

It has been demonstrated that there are a variety of methods for assessing regional ice thickness, with those previously applied to the New Zealand Southern Alps shown in Table 2.2. At the simplest level, ice thickness and volume can be estimated by in-field measurements followed by interpolation to a full surface (e.g. Fischer & Kuhn, 2013). However, there are very few field measurements of ice thickness in New Zealand, with only the Tasman glacier perhaps studied in sufficient detail to currently construct a bed topography map (see Figure 2.10b). Whilst airborne radar has recently opened up opportunities for regional scale mapping of ice-sheet bed topography (e.g. Fretwell *et al.*, 2013), this method is expensive and the coarse resolution is not suitable for assessing the intricacies of mountain valley glacier systems such as the Southern Alps. This has led to the development and application of various modelling approaches such as VOLTA. With an increased research interest in ice volume and distributed thickness, combined with advances in remote data collection and computing power/efficiency, modelling of regional ice thickness distribution has become increasingly popular.

2.6.1.1 Scaling approaches

The simplest models for estimating glacier volume utilise scaling approaches, relying on empirical relationships between glacier volume and other parameters (most commonly glacier area) (Bahr *et al.*, 2015). Once an empirical relationship has been defined, volume-area scaling requires just the knowledge of glacier area and has successfully been used to estimate the volume of glaciers around the world (Grinsted, 2013a) and for regional scale assessments including that of the New Zealand Southern Alps (Chinn, 2001). However, a major drawback of this method is that it provides just a single volume estimate for each glacier, with alternative methods required if the distributed thickness is sought. Furthermore, despite its prevalence in the literature, there is some confusion regarding the correct application (Bahr *et al.*, 2015). Whilst some studies rely on a volume-area

relationship derived purely from empirical data (e.g. Chinn, 2001), Bahr *et al.* (1997) demonstrated how the approach is physically justified using a power relationship:

$$\boldsymbol{V = c\, S^{e}}$$

Equation 9

Theory predicts the exponent *e* is a constant for a given geometric class (i.e. glacier type), determined as 1.375 for valley glaciers (see Bahr *et al.* (1997) for a full derivation), whilst the scale factor *c* may be variable by glacier, region, slope, climate or other factor (Bahr *et al.*, 2015). Despite the theoretical underpinning, Bahr *et al.* (2015) noted how applications have often incorrectly derived varying exponents and assumed a constant scale factor (e.g. Grinsted, 2013a).

As discussed in section 2.4.9, this thesis utilises volume area scaling to model the thickness of small glaciers (< 1 km^2) of the Southern Alps as it has been proven to work for all sizes of glacier (Bahr *et al.*, 2015) whilst the assumptions of alternative models have been shown to not hold true for smaller glaciers (Driedger & Kennard, 1986a). Whilst a distributed bed topography will not be created for these smaller glaciers, they are likely to be thin: a 1 km^2 glacier is estimated to have an average thickness of 37 m using the relationship of Bahr *et al.* (1997), with the average thickness used to approximate the bed.

Whilst there are no field based volume observations in New Zealand to build an initial relationship from, Bahr *et al.* (1997) derived a relationship from 144 glaciers (not including ice caps) located in Europe, North America, central Asia and the Arctic (Equation 8). This relationship is therefore considered to be a well-defined worldwide mean for mountain valley glaciers (Bahr *et al.*, 2015), applicable to those found in New Zealand. Although other relationships are available in the literature (Table 2.7), these are often based on specific locations with different glaciological characteristics to New Zealand (e.g. Grinsted, 2013a) and/or based on a smaller sample size. For example, Chen and Ohmura (1990) based their relationship on just 63 glaciers compared to the 144 of (Bahr *et al.*, 1997). For these reasons, the relationship of Bahr *et al.* (1997); Equation 8 was used.

2.6.1.2 Ice-mechanics methods

A more complex set of models for estimating volume and distributed ice thickness has recently been developed, based on glacier mass turnover and ice-flow mechanics (Farinotti *et al.*, 2009). This method has the major advantage over volume area scaling of being able to output fully distributed bed topography rather than simply an overall volume estimate. According to the principles of mass conservation, the mass balance distribution of a glacier should be in equilibrium with the ice flux divergence and the resultant ice surface elevation change, with the overall ice thickness then inferred from the ice fluxes (Farinotti *et al.*, 2009). This method has been successfully used as the basis for estimating the distributed ice thickness of all glaciers in the world (Huss & Farinotti, 2012; Huss & Hock, 2015) and is thought to provide the first assessment of distributed ice thickness for the New Zealand Southern Alps.

Whilst input datasets are minimal, requiring just a DEM and glacier outlines, a number of assumptions and extensive parameterisation is required. The main parameter is the 'apparent mass balance distribution', calculated from altitudinal gradients of the accumulation and ablation areas, with smaller gradients assumed in the accumulation area. The 'continentality' of each glacier is also estimated from latitude and air temperature at the ELA (see Huss and Farinotti (2012) for full derivation) and used in conjunction with glacier surface area to define a 'sliding factor'. Comparison with measured ice thickness profiles found that the model reproduced ice thickness with an average deviation of ~25% (Farinotti *et al.*, 2009), showing the current level of accuracy for such ice thickness estimation models.

The underlying method of Farinotti *et al.* (2009) has been used as the basis to estimate the volume of the New Zealand Southern Alps on two separate occasions (Huss & Farinotti, 2012; Huss & Hock, 2015), with volume estimates of 70 km^3 and 59.5 km^3 respectively. As both studies used the same SRTM v 4.0 DEM as an input (Jarvis *et al.*, 2008), this ~15% difference in volume estimate is attributed to using different glacer outlines. Although both studies utilised the RGI outlines (see section 2.3), Huss and Farinotti (2012) utilised version 2.0 whilst Huss and Hock (2015) used

version 4.0. The only change between these two versions was the deliniation of glacier complexes into separate individual glaciers (Arendt *et al.*, 2015), highlighting the sensitivity of the method presented by Farinotti *et al.* (2009) to a seeminly minor alteration of the input data.

2.6.1.3 Perfect Plasticity Approaches: VOLTA

'Perfect plasticity' based modelling approaches are also proving a popular choice for estimating ice thickness, based on the theory originally described by Nye (1951). Some of these approaches have the ability to estimate distributed ice thickness (e.g. Linsbauer *et al.*, 2009), with a basic version previously applied on the mountain chain scale (Linsbauer *et al.*, 2012). Development of the method to include a side drag component (Li *et al.*, 2012) and the ability to automatically derive glacier centrelines (Le Bris & Paul, 2013) has led to the creation of the VOLTA model, allowing the fully automated, rapid estimation of distributed ice thickness from a DEM and glacier outlines. VOLTA can be seen as a simpler model than the ice mechanics methods outlined in section 2.6.1.2, requiring less parameterisation whilst outputting fully distributed ice thickness unlike scaling methods (section 2.6.1.1). Validation of VOLTA against 'measured' ice thickness data (section 2.4.7) and of other perfect plasticity approaches by Li *et al.* (2012) suggests they perform to a similar level as ice mechanics methods for mountain valley glaciers, representing a useful alternative method for ice volume estimation.

2.6.2 Modelling of the Southern Alps: data requirements and sensitivity

2.6.2.1 Digital Elevation Model (DEM)

VOLTA requires just a DEM and glacier outlines as inputs, with the various sources used for modelling the Southern Alps discussed in section 2.4.10. It is known that the volume of the Southern Alps is changing rapidly, with Chinn *et al.* (2012) estimating a 15 % reduction in total volume between 1976 and 2008. It is therefore considered essential to consider the 'capture date' of any input datasets used for modelling as this may influence the results, although this is rarely discussed in the literature. With

the ability to rapidly model distributed ice thickness, VOLTA was run on a variety of input datasets (DEM and outlines) to assess the sensitivity of the model and the temporal changes between datasets (Table 2.6).

VOLTA appears to be not very sensitive to the DEM used; with the difference in overall estimated volume just 1.4% between the Geographix 8m DEM and the SRTM DEM using the same set of outlines (Table 2.6). It is not possible to define an exact capture date for the Geographix DEM as it is made from a composite of data sources (Geographix, 2012). Whilst the topography/extent of some important glaciological features (e.g. proglacial lakes) is based on recent c. 2012 extents, it is mainly derived from 1986 topographic data and is therefore considered to overall represent an earlier surface than the SRTM DEM which was captured in 2000 (Jarvis *et al.*, 2008). The difference in estimated volume may be explained by change in glacier surface slope over the period, with Figure 2.14 showing the surface elevation differential of glaciers in the Mount Cook region between the DEMs. Surface lowering is most pronounced in the lower ablation regions, effectively increasing the overall ice surface slope and thus being reflected in the perfect plasticity based calculations. For glaciated areas (defined here from RGI V5 outlines), the Geographix DEM is on average 0.87 m lower than the SRTM DEM, equivalent to 1.01 km^3 of ice. The spatial distribution of variation in the Mount Cook region is shown in Figure 2.14. Whilst some differences may be due to the methods of DEM capture and processing techniques, there appears to be a general pattern of mass loss in the lower ablation zones and mass gain in the accumulation areas. This is most likely due to glacier downwasting occurring in the ablation zones between the acquisition of the earlier (c. 1986) Geographix DEM and the later (2000) SRTM DEM, a phenomenon observed directly by other studies (e.g. Hochstein *et al.*, 1995). The elevation 'gain' observed in the accumulation zones may be due to shorter term changes in mass balance, with the years preceding 2000 known to have had unusually low end of summer snowlines (Willsman, 2011).

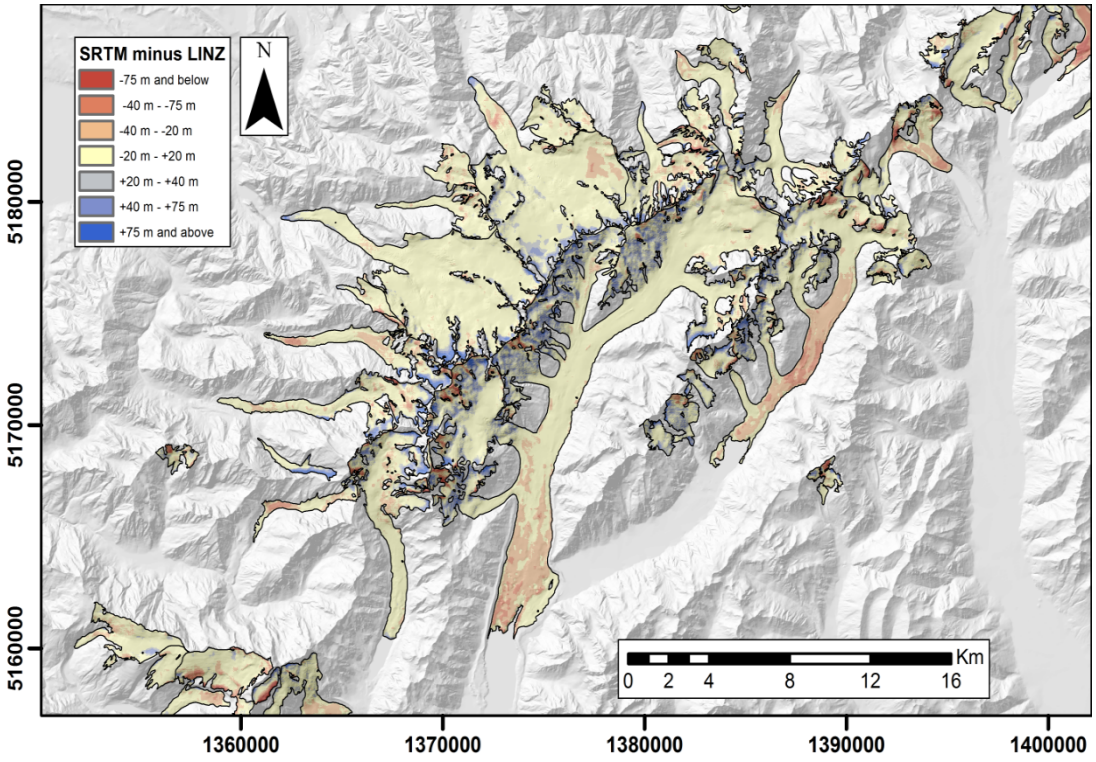

Figure 2.14 Surface elevation change between the SRTM and Geographix DEMs.

Whilst there are differences between the DEMs used and that some changes in ice elevation have occurred, this does not greatly influence the overall volume estimate if the same outlines are used, with a 1.4 % difference observed. This may be because whilst elevation change has occurred, this is relatively minor compared to the overall ice thickness. Furthermore, the thickness calculation of VOLTA relies on the surface slope along the centreline, which may not have changed in the same manner as the ice elevation on other parts of the glacier.

2.6.2.2 Outlines

VOLTA was also run on different outlines, with analysis of the Mt. Cook area providing a comparison between those mapped in 1978 and in 2009. To assess changes between the original 1978 outlines and the updated 2009 outlines, an initial comparison study of planform area was conducted (Table 2.8, Figure 2.15). As the 2009 outlines only cover the Mt. Cook region, comparison was only possible for this area, with the 1978 outlines clipped to the same extent using a minimum bounding geometry (MBG) polygon.

Table 2.8 Planform area of glacial ice calculated from both the 1978 (Chinn, 1978) and 2009 (Sirguey, 2010) surveys.

	1978 Area (km^2)	2009 Area (km^2)	Change %
Central Southern Alps (Mt Cook)	400.3	351.4	-12.2
Franz Josef Glacier	33.1	33.0	- 0.06
Fox Glacier	34.7	34.1	- 1.60
Hooker Glacier	14.3	12.4	- 13.48
Tasman Glacier	95.2	87.3	- 8.35

Overall, the Mt Cook region experienced an area loss of 12.2 % between 1978 and 2009, with individual glaciers analysed all showing a reduction in area. This is in general agreement with Gjermundsen *et al.* (2011) who calculated an area loss of 16.6 % between 1978 and 2002 for a portion of the central Southern Alps. Figure 2.15 shows that the pattern of ice loss is complex, with reduction in some areas and gain in others. Evidence of terminus retreat is visible, with the La Perouse and Balfour glaciers retreating approximately 1.8 km and 1.4 km respectively (Figure 2.15c). There is also evidence of potential downwasting, with the 2009 margins of the Hooker glacier (Figure 2.15a) and the Tasman glacier (Figure 2.15d) mapped well inside the boundary of the 1978 outlines.

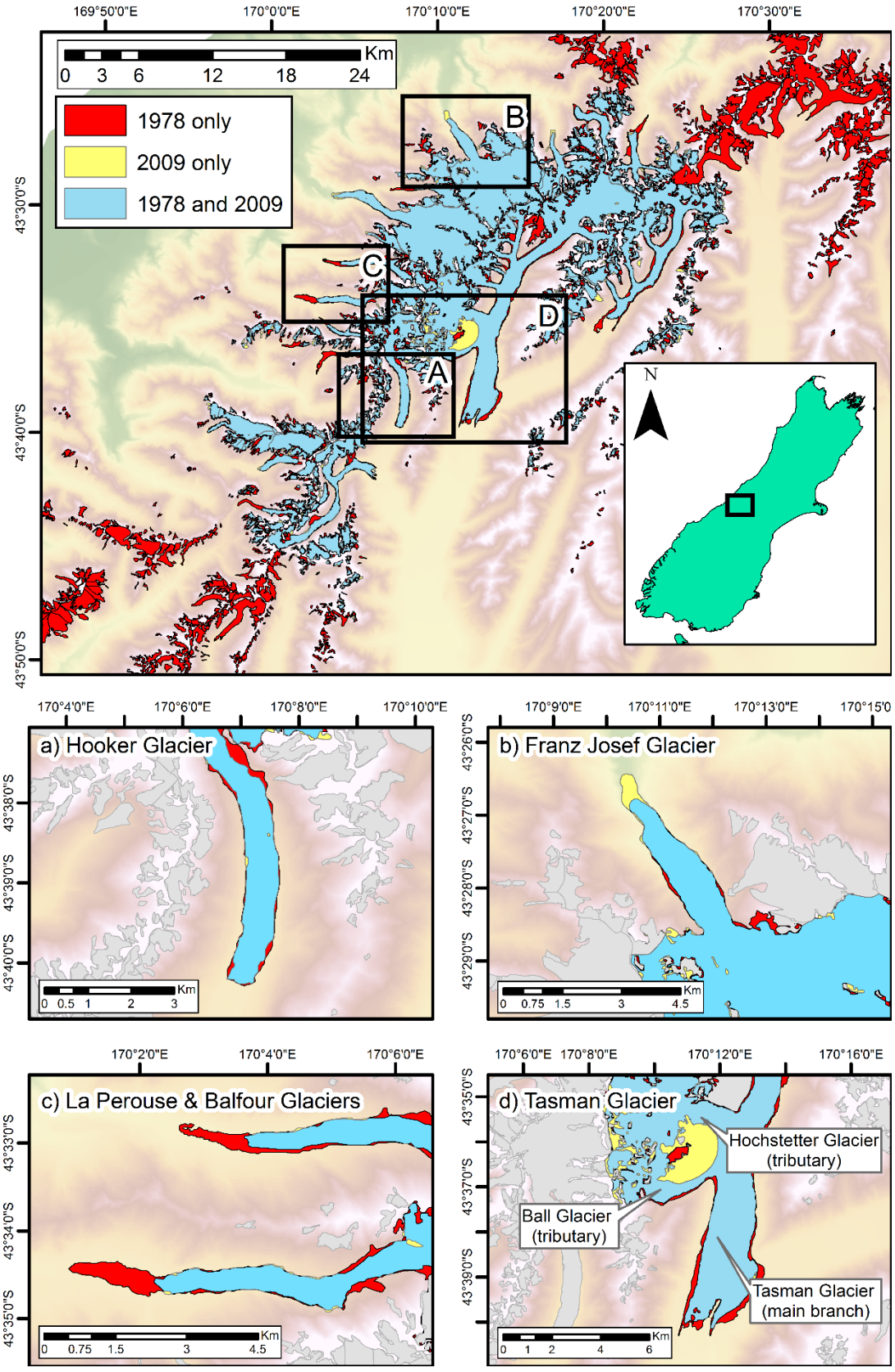

Figure 2.15 Glacial ice covered by the 1978 outlines (Chinn, 1978) and the 2009 survey (Sirguey, 2010).

Interestingly, there are also some 'new' areas of ice in the 2009 survey which were not included in the original 1978 outlines. This may be due to glacier advance and expansion or due to differences/errors in the classification of either survey. The largest such region is situated within the Tasman glacier complex, between the Ball and Hochstetter tributaries (Figure 2.15d), covering an area of 6.28 km^2. Analysis of satellite imagery from February 2013 (Google Earth, 2013) shows the area as largely snow and ice-free, with misclassification therefore a likely cause for it being included in the 2009 survey. There are also notable areas of new ice at the terminus of the Franz Josef Glacier (Figure 2.15b), Fox Glacier and Spencer Glacier which are not covered by the 1978 outlines. These additional areas of ice at the terminus of glaciers on the West coast are likely to be due to short-term phases of advance, known to have occurred at both the Franz Josef glacier and Fox glacier within the period of interest (Purdie *et al.*, 2014). It should be noted that despite the advancing terminus, the overall area of both the Franz Josef and Fox glaciers decreased by 1.6 % and 0.06 % respectively due to area loss at the margins elsewhere.

When using the updated outlines for VOLTA modelling, the volume estimate was 6.04 % lower than when using the 1978 outlines (Table 2.6). This overall pattern of volume loss is in general agreement with Chinn *et al.* (2012) who calculated a volume reduction of 15 % for approximately the same period (although for the entire Southern Alps domain). The lower mass loss predicted by VOLTA may be expected due to the use of the same DEM for both studies, although this has been shown to have a minimal impact on volume calculations (section 2.6.2.1). Other potential factors for the difference may include differences in model domain (Entire Southern Alps vs. Mt Cook region only) and inaccuracies with either model.

2.6.2.3 Total volume and distributed thickness of the Southern Alps

The total volume of the Southern Alps is estimated at 50.67 km^3, in good correspondence to the widely cited estimate of 53.29 km^3 by Chinn (2001). Whilst the estimate presented here is lower than the latest ice-mechanics based method of 59.31 km^3 by Huss and Hock (2015), it is well within the bounds of uncertainty of such studies and is thus deemed an appropriate tool for modelling glacier ice volume and distributed thickness of the Southern Alps. The ability to derive distributed

thickness is of great value, with applications for glaciological hazards assessment (e.g. Carrivick, 2007; Staines & Carrivick, 2015), for understanding subglacial lake formation (e.g. Frey *et al.*, 2010) and palaeoglacier reconstruction (Benn & Hulton, 2010).

This thesis employed a composite approach for ice volume estimation, using the VOLTA model for all glaciers over 1 km^2 in area and volume area scaling for the remaining smaller glaciers. These small glaciers contributed to 19.5 % of the total volume, highlighting their importance in the Southern Alps. Analysis of various scaling relationships in the literature revealed a large variation in estimated volume (Table 2.7), ranging between 6.4 km^3 and 14.66 km^3. This shows the importance of picking an appropriate scaling scheme and the uncertainty involved with the technique. The rationale for choosing the relationship of Bahr *et al.* (1997) for New Zealand is discussed in section 2.6.1.1 with the resulting estimate of 9.9 km^3 comparing favourably to that of 9.41 km^3 from an ice-mechanics approach of (Huss & Hock, 2015). This close correspondence with an alternative approach further suggests that the relationship of Bahr *et al.* (1997) is appropriate for the New Zealand Southern Alps.

2.7 Conclusions

The glaciers of New Zealand fill a huge gap in the global distribution, with an understanding of their volume and distributed thickness of use for understanding worldwide glacier-climate interactions. Locally, contemporary ice thickness distribution and volume is of great importance for the hydrology, ecology and economy of New Zealand (Fitzharris *et al.*, 1999), resulting in a considerable research interest. Despite this, there are very few direct observations of ice thickness and a considerable amount of uncertainty in the literature surrounding the total contemporary ice volume. Furthermore, almost all of the published estimates of ice volume rely on a volume-area scaling technique which is unable to predict thickness distribution.

In an attempt to improve our understanding of distributed ice thickness and volume of the New Zealand Southern Alps, the VOLTA model has been developed for the rapid and data-efficient 3D modelling of glaciers. VOLTA requires just a DEM and glacier outline(s) as inputs, both of which can be obtained free of charge with an almost global coverage for research purposes (e.g GLIMS, 2014; USGS, 2014). Whilst the basic perfect plasticity assumption is applicable for ice sheets (Nye, 1951), VOLTA also takes into account a valley side drag component of the force balance equation, making it especially applicable where glaciers are constrained by topography such as in the Southern Alps of New Zealand. As such, VOLTA can be applied with confidence to any region where the appropriate datasets are available and has recently been successfully applied to the glaciers of South America (Carrivick *et al.*, IN REVIEW-b) and the Antarctic Peninsula (Carrivick *et al.*, IN REVIEW-a). Compared with other existing methods, key advantages of VOLTA are: a fully automated workflow, improved centreline generation that can accommodate glaciers with multiple branches, inclusion of a side drag component in the force balance equation, GIS consistent geometry, individual glacier basal shear stress estimation, fully distributed ice thickness and bed topography outputs and a user friendly graphical user interface (GUI). In comparison of VOLTA-derived ice thickness and volume against independent data from five glaciers where the bed topography was well

constrained, total volume estimates fell between 26.5 % (underestimate) and 16.6 % (overestimate) of the volume estimated from field measurements. The greatest field based-modelled differences were where bed elevation formed an asymmetric valley shape or valley infilling had occurred.

VOLTA was used to estimate the distributed thickness and volume of all glaciers over 1km^2 in the New Zealand Southern Alps, with the remainder estimated using the volume-area scaling relationship of Bahr *et al.* (1997). The total combined volume estimate is 50.67 km^3, comprised of 9.9 km^3 for glaciers under 1 km^2 and 40.68 km^3 for larger glaciers using VOLTA.

With present knowledge of ice thickness distribution being remarkably limited, VOLTA has the potential to improve our database of estimated ice thickness and thus also of estimated glacier volume. With the ability to produce an 'ice-free' DEM, an important prerequisite for addressing a range of glaciological and hydrological issues can be provided quickly. The creation of such an 'ice free' DEM for New Zealand represents the first step towards the required input for palaeoglacier reconstruction models (e.g. Benn & Evans, 2010), a DEM of bed conditions for the specified time period. This is explored further in Chapters 3 and 4 where former glaciers of the last glacial maximum are reconstructed for the New Zealand Southern Alps.

Chapter 3. Synthesis and analysis of data to produce a refined consideration of ice extent during the Last Glacial Maximum in the New Zealand Southern Alps.

3.1 Introduction

The New Zealand Southern Alps has a remarkable imprint of former glaciations preserved in landforms and near surface deposits (Suggate, 1990). Being one of the few land masses in the Southern Hemisphere which has experienced multiple glacial cycles, the record is of great importance for research into the natural behaviour of the Earth's climate system (Barrell *et al.*, 2011). The aim of this chapter is to compile, critically assess, synthesise and process datasets to produce a refined consideration of the geomorphological evidence for ice extent during the LGM in the Southern Alps, New Zealand. This assessment of down-valley ice extents is a necessary precursor, alongside knowledge of contemporary ice thickness (Chapter 2) to making 3D ice thickness reconstructions with the REVOLTA model (Chapter 4).

The major objectives of this chapter are: a) to amalgamate and review the most up to date literature and datasets regarding the lateral extent of LGM glaciation in the Southern Alps, producing an updated 'outline' of LGM glaciation and b) to produce a DEM of LGM bed topography conditions to best represent the former glacier beds.

3.2 Glacial history of the New Zealand Southern Alps

The study of former glaciations in New Zealand began with early geological surveys in the 1860's, shortly after the discovery of evidence of former glaciations in the Northern Hemisphere (Agassiz, 1840). Since then, the down-valley extent of palaeoglaciers has been the subject of intense research, with various interpretations and mapping of glacial geomorphology and sediments (e.g. Speight, 1934; McKellar, 1960). However, the recognition of multiple glacial phases in New Zealand is a relatively recent concept, with compound glacial advances first convincingly documented in the mid-20th century (e.g. Soons, 1963) and the first major attempt to correlate between valley systems made in 1973 by the New Zealand Geological Survey (New Zealand Geological Survey, 1973).

3.2.1 Late Pliocene and Quaternary glaciations

The exact number of glacial cycles to have occurred in New Zealand is unknown as evidence for older glaciations is increasingly fragmentary, although at least eight glaciations have been formerly recognised and named (Barrell, 2011). Table 3.1 summarises the sequence of glacial-interglacial cycles in New Zealand, with the approximate age and corresponding Marine Isotope Stage (MIS) shown. In addition to these regional glaciation names, local stratigraphical names have also been developed for individual regions or catchments (Table 3.2). This approach was originally adopted as a method for overcoming the difficulties of quantifying ages of glacial deposits, enabling a succession of relative ages to be constructed for each valley. These local stratigraphies are correlated between catchments with varying degrees of confidence (Barrell, 2011), although advances in absolute age dating techniques (see section 3.2.8) is improving the situation, with subsequent revisions being made locally (e.g. Shulmeister *et al.*, 2010).

Table 3.1 New Zealand names for mid to late Quaternary glaciations and interglacial periods with corresponding MIS stages and approximate ages. Modified from Barrell (2011)

<table>
<tr><th>Marine Isotope Stage (MIS)</th><th colspan="2">Glaciation</th><th colspan="2">Interglacial</th><th>Approximate Age (cal. ka)</th></tr>
<tr><td>1</td><td colspan="2"></td><td>Holocene</td><td rowspan="2">Aranui</td><td>0–11.7</td></tr>
<tr><td rowspan="3">2

3

4</td><td colspan="2">Late Glacial</td><td rowspan="3"></td><td>11.7 – 14.5</td></tr>
<tr><td rowspan="3">Otira (Last Glaciation)</td><td>Late Otira</td><td>14.5 - ~18
~18 - ~30
(LAST GLACIAL MAXIMUM)
~45</td></tr>
<tr><td>Early Otira</td><td>~45
~65
~74</td></tr>
<tr><td>5</td><td colspan="2"></td><td>Kaihinu</td><td></td><td>~74 - ~130</td></tr>
<tr><td>6</td><td colspan="2">Waimea</td><td></td><td></td><td>~130 - ~190</td></tr>
<tr><td>7</td><td colspan="2"></td><td>Karoro</td><td></td><td>~190 - ~244</td></tr>
<tr><td>8</td><td colspan="2">Waimaunga</td><td></td><td></td><td>~244 - ~303</td></tr>
<tr><td>9</td><td colspan="2"></td><td>(No name)</td><td></td><td>~303 - ~ 339</td></tr>
<tr><td>10</td><td colspan="2">Nemona</td><td></td><td></td><td>~339 - ~362</td></tr>
<tr><td>11</td><td colspan="2"></td><td>(No name)</td><td></td><td>~362 - ~423</td></tr>
<tr><td>12</td><td colspan="2">Kawhaka</td><td></td><td></td><td>~423 - ~478</td></tr>
<tr><td colspan="6">Earlier glacial and interglacial episodes have not been assigned formal names</td></tr>
<tr><td colspan="6">Porika >1.8 Ma, ?<2.6 Ma</td></tr>
<tr><td colspan="6">Ross ?<2.6 Ma</td></tr>
</table>

.

Table 3.2 Quaternary stratigraphic names for selected South Island catchments, in relation to the classification scheme used by Barrell *et al.* (2011). Adapted from Barrell *et al.* (2013).

SOUTHERN ALPS	Westland Lowlands	Waimakariri	Rakaia	Lake Heron-Arrowsmith Range	Rangitata-Clearwater	Mackenzie Basin	Canterbury Plains	Barrell et al (2011)* Moraine/Outwash	MIS	Approx. Age (yrs.)
Latest Holocene								**Latest Holocene**		
Holocene	**Nine Mile**	*Barker*	*Whitcombe*	*Arrowsmith*		Ben Ohau	**Springston**	**Holocene**	1	~1,000
		O'Malley	*Lyell*	*Younger Marquee*						
			Meins Knob	*Older Marquee*						
Late-Glacial	**Waiho**	*Arthur's Pass*	*Reischek*	***Wildman***		**Birch Hill**		**Late Glacial**		~11,700
			Jagged Stm							
		McGrath	***Lake Stream***		**Two Thumbs**			**Latest Late Otiran**	2	~14500
Latest Last Glacial Maximum	**Moana** *(M6)*	***Poulter***	***Acheron***	**Lake Heron**	**Spider Lakes**	**Tekapo**	(St Bernard) **Burnham**			~19000
			Bayfield	**Johnstone Stm**	**Hakatere**			**Late Otiran**		
Last Glacial Maximum	**Larrikins** *(M4b - M5)*	***Blackwater***	***Tui Creek***	**Emily**	**Trinity Hill**	**Mt John**	(Windwhistle)		3	
		Otarama								~45000
	Loopline	*Woodstock*	**Woodlands**	**Dogs Hill**	**Dogs Hill**	**Balmoral**	**Woodlands**		4	
	Waimea								6	
	Tansey	***Avoca***	**Hororata**	(Pyramid)	(Pyramid)	**Wolds**	**Hororata**	**Early Otiran & Older**	8	
	Cockeye								10	

Well defined age range

Age range with uncertainty

* Colours relate to landform classification mapping by (Barrell *et al.*, 2011). See Figure 3.1 for full description.

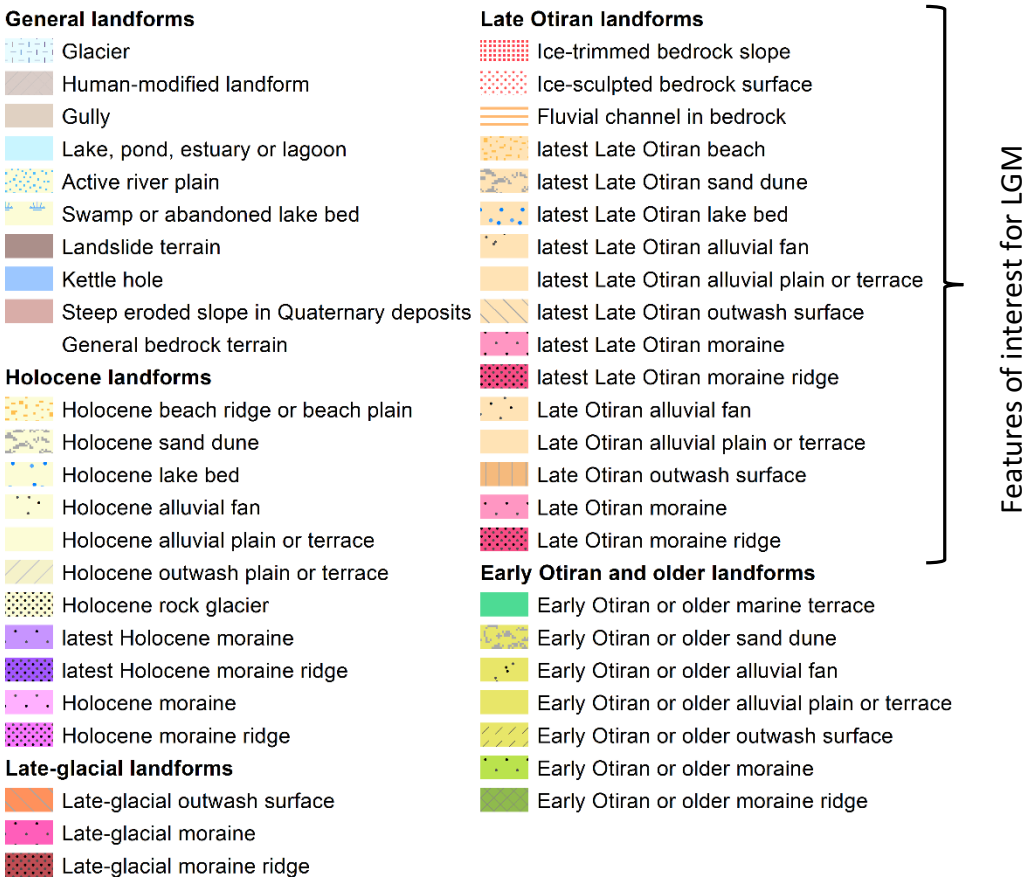

Figure 3.1 Legend for glacial geomorphological mapping by Barrell *et al.* (2011). Associated maps are used extensively during analysis and presentation in this thesis.

As with the contemporary pattern of glaciation, all known former glaciers of the Southern Alps originated in the central snowfields of the main ranges and flowed down-valley towards the lowlands of the Canterbury Plains to the east of the main divide and towards the present day coastline on the west (Suggate, 2004). New Zealand's earliest known ice advance is termed the Ross glaciation and is thought to have occurred in the Early Pleistocene (< 2.6 Ma). This was followed by the younger Porika glaciation (approximately 2 Ma), although the ice limits and extent are currently undefined for both (Barrell, 2011). A gap of over 1 million years then exists in the glacial record, assumed to be due to uplift and erosion removing geomorphological evidence (Suggate, 2004).

Pulses of glaciation as summarised in Table 3.1 and Table 3.2 have produced geomorphological and sedimentary records of varying length and quality, according to the tectonic situation and ease at which more recent ice advances could overrun and destroy evidence of older ones (Barrell, 2011). This removal and modification of

records has resulted in few data existing that directly constrain the timing of glaciation phases pre-LGM (Sutherland *et al.*, 2007).

3.2.2 The Otiran glaciation and the Last Glacial Maximum (LGM)

The Otiran glaciation (Table 3.1) is regarded as broadly equivalent to MIS 4, 3 and 2, with glacial deposits from MIS 4, a limited number of 'cool climate' deposits representing MIS 3 and a complex set of 'Late Otiran' deposits representing MIS 2 (Suggate & Almond, 2005), with the last major advance of the Otiran glaciation commonly referred to as the 'Last Glacial Maximum' (LGM) (Barrell *et al.*, 2011).

On a global scale, the term 'Last Glacial Maximum' is conventionally defined as the most recent interval where global ice sheets reached their maximum integrated volume, with an age range defined as 23 to 19 ka (Mix *et al.*, 2001). Some studies in New Zealand have found evidence to support synchronicity between Southern Hemisphere glaciations and those in the northern hemisphere (e.g. Schaefer *et al.*, 2006). However, there is growing recognition that this maximum global integrated volume does not necessarily coincide with local glacier maxima (e.g. Suggate & Almond, 2005), with evidence suggesting that New Zealand and other Southern Hemisphere locations reached maximum glacial extents by around 30 ka and persisted longer than in the Northern Hemisphere (Vandergoes *et al.*, 2005; Suggate & Almond, 2005; Rother *et al.*, 2014), with the last glacial-interglacial transition (LGIT) commencing at approximately 18 ka (Barnes, 2009; Clark *et al.*, 2009; Rother *et al.*, 2014). This apparent mismatch between the global LGM and that in New Zealand has led to the emergence of a variety of new terms in the literature to differentiate the period in New Zealand such as the 'Last Glacial Coldest Period' (Alloway *et al.*, 2007) and the 'Local Last Glacial Maximum, (LLGM)' (Putnam *et al.*, 2013b). To avoid confusion between terms, this thesis uses the term 'Last Glacial Maximum' (LGM) to describe the period of interest for New Zealand (~30 to 18 ka), in common with other New Zealand based glacier reconstruction studies (Golledge *et al.*, 2012). Any subsequent reference to the global LGM (Mix *et al.*, 2001) rather than for New Zealand will be clearly stated.

3.2.3 Holocene glacier fluctuations

Since the onset of the last glacial-interglacial transition (LGIT) ~18 to 17 ka (Barnes, 2009; Clark *et al.*, 2009; Rother *et al.*, 2014), general deglaciation has been interrupted with short-lived periods of glacier terminus re-advance. Whilst being of a smaller magnitude than during full glacial conditions, these Holocene events have modified and reworked the landscape and provide an insight into glacial processes and climatic conditions.

Records from the Irishman Stream catchment in the Southern Alps indicate a late-glacial cooling event (around 13 ka) approximately coeval with the Antarctic Cold Reversal (ACR) (Doughty *et al.*, 2012). Modelling suggests that cooling of 2.3 – 3.2 ^{o}C with +/- 20% precipitation change would be required to form the moraines associated with the event, approximately 45 km up valley from the corresponding LGM moraines (Doughty *et al.*, 2012). Additionally, surface exposure dating from the same catchment indicates glacier retreat and warming after ~13 ka (Kaplan *et al.*, 2010), suggesting that the Younger Dryas stadial (12.9 to 11.7 ka), which is widely recognised in the northern hemisphere, was not global in nature, although previous studies have inferred cooling in New Zealand during this period (Denton & Hendy, 1994).

3.2.4 Little Ice age (LIA)

Most recently, the largest glacier oscillation in historical times occurred during the Little Ice Age (Grove, 1988), although there is still debate surrounding its exact timing and synchronicity between the northern and southern hemispheres (Winkler, 2000). On a global scale, Grove (1988) suggests that the Little Ice Age culminated between the mid-sixteenth and mid-nineteenth century, when lower temperatures were sufficient to affect plant growth and agriculture, especially in marginal areas. However, due to regional variations, it is difficult to give a precise date range. As a consequence, Winkler (2004) suggests the term should be used in a broader sense to describe the latest period of advance, terminating around AD 1900.

The Franz Josef glacier serves as an excellent example of the range of proposed dates for LIA maximum extent in New Zealand and highlights the uncertainty in the

literature. An initial estimate of AD 1750 was postulated by Lawrence (1965) based on the general size and structure of the vegetation. A more in depth study by Burrows (1990) revised the date of maximum extent to AD 1450, inferred from the size of southern rata trees (*Metrosideros umbellate*) growing on moraines. The chronology was further refined by McKinzey *et al.* (2004), using a range of tree species to conclude that the LIA maximum occurred around AD 1500 with subsequent, smaller re-advances around AD 1600 and AD 1800 (McKinzey *et al.*, 2004). Similar complex LIA records with re-advances have been detected at other glaciers, with Winkler (2000) estimating an LIA maximum at Mueller glacier at approximately AD 1725 to 1730, followed by successive advances and stillstands around 1740, 1860, 1895 and 1905. At this stage it should be noted there is debate in the literature surrounding the climatic significance of such moraines (Reznichenko *et al.*, 2016), with a detailed case study of such a case presented in section 3.2.9.

Geomorphological evidence in the form of moraines and trimlines show that at the LIA maximum, glaciers in the South Island were still clearly confined to valleys in an alpine style glaciation. For example, dated moraines in the foreland (< 1 km from the present terminus) of the Mueller glacier (Winkler, 2000) and trimlines on the valley sides approximately 300 m above the present ice level of the Franz Josef glacier (McKinzey *et al.*, 2004) are well within the valley constraints.

3.2.5 Post Little Ice Age

Warming since the end of the LIA has seen a global contraction of glaciers, with a study of 169 glaciers from around the world by Oerlemans (2005) finding an average length decrease of 1800 m. This is consistent with New Zealand, where Chinn (1996) found a sample of 127 glaciers shortened by 38 % on average. Furthermore, the rate of retreat appears to be increasing, with a study of 640 mountain glaciers in the Patagonian Andes finding that mean glacier shrinkage is now faster than it was at the end of the LIA (Davies & Glasser, 2012).

Within New Zealand, the most complete record of changes in terminus position since the LIA are from the Franz Josef glacier, currently approximately 11 km long with a surface area of approximately 35 km^2 (Anderson *et al.*, 2008). The glacier was first

photographed by T. Pringle in 1867, and unlike other glaciers in New Zealand, continuous measurements have been made on a regular basis since then (e.g. Speight, 1914). Historical length records of the Franz Josef and Fox glaciers have been collated and analysed by Purdie *et al.* (2014), demonstrating that both glaciers have shortened by approximately 3 km since the 1800s (Figure 3.2). Within the overall trend of retreat, both glaciers have also experienced periods of re-advance of up to 1420m. The major re-advance of both glaciers between ~1983 and 1998 is clearly visible in Figure 3.2.

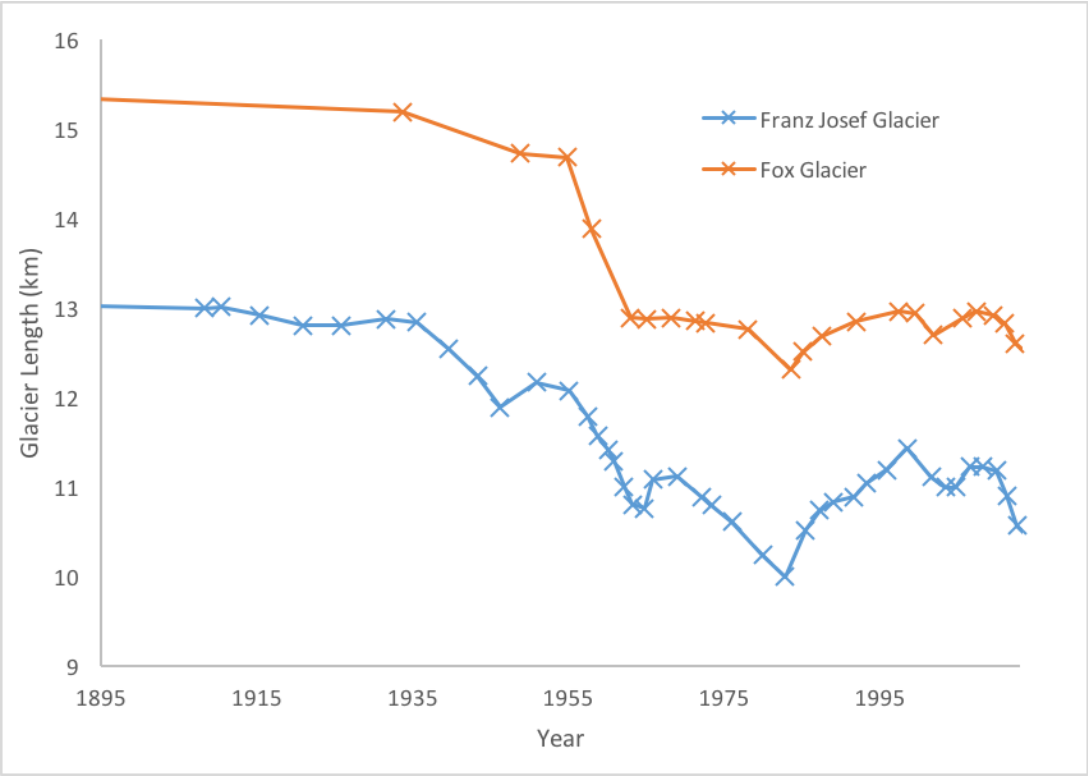

Figure 3.2 Summary of length changes at Fox and Franz Josef glaciers from 1985 until present. Adapted from Purdie et al. (2014).

3.2.5.1 Proglacial lake development

During the late 20th Century, proglacial lakes developed at a number of New Zealand's glaciers (Warren & Kirkbride, 1998), with Figure 3.3 showing examples of the Hooker and Mueller Lakes in the Mt. Cook region. These commonly occur at the terminus of large, low gradient valley glaciers to the east of the main divide following the coalescence of thermokast ponds after progressive downwasting since the Little Ice Age (Kirkbride, 1993). These lakes are generally constrained by post-LGM outwash gravels, upon which Little Ice Age (LIA) and older late Holocene moraines

have developed (Dykes *et al.*, 2010). The largest such lake is found at the Tasman glacier, measuring 5.96 km^2 in area, 0.51 km^3 in volume and has a maximum depth of 240 metres (2012 values) (Robertson *et al.*, 2012), with other notable examples at the Hooker, Mueller, Godley and Maud glaciers. Many of these lakes are developing rapidly and at an increasing rate – the area of Tasman lake doubled between 2000 and 2007 alone (Quincey & Glasser, 2009). The bathymetry of a number of these lakes is further investigated in section 3.5.3 where the lake presence masks the topography of the proglacial zone.

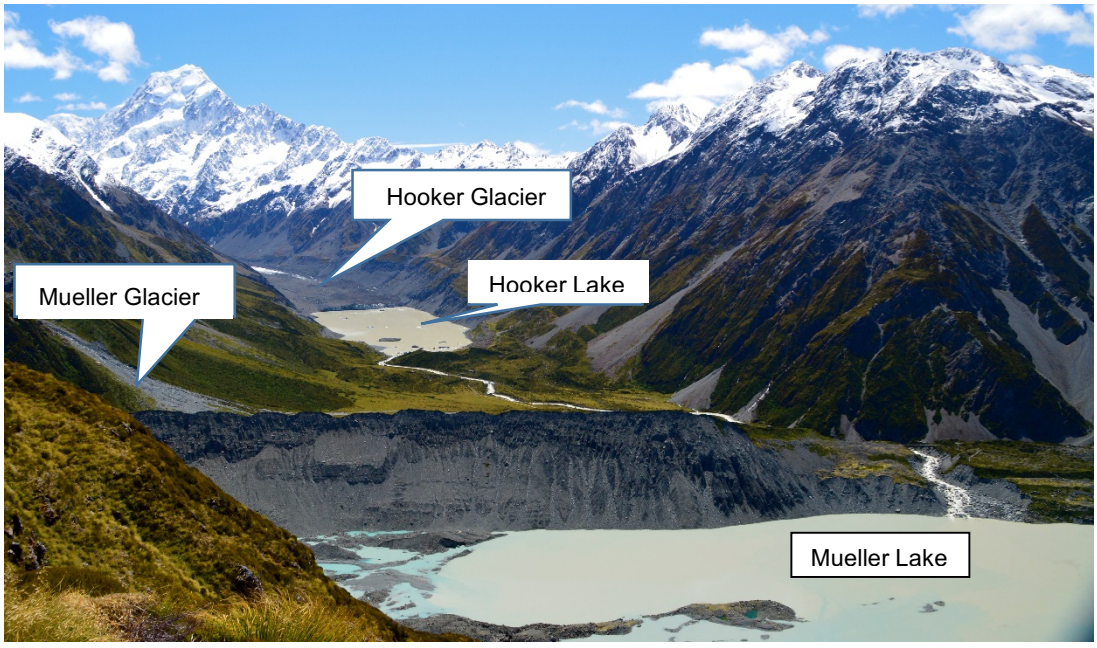

Figure 3.3 Proglacial lakes at the terminus of the Mueller and Hooker glaciers. (W. James)

The development of proglacial lakes has effectively 'decoupled' the associated glaciers from changes in climate, with the switch to calving termini overriding climatic inputs (Warren & Kirkbride, 2003). As such, the onset of calving has dramatically influenced retreat rates of affected glaciers, increasing from an average of 12 m yr^{-1} pre lake formation to 50 m yr^{-1} once lake development and calving was initiated (Purdie & Fitzharris, 1999). This phenomenon complicates the links between terminus position change and climatic signals, with individual glacier systems no longer reliable indicators of overall deglaciation trends at a regional level (Rother *et al.*, 2014). Whilst this phenomenon is widely recognised for contemporary glaciers (Warren & Kirkbride, 2003; Kirkbride, 1993), there is emerging evidence to suggest a similar process may have occurred during previous periods of deglaciation.

Rother *et al.* (2014) suggests that a similar mode of retreat was common during the post-LGM period, evidenced by widespread glaciolacustrine deposits. Care must therefore be taken when using such glacier systems to infer regional deglaciation trends or for palaeoclimatic research.

3.2.6 A note on debris cover

The larger glaciers of the Southern Alps are renowned for their debris covered surfaces, covering approximately 25 % of the total glaciated area of the Southern Alps (Chinn, 1996). The Tasman glacier has the most-extensive and best-studied debris, covering approximately 30 % of the surface area (Anderson & Mackintosh, 2012) and generally between zero and 3 m in thickness (Kirkbride, 1989), although up to 7.6 m has been measured (Hart, 2014). Whilst it has historically been reported that debris cover is more extensive on glaciers to the east of the main divide (e.g. Harper, 1893), more recent research by Chinn (2001) shows this is not the case, with the unfounded notion of an east-west differential attributed to simplistic comparisons between the unusually 'clean' Fox and Franz Josef glaciers and the heavily covered Tasman glacier.

Figure 3.4 The debris covered surface of the Tasman glacier, up to 7.6 m thick in places. (W. James)

Local topography and geology is a major control on debris cover and distribution, with Chinn (2001) suggesting that the following factors favour the accumulation of debris on the glacier surface across the Southern Alps:

- A high ratio of debris to snow accumulation;
- Steep headwalls that enhance rockfalls and avalanches, feeding material directly onto the glacier surface;
- Disconnected icefalls exposing the glacier bed. This allows basal debris to be physically mixed and transported to the surface;
- Large glacier trunks with a low slope angle and high ablation rates that permit steeply emerging and decelerating ice to transport basal debris to the surface.

Where debris cover does exist, it can profoundly influence surface energy balance and ablation rates. Field experiments show that there is a consistent, non-linear relationship between debris cover thickness and melt rates (e.g. Kayastha *et al.*, 2000) due to two opposing effects. When debris cover is thin (below approximately 2 cm) ablation rates are increased due to debris having a lower albedo than ice, thus absorbing additional shortwave radiation and increasing energy available for melting. However, once thicker deposits develop, debris acts as a thermal barrier, insulating the ice below and reducing ablation exponentially (Benn & Evans, 2010).

Whilst early observations (e.g. Brodrick, 1894) suggests that debris cover was present on the glaciers of the Southern Alps at the turn of the 20th Century, little is known regarding its presence before historical records. Although there is no direct evidence, McKinnon *et al.* (2012) suggests that debris cover was likely to have been minimal in the Southern Alps during the LGM due to the conditions prevalent at the time. Specifically, LGM glaciers extended away from the main divide into regions of lower uplift and erosion, whilst snow and ice also covered a greater proportion of the catchment, thus reducing the debris-snow ratio.

3.2.7 Thresholds and feedbacks: recent wastage of debris-covered calving glaciers

As noted in section 3.2.5.1, many of the large valley glaciers of the Southern Alps now exhibit proglacial lakes and an associated calving terminus. The change from melting to calving termini represents a major threshold in the retreat process, which is thought to be irreversible at the century and probably millennial scale (Kirkbride

& Warren, 1999). This transition is a complex process with a number of feedbacks and thresholds related to debris cover and changes in the longitudinal glacier profile.

Glaciers of the Southern Alps are initially vulnerable to calving due to thick debris cover in the ablation region generating a specific longitudinal profile. As discussed in section 3.2.6, thick debris cover is a common feature of glaciers in the Southern Alps due to both low magnitude / high frequency rockfalls and less frequent large rock avalanches. This debris is a highly effective insulator, reducing melt rates of the ice underneath by up to 90 % (Chinn, 1996). Furthermore, a number of feedbacks involving ablation rate, ice velocity and debris emergence pathways results in the up-glacier spread of debris and the region of maximum ablation (Kirkbride & Warren, 1999). This process leads to the preservation of a low gradient ice tongue at low elevation, with little terminus retreat from the outwash head, as evident in the recent evolution of the Tasman glacier (Kirkbride, 2000).

Once the characteristic low gradient profile is achieved, the emergence and coalescence of thermokast ponds in the terminus region can result in the formation of an ice contact proglacial lake, allowing calving to occur. As noted in section 3.2.5.1, the development of proglacial lakes and calving effectively 'decouples' the glacier from changes in climate, with the switch to calving termini overriding climatic inputs (Warren & Kirkbride, 2003). As such, the onset of calving has dramatically influenced retreat rates of affected glaciers, increasing from an average of 12 m yr^{-1} pre lake formation to 50 m yr^{-1} once lake development and calving was initiated (Purdie & Fitzharris, 1999). Whilst the process can currently be observed at many of the large valley glaciers of the Southern Alps it is also thought to be analogous to the retreat phase of earlier glaciations, and needs to be considered when interpreting the geomorphological record.

3.2.8 Absolute age dating of glacier extents

Whilst the former position of glaciers has been the subject of research since the beginning of the 20th century (e.g. Speight, 1914), the advance of knowledge had, for some time, been held back by the lack of quantitative age control (Barrell, 2011). There are now a number of techniques available for the absolute age estimate of glacier fluctuations, although the time frame in question and local environmental

conditions need to be carefully considered for selecting an appropriate method (Hubbard & Glasser, 2005). For example, whilst lichenometric dating (e.g. Winkler, 2004) and dendrochronology (e.g. McKinzey *et al.*, 2004) are popular choices for dating of the Little Ice Age in the Southern Alps they are not suitable for the earlier LGM phase. As such, pioneering LGM age-control relied primarily on radiocarbon dating, based on the predictable radioactive decay rate of ^{14}C in organic material (Grant-Taylor & Rafter, 1971). However, the harsh environments and subsequent lack of organic material associated with glaciated regions means that ^{14}C dating is not always applicable (Hubbard & Glasser, 2005). Furthermore, in New Zealand specifically, radiocarbon dating is especially problematic in the western ranges of the Southern Alps as the high rainfall commonly leads to contamination of samples with modern carbon (Suggate, 2004).

Recent advances in cosmogenic nuclide (surface exposure dating, SED) dating techniques have enabled the absolute age of rock surfaces (e.g. moraine boulders) to be estimated and has consequently re-energised research into the glacial history of New Zealand. The method relies on the time dependent production of measurable quantities of cosmogenic nuclides in geological substrate, acting as a geochronometer of the time elapsed since exposure (i.e. moraine formation). The following text is intended to provide a brief overview of cosmogenic nuclide (surface exposure) dating in regards to palaeoglacier applications. Whilst the detailed theory and application is beyond the scope of this thesis, the subject has been well reviewed by other authors, with the reader directed to Dunai (2010) and Gosse and Phillips (2001) for more detail.

Figure 3.5 Moraine boulders on the 'Ohau II' ridge (Lake Ohau) sampled for cosmogenic analysis by Putnam *et al.* (2013b). (W. James)

As the Earth's upper atmosphere is bombarded with high energy charged particles (cosmic rays), a wide array of secondary particles are created (e.g. protons, neutrons, muons, mesons) which consequently cause further nuclear interactions resulting in a complex particle shower. These secondary particles hit the Earth's surface, penetrating the upper few metres of the lithosphere (Gosse & Phillips, 2001). Theoretically, any stable geological surface which is continuously exposed to these particles can be dated by measuring the abundance of cosmogenic nuclide, thus enabling the timing of the land forming process (i.e. moraine formation) to be constrained (Dunai, 2010). Whilst many forms of nuclides are produced by cosmic rays, only those meeting several conditions are useful for geomorphological applications. A detailed list of conditions is provided by Dunai (2010), with the following of most importance:

i) The nuclide should be naturally rare, ideally not occurring in rocks if not produced by cosmic rays.

ii) The nuclide should be long-lived radioactive or stable with a half-life of the same order or greater than the period of investigation.

iii) The production rate in rocks must be high enough to produce concentrations detectable using existing analytical methods

These conditions have resulted in six terrestrial cosmogenic nuclides (TCNs) being commonly used for geological / geomorphological investigations: ^{3}He, ^{10}Be, ^{14}C, ^{21}Ne,

^{26}Al and ^{36}Cl (Gosse & Phillips, 2001). Of these, ^{10}Be is the most widely used for exposure dating of formerly glaciated regions as it uses quartz minerals from common lithologies in moraines and ice carved bedrock (e.g. granites, sandstones) and has a half-life of 1.5 Ma, suitable for glacial timescales (Rother, 2006), including that of the LGM.

An accurate knowledge of the production rate of cosmogenic nuclides and their spatial variability (altitude and latitude) is perhaps the most important consideration for the successful application of cosmogenic nuclide dating to glacial geomorphology. Whilst the ^{10}Be production rate has been measured at various sites worldwide (Stone, 2000), it is highly spatially variable, with an approximate twofold increase from the equator to the poles (at sea level) and a three-fold increase from sea level to 1500 m altitude (Putnam *et al.*, 2010). Traditionally, ^{10}Be ages calculated for New Zealand depended on production rates from sites in the Northern Hemisphere that were extrapolated to the Southern Hemisphere (e.g. Shulmeister *et al.*, 2005; Ivy-Ochs *et al.*, 1999), thus incorporating uncertainties related to the extrapolation models.

Recently, the establishment of a local ^{10}Be production rate for New Zealand by Putnam *et al.* (2010) significantly improved the accuracy of exposure age dating in the Southern Alps, finding previous studies using extrapolated production rates likely to underestimate true ages by around 15 %. Consequently, exposure ages from the Southern Alps calculated using a global production rate (i.e. any studies pre 2010) are now considered to underestimate landform ages by 1.4 ka to 2.8 ka when considering the LGM (Rother *et al.*, 2014). As such, exposure ages used in this thesis have been adjusted to the local production rate of Putnam *et al.* (2010) where necessary.

The earliest study to employ exposure dating in New Zealand to assess palaeoglacier fluctuations was by (Ivy-Ochs *et al.*, 1999) and since then a multitude of studies has resulted in the Southern Alps having some of the most comprehensive cosmogenic nuclide chronologies in the world. One of the best examples is the Lake Pukaki moraine sequence which has over 200 individual samples when various studies are combined (e.g. Schaefer *et al.*, 2006; Kelley *et al.*, 2014; Doughty *et al.*, 2015).

Extensive datasets are also available for the Rakaia valley (Shulmeister *et al.*, 2010; Putnam *et al.*, 2013a), Waimakiri catchment (Rother *et al.*, 2015), Lake Ohau moraine sequence (Putnam *et al.*, 2013b), Milford Sound (Dykstra, 2012) and North-West Nelson region (Shulmeister *et al.*, 2005) amongst others. These datasets are more fully presented and critically analysed in section 3.4.1 where their implications for the extent and timing of the LGM are also discussed.

3.2.9 A cautionary tale of interpreting landforms: The Waiho Loop

The glacial stratigraphies discussed in section 3.2.1 are derived mainly from geomorphological mapping and landform interpretation, with absolute ages assigned using the techniques outlined in section 3.2.8. It is important to note that there is still substantial debate and uncertainty surrounding many of the chronologies and assigned dates, with ongoing research leading to regularly updated and refined boundaries (e.g. Shulmeister *et al.*, 2010).

Issues of landform interpretation and age control are well illustrated at the Franz Josef Glacier on the Western flank of the Southern Alps, one of the most intensively studied glaciers in the world (Alexander *et al.*, 2014). Here, the associated 'Waiho Loop' landform (Figure 3.6) is of particular interest for palaeoglacier and paleoclimate reconstructions. This prominent, steep sided moraine rises more than 100 m above the plains of the glacier foreland has attracted much scientific attention, with on-going debate in high profile journals over the last 25 years. The geomorphological interpretation, absolute dating and significance of the Waiho Loop highlights some of the issues involved with geomorphological mapping and emerging dating techniques, providing an insight into the difficulties associated with such studies.

Figure 3.6 The tree-covered Waiho Loop landform, Franz Josef glacier. (GNS science)

The landform was initially assumed to represent a phase of glacial advance with ^{14}C dating used as evidence of a Younger Dryas event in the Southern Hemisphere and synchronicity of climate change between the northern and southern (Denton & Hendy, 1994), although Singer *et al.* (1998) suggested the advance was rather a consequence of increased precipitation or local variation not representative of regional thermal decline. A temperature-precipitation reconstruction by Anderson and Mackintosh (2006b) found that the climatic conditions required for the advance were similar to those proposed for the LGM, inferring a major late-glacial cooling event. Further debate was added when surface exposure dating by Barrows *et al.* (2007) suggested ice retreated from the moraine around 1100 years after the end of the Younger Dryas and was therefore not associated with the cooling event. This conclusion was controversial at the time (Applegate *et al.*, 2008), with the local ^{10}Be production rate for the Southern Alps by Putnam *et al.* (2010) (see section 3.2.8) published soon after suggesting true ages were likely to be around 15 % older. More significantly, there was a growing body of evidence to suggest that the loop moraine did not represent a climatically driven advance, with the composition and type of

clasts indicating a landslide origin which consequently triggered the advance (Tovar *et al.*, 2008; Shulmeister *et al.*, 2009; Evans, 2008). Most recently, the perception that the landform represents a period of advance at all has been challenged, with Alexander *et al.* (2014) concluding that the landslide deposit could not have generated the advance, with formation actually occurring over more than 30 years as the terminus slowly retreated from an overdeepened trough.

3.3 Rationale for concentrating on the LGM

This thesis concentrates on the LGM (herein assigned to the period 30 ka to 18 ka: see section 3.2.2) because it has an excellent geomorphological record in terms of spatial and temporal coverage and therefore has great potential for improving our understanding of former climatic conditions and functioning of natural systems.

This LGM period is of great interest as it represents a climate state dramatically different to that of present, providing a useful test of climate models' sensitivity to change (Mix *et al.*, 2001). The LGM was a phase of 'equilibrium state' climate, with short term variability smaller than during other phases such as MIS stage 3, which was dominated by numerous short-term oscillations (Mix *et al.*, 2001). These stable climatic conditions consequently allowed glaciers to reach near steady state conditions, achieved when mass balance remains constant for many years (Benn & Evans, 2010). Steady state glaciers have characteristic surface profiles whose shape depends only slightly on mass balance, approximating a parabola for an ice cap on a horizontal bed (Paterson, 1994). The assumption of steady state meets the criteria for a number of surface reconstruction models (Schilling & Hollin, 1981; Benn & Hulton, 2010) and for the calculation of other parameters of glaciological and climatological importance such as the Equilibrium Line Altitude (ELA) (Pellitero *et al.*, 2015). Furthermore, with the New Zealand land mass largely in its present configuration by the mid-Pleistocene (Barrell, 2011), primary boundary conditions for the LGM are well known (Mix *et al.*, 2001), allowing greater confidence with modelling studies compared to older glaciations.

Being the most recent episode of 'ice age' climate, the LGM produced very distinctive and recognisable glacier landforms which are much better preserved than those

from earlier episodes (Barrell, 2011). With geomorphological study still one of the principle methods for determining glacial sequences (Hubbard & Glasser, 2005), the LGM is particularly suitable for palaeoglacier study and is the only glacial period for which sufficient geomorphological evidence is available for detailed regional scale mapping of down valley extent in New Zealand (e.g. Barrell, 2011; Suggate, 1990). Furthermore, being in the range of a number of absolute age dating techniques (see section 3.2.8) (Mix *et al.*, 2001), there is an ever growing database of quantitative age-controlled sites (e.g. Kelley *et al.*, 2014; Rother *et al.*, 2015).

3.3.1 Uncertainty and unresolved questions regarding the LGM

Despite its importance, there are still a number of unresolved questions regarding the LGM in New Zealand, the Southern Hemisphere and globally, which have caused debate in the literature. This has led to the behaviour of southern mid-latitude glaciers during the Last Glacial Maximum and the associated glacial-interglacial transition being the focus of intense debate for over 20 years.

3.3.1.1 Air temperature of the Southern Alps at the LGM

Temperature at the LGM has been reconstructed using a variety of methods for the New Zealand Southern Alps, with Table 3.3 providing a synthesis of results. There is a large range of estimated temperatures, from 9°C of cooling from present (Barrows & Juggins, 2005) to little change from current conditions (Marra *et al.*, 2006). Some of the variations may be explained by the specific locations (e.g. North Island vs South Island) whilst it is also likely that temperature oscillated during the LGM period, with cooler periods punctuated by comparatively warmer phases (Marra *et al.*, 2006). Although the wide range of temperature reductions make it difficult to compare New Zealand to other locations worldwide, the results are within the range of those from other regions, with Seltzer *et al.* (2015) noting a 'striking similarity' between their estimation of 4.6 °C cooling (for New Zealand) with the ~5°C of cooling estimated for a number of Northern Hemisphere sites using similar methods (Beyerle *et al.*, 1998; Ma *et al.*, 2004).

Table 3.3 Estimated temperature change from present for the LGM in New Zealand. Adapted from McKinnon *et al.* (2012).

Bibliographic reference	Temperature change from present (°C)	Site Location	Notes / Methods
(Marra *et al.*, 2006)	+0.5 to – 1.9 (Summer, LGM stadial)	Canterbury foothills, South Island	Beetle fossils
	+1 to -2.2 (Winter, LGM interstadial)		
(Samson *et al.*, 2005)	-0.9 (Winter)	Bay of Plenty, North Island	Foram-based sea surface temperature (SST)
	-1.5 (Summer)		
(Barrows & Juggins, 2005)	-1 to -3	Bay of Plenty, North Island	Foram-based sea surface temperature (SST)
	-3 to -5	Central and northern NZ, east and west coasts	
	-7 to -9	Southern NZ, east coast	
(Rother & Shulmeister, 2006)	-1 to -4	Central alpine region	Snow mass balance model
(Sikes *et al.*, 2002)	-4	North of Chatham Rise	Foram- and alkenone based sea surface temperature
		South of Chatham Rise	
(Sandiford *et al.*, 2003)	<-4	Auckland, North Island	Pollen assemblages
(Seltzer *et al.*, 2015)	-4.6 ± 0.5	New Zealand average	Dissolved noble gases in groundwater
(Drost *et al.*, 2007)	-4.6	New Zealand average	Regional climate modelling
	-6.5 to -6.9	Southern Alps	
(Weaver *et al.*, 1998)	-4 to -6	North of Chatham Rise	Foram-based sea surface temperature (SST)
	-8	South of Chatham Rise	
(Wilmshurst *et al.*, 2007)	-5.3	Maratoto, North Island	Pollen assemblages
(Shulmeister *et al.*, 2001)	-6.3 to -7.8	Lake Poukawa, North Island	Pollen assemblages
(Golledge *et al.*, 2012)	-6 to -6.5	Southern Alps	Glacier-climate modelling
(McKinnon *et al.*, 2012)	-7 to -8	Pukaki glacier, South Island	Glacier modelling

The method of temperature reconstruction, area and scope of study (e.g. New Zealand specific or wider region) should be carefully considered when assessing the estimates shown in Table 3.3. A number of the studies suggesting limited cooling at the LGM are thought to be unrepresentative of the glaciated regions of the Southern Alps as they are based on lowland regions (Marra *et al.*, 2006) or on data from far afield ocean sites (Barrows & Juggins, 2005; Samson *et al.*, 2005). As such, for the scope of this thesis (glaciated regions of the Southern Alps), LGM cooling of between 1 °C and 8 °C are considered as previously estimated values.

3.3.1.2 Precipitation at the LGM

Palaeo-precipitation in the Southern Alps during the LGM is poorly recorded by terrestrial proxies (Golledge *et al.*, 2012) resulting in very few quantitative studies regarding precipitation regime for the Southern Alps during the LGM. Drost *et al.* (2007) provides perhaps the most comprehensive study of precipitation in the

Southern Alps at the LGM, using the United Kingdom Met Office global (HadAM3H) and regional model (HadRM3H) to reconstruct former conditions. This study found precipitation levels during the LGM were generally less, although there was 'remarkable' regional variation (Table 3.4). Alongside spatial variation, temporal variations in precipitation are likely to have occurred during the LGM period, with changes in circulation resulting in short-lived wetter episodes (Drost *et al.*, 2007; Whittaker *et al.*, 2011)

Table 3.4 Simulated annual precipitation at the LGM for various regions of the Southern Alps. *Contemporary values relate to pre industrial simulation. Adapted from Drost *et al.* (2007).

Region	LGM precipitation (mm yr^{-1})	Present* precipitation (mm yr^{-1})	Change (%)
South Island (North)	2302	2680	-14.1
South Island (West and South)	3638	3864	-5.8
South Island (East)	866	844	+2.5
New Zealand	**2182**	**2363**	**-7.6**

Palaeo-vegetation studies suggest a major reorganisation of vegetation patterns during the LGM in New Zealand, with a general consensus of drier conditions overall (McGlone *et al.*, 1993). This is consistent with studies finding an increase of loess (thought to originate from exposed floodplains), indicating a drier and windier climate (Eden & Hammond, 2003). Conversely, some studies have postulated 'relatively wet' conditions due to enhanced westerlies and an enhanced orographic effect as a consequence of reduced sea level resulting in the Southern Alps forming a larger barrier (Shulmeister *et al.*, 2004). With no suggestion that precipitation changes were particularly severe, Golledge *et al.* (2012) restricted glaciological modelling to precipitation changes of ± 25% from contemporary values, finding that a precipitation reduction of 25 % (combined with a 6.5 °C temperature reduction) produced a 'best fit' to the geomorphological evidence.

3.3.1.3 Style of glaciation at the LGM

Alongside climatic conditions, there is also uncertainty regarding the 'style' of LGM glaciation in New Zealand. Published interpretations of LGM ice extent (Barrell, 2011; Golledge *et al.*, 2012) show an 'ice sheet/cap' style of glaciation, with little or few nunataks present. This view of an 'ice cap' style glaciation is supported by Rother and Shulmeister (2006) who suggest that reduced sea level during the LGM increased

the relative height of the Southern Alps as a barrier for moist air masses, resulting in increased precipitation and produced an ice cap/field approximately 30 km wide.

However, this view is not shared by Anderson and Mackintosh (2006b) who suggest the geomorphological evidence does not support the notion of such an ice cap. They proposed that the LGM glaciation was largely confined to separate valley systems and did not overtop many of the peaks. They argue that that jagged topography found in the Southern Alps is indicative of glaciations confined to the lower valleys, rather than smooth and rounded peaks which would be expected if they had been over-ridden by glacial ice.

As an intermediate view, Chinn *et al.* (2014) postulates a north-south transition between an ice cap style of glaciation and mountain valley glaciation, with the Darran range (adjacent to Milford Sound) marking the approximate boundary. This concept is based on the observation that peaks to the south are moderately smoothed and barely penetrate the contemporary ELA, suggesting an ice cap free of central nunataks. In contrast, the higher peaks to the north are jagged, suggesting they rose above any regional ice cap.

3.3.1.4 Regional variability

There is further debate regarding catchment scale patterns and timing of LGM glaciation, with a growing body of evidence to suggest that the LGM and associated retreat was not synchronous between catchments (Rother *et al.*, 2014). The formation of proglacial lakes is one way in which glaciers and their associated geomorphological record may become 'decoupled' from climate, making such individual glaciers unreliable for inferring regional trends. For example, surface exposure dating by Putnam *et al.* (2013a) found a rapid recession of the Rakaia glacier between 17.8 to 15.6 ka, with glacier length reducing by approximately 50 % in this timespan. Exposure ages show the glacier margin was at the 'Big Ben' moraine 17.8 ka and by 16.9 ka 'Double Hill' was ice free, implying a recession of ~28 km in this time period (Figure 3.7).

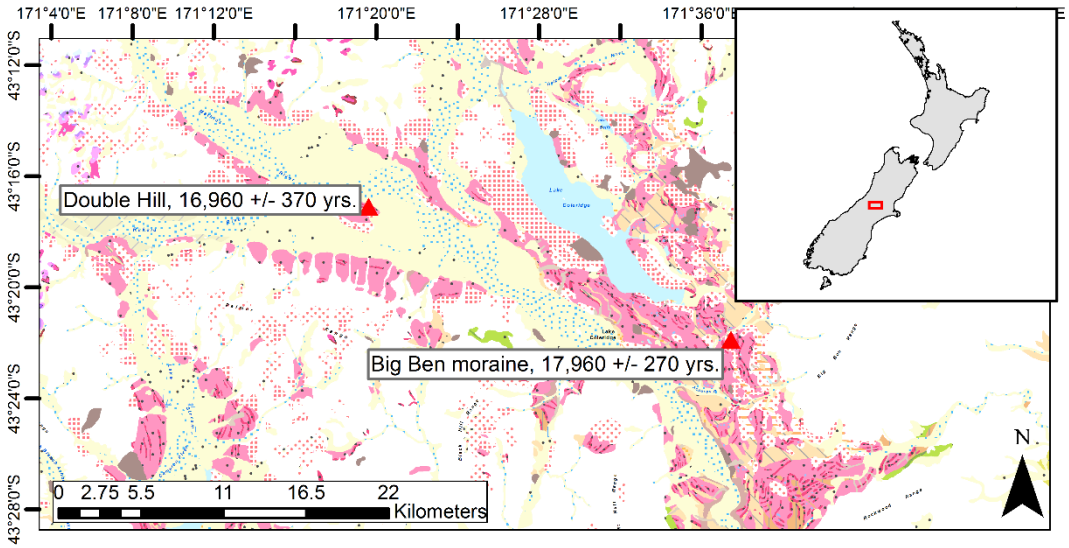

Figure 3.7 Location map of 'Big Ben' moraines and 'Double Hill' with corresponding exposure ages calculated by Putnam *et al.* (2013a)

Whilst Putnam *et al.* (2013a) used this chronology for regional palaeoclimatic reconstruction, Rother *et al.* (2014) suggested that the recession rate in the Rakaia valley was localised to the catchment and decoupled from climate due to the formation of a large proglacial lake as evidenced from the sedimentary record (Shulmeister *et al.*, 2010). Whilst this is generally an issue for inferring deglaciation trends rather than maximum extent, it highlights how the position of an individual glacier may not be a reliable climate proxy and that caution should be used when extrapolating the glacial record across multiple catchments.

3.4 An updated geodatabase of LGM extents for the Southern Alps

This section aims to review the most up to date knowledge regarding LGM extent in New Zealand, combining existing regional extent mapping with catchment specific studies to create an updated LGM extent geodatabase for the Southern Alps.

Since early attempts to correlate glacier advances between valley systems (e.g. New Zealand Geological Survey, 1973), there have been various efforts at constructing regional scale compilations of glacier extents at the LGM. Expanding on his early work (Suggate, 1965), ice advance limits were progressively compiled by R.P. Suggate at a scale of 1:250,000 (Suggate, 1990; Suggate, 2004). This was subsequently updated and revised by Barrell (2011), including revisions based on the QMAP (Quarter Million Scale Mapping) project, a nationwide geological mapping project

where the ages of Quaternary deposits were mapped in terms of MIS stages (Heron, 2014). Although some extents are defined by well-known moraines and geomorphological evidence, other parts of the map reflect personal interpretation by D. Barrell, who states that the mapping:

"*represents inferred extents of LGM ice that I hope will motivate further investigation and in turn be tested and refined by future research and dating*" (Barrell, 2011 p. 1050).

In conjunction with this regional LGM ice extent map, a detailed geomorphological map for the central sector of the Southern Alps has also been produced by Barrell *et al.* (2011), with its extent shown in Figure 3.8. This 1:100,000 scale mapping project separates glacier landforms according to their ages, with the belts of moraines and other geomorphological features delineating the extent of glaciations at a high resolution. These maps are used extensively for analysis and presentation later in this project with Figure 3.1 providing a legend with features of interest for LGM glaciation highlighted.

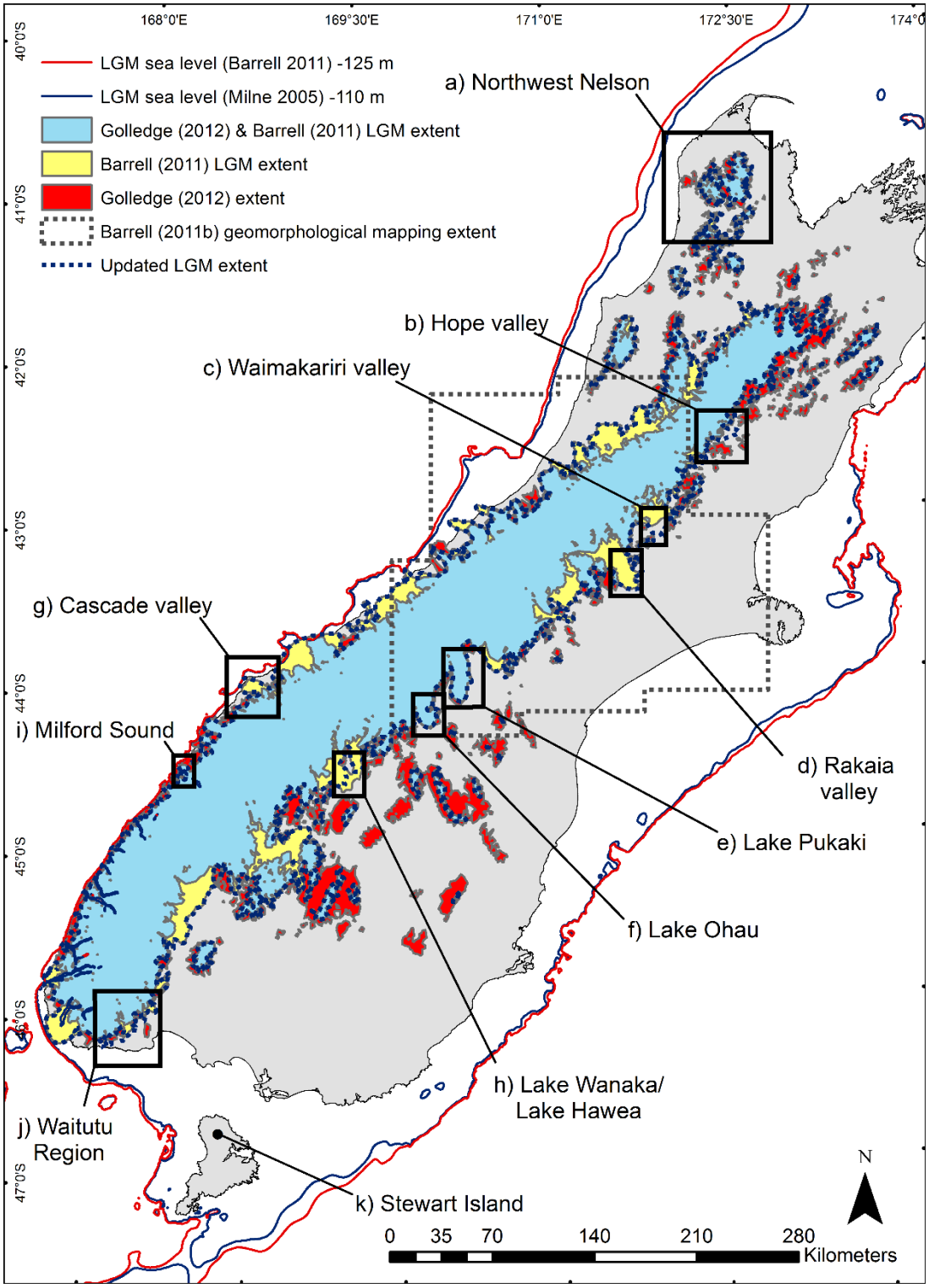

Figure 3.8 Overview map of existing LGM extent interpretations and locations of detailed extent analysis

A further delineation of ice limits is provided by Golledge *et al.* (2012), who used the Parallel Ice Sheet Model (PISM) to simulate the Southern Alps icefield at the LGM. The specifics of the model and results of the corresponding distributed ice thickness distribution will be discussed in detail in Chapter 4, with analysis in this chapter restricted to the planform extent. This model was parameterised to 'best fit' the

geomorphological evidence (e.g.Barrell, 2011), with results indicating that an LGM cooling of 6.5 ^{o}C and 25 % reduction in precipitation was required to reproduce mapped glacier extents. Being parameterised to match the geomorphological evidence, the extents delimited cannot be viewed as an alternative to those of Barrell (2011). However, with some areas of the Barrell (2011) mapping reflecting 'personal interpretation' (Barrell, 2011 p. 1050) and even being depicted 'schematically' in some cases (Barrell, 2011 p. 1059), the modelling by Golledge *et al.* (2012) provides a useful tool for comparing the interpreted extents with those from a physically justified model.

As shown in Figure 3.8, the extents derived from the best fit scenario by Golledge *et al.* (2012) are in general agreement with the geomorphological limits defined by Barrell (2011). However, there are some locations where the model does not align with the extents of Barrell (2011), either overestimating or underestimating ice extent in comparison. The greatest 'underestimates' by Golledge *et al.* (2012) exist in the eastern outlets such as the Rakaia and Wakatipu where glaciers are modelled significantly further up valley compared to geomorphological records. Conversely, Golledge *et al.* (2012) predicts more extensive LGM ice at a number of locations compared to Barrell (2011), mostly in eastern areas separated from the main ice field (Figure 3.8).

3.4.1 Catchment scale analysis of LGM extents

In conjunction with the regional scale extents encompassing the entire Southern Alps presented in Figure 3.8, there have been a number of individual catchment scale studies which have delineated ice extents through a variety of methods. Recent advances in age control techniques (section 3.2.8) has improved our understanding of palaeoglacier fluctuations, with an ever improving database of LGM age constrained sites. The following section provides a detailed overview of knowledge of former glacier extents in key locations, focussing on LGM limits and recent advances in age control which have in some cases verified the extents delineated by geomorphological mapping and contradicted them in others. Where sufficient evidence exists to dispute the extents delineated in regional mapping projects (Barrell, 2011; Golledge *et al.*, 2012) they have been updated accordingly in this

thesis, thereby producing the synthesised and critically evaluated LGM extent shown in Figure 3.8.

3.4.1.1 Northwest Nelson

The Tasman Mountains (Figure 3.8a) are ice free today, but represented the northern tip of LGM glaciation in the Southern Alps. There is some disagreement in the literature surrounding the style and extent of glaciation in the region, with reconstructions of the Boulder and Snow glaciers by McCarthy *et al.* (2008) inferring glaciers were restricted to their individual catchments (Figure 3.8a). Conversely, Barrell (2011) suggested an ice field style of glaciation in the region covering the major peaks, with the modelled extents of Golledge *et al.* (2012) predicting even more substantial ice coverage (Figure 3.8b). The notion of expansive ice cover is consistent with surface exposure dating by Shulmeister *et al.* (2005) who constructed a glacial chronology of the Cobb valley, describing deglaciation from LGM conditions. Age estimates of an elevated bench over 100 m above the modern Cobb valley floor revealed an average age of 21.05 ka (adjusted to the Putnam *et al.* (2010) production rate), indicating a substantial LGM advance at this site. With these age controlled samples suggesting expansive ice coverage, this thesis has utilised the limits defined by Barrell (2011), with minor adjustments in the lower Cobb valley to accommodate the down valley SED ages of Shulmeister *et al.* (2005) (Figure 3.8b).

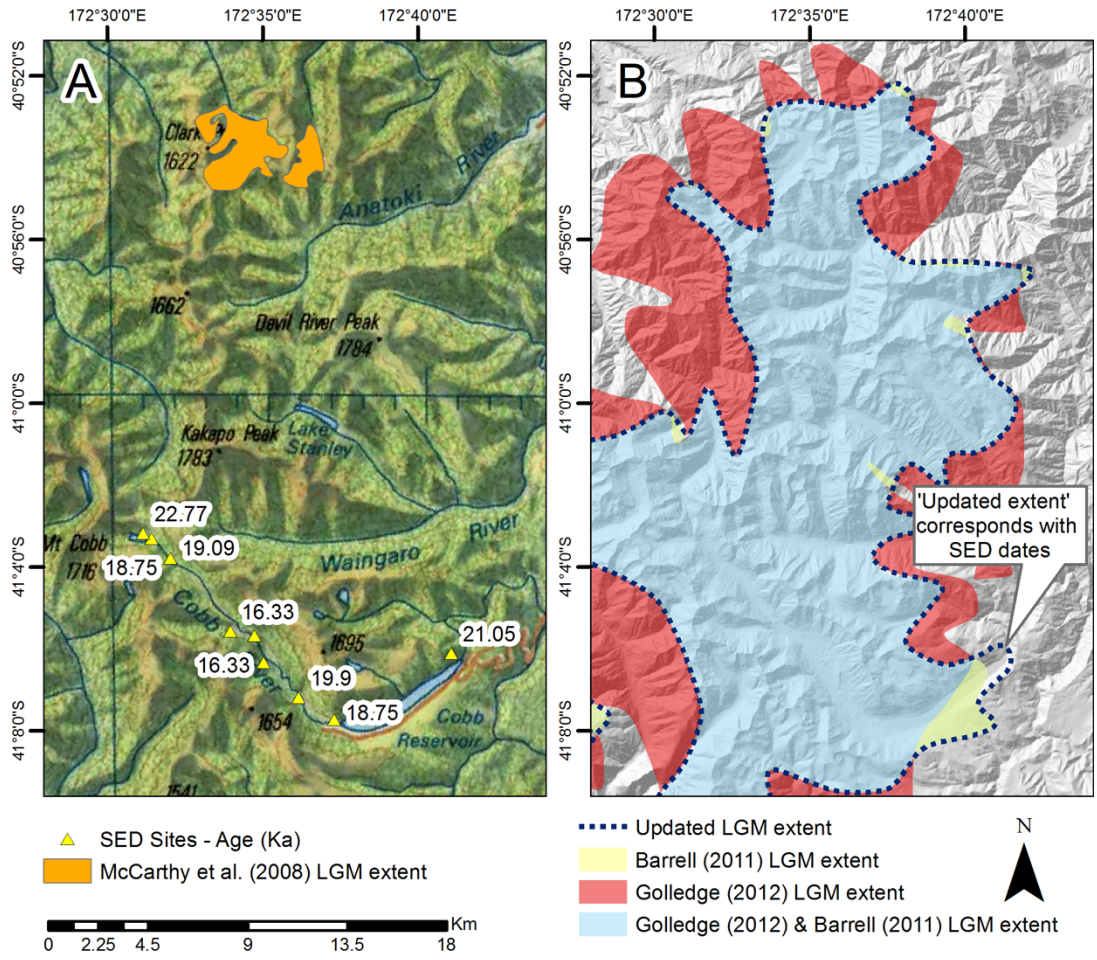

Figure 3.9 a) Site specific data related to LGM extent in Northwest Nelson. b) LGM extent in Northwest Nelson from regional datasets including the 'updated extent' used in this thesis.

3.4.1.2 Hope Valley

Mapping of glacial deposits in the Hope-Waiau valleys (Figure 3.8b) formed part of the seminal work '*Late Pleistocene geology of the northern part of the South Island, New Zealand*' by Suggate (1965). Detail was improved by Clayton (1968), identifying six late Pleistocene advances in the region, which in order from oldest to youngest were termed the Kakapo, Horseshoe, Leslie Hills, Glenhope, Glynn Wye and Lewis advance. The Glynn Wye moraines are the largest and most prominent, originally thought to represent the LGM (Clayton, 1968; Cowan, 1990), as mapped by Barrell (2011). However, this assumption has recently been challenged, with dating of the Glynn Wye moraine yielding an age of 15.2 to 18.8 ka (Rother, 2006), which is younger than would be expected for an LGM terminal position. Furthermore, Kakapo Hill (Figure 3.9a), the highest glacial surface in the Hope Waiau valleys, yielded an age of 20.5 ± 1.7 ka, which is substantially younger than the Oxygen Isotope Stage

(OIS) 8 (290 – 240 ka) age inferred by Clayton (1968). This suggests that Kakapo hill was overrun by ice during the LGM, with the Glynn Wye terminal moraine (Figure 3.9a) 200 m below unable to generate the geometry required. Whilst it is acknowledged that some caution should be exercised when interpreting this single exposure age from Kakapo Hill (Rother, 2006), when considered in conjunction with the LGM age determined for the Glynn Wye moraine (Rother & Shulmeister, 2006), it appears that the down valley extent is greater than previously thought. Rother (2006) suggests that the 'Glenhope advance' (Figure 3.9a) is most likely to represent the LGM terminal position, with the Glynn Wye moraine instead attributed to a later retreat phase.

The LGM outline for this thesis has subsequently been updated to take into consideration the SED ages presented by Rother and Shulmeister (2006) as shown in Figure 3.9b The updated limits continue downstream to the 'Glenhope' advance position as mapped by Rother and Shulmeister (2006).

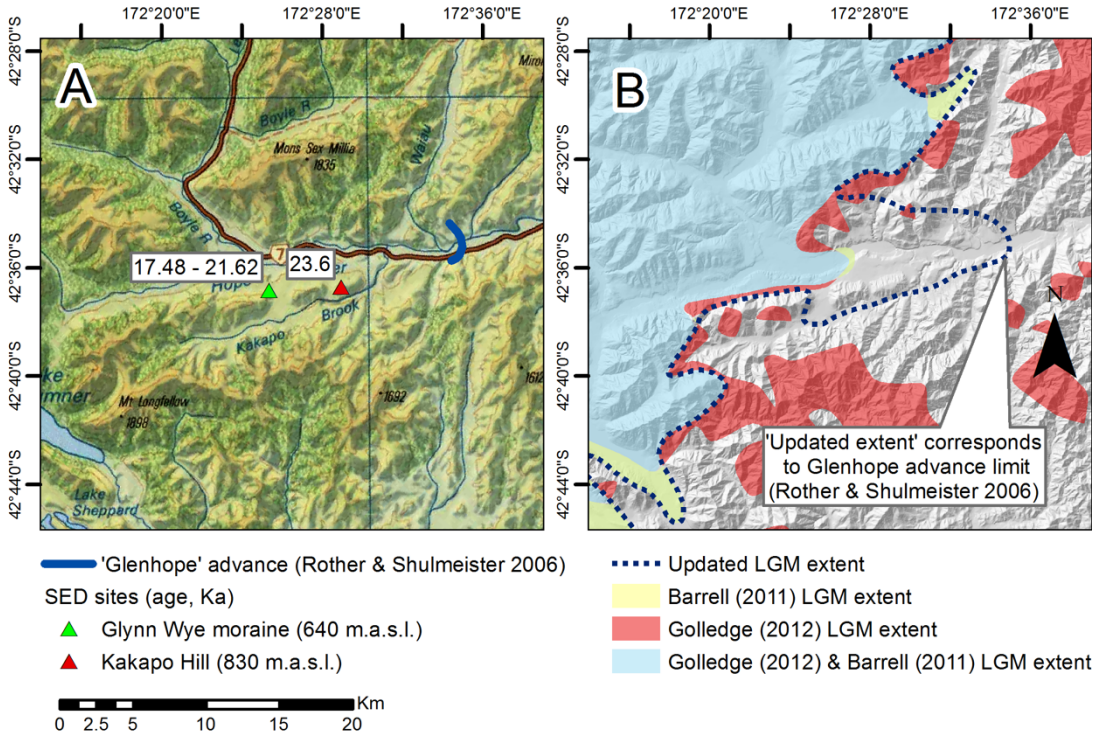

Figure 3.10 a) Site specific data related to LGM extent in the Hope Valley. b) LGM extent in the Hope Valley from regional datasets including the 'updated extent' used in this thesis.

3.4.1.3 Waimakariri Valley

The Waimakariri Valley (Figure 3.8c) represents a major glacier outlet system of the Southern Alps, with clear geomorphological evidence making it a prime focus for palaeoglacier studies (e.g. Rother *et al.*, 2015). Five major glacial advances were initially identified in the valley, termed (from oldest to youngest) the Avoca, Woodstock, Otarama, Blackwater and Poulter (Table 3.2). It was initially assumed that the Poulter advance represented a late MIS 2 event and the Blackwater advance was correlated with the main LGM advance (Suggate, 1990). This sequence was recently reassessed by Rother *et al.* (2015), with surface exposure dating from the Avoca Plateau (Figure 3.11a) 250 m above the valley floor yielding a mean age of 26.5 ka, inferring the Waimakariri glacier overtopped this surface during the LGM, which would not fit with the previous model. Rother *et al.* (2015) therefore concluded that the Otarama moraine (Figure 3.11a) marked the local LGM ice limit, approximately 15 km beyond the previously defined limits (Suggate, 1990; Barrell *et al.*, 2011). Based on these new exposure ages (published after the compilation by Barrell (2011), the LGM outline has been updated in this thesis to extend to the Otarama moraine following the inferred extent presented by Rother *et al.* (2015) as shown in Figure 3.11b.

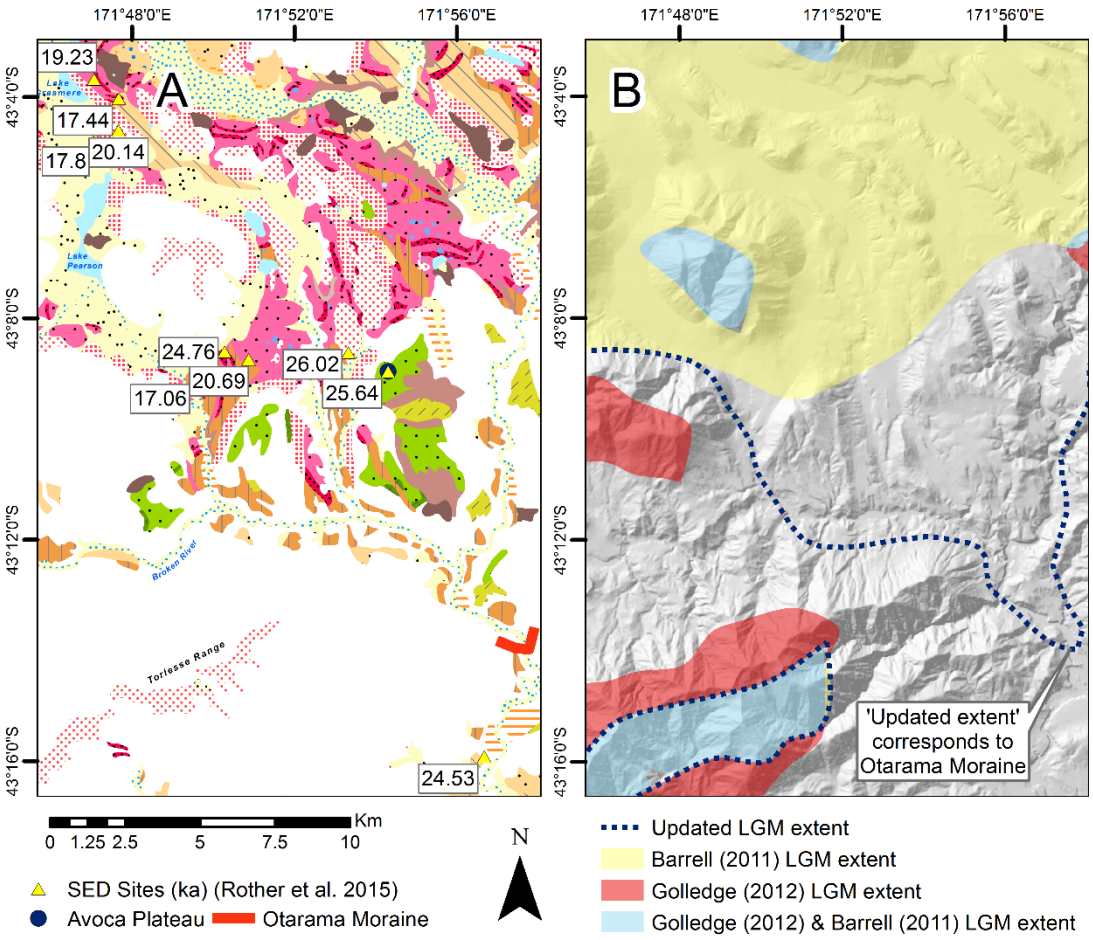

Figure 3.11 a) Site specific data related to LGM extent in the Waimakiri Valley. b) LGM extent in the Waimakiri Valley from regional datasets including the 'updated extent' used in this thesis.

3.4.1.4 Rakaia Valley

The Rakaia valley (Figure 3.8d) currently contains the Lyell and Ramsay glaciers. The valley has undergone at least five major glaciations during the Quaternary (Rowan *et al.*, 2012), with glaciers reaching the Canterbury plains at least twice. During the LGM the valley was occupied by a single large glacier, formed by the coalescence of ice from the Wilberforce, Mathias and Upper Rakaia valleys (Putnam *et al.*, 2013a). LGM glaciation was complex, with a reversal of flow at the Lake Stream tributary indicated by southward dipping lateral moraines at prospect hill (Pugh, 2008). This drainage capture reduced the effective drainage area of the catchment by approximately 7 % (Rowan *et al.*, 2013). The landscape is dominated by glacial-fluvial landforms, containing some of the best preserved relict glacial geomorphological features in New Zealand (Soons, 1963). This region is also of interest as it is one of the major catchments for which Golledge *et al.* (2012) acknowledges their model

performs poorly, with LGM limits estimated approximately 40 km upstream from the extents delineated by Barrell (2011). An in-depth review of the existing evidence will therefore help to understand if the model by Golledge *et al.* (2012) is a true underestimate or if the mapping by Barrell (2011) is an overestimate.

The glacial history of the valley has long been studied, with early descriptions of deposits by Speight (1934). The first attempt to define the limits of glaciation was by Soons (1963), identifying four separate moraine sequences. The outermost (Woodlands) sequence extends into the Canterbury Plains and is defined by a discontinuous moraine loop. Successive up-valley components are ascribed to the Tui Creek, Bayfield and Acheron advances. These more recent moraine sequences have been subsequently sub-divided into smaller re-advances (e.g. Acheron I,II,III) in various ways by different authors, with Carryer (1967) suggesting a further Blackford advance, although Soons and Gullentops (1973) group this with the Bayfield (Figure 3.12a).

.

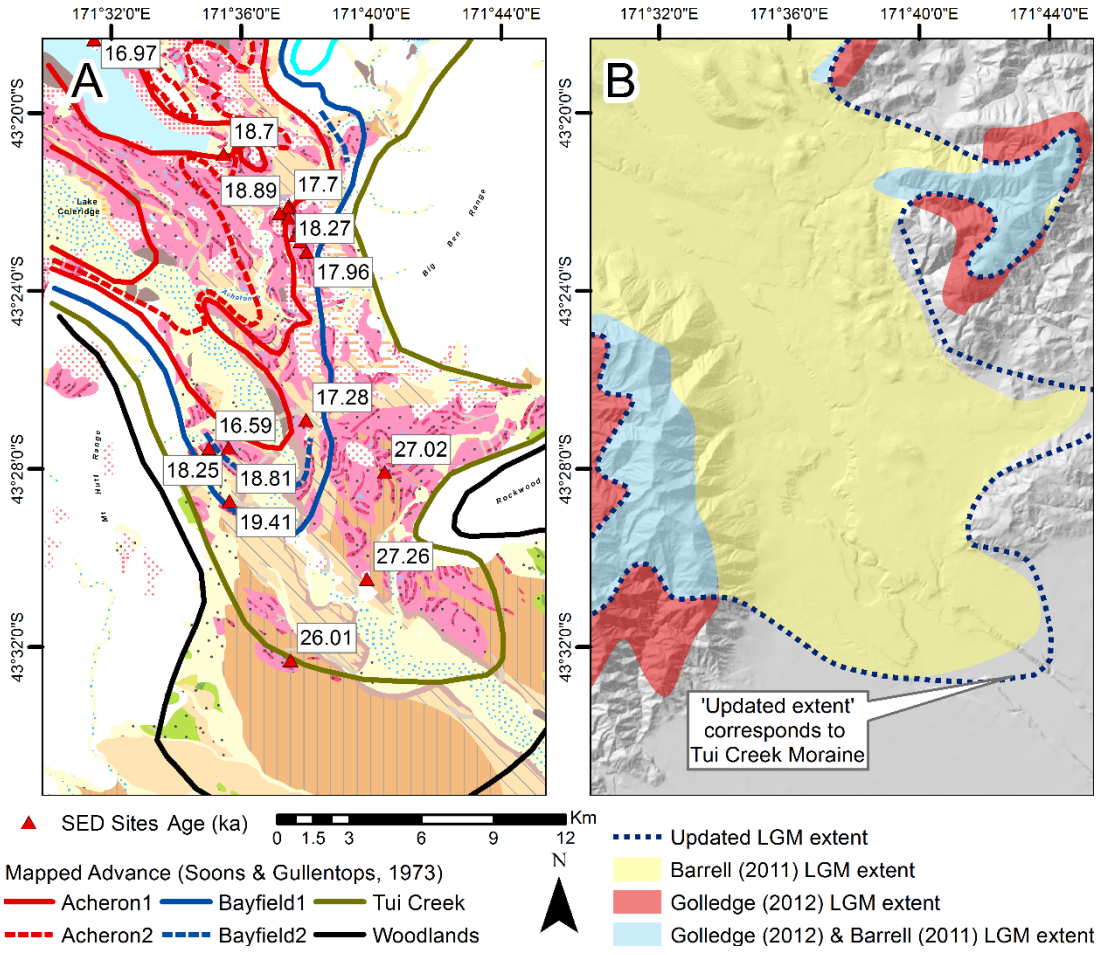

Figure 3.12 a) Site specific data related to LGM extent in the Rakaia Valley. b) LGM extent in the Rakaia Valley from regional datasets including the 'updated extent' used in this thesis.

Prior to the advent of geochronological dating techniques, it was assumed that each component represented an advance followed by a major recession or interglacial (Soons & Gullentops, 1973). This view has been disproved by Shulmeister *et al.* (2010), with surface exposure dating revealing that the Tui Creek, Bayfield and Acheron complexes document a retreat from LGM conditions. Samples from Tui Creek, previously ascribed to MIS 4 (Soons & Gullentops, 1973; Suggate, 1990) yielded an age estimate of 26 ka (after recalibration to Putnam *et al.* (2010) production rate) and are now considered to define the LGM advance limits, whilst the Acheron and Bayfield moraines are now deemed to be the product of minor advances / still-stands superimposed on a long term pattern of retreat (Shulmeister *et al.*, 2010). Early ice advances (the Woodlands) extended approximately 7 km beyond the Rakaia gorge onto the Canterbury plains and has been dated to 114 ka (Shulmeister *et al.*, 2010).

Based on this evidence, the updated LGM boundary (Figure 3.12b) largely follows the extents delineated by (Barrell, 2011), with minor adjustments to coincide with the Tui Creek moraine crest in agreement with Soons and Gullentops (1973). This assertion further suggests that the modelling by Golledge *et al.* (2012) is underestimating the ice extent in the Rakaia valley, with age control largely verifying the original interpretation by Barrell (2011).

3.4.1.5 Tasman valley (Lake Pukaki)

The catchment feeding Lake Pukaki (Figure 3.8e) drains the highest peaks of the Southern Alps and currently contains four of New Zealand's largest glaciers – the Tasman, Murchison, Hooker and Mueller. During the LGM, these glaciers coalesced to form a large valley glacier up to 80 km long, commonly referred to in the literature as the Pukaki glacier (McKinnon *et al.*, 2012). The ice tongue formed a complex of outwash plains and moraines which enclose the glacial trough (Schaefer *et al.*, 2015) and evidence of the upper limit of LGM ice can be traced along its length (Mathews, 1967). Moraine belts and outwash plains show evidence of at least four glacial advances (Kelley *et al.*, 2014), with the dry rain shadow climate aiding the preservation of the landforms (Barrell, 2011). The oldest advance is referred to as the Wolds advance, followed by the Balmoral, Mt. John and Tekapo (Table 3.2). The outermost (Wolds) complex is discontinuous and subdued, while increasingly well preserved landforms are found closer to the contemporary lake shore (Barrell & Read, 2014).

A number of recent studies have applied surface exposure dating to the Tasman valley region (e.g. Doughty *et al.*, 2015; Kelley *et al.*, 2014; Schaefer *et al.*, 2015), providing excellent constraints on the downstream and vertical extent of LGM glaciation. These studies have confirmed that the inner moraines represent the global LGM and that during formation of the Balmoral moraines, the Pukaki glacier was more extensive than during the LGM (Schaefer *et al.*, 2015). Figure 3.13a presents the first amalgamation of surface exposure dating studies in the region, representing a total of 151 dated sites. From these points, 30 ka and 19 ka ice limits were interpolated to estimate the approximate extents for when the Southern Alps are believed to have first reached LGM conditions and at the initiation of the last

glacial-interglacial transition (LGIT) respectively (Rother *et al.*, 2014; Vandergoes *et al.*, 2005).

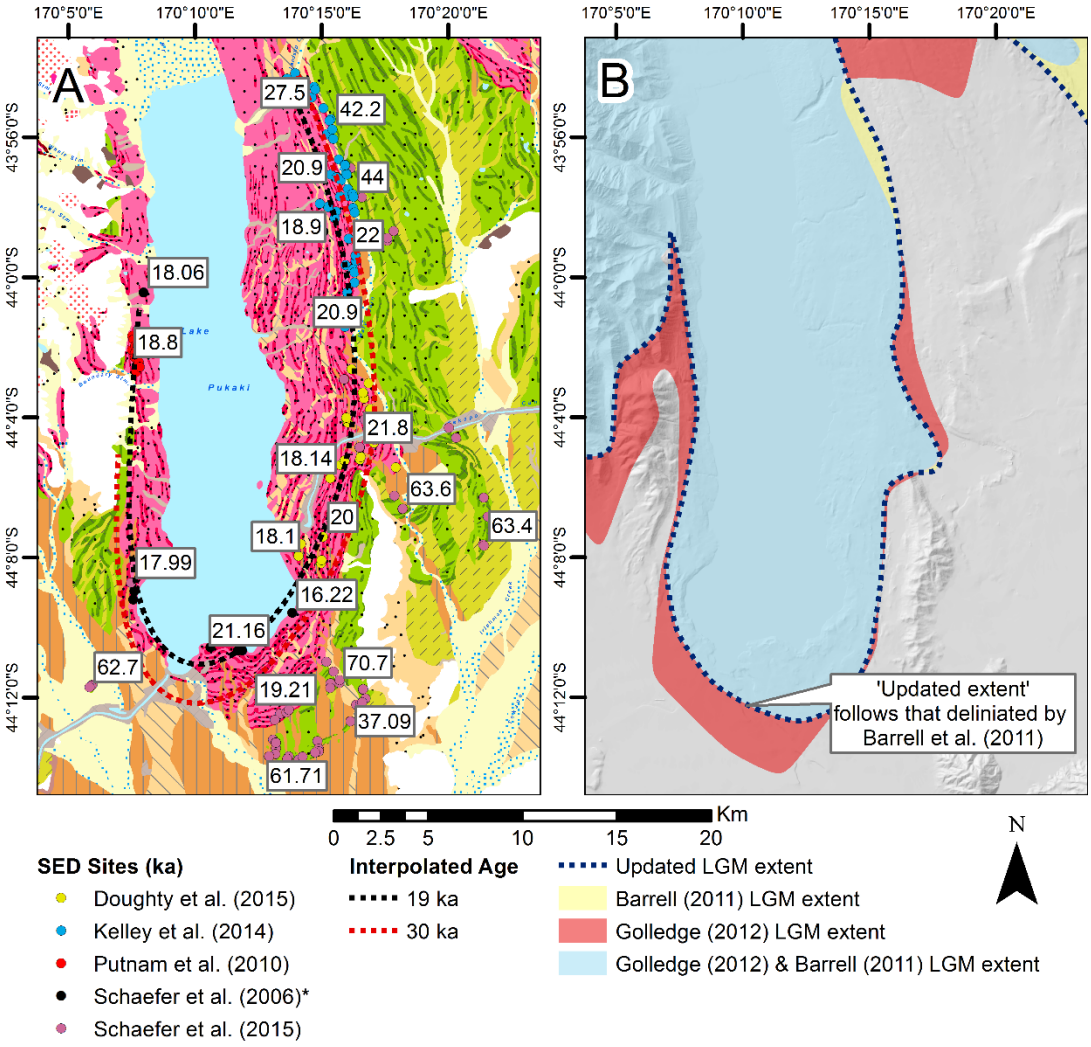

Figure 3.13 a) Site specific data related to LGM extent in the Tasman Valley (Lake Pukaki). b) LGM extent in the Tasman Valley (Lake Pukaki) from regional datasets including the 'updated extent' used in this thesis.

Figure 3.13b demonstrates that the extents delineated by Barrell (2011) are consistent with the interpolated limits, and have therefore been used in this study. The modelled extents by Golledge *et al.* (2012) are more extensive than those from geomorphological evidence, extending beyond the interpolated 30 ka limit, suggesting their model is overestimating the LGM limits in this region.

3.4.1.6 Hopkins-Dobson valley (Lake Ohau)

During the LGM, coalescence of ice from the Dobson and Hopkins catchments formed the Ohau glacier, terminating at the present location of Lake Ohau (Figure 3.8f). The dry rain-shadow climate of the region has aided the preservation of

moraine sequences and outwash plains, with detailed geomorphological mapping carried out by Barrell *et al.* (2011). Exposure dating by Putnam *et al.* (2013b) has allowed age control of the moraine sequences, with Figure 3.14a showing the sample locations and associated ages. The extents delineated by Barrell (2011) largely agree with sites dated to approximately 30 ka, the period at which LGM conditions in New Zealand were first thought to have been reached (Rother *et al.*, 2014), and have therefore been used in this thesis for the updated LGM extent Figure 3.14b. LGM ice extents modelled by Golledge *et al.* (2012) extend further to the east, beyond sites dated at 31 to 33 ka, suggesting their model is overestimating LGM extents in the Ohau valley.

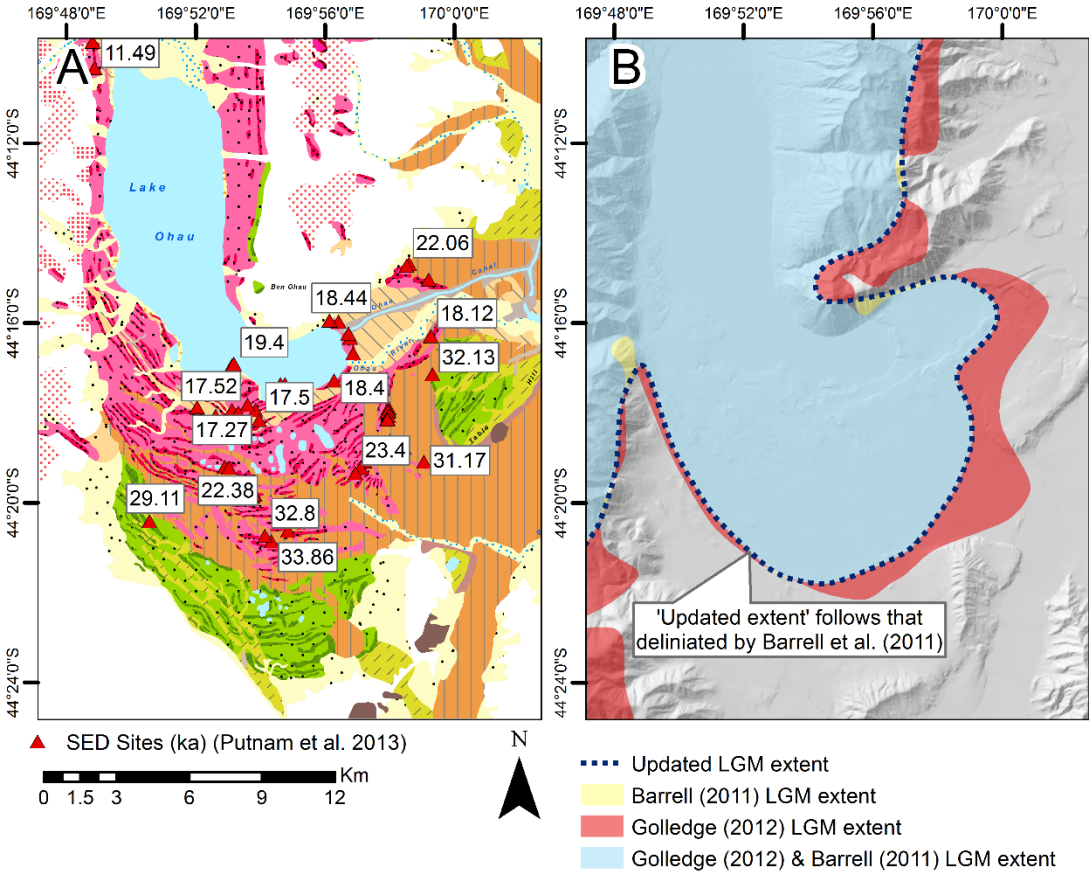

Figure 3.14 a) Site specific data related to LGM extent in the Hopkins/Dobson Valley (Lake Ohau). b) LGM extent in the Hopkins/Dobson Valley (Lake Ohau) from regional datasets including the 'updated extent' used in this thesis.

3.4.1.7 Cascade Valley

The Cascade Valley (Figure 3.8g) has one of the most complete glacial records in the Southern Hemisphere and represents a key location for defining the extent of LGM

glaciation on the west coast of the New Zealand Southern Alps. Evidence from over thirty advance-retreat cycles is identifiable in the region (Sutherland *et al.*, 2007), with lateral moraines of over 13 km in length clearly identifiable in the landscape and visible on aerial photographs (Figure 3.15a) and on the hill-shaded DEM (Figure 3.15b).

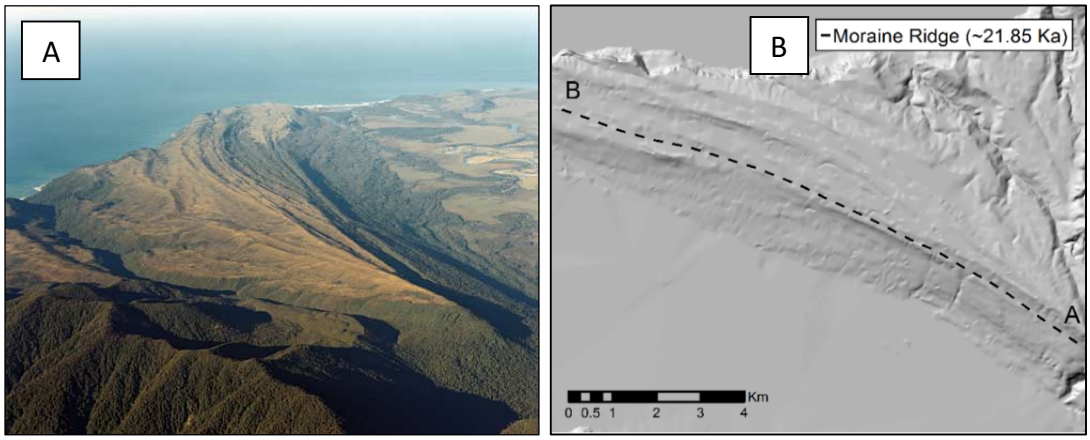

Figure 3.15 a) Oblique aerial photo of the Cascade Plateau showing lateral moraine ridges approximately 14 km in length. (GNS Science). b) Hillshaded DEM of the same region, with the LGM lateral moraine identified by SED by Sutherland *et al.* (2007)

Sutherland *et al.* (2007) carried out surface exposure dating along the moraine sequence, assigning an LGM age of 21.85 ka (after recalibration to the production rate of Putnam *et al.* (2010) to the ridge marked on Figure 3.15b, for which the corresponding transect is shown on Figure 3.16 and Figure 3.17a. With no geomorphological evidence of terminus position, in this thesis the updated LGM extent has been estimated by extrapolating the lateral moraine as shown in Figure 3.16, resulting in a tidewater terminating scenario at LGM sea level.

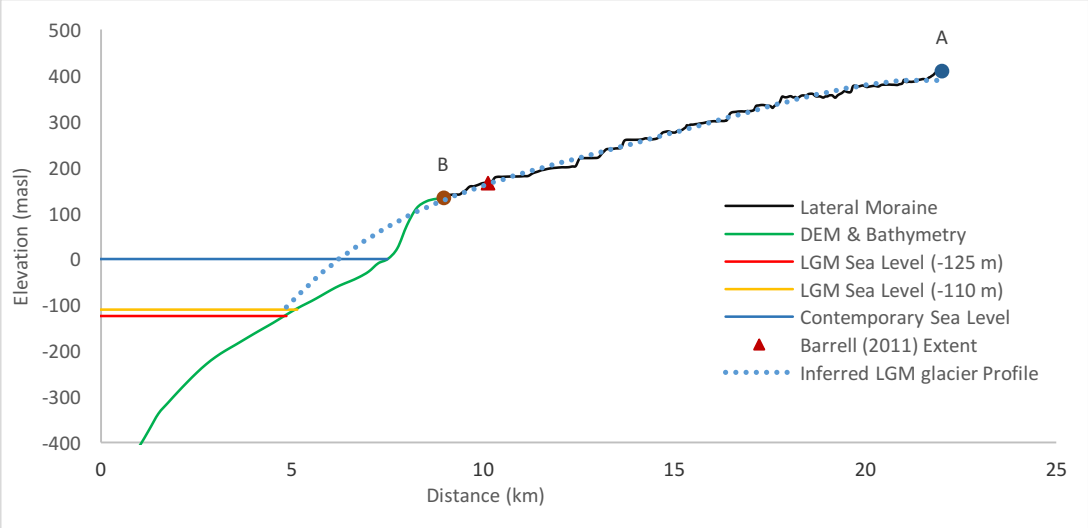

Figure 3.16 LGM moraine ridge (transect A - B on Figure 3.15b) with extrapolated profile required for the glacier to terminate at LGM sea level. Note how the extent delineated by Barrell (2011) is 6 km up valley from the inferred terminus.

As shown in Figure 3.16, comparison with the extents delineated by Barrell (2011) shows that the mapped limit is 6 km up valley from this inferred extent and 1 km up valley of the clearly defined geomorphological evidence, indicating LGM extents have previously been underestimated in the valley. With the possibility of a tidewater termini at the LGM, the exact nature of the former glacier is difficult to assess, with Figure 3.18 showing modern examples of tidewater terminating glaciers. With the extrapolated profile suggesting the glacier would have only just reached the LGM coastline, the extent has been delineated to reflect little ocean influence (Figure 3.17b), in common with other sites on the west coast (e.g. Milford Sound, see section 3.4.1.9).

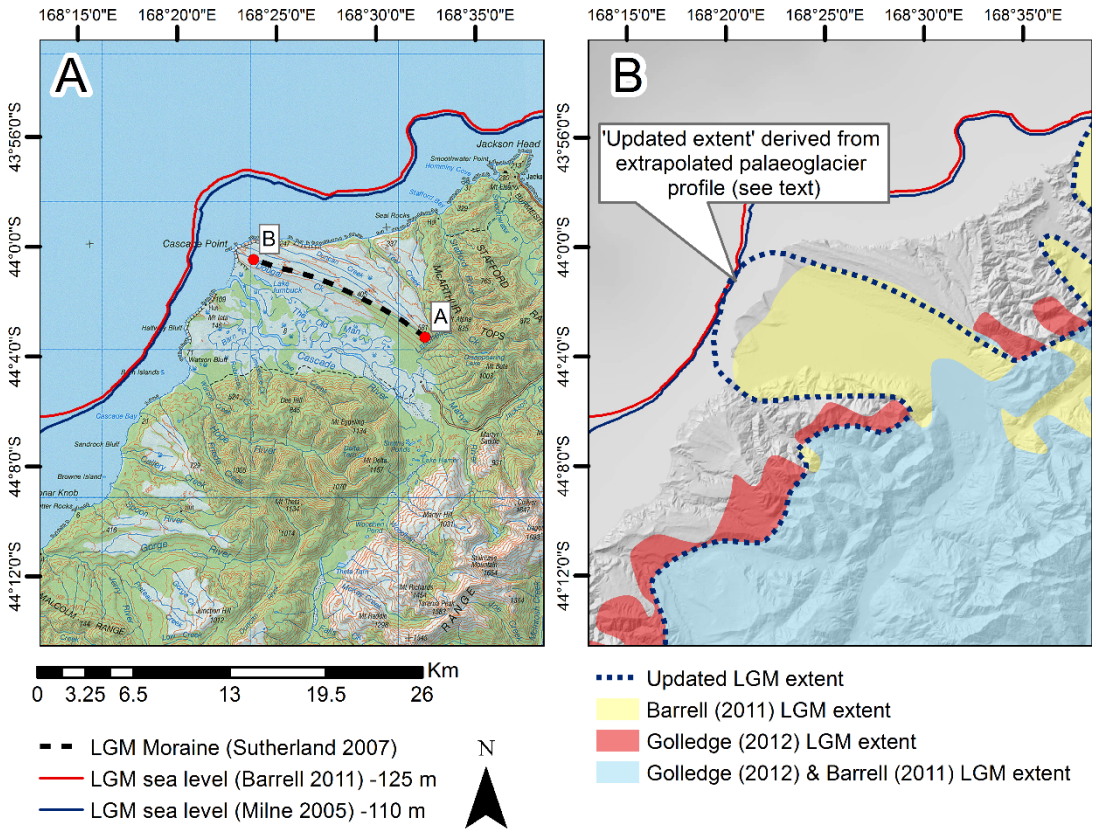

Figure 3.17 a) Site specific data related to LGM extent in the Cascade Valley. b) LGM extent in the Cascade Valley from regional datasets including the 'updated extent' used in this thesis.

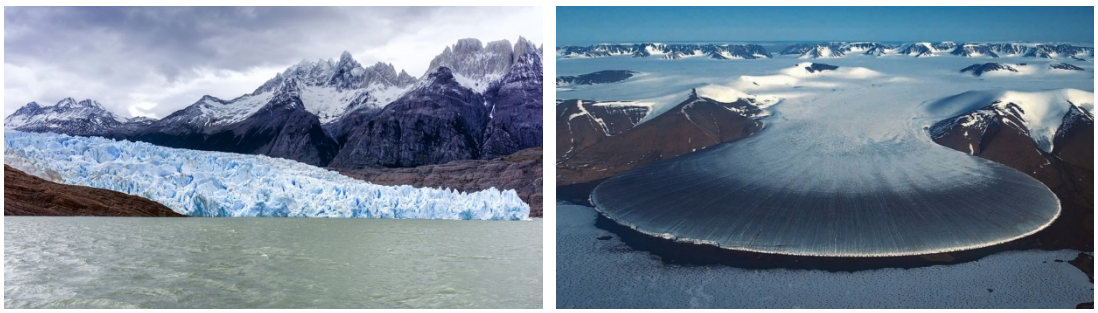

Figure 3.18 Contemporary examples of ice margins for tidewater terminating glaciers. a) Grey Glacier, Chile (G. Collier). b) Elephant foot glacier, Greenland (T. Bolch).

3.4.1.8 Upper Clutha valley (Lake Hawea & Lake Wanaka)

The Upper Clutha (Lake Hawea and Lake Wanaka) area (Figure 3.8h) has previously received attention in the literature, with McKellar (1960) identifying five separate moraine systems, locally named the 'Hawea', 'Albert Town', 'Luggate', 'Lindis' and 'Clyde' advances. Infrared stimulated luminescence (IRSL) dating by Wyshnytzky (2013) constrained the retreat from the Mt Iron position to approximately 32 ka to 26 ka, whilst radiocarbon dating by McKellar (1960) yielded an age of 17.5 ka, providing a minimum date for retreat from the Hawea moraine (Figure 3.19a). Taken

together, these dates broadly constrain formation of the Mt. Iron moraine to the LGM. This is in contradiction to the mapping by Barrell (2011) which depicts ice convergence at the head of Lake Wanaka and Lake Hawea (Figure 3.19b) whilst the modelled extents of Golledge *et al.* (2012) predict substantially less ice, with the areas directly upstream of the Mt. Iron moraine completely ice free. With such large disagreement between the regional extents delineated by (Barrell, 2011) and (Golledge *et al.*, 2012), this thesis conforms to the clear geomorphological evidence with supporting age control (Wyshnytzky, 2013; McKellar, 1960), delineating the LGM extent to that of the Mt. Iron moraine position, with no coalescence of ice between Lake Hawea and Lake Wanaka (Figure 3.19b).

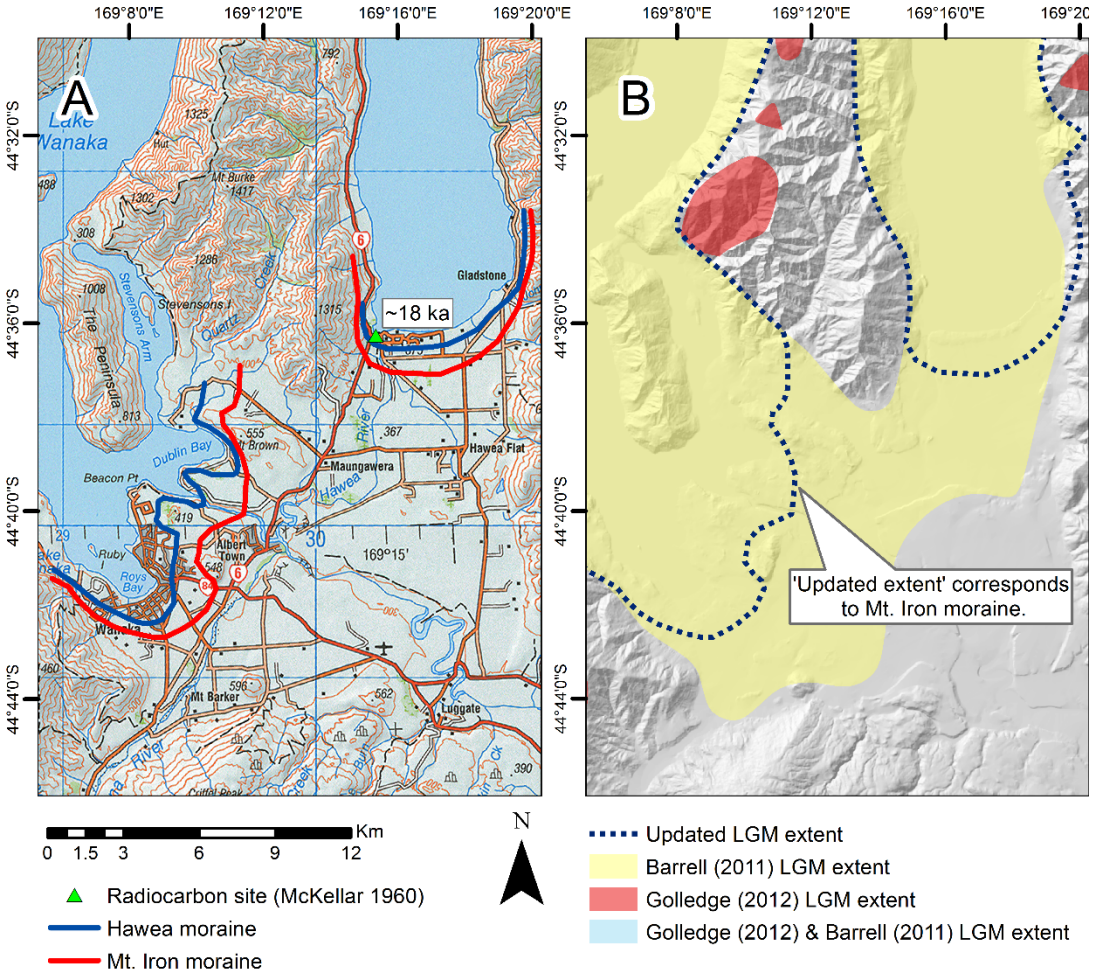

Figure 3.19 a) Site specific data related to LGM extent in the Upper Clutha region (Lake Hawea and Lake Wanaka). b) LGM extent in the Upper Clutha region (Lake Hawea and Lake Wanaka) from regional datasets including the 'updated extent' used in this thesis.

3.4.1.9 Milford Sound

South of approximately 43°30'S, the continental shelf is narrow and some LGM glaciers are thought to have had tidewater-calving termini, reaching the ocean at periods of sea level minima/full glacial extent (Barrell, 2011). In general, catchments to the west of the main divide contain a relatively poor geomorphological record, with Milford Sound (Figure 3.8i) providing an exception, where evidence of the former LGM glacier terminus position has been preserved in the form of an extensive terminal moraine sequence in the submarine environment (Dykstra, 2012). This geomorphological evidence is supplemented by surface exposure dating at a number of sites along the fjord (Figure 3.20a), describing deglaciation from LGM conditions. Figure 3.20b shows that the LGM ice extents delineated by Barrell (2011) largely agree with these SED dates, suggesting this interpretation for the region is largely appropriate. As such, Figure 3.20b shows how this thesis largely follows the extents derived by Barrell (2011) with minor changes to accommodate the more detailed moraine mapping of Dykstra (2012) where available.

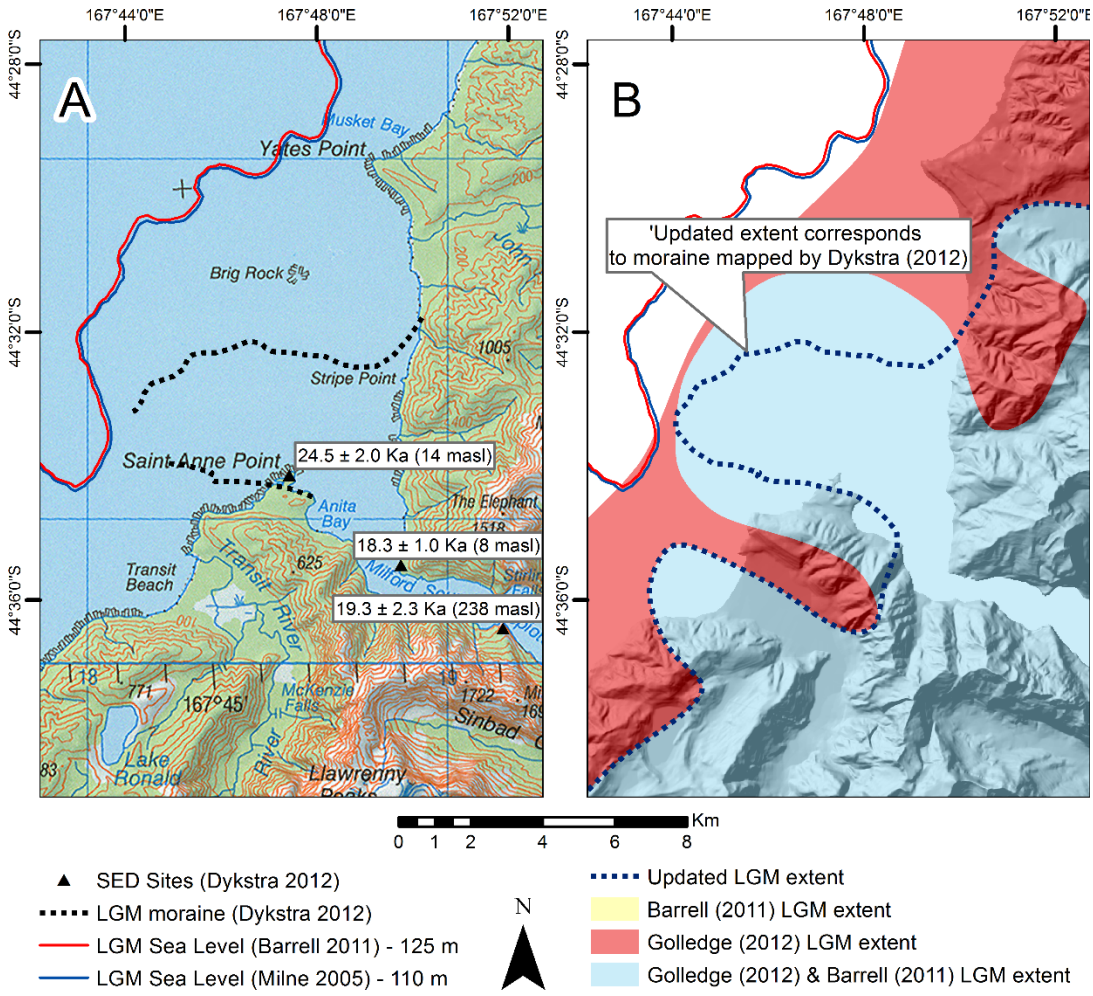

Figure 3.20 a) Site specific data related to LGM extent in the Milford Sound region. b) LGM extent in the Milford Sound region from regional datasets including the 'updated extent' used in this thesis.

3.4.1.10 Waitutu Region

During the LGM, the Waitutu region (Figure 3.8j) contained the large Poteritiri and Hauroko glaciers, representing the southern tip of LGM glaciation on the South Island mainland. Ward (1988) first mapped their extent based on geomorphological evidence (Figure 3.21a), inferring that the glaciers terminated at the inner of two terminal moraine sequences 250 m apart, with the outer sequence presumed to relate to an earlier Otiran advance. The regional extent mapping by Barrell (2011) depicts the ice margin largely inside of the moraines identified by Ward (1988) and up-valley of the contemporary lakes, which would not be expected if they were formed by glacial erosion processes as commonly accepted (Rother *et al.*, 2014). As such, whilst there is no direct age control for the region, the updated LGM outline for this thesis (Figure 3.21b) follows the extents delineated by Ward (1988) as this is

believed to represent a more plausible scenario due to the geomorphological evidence and relative lake positions.

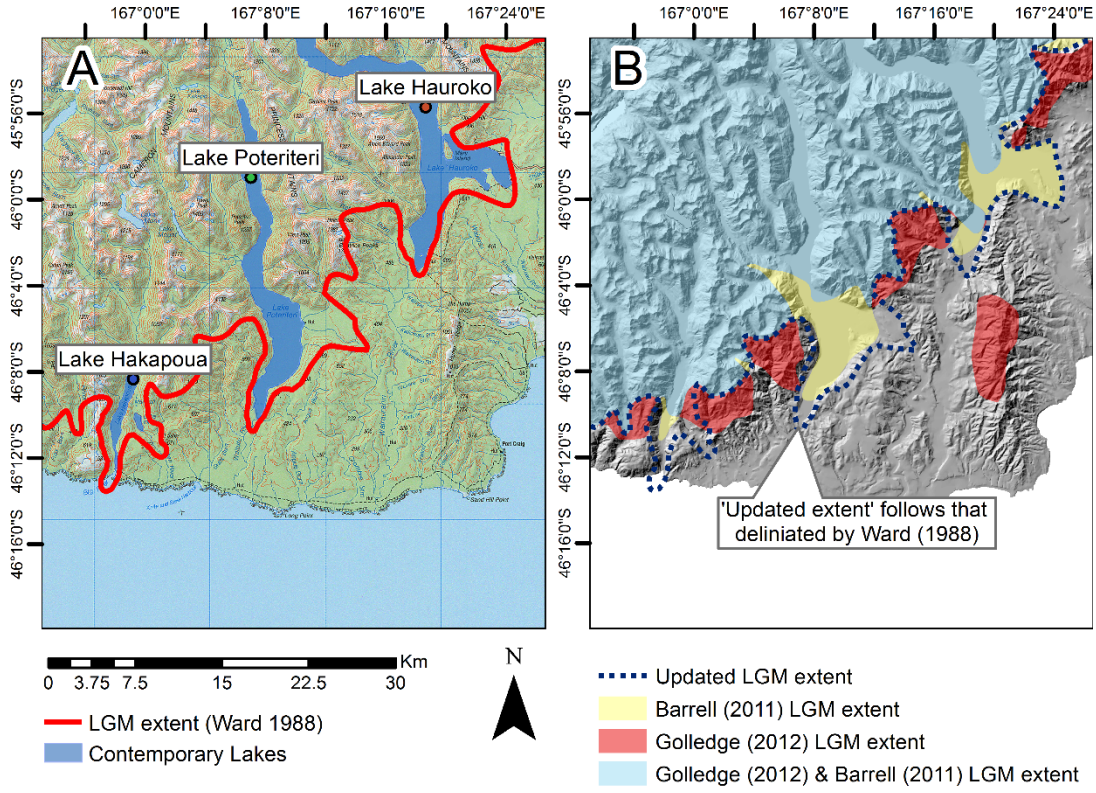

Figure 3.21 a) Site specific data related to LGM extent in the Waitutu region. b) LGM extent in the Waitutu region from regional datasets including the 'updated extent' used in this thesis.

3.4.1.11 Stewart Island

Stewart Island (Figure 3.8k), situated 35 km off the south coast of the South Island is the smallest of the three main islands that form the New Zealand archipelago. During the LGM it was connected to the mainland as a reduced sea level exposed the Foveaux Strait, currently 35 m deep (Brook, 2009). The presence of an ice cap on Stewart Island during the LGM is thought to be unlikely due to the relatively low relief, with glaciation restricted to 'very favourable' locations with small cirques on the highest peaks only (Brook, 2009). With very limited geomorphological evidence and no ice cover delineated by either Barrell (2011) or Golledge *et al.* (2012), the revised LGM outline for this thesis does not include any glacial ice on Stewart Island.

3.5 Constructing a DEM of LGM bed conditions

Former glacier bed topography can be used to reconstruct palaeoglaciers (Benn & Hulton, 2010), and the resultant equilibrium-line altitudes are a widely-used source of palaeoclimatic information (e.g. Benn & Ballantyne, 2005). Whilst contemporary DEMs are often used to represent former glacier beds (Trommelen & Ross, 2010; Golledge *et al.*, 2012), it needs to be considered that landscape modification may have occurred between the capture of elevation data (DEM) and the time of ice occupation, resulting in the DEM not truly representing former glacier bed conditions (Finlayson, 2013). A major objective of this thesis is to explore how the landscape (and associated DEM) of the Southern Alps has changed since the LGM and methods by which the contemporary DEM may be modified to better represent former LGM bed conditions better. The following section of this chapter discusses Holocene activity which may result in the contemporary DEM constituting a poor representation of LGM conditions. Subsequently, a number of 'DEM correction' techniques are presented to modify the DEM as appropriate to better represent LGM bed conditions and thus to provide the primary data input to the REVOLTA model (Chapter 4). The corrections applied are all novel, never having been applied in previous reconstructions of LGM ice in New Zealand. Specifically, they concern (i) removing modern-day glaciers from the DEM, (ii) considering offshore bathymetry as some of New Zealand's west coast LGM glaciers extended onto the continental shelf, (iii) removing modern-day lakes that were inundated by LGM ice, and (iv) considering Holocene valley in-fill sediments.

3.5.1 Removal of contemporary ice from the DEM

Where contemporary glacier ice exists, topographic maps and DEMs will express the present ice surface rather than the Earth's surface below. This discrepancy between ice surface and land elevation needs to be considered when calculating former ice volumes and former ice thickness by 'subtracting' reconstructed surfaces from the DEM because the volume of contemporary ice will effectively be ignored if the standard DEM is used. Furthermore, when using a DEM as the input for reconstruction models e.g. REVOLTA (Chapter 4), (Benn & Hulton, 2010), a DEM representing the palaeoglacier bed is required, which is effectively masked by

contemporary ice if present. These issues need to be considered for the New Zealand Southern Alps where over 3000 glaciers cover an area of 1,157 km^2 (Chinn *et al.*, 2012). These glaciers are estimated to have a volume of 50.67 km^3 (Chapter 2) using the VOLTA model detailed by James and Carrivick (2016), with field thickness measurements exceeding 500 m in places (Hart, 2014). Despite their prevalence, contemporary glaciers have previously been either ignored (e.g. Putnam *et al.*, 2013b) or dealt with in a primitive manner (e.g. Golledge *et al.*, 2012) in reconstructions of LGM glaciers.

In this thesis, contemporary ice has been 'subtracted' from the DEM to help produce a surface which better represents LGM bed conditions. This has been achieved using the results of the VOLTA model described in Chapter 2, helping to produce a surface suitable for palaeoglacier reconstruction from bed topography using the REVOLTA model (Chapter 4). Figure 2.13 shows an example of the ice thickness distribution generated by VOLTA for the central section of the Southern Alps, which is subsequently subtracted from the existing DEM.

3.5.2 Sea level rise: appending an offshore DEM

Sea level during the LGM was approximately 125 m lower than present (Barrell, 2011; Milne *et al.*, 2005). Whilst the geomorphological record clearly shows that glaciers flowing towards the east coast terminated well inland (e.g. Shulmeister *et al.*, 2010), some glaciers on the west coast are known to have extended beyond the present coastline and in some cases likely had tidewater-calving termini (Milne *et al.*, 2005).

Analysis of the updated LGM limits (see section 3.4) reveals just 2.7 % of a total LGM glaciated area occurred beyond the present coastline and consequently outside the limits of standard DEMs (Geographix, 2012). Therefore, an alternative topographical source is required for these presently-offshore areas. For this purpose, 250 m resolution offshore bathymetry data was obtained in the form of the NIWA bathymetric dataset (Mitchell *et al.*, 2012) and these data were appended to the LGM DEM used in this thesis. Although the spatial accuracy of the bathymetric dataset is stated to be variable (Mitchell *et al.*, 2012), the majority of palaeoglacier offshore locations fall within areas mapped by multibeam swath sounders, and so

this research assumes that the bathymetry data for the areas of interest is likely to be sufficiently accurate for the modelling purposes of this project. To create a continuous composite elevation model dataset, the ocean bathymetry had to be resampled to the resolution of the land surface DEM (8 m) and merged.

3.5.3 Contemporary Lakes

Whilst palaeoglaciers are known to have extended past the contemporary coastline and DEM limits, they also occupied areas where contemporary lakes exist, for which standard DEMs only represent the water surface level and not bathymetric data, thus obscuring the former glacier bed. Lakes are especially prevalent in New Zealand as the high sediment flux promotes the formation of large outwash heads and fans, allowing lake development as the glacier retreats. Lakes in the Southern Alps are up to 344 km^2 in area (Lake Te Anau) and up to 462 m deep (Lake Hauroko), (Irwin, 1980), highlighting their potential influence in reconstruction models (Table 3.5).

Table 3.5 Bibliographic reference for original lake bathymetry data and calculated lake volume. Maximum depth and area values are taken from the original reference.

Lake Name	Reference	Volume km^3	Max depth m	Area km^2
Aviemore	(Irwin, 1987)	**0.45**	41	28.1
Te Anau	(Irwin, 1971)	**48.25**	417	344.2
Hooker	(Robertson, 2012)	**0.06**	140	1.22
Maud	(Warren & Kirkbride, 1998)	**0.08**	90	1.40
Godley	(Warren & Kirkbride, 1998)	**0.08**	90	1.99
Mueller	(Robertson, 2012)	**0.02**	83	0.87
Pukaki	(Irwin, 1970b)	**8.9**	98	172.8
Rotoroa	(Irwin, 1982b)	**2.17**	145	23.6
Tasman	(Dykes *et al.*, 2010)	**0.54**	240	5.96
Tekapo	(Irwin, 1981c)	**6.94**	120	96.5
Monowai	(Irwin, 1981c)	**2.56**	161	32.0
McKerrow	(Irwin, 1983)	**1.69**	121	22.9
Manapouri	(Irwin, 1969)	**22.47**	444	138.6
Kaniere	(Irwin, 1982a)	**1.38**	198	14.7
Hawea	(Irwin, 1975)	**24.49**	384	151.7
Hauroko	(Irwin, 1980)	**10.97**	462	71.0
Ohau	(Irwin, 1970a)	**4.56**	129	59.3
Sumner	(Irwin, 1979)	**1.1**	134	13.7
Coleridge	(Flain, 1970)	**3.65**	200	36.9
Benmore	(Irwin, 1981a)	**1.84**	91	75.4
Brunner	(Irwin, 1981b)	**2.24**	109	40.6
Wanaka	(Irwin, 1976)	**31.92**	311	198.9
Wakatipu	(Irwin, 1972)	**64.2**	380	295.4

To produce a DEM representative of LGM conditions, the water depth of each of the lakes shown in Table 3.5 was 'subtracted' from the contemporary DEM. This dataset includes all lakes over 10 km^2 in area, other than Lake Poteriteri which has never

been surveyed. Original lake bathymetry was provided by NIWA and from other scientific publications mainly in the form of scanned paper maps. In this research, each map was georeferenced, with water depth contours ranging in interval between 5 m and 100 m digitized. Bathymetry was adjusted to the lake level of the DEM before a gridded surface was interpolated using the ANUDEM routine (Hutchinson, 1989) with the resultant bathymetry shown in Figure 3.22. These data were subsequently merged with the DEM, helping to produce a surface more representative of LGM bed conditions.

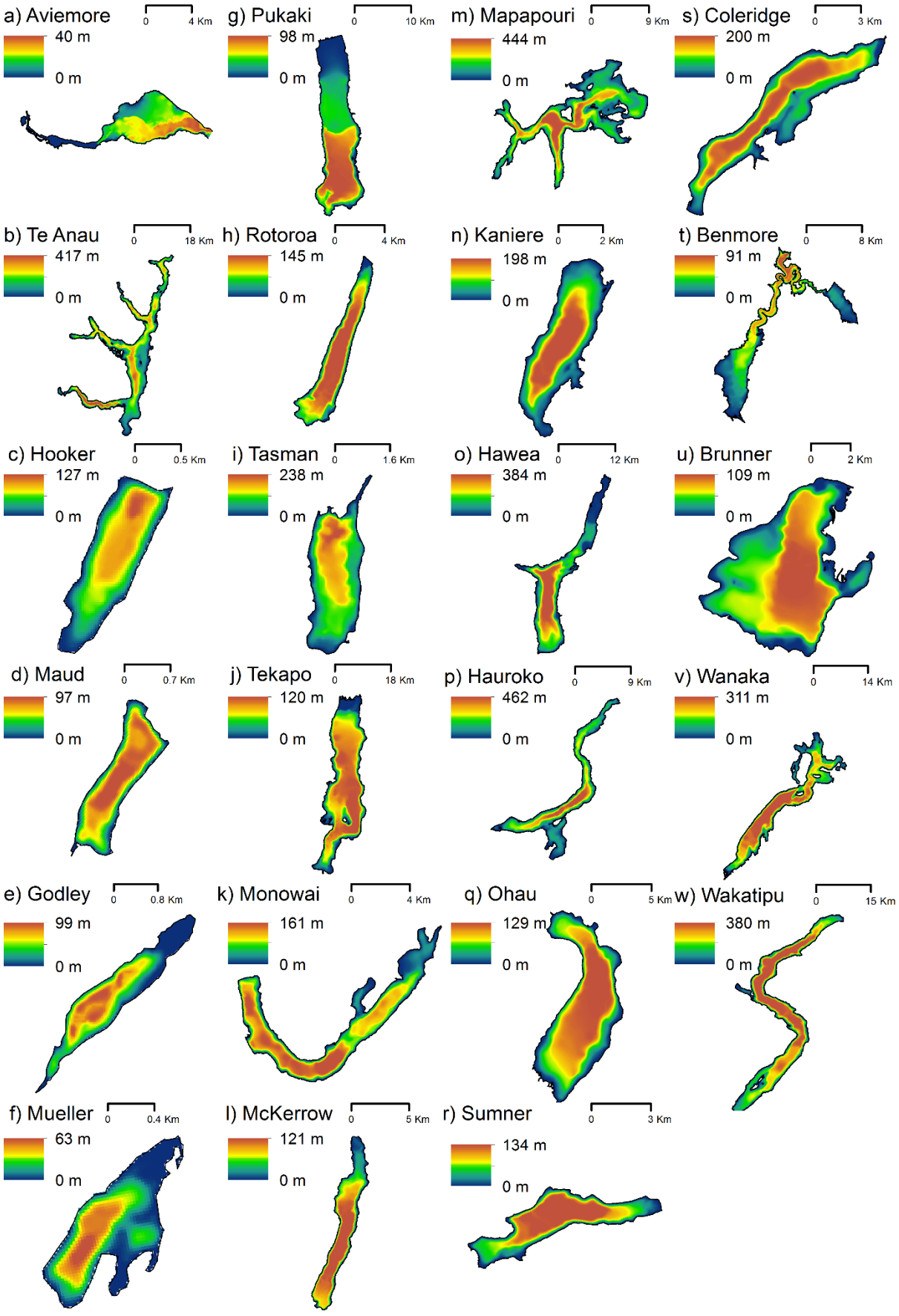

Figure 3.22 Rasterised bathymetry of contemporary lakes in the Southern Alps. Note the wide range of scales.

Digitisation of the bathymetry also permitted calculation of individual lake volume (Table 3.5) which has not been previously quantified in the literature. Interestingly, this reveals that whilst the title of the 'largest lake of the South Island' is often given to Lake Hauroko because it is the deepest recorded at 462 m, or else to Lake Te Anau because that has the largest surface area at 344 km^2, volumetrically the largest is Lake Wakatipu at 64.2 km^3.

3.5.4 Uplift and denudation

New Zealand has one of the world's most dynamic landscapes, with numerous active faults and exceptionally high rates of both uplift and denudation. A startling reminder of the dynamic nature of the Southern Alps occurred on 14th December 1991 when a huge (non-seismic) rock avalanche occurred at Aoraki/Mt. Cook, reducing the height of New Zealand's highest peak by 10 m (Figure 3.23).

Figure 3.23 Peak of Mt. Cook shortly after the rock avalanche of December 1991. (T.Chinn).

Uplift and denudation are processes by which the land surface elevation may be altered over time. Care must therefore be taken when using contemporary DEMs to represent past glacier beds as such landscape evolution between glacial occupation and capture of elevation data may affect the geomorphic expression. For example, ancient lake levels may no longer be horizontal and lateral terraces or moraines may become offset due to differential uplift. Whilst these changes are commonly too

small to introduce significant error (Finlayson, 2013) and are thus commonly ignored in the literature related to palaeoglacier reconstruction in the New Zealand Southern Alps (e.g. Golledge *et al.*, 2012; McKinnon *et al.*, 2012), they at least need to be critically evaluated with respect to the scope of the research to which they are applied.

The Southern Alps of New Zealand did not experience ice sheet glaciation as extensive as in the Northern Hemisphere, and thus isostatic rebound in New Zealand has been minimal (Pickrill *et al.*, 1992), with Mathews (1967) suggesting a maximum of 30 m post-LGM rebound. However, tectonic uplift rates in New Zealand and especially in the Southern Alps are amongst the highest in the world, with the Pacific plate being compressed into the Australian plate (Coates, 2002). Whilst long term Cenozoic uplift rates of 0.1 – 0.3 mm yr^{-1} were estimated by fission track thermochronology (Tippett & Kamp, 1993), rates during the Pleistocene and Holocene are thought to have been considerably greater (Adams, 1980). The Paringa river site on the west coast provides one of the few robust constraints, where marine deposits in an infilled postglacial fiord reach inland of the alpine fault (Putnam *et al.*, 2010). Here, Pleistocene to Holocene uplift rate has been calculated at 8 ± 1 mm yr^{-1} (Norris & Cooper, 2001). The uplift pattern of the Southern Alps is also known to be highly spatially variable, with Adams (1980) inferring the pattern from tilted lake shorelines as shown in Figure 3.24.

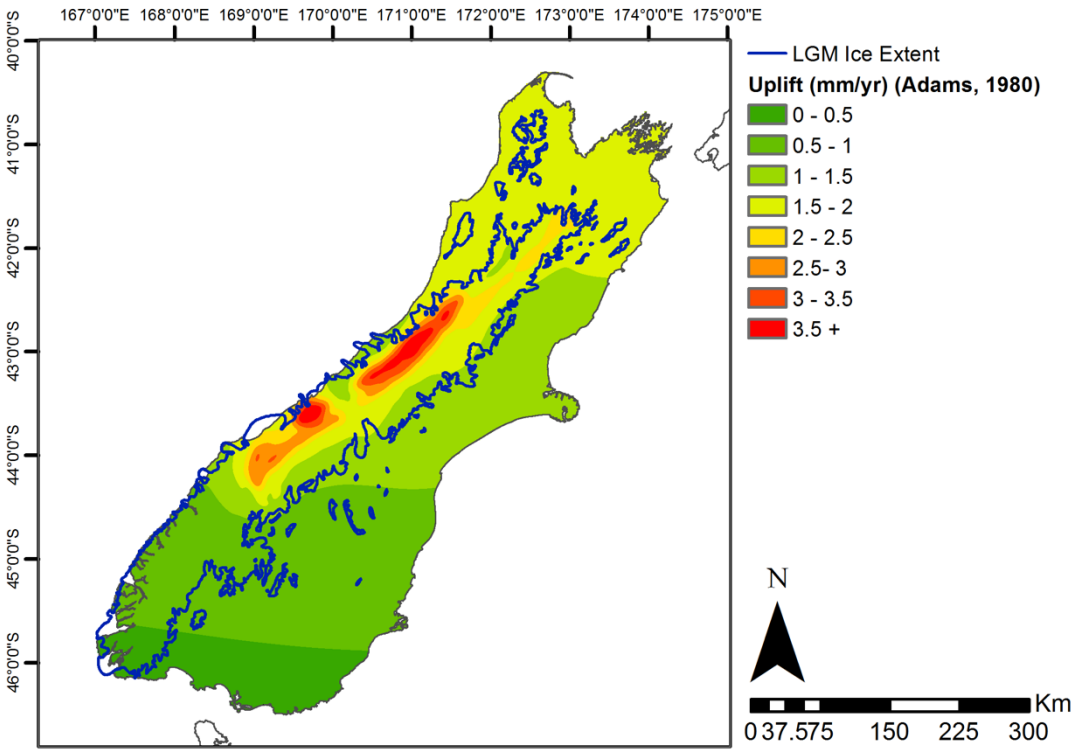

Figure 3.24 Uplift map of the South Island inferred from tilted lake shorelines (adapted from Adams, 1980).

Since AD 2000 semi-continuous and continuous GPS measurements have been collected along a transect running broadly perpendicular to the alpine fault, providing an insight into current uplift rates. Results of the most recently published data (Beavan *et al.*, 2007) shows a maximum average vertical rate of 5.4 mm yr^{-1} for the transect. However, and critically, rates of uplift reduce rapidly with distance from the alpine fault, with the 'NETT' station (29 km from the alpine fault) recording an uplift rate of just 1.8 ± 1 mm yr^{-1} and the Mount John station (68 km from the alpine fault) recording no significant vertical rise (Beavan *et al.*, 2007). As these GPS measurements record current rates, it is acknowledged that they are not necessarily applicable to longer (glacial) timescales. Nonetheless, with contemporary uplift rates reducing exponentially with distance from the alpine fault and no significant rise recorded at 68 km from the fault, and in lieu of any other geological data pertaining to long-term and spatially-distributed uplift rates, it is assumed in this research that it is likely that much of the model domain for an LGM reconstruction would fall within relatively low uplift areas. This is consistent with the inferred uplift pattern by Adams (1980), with the majority of the LGM ice extent occupying low uplift regions as shown in Figure 3.24.

Alongside tectonic uplift, denudation is a major control on the form of the New Zealand Southern Alps, with the tectonically and climatically dynamic environment producing rates up to ten times the global average. Whilst there are relatively few estimates in the literature and no known regional scale maps, Tippett and Kamp (1993) used fission track thermochronology to estimate long term Cenozonic denudation rates ranging from ~2.5 – 0.5 mm yr^{-1}, decreasing with distance from the alpine fault. This is supplemented by contemporary measurements by Adams (1980) who estimated the total river load of the Southern Alps to be 700 ± 200 x 10^9 kg yr^{-1} whilst basin averaged rates for the Nelson/Tasman region are estimated to be between 112 and 298 t km^{-2} yr^{-1} (Burdis, 2014).

Importantly, denudation effectively counteracts uplift, with long term rates in the Southern Alps approximately equal (Adams, 1980). This results in relatively little landscape change when considering the dynamic nature of the Southern Alps. For example, whilst the highest peak in the Southern Alps (Aoraki, Mount Cook) is 3,724 m, the total amount of uplift during orogeny is estimated to be approximately 15 to 20 km (Kamp *et al.*, 1989), highlighting the counterbalance between uplift and erosion. With insufficient data to develop a regional distribution of denudation rates, it is assumed in this thesis that denudation and uplift counteract each other across the Southern Alps, with the contemporary land surface effectively mimicking that at the LGM. With the New Zealand land mass largely in its present configuration by the mid-Pleistocene (Barrell, 2011), this is thought to be a reasonable assumption for the LGM glaciation and more recent glacial episodes, although it may need further consideration if addressing earlier glacial phases.

In summary, whilst it is acknowledged that uplift and denudation may have modified the geomorphic expression of the landscape, there is not enough data to 'correct' the DEM for such changes, and this is a view shared by other authors of studies reconstructing LGM ice across the Southern Alps (e.g. Golledge *et al.*, 2012). These issues of tectonic deformation and denudation will become increasingly prevalent for older glaciations, so care must be taken if other studies were to seek to reconstruct glaciers preceding the LGM.

3.5.5 Postglacial sediment valley infill

Large volumes of sediment accumulated in valley floors is a commonly noted feature of the Southern Alps (Figure 3.25), with high denudation rates and sediment fluxes resulting in thick deposits of up to 500 m in places (McKinnon *et al.*, 2012). This process of landscape modification has previously been recognised as a potential source of uncertainty when reconstructing palaeoglaciers in New Zealand (Golledge *et al.*, 2012) and needs to be considered when using a DEM to represent a former glacier beds. The volume of any sediment accumulated post-glacially will effectively be omitted from palaeo-ice volume calculations if using the contemporary DEM as the baseline (Golledge *et al.*, 2012) whilst also influencing reconstructed ice surface profiles if the contemporary land surface is used as a model input (e.g. Benn & Hulton, 2010; Schilling & Hollin, 1981).

Figure 3.25 The flat valley floor of the Hooker/Tasman valley due to substantial post-glacial sedimentation (W. James)

High resolution DEMs, geophysical methods and GIS have opened up new possibilities for the quantification of sediment volumes and distribution (Otto *et al.*, 2009). As an initial step, planform areas of postglacial valley fill need to be identified, which can be achieved using geomorphological field mapping techniques (e.g. Otto *et al.*, 2009) or using automated approaches (e.g. Straumann & Purves, 2008; Straumann & Korup, 2009). In this thesis, a Python-based ArcGIS script was developed to allow rapid delineation of valley fill storage areas based on the 'region

growing' concept described by Straumann and Korup (2009), requiring just a DEM as the initial input. This method uses the cells along a GIS derived stream network as initial starting points (sediment cells), iteratively assessing neighbouring cells based on their relative elevation difference as shown in Figure 3.26. If the appropriate condition is met, the cell being analysed is assigned as a 'sediment' cell and the process repeated until no more sediment cells are found. For computational efficiency, this process was coded in the Python scripting language, with raster analysis performed using the Numpy package.

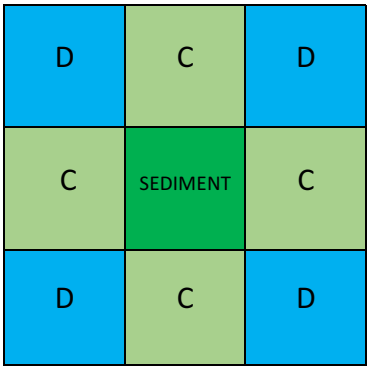

C = Cardinal neighbour, D = Diagonal neighbour.

Cardinal neighbours (C): $\tan(\gamma_c)\,\lambda \geq \Delta E \geq 0$

Diagonal neighbors (D): $\tan(\gamma_c)\,\lambda\sqrt{2} \geq \Delta E \geq 0$

Where γ_c is the gradient threshold, set at 1.5° as described by Straumann and Korup (2009), λ is the cellsize of the DEM and ΔE is the elevation difference between the cell being analyzed and the sediment cell.

Figure 3.26 Diagram of the 'region growing' algorithm initially developed by Straumann and Korup (2009)

Once the sediment areas have been delineated using this method, the total volume of valley infill may be estimated using a volume-area scaling approach. This technique relies upon an empirical relationship between sediment storage area and volume, with this thesis using the relationship developed by Hinderer (2001) which was derived from 16 alpine basins:

$$V = 20.3\,A$$

Equation 10

Where A is the sediment storage unit area (km^2) and V is the sediment storage unit volume (km^3).

For testing purposes, this process was applied to the Pukaki basin in the central New Zealand Southern Alps, where sediment thickness has been measured to a maximum of 510 m (Broadbent, 1974), in agreement with modelling studies (McKinnon *et al.*, 2012). Once the initial stream network was created using the standard 'flow direction' and 'flow accumulation' tools in ArcGIS, the algorithm (Figure 3.26) was applied, delineating a total storage area of 461.8 km^2, as shown in Figure 3.27. Using

the relationship described in Equation 10 the volume of the storage unit was estimated to be 9.37 km^3.

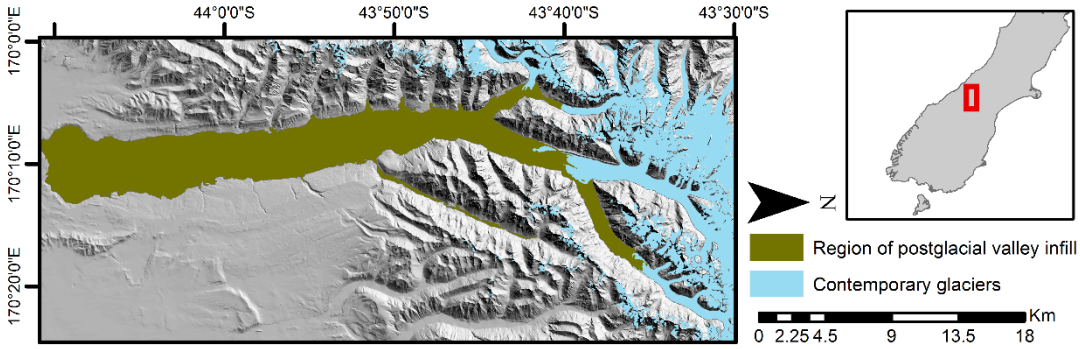

Figure 3.27 Areas of valley infill delineated for the Pukaki basin using the approach outlined in Figure 3.26

Whilst this method demonstrates it is possible to estimate the total volume of sediment stored, it does not give any indication of the distributed sediment thickness or underlying topography, the required input for various palaeoglacier models. (e.g. Benn & Hulton, 2010; Schilling & Hollin, 1981) and the REVOLTA model introduced in Chapter 4.

To address this issue, estimation of fully distributed thickness (to bedrock) may be achieved by extrapolating a quadratic equation fitted to exposed bedrock sections of the valley (Harbor & Wheeler, 1992) or by using a sloping base level approach (Jaboyedoff & Derron, 2005). However, whilst useful in some circumstances, these techniques remove the entire valley fill (to bedrock), which the following recent evidence suggests is unlikely to be suitable for LGM conditions in New Zealand.

It was initially postulated that the majority, or entirety of valley fill in the New Zealand Southern Alps was deposited post LGM (Suggate, 1965; Adams, 1980), simply due to the 'absence of any conflicting evidence' (Adams, 1980 p. 77). This notion has been challenged by recent studies, with Rother *et al.* (2010) suggesting that recent glaciations (including the LGM) were not powerful enough to cause extensive erosion and overrode pre-LGM sediments rather than removing them. Infrared stimulated luminescence (IRSL) dating and sediment analysis of deposits in the Hope valley found the majority of material was deposited during the pre-LGM period of 95.7 to 32.1 ka with only approximately 30 m of sediment accumulation occurring post LGM, overriding 200 m of previous deposits (Rother *et al.*, 2010). This

is consistent with a seismic investigation in the Franz Josef valley by Alexander *et al.* (2014), suggesting that the base of LGM ice was well above the bedrock, with a comparatively minor volume of sediment deposited thereafter. Results of this study are presented in Figure 3.28 with transect W1-W2 showing total sediment thickness (to bedrock) was found to vary between 260 m and 150 m whilst the inferred thickness of post LGM sediments was just 94 m to 47 m.

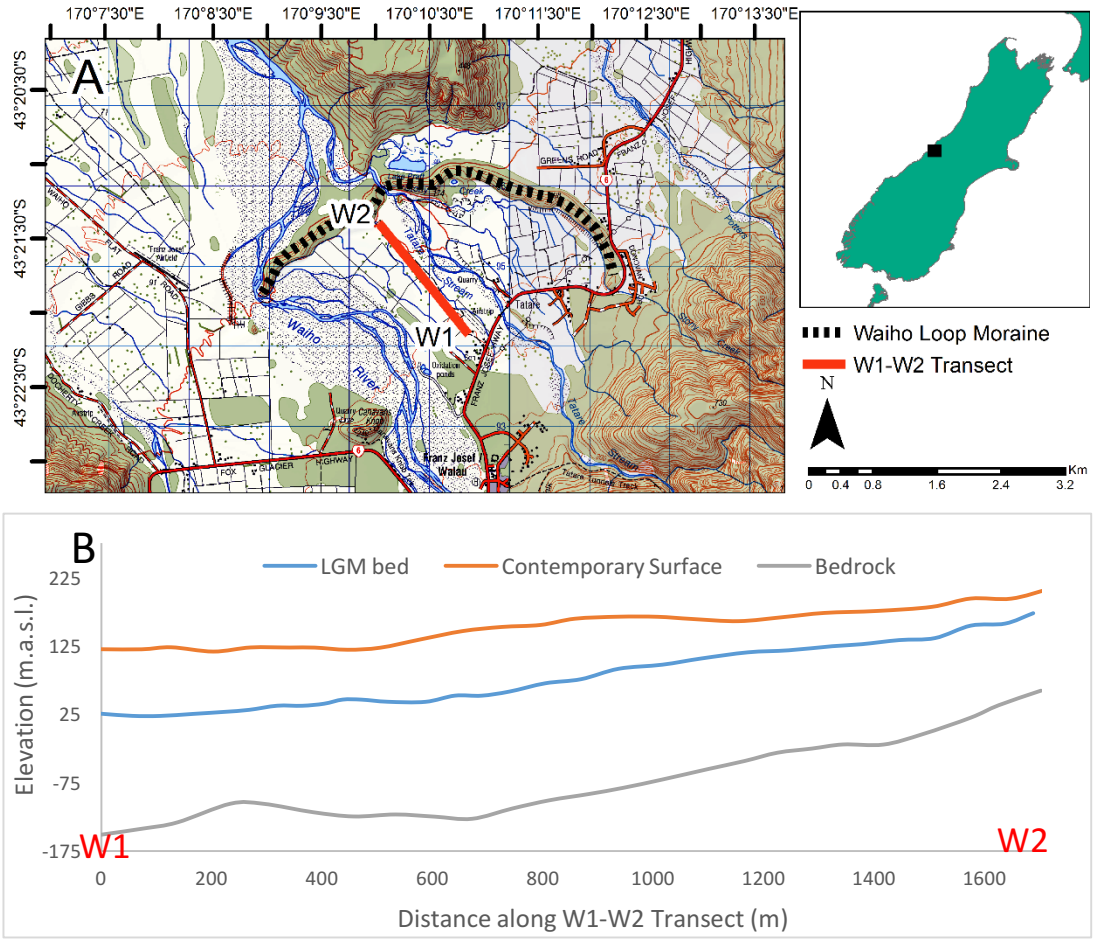

Figure 3.28 a) Location of Waiho Loop landform and W1-W2 seismic investigation transect (Alexander et al. (2014). b) Contemporary surface, LGM bed and bedrock profile along W1-W2 transect. Adapted from Alexander et al. (2014).

Alongside the field based observations discussed above, modelling studies in the New Zealand Southern Alps also support the concept of LGM glaciers overriding sediment from previous glaciations, with McKinnon *et al.* (2012) using mass-flux balance, perfect plasticity and theoretical erosion models to simulate the LGM bed of the Pukaki glacier, all of which simulated the bed well above the imaged bedrock. Figure 3.29 presents the results of McKinnon *et al.* (2012), showing the location of the transect used, the imaged bedrock and the modelled LGM bed profile using their

preferred mass flux balance model. The results are consistent with field based observations from other studies (Alexander *et al.*, 2014; Rother *et al.*, 2007), with the LGM bed overriding up to 300 m of pre-LGM sediment.

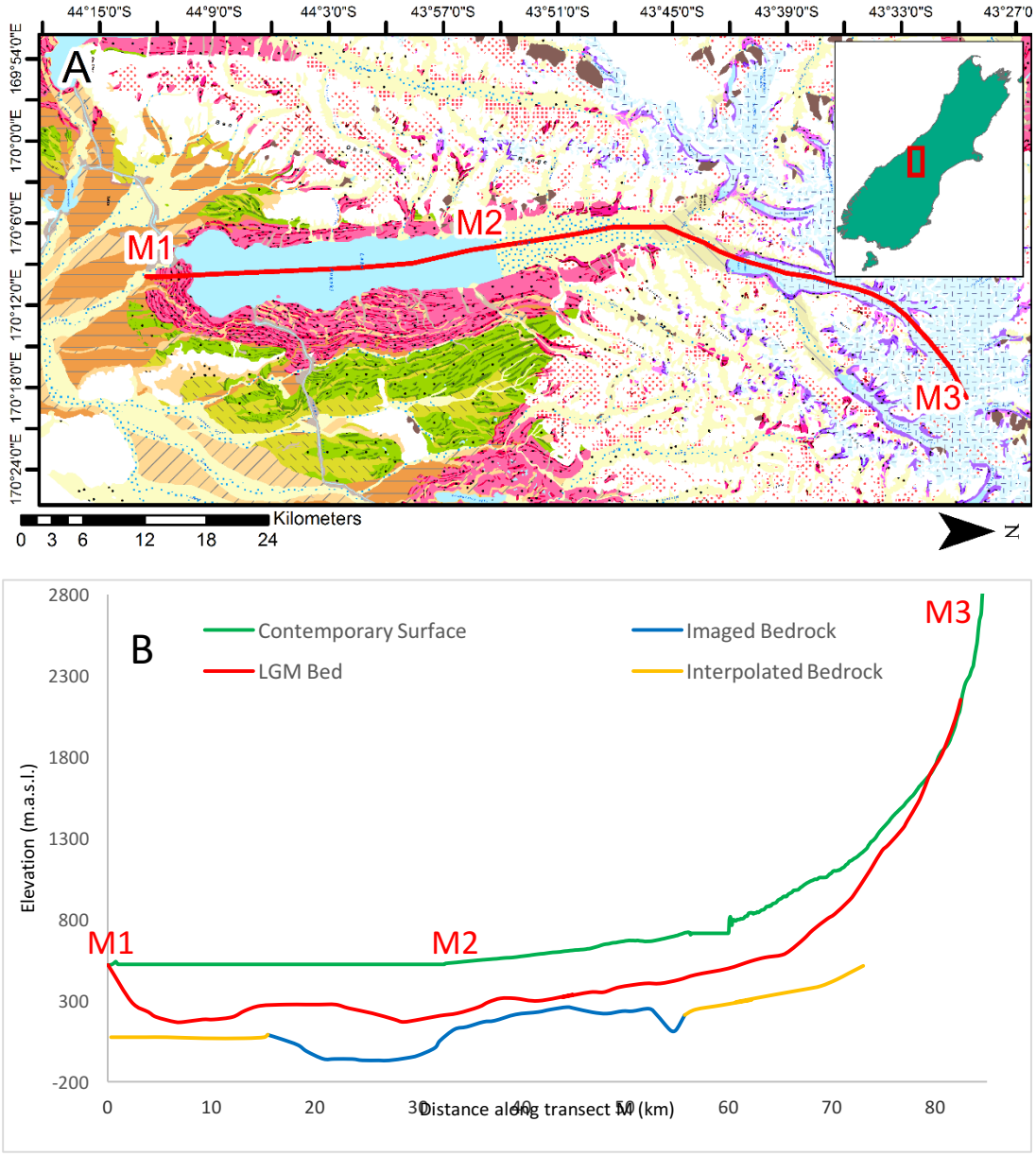

Figure 3.29 a) Glacial geomorphology of the Pukaki/Tasman valley (Barrell et al. 2011) and transect used by McKinnon et al. (2012). b) Contemporary surface, LGM bed and bedrock profiles along M profile (adapted from McKinnon et al. (2012).

In summary, recent field based observations and modelling studies are in agreement that LGM glaciers overrode pre-existing sediments and did not reach the bedrock below. The notion of pre-LGM sediment surviving in glaciated valleys is also consistent with studies outside of the New Zealand Southern Alps, with pre LGM deposits found beneath more recent sediments in the European Alps (e.g. Hinderer,

2001). As such, whilst automated techniques exist to estimate and remove the entirety of sediment infill from a DEM (Harbor & Wheeler, 1992; Jaboyedoff & Derron, 2005), this approach is not appropriate for modelling LGM glaciers of the New Zealand Southern Alps.

3.5.5.1 Distributed post LGM sediment thickness and DEM of the lower Pukaki valley

Whilst there is insufficient data to construct a regional assessment of post-LGM sediment thickness for the New Zealand Southern Alps, this is possible for the Pukaki catchment where the LGM bed profile has been modelled along the valley centreline (McKinnon *et al.*, 2012) (Figure 3.29). In this thesis, estimation of distributed post LGM sediment thickness was achieved by initially using the region growing algorithm introduced in section 3.5.5 to delineate regions of sediment infill (Figure 3.27), followed by interpolation of the LGM sediment thickness estimates provided by McKinnon *et al.* (2012) (Figure 3.29) using the ANUDEM routine (Hutchinson, 1989). Analysis was restricted to the lower 35 km of the valley (transect M1-M2 in Figure 3.29) due to the confluence of tributaries with no thickness estimates. Results are shown in Figure 3.30 with the resultant DEM used in Chapter 4 to assess the sensitivity of the REVOLTA palaeoglacier reconstruction model to postglacial valley infill.

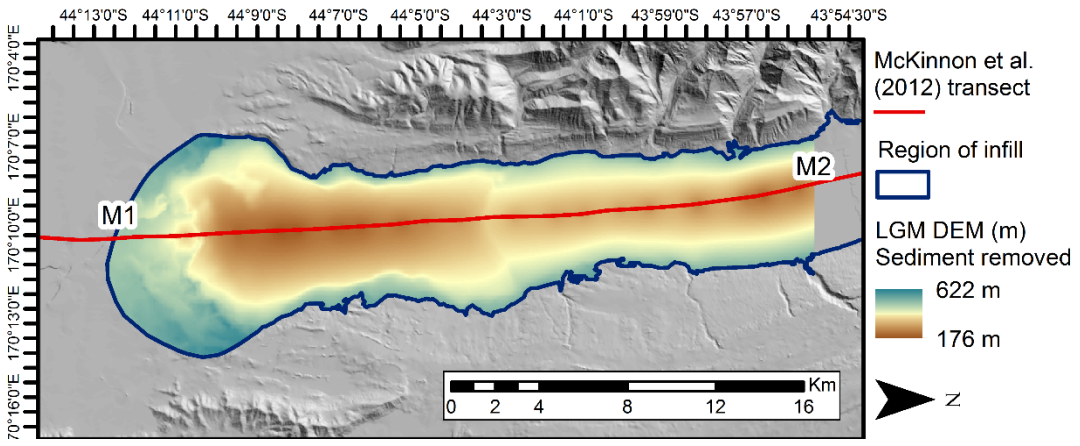

Figure 3.30 Estimated distributed post-LGM sediment thickness for the lower Pukaki valley. The area analysed represents 28.5 km^3 of sediment infill since the LGM.

In summary, the LGM bed elevation will lie somewhere between the contemporary DEM and the level that would exist if all postglacial valley-fill were removed. However, since inferred LGM sediment depths are only available for a few select

locations (Rother *et al.*, 2007), there are not enough data to generate a regional distribution of the LGM bed surface beneath Holocene valley fill sediments. Therefore, with the consensus in the literature suggesting that the majority of sediment was present pre-LGM, in this research, the REVOLTA model (Chapter 4) will be initially applied without removing post LGM sediment. To test the sensitivity of the model to valley infill, scenarios will also be run on the lower Pukaki valley where sufficient data exists to construct a DEM with post LGM sediment removed (Figure 3.30).

3.6 Conclusions

It is clear that there are still many research gaps and unanswered questions surrounding the timing and nature of the LGM (and other glaciations) in the Southern Alps, although recent advances in age control techniques have re-invigorated research and resulted in the traditional models of glaciation being reassessed in some cases. As more high quality samples are processed, it is expected this trend will continue, with an increasingly refined appreciation of LGM conditions. By reviewing the latest research and combining with GIS techniques, this thesis has created the most up to date synthesis of LGM terminus positions currently possible.

New Zealand is a highly dynamic location and it has long been recognised that landscape modification has occurred since glacial occupation. This chapter has attempted to analyse, quantify and evaluate changes which have occurred, with novel techniques explored to 'reverse' these changes from the DEM, generating a surface more representative of the LGM bed. It has been demonstrated that contemporary ice can be successfully 'stripped' from the DEM using the VOLTA model (Chapter 2), the former bed of offshore locations has been approximated using bathymetric data whilst present day lakes have been effectively removed from the DEM by digitizing their bathymetry for the first time.

Whilst it is acknowledged that uplift and denudation has had an impact on the geomorphic expression of the landscape since the LGM, after critical appraisal of the available evidence it is thought that post LGM modifications have been too minor to cause significant error in LGM reconstruction models, although would need to be considered for older glaciations. Furthermore, review of the latest literature regarding valley infill by postglacial sediments suggests that LGM glaciers overrode older sediments, with much of the observed sediment deposited pre-LGM. For these reasons, regional palaeoglaciers reconstructions (Chapter 4) will utilise a DEM with no sediment removed. For catchments where sufficient data exists regarding post LGM sediment thickness, additional modelling will be performed using a 'sediment removed DEM' to assess sensitivity to valley infill.

This chapter has reviewed and amalgamated the most up to date literature and datasets regarding the lateral extent of LGM glaciation in New Zealand, producing

an updated outline of LGM glaciation and a DEM of LGM conditions to represent the former glacier beds. Whilst both of these outputs are novel and useful in their own right, they will also be used as the primary inputs for modelling the former thickness distribution of glacial ice during the LGM in New Zealand (Chapter 4).

Chapter 4. Palaeoglacier and climatic reconstruction of the New Zealand Southern Alps during the Last Glacial Maximum (LGM)

4.1 Introduction

There is debate in the literature concerning both climatic conditions and the 'style' of glaciation during the LGM in the Southern Alps (section 3.3.1). Improved knowledge of distributed ice thickness at the LGM has the potential to address both of these issues, with delineation of vertical ice limits providing an insight into the form of glaciers (e.g. valley constrained vs ice cap) whilst reconstructed glacier geometry and associated equilibrium line altitudes can be used to estimate palaeoclimatic conditions (Benn & Ballantyne, 2005; Ohmura *et al.*, 1992).

With an excellent record of lateral ice extent at the LGM (Chapter 3) combined with well constrained estimates of LGM bed topography (section 3.5), the New Zealand Southern Alps presents an excellent opportunity for LGM glacial reconstructions based on geomorphological evidence. As such, this chapter introduces the REVOLTA (**Re**construction of **Vo**lume and **T**opography **A**utomation) model, with the resultant ice thickness distribution used to estimate climatic conditions.

4.1.1 Previous (3D) palaeoglacier reconstructions of the New Zealand Southern Alps

4.1.1.1 Landform (field based) reconstructions

Until recently, palaeoglacier reconstructions in New Zealand were restricted to individual glaciers, often relying on the interpolation or extrapolation of geomorphological evidence from field-based observations. One of the earliest such studies is presented by Mathews (1967) who used the well-defined landform evidence on the valley walls of the Pukaki and Godley catchments to estimate late Pleistocene glacier ice surface profiles. A similar method was used by Porter (1975) to reconstruct the Pukaki glacier at the Birch Hill, Tekapo, Mt. John and Balmoral stages. These reconstructions were subsequently used to infer former ELAs, which are a very useful parameter for paleoclimate reconstruction (Benn & Ballantyne, 2005). More recently, Kaplan *et al.* (2010) utilised geomorphological-based reconstructions in combination with surface exposure dating to determine climatic conditions during the Younger Dryas stadial in New Zealand, suggesting a distinct warming of the Southern mid-latitudes during this period.

Whilst these studies show that landform based research is a useful tool for reconstructing former glaciers and paleoclimate, they have been restricted to a relatively small sample of catchments where sufficient landform data exists. With growing recognition that individual catchments may not be representative of regional glacial trends or climatic conditions (Rother *et al.*, 2014), caution must be applied when using such localised studies to infer regional trends. Furthermore, whilst these studies may be able to help to constrain the former geometry of individual glaciers, regional analysis is needed to assess the overall style of LGM glaciation in the Southern Alps, which is not possible using field based reconstructions alone.

4.1.1.2 Model based reconstructions

The resources required for fieldwork and the incomplete landform records have resulted in the development of a variety of modelling approaches for palaeoglacier and subsequent paleoclimate reconstruction. Within the New Zealand Southern Alps, reconstruction models have been applied to a number of former glaciers including the Pukaki Glacier (McKinnon *et al.*, 2012), Ohau Glacier (Putnam *et al.*, 2013b), Milford Sound Glacier (Dykstra, 2012) and the Franz Josef glacier. The latter is perhaps the most studied glacier in New Zealand and has been the subject of many reconstructions due to its excellent terminus position record (Purdie *et al.*, 2014) and geographically important location (Anderson *et al.*, 2008). It therefore provides a useful case study of the types of reconstruction models previously applied in New Zealand Southern Alps. An early study by Oerlemans (1997) successfully simulated the position of the terminus in relation to climatic variability using a mass flux model with just topographical and local meteorological data as inputs, inferring an average warming of 0.6 °C per century since the Little Ice Age maximum. This study was later complemented by Anderson *et al.* (2008) who used reconstructed mass balance records to drive an ice flow model, simulating the pattern of retreat throughout the 20th Century and predicting a terminus retreat of 5 km and volume loss of 38 % by the year 2100. Earlier glacial phases have also been modelled, with Anderson and Mackintosh (2006b) using a process based numerical model to conclude a cooling of 3 to 4 °C at 13 ka was required to generate the geometry required for the formation

of the Waiho Loop moraine, although this interpretation has since been questioned (see section 3.2.9).

Whilst the modelling approaches outlined above are able to successfully simulate the former terminus position and potential climatic conditions, data requirements mean they are still confined to individual catchments and provide no information on distributed ice thickness, which is a crucial output for assessing the former style of glaciation and regional climatic variability. As such, additional modelling approaches have also been used to reconstruct the 3D distributed thickness of palaeoglaciers in the Southern Alps. On an individual catchment scale, the distributed thickness of LGM ice in the Ohau valley (section 3.4.2.6) was reconstructed by Putnam et al. (2013b) using a modified version of the University of Maine Ice Sheet Model (UMISM), parameterised by geomorphological evidence, estimating a total ice volume of 280 km^3. The same catchment was also the subject of a coupled energy balance and ice flow model by Doughty *et al.* (2012) generating a distributed ice thickness map for a late glacial advance (14.5 to 12.5 Ka) and inferring an associated cooling of 2.3 to 3.2 °C. These studies have shown the potential for estimating former distributed ice thickness in the Southern Alps, although critically are still only applied to individual catchments and as such may not be reliable indicators for inferring overall regional glacial trends or for reconstructing regional climatic signals (Rother et al. 2015)

4.1.1.3 Regional scale reconstructions of the entire Southern Alps

The questions and uncertainties regarding the Southern Alps LGM discussed in section 3.3.1 (palaeoclimatic conditions, glaciation 'style' and inter-catchment variability in timing) require a regional reconstruction approach of distributed ice thickness that encompasses the entirety of the formerly glaciated Southern Alps. As such, these questions cannot be appropriately addressed using the 2D and catchment specific techniques discussed in sections 4.1.1.1 and 4.1.1.2.

Such a regional simulation presents significant challenges as the steep topography, high precipitation and mild temperatures of the Southern Alps gives rise to a complex yet large-scale system (Chinn *et al.*, 2014). To date the work by Golledge et al. (2012) is the only attempt at such a reconstruction, and that was achieved using

the Parallel Ice Sheet Model (PISM) (www.pism-docs.org) to reconstruct the LGM distributed ice thickness of the entire Southern Alps at a resolution of 500 m. Using topographic (DEM) and climatic inputs, a 'best fit' scenario to the geomorphological limits (Barrell, 2011) was found, with the optimal output shown in Figure 4.1a.

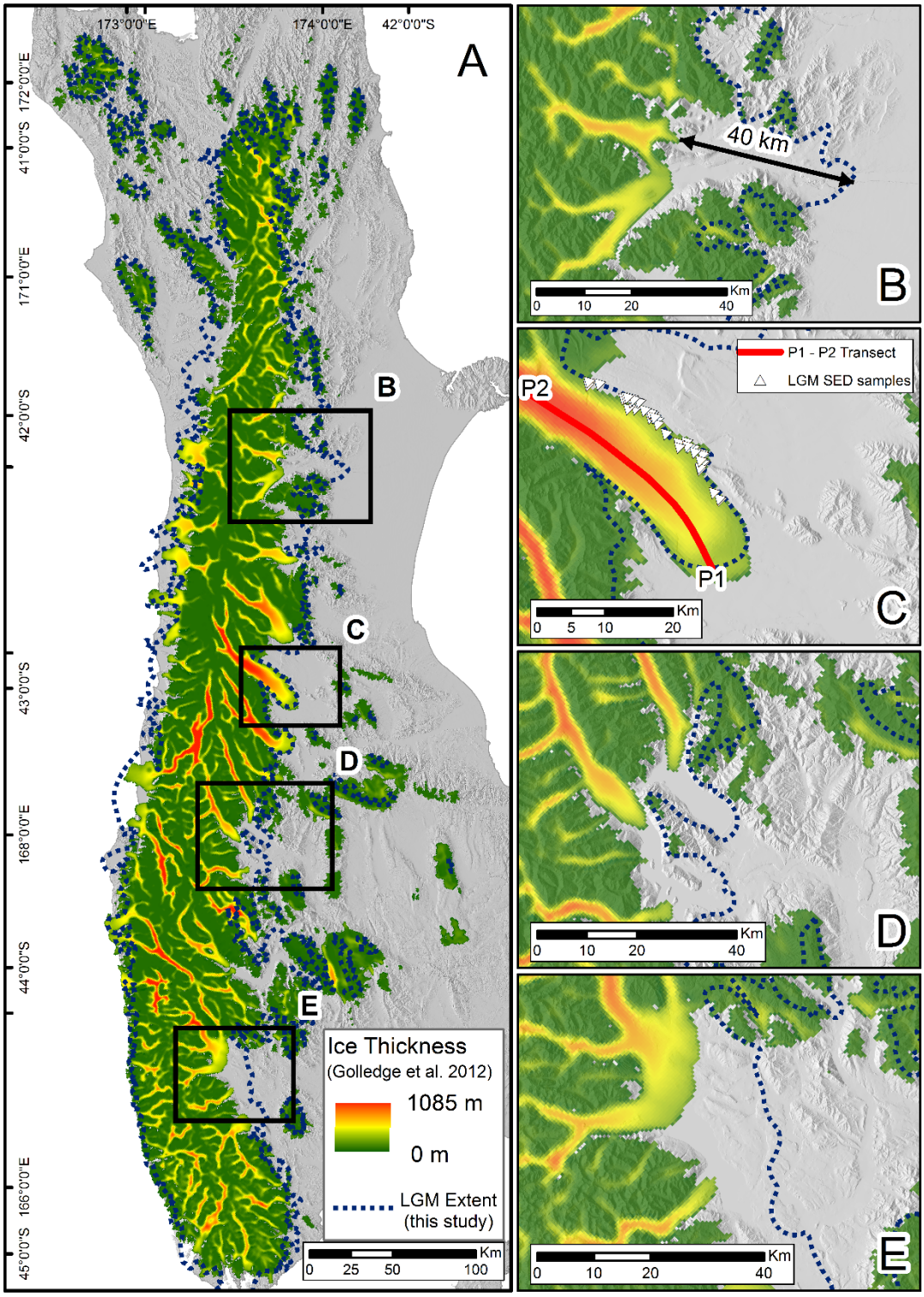

Figure 4.1 a) Simulation of LGM ice thickness for the Southern Alps by Golledge et al. (2012) alongside mapped limits (see section 3.4). Detailed view of: b) Rakaia valley. C) Pukaki valley. d) Lake Hawea / Wanaka region. E) Te Anau region.

To generate the 'best fit' ice thickness distribution, Golledge *et al.* (2012) parameterised a cooling of 6.5 ^{o}C combined with a 25 % reduction in precipitation (from present values) across the entire Southern Alps domain. Warmer scenarios generally resulted in the under prediction of glaciers on the east coast whilst greater cooling inundated lowland regions beyond the geomorphological limits.

Comparison of the 'best fit' scenario against the latest planform ice extents derived from geomorphological evidence (see section 3.4) shows a generally good correspondence (Figure 4.1a), with good agreement in certain individual catchments (e.g. Pukaki Glacier, Figure 4.1c). However, a number of glaciers, especially on the eastern flanks, remain poorly resolved. For example, the simulated extent of the Rakaia Glacier (Figure 4.1b) lies over 40 km from the accepted LGM limits (section 3.4.1.4), with comparable deficiencies in the Lake Hawea / Wanaka region (Figure 4.1d) and Te Anau catchment (Figure 4.1e).

Comparison of the vertical ice extent modelled by Golledge *et al.* (2012) is also possible where sufficient independent evidence exists. Figure 4.2 shows the simulated profile of the Pukaki glacier by Golledge *et al.* (2012) and the location of dated LGM landforms (Kelley *et al.*, 2014; Doughty *et al.*, 2015; Schaefer *et al.*, 2015). Whilst the relative shape of the profile is consistent with the geomorphological evidence, the simulation is higher than the landform evidence by approximately 150 m. Most crucially, despite the lateral extents appearing to match the evidence relatively well (Figure 4.1c), the steep valley sides result in small lateral discrepancies being translated into large vertical errors. Although it may be expected for the centreline profile to be above the associated landforms on the valley sides due to the generally convex shape of glaciers in the ablation zone (Nesje, 1992), the difference is likely to be in the region of 50 m (Glasser *et al.*, 2011) and is therefore unlikely to explain the entirety of the offset observed here.

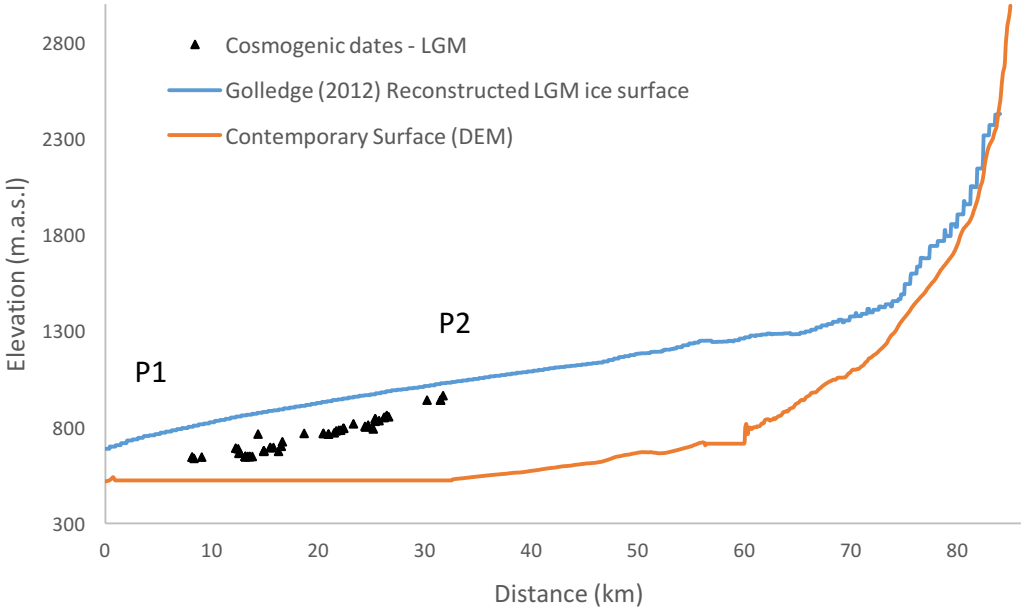

Figure 4.2 Centreline profile of Pukaki glacier modelled by Golledge et al. (2012) and corresponding dated landforms. P1 - P2 transect shown on Figure 4.1.

In summary, from the analysis of the lateral and vertical ice extent evidence, it is clear that whilst the simulation by Golledge *et al.* (2012) provides a good initial reconstruction, it has serious deficiencies in some valley systems (most notably to the east of the main divide) where it is unable to recreate lateral limits or ice thickness derived from field based observations and independent dating studies.

With the synthesis of geomorphological evidence presented in Chapter 3 combined with the availability of high resolution digital elevation models (e.g. Geographix, 2012), there is scope to improve our understanding of LGM conditions by developing a model driven by geomorphological evidence. Such a 'bottom up' approach can be seen as an alternative to the climate driven 'top down' approach of Golledge *et al.* (2012), providing a valuable new approach for researching LGM conditions.

As such, the major objectives of this chapter are: a) to introduce the REVOLTA (**RE**construction of **VOl**ume and **T**opography **A**utomation) tool for reconstructing palaeoglaciers from geomorphological evidence, b) to apply REVOLTA to the Southern Alps of New Zealand to simulate distributed ice thickness at the LGM and c) to use the subsequent glacial reconstruction to estimate palaeo-equilibrium line altitudes and infer potential climatic conditions (specifically temperature and precipitation) at the LGM.

4.2 Methods

4.2.1 REVOLTA: A new tool for reconstructing distributed ice thickness

With the availability of high resolution DEMs of New Zealand (e.g. Geographix, 2012) and well-defined down-valley extent of glaciation (Chapter 3), regional scale modelling is possible within a GIS environment. To help improve our understanding of LGM conditions in the Southern Alps, the REVOLTA (**RE**construction of **VO**lume and **T**opography **A**utomation) model has been developed in this thesis. This model is implemented as an ArcGIS tool, is coded in the Python scripting language and utilises the Scipy package for computational efficiency, allowing it to run on a standard laptop or desktop PC.

In common with the VOLTA model for estimating contemporary ice thickness distribution (James & Carrivick, 2016) outlines in Chapter 2, REVOLTA is a 'perfect plasticity' model, based on the assumption that glacial ice deforms only when a critical yield stress is reached and most suitable for steady-state (equilibrium) glaciological conditions (see section 2.4.4 for further details). REVOLTA requires just a DEM of glacier bed conditions and the down-valley extent of glaciation as initial inputs, and generates a fully-distributed, 3D ice thickness dataset. The workflow of REVOLTA is displayed in flowchart format in Figure 4.3, with additional information on key processes outlined below.

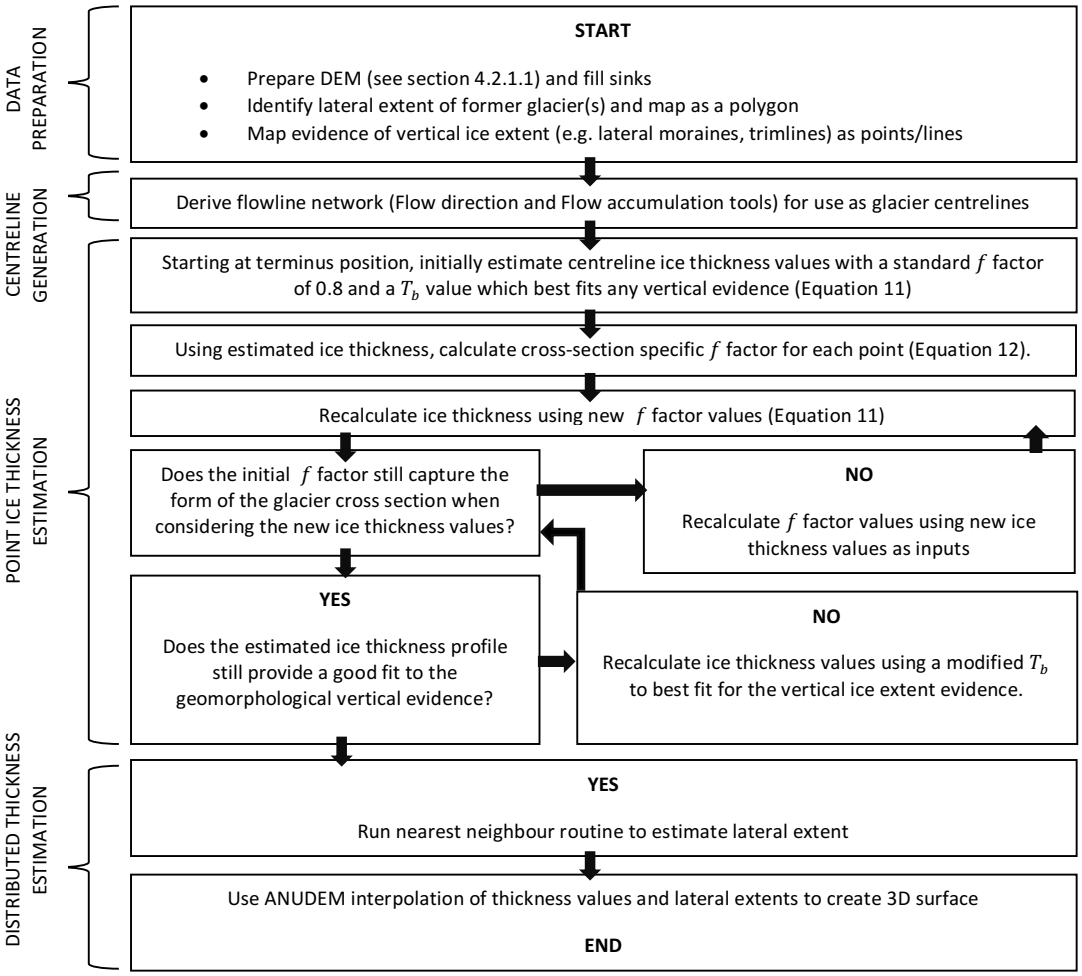

Figure 4.3 Flowchart conceptually illustrating the REVOLTA model

4.2.1.1 Data preparation

REVOLTA requires a DEM of palaeoglacier bed topography as an initial input. If the land surface is unchanged since deglaciation, a contemporary DEM will reflect these conditions and can be used unmodified. However, there are a number of processes which may result in a contemporary DEM no longer representing former bed conditions, which need to be considered for such modelling studies (Finlayson, 2013). Section 3.5 discusses the issues of uplift, denudation, sedimentary infill, contemporary lakes, sea level rise and contemporary glaciers, assessing their potential impact on the DEM record and how they are taken into account to produce a DEM best representative of LGM bed conditions.

The other major requirement of REVOLTA is the location of the down valley extent of glaciation, which can often be inferred from geomorphological evidence. An in depth review of LGM ice extent across the Southern Alps is provided in section 3.4 of this thesis, with an updated synthesis dataset of that evidence. This dataset

provides the down valley extent of LGM glaciation for all major catchments in the Southern Alps, permitting regional scale modelling.

4.2.1.2 Centreline generation

REVOLTA initially estimates ice thickness values at points along a network of centrelines. In common with other glaciological studies (Schiefer *et al.*, 2008; Machguth & Huss, 2014), centrelines are derived using a GIS approach, using a hydrological routing approach. This method requires any sinks (closed depressions or basins) in the DEM to be filled and uses the 'Flow Direction' and 'Flow Accumulation' tools in ArcGIS. Each centreline is subsequently clipped to the mapped down valley extent.

4.2.1.3 Point ice thickness estimation

Once centrelines have been generated, ice thickness values are iteratively calculated at points along the centrelines using a perfect plasticity approach, in a similar manner to the Excel™ program developed by Benn and Hulton (2010). The original basis for this method was introduced by Schilling and Hollin (1981), stating that:

$$h_{i+1} = h_i + \left(\frac{T_b/f}{H}\right)_i \frac{\Delta x}{pg}$$

Equation 11

Where h is the ice surface elevation, H is the ice thickness, T_b is the basal shear stress (equal to the yield stress), f is a 'shape factor' representing the proportion of the driving stress supported by the bed (see section 2.4.4 for more details), p is ice density (917 kg m^{-3}), g is gravitational acceleration (9.81 m s^{-2}) and Δx is a specified interval of distance along the centreline. Full details of the final derivation can be found in Benn and Hulton (2010) and the original Excel™ program can be downloaded from doi:10.1016/j.cageo.2009.09.016. Although this is an excellent user-friendly implementation for the 2D reconstruction of glacier surface profiles along a centreline, it provides no information on the 3D distributed ice thickness. Furthermore, it requires the user to manually extract and input the initial bed topography information, which is a time consuming process, especially when considering multiple glaciers and centrelines. REVOLTA improves upon the original

model by: a) providing a fully distributed ice thickness output and b) automating the process in a GIS environment, allowing the rapid reconstruction of palaeoglaciers at a regional scale.

4.2.1.4 Shear Stress

Under Equation 11, the basal shear stress (T_b) is a critical parameter for estimating palaeo ice thickness as it determines when ice will deform. T_b is generally between 50 and 150 KPa for mountain valley glaciers (Paterson, 1994), although it may vary between individual glaciers due to various factors (e.g. basal sliding, ice viscosity, subglacial deformation). Whilst REVOLTA has the option to vary T_b along an individual centreline if appropriate data are available, a constant value along the profile is usually sufficient for modelling purposes as this has been shown to adequately reproduce thickness estimates along the length of a centreline (Li *et al.*, 2012) and successfully applied to palaeoglacier reconstruction studies (e.g. Rea & Evans, 2007).

Defining the basal shear stress value so that the reconstructed profiles match independent (usually landform based) ice thickness estimates is a standard and accepted method for parameterising perfect plasticity based models (e.g. Schilling & Hollin, 1981; Benn & Hulton, 2010; Murray & Locke, 1989). In the event of insufficient evidence being available, a global average value - often 100 kPa (Nye, 1952) is sometimes used. For example, Rea and Evans (2007) employed a constant value of 100 kPa for the entire Øksfjordjøkelen region of Norway whilst Locke (1995) used the same value for reconstructing former glaciers in the Rocky Mountains.

Although the standard perfect plasticity model assumes motion by internal deformation only, basal sliding may also contribute to motion if glaciers are wet based. With the general consensus of a relatively temperate climate during the LGM in New Zealand (see section 3.3.1.1) it is highly likely that LGM glaciers in New Zealand were wet-based and basal sliding was occurring. This notion is supported by geomorphological evidence in the form of striated and abraded bedrock, deformable subglacial till and the transport of erratics through subglacial pathways (Mager & Fitzsimons, 2007). Basal sliding can be accommodated within perfect plasticity based models by prescribing a softer ice rheology via a lower T_b value (Veen, 2013;

Golledge, 2015). Thus basal sliding will be implicitly considered if using landform based evidence (from the location being studied) to parameterise T_b but needs to be considered if using an average value from the literature (by manually changing T_b). Whilst prescribing a softer ice-rheology via landform based evidence is suitable for reconstructing former profiles, it should be noted that in these cases T_b effectively becomes a 'lumped parameter' and further calculations, such as estimates of ice velocity, requiring just T_b as an input may be spurious (Golledge, 2015). As such, the results of this thesis are restricted to volume and thickness distribution with no attempts made to infer ice dynamics.

4.2.1.5 Shape factor

In the case of valley glaciers and other topographically-controlled ice bodies, it is unrealistic to assume that the bed shear stress equals the driving stress as side-drag from the valley walls provides resistance to the flow (Paterson, 1994). This effect is commonly incorporated into perfect plasticity models using a 'shape factor' (f) as shown in Equation 11. Whilst other studies simply assign a standard f value of 0.8 (Linsbauer *et al.*, 2012), REVOLTA dynamically adjusts f depending on the local valley geometry using a modified version of the method described by (Benn & Hulton, 2010):

$$f = \frac{A}{Hp}$$

Equation 12

Where A is half the glacierised area, p is half the glacierised perimeter and H is the ice thickness at the centreline (Figure 4.4). As described in the REVOLTA flowchart (Figure 4.3), an initial approximate ice surface elevation and cross section is generated by using a standard f value of 0.8 (Nye, 1965). From this initial cross section, a 'valley geometry based' f value can be calculated using Equation 12 as shown in Figure 4.4, which is subsequently used to update the ice surface elevation. In a similar approach to that of Benn and Hulton (2010) an iterative process is now applied to determine if the valley geometry based f value adequately describes the updated cross section (here defined as within an error of ± 0.1), recalculating the ice

surface elevation and valley geometry based f value until an appropriate solution is found.

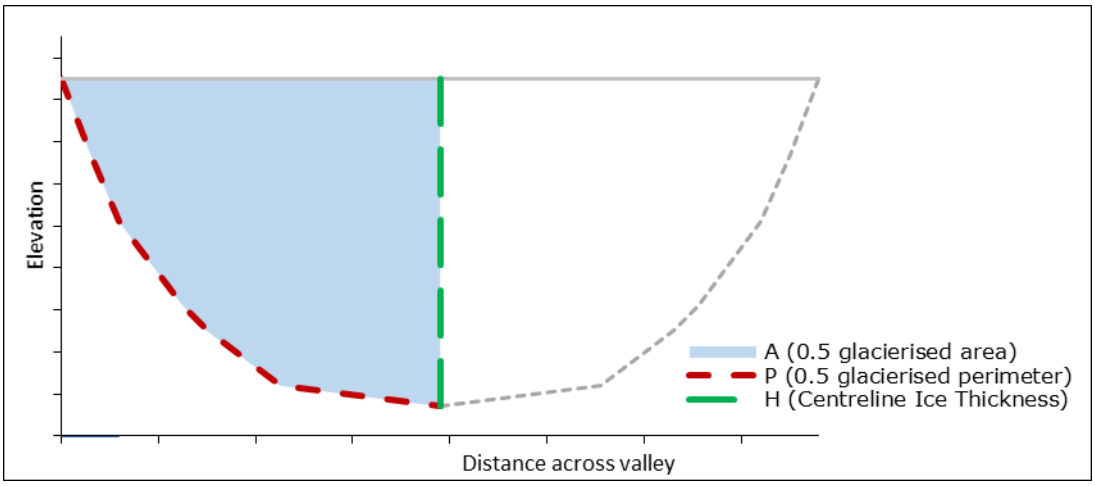

Figure 4.4 Conceptual diagram of valley cross-section and parameters for calculating shape factor (f)

Whilst the original Excel™ program by Benn and Hulton (2010) requires the manual extraction of cross-sectional profiles from topographic maps, the process is automated in REVOLTA using a novel 'nearest neighbour' technique. At each ice thickness point along the centreline, REVOLTA searches for the nearest DEM cell which is of equal or greater elevation. This process identifies a single point on a valley side where the ice surface cross-section intersects (Figure 4.5), thereby permitting the automatic generation of valley cross sections.

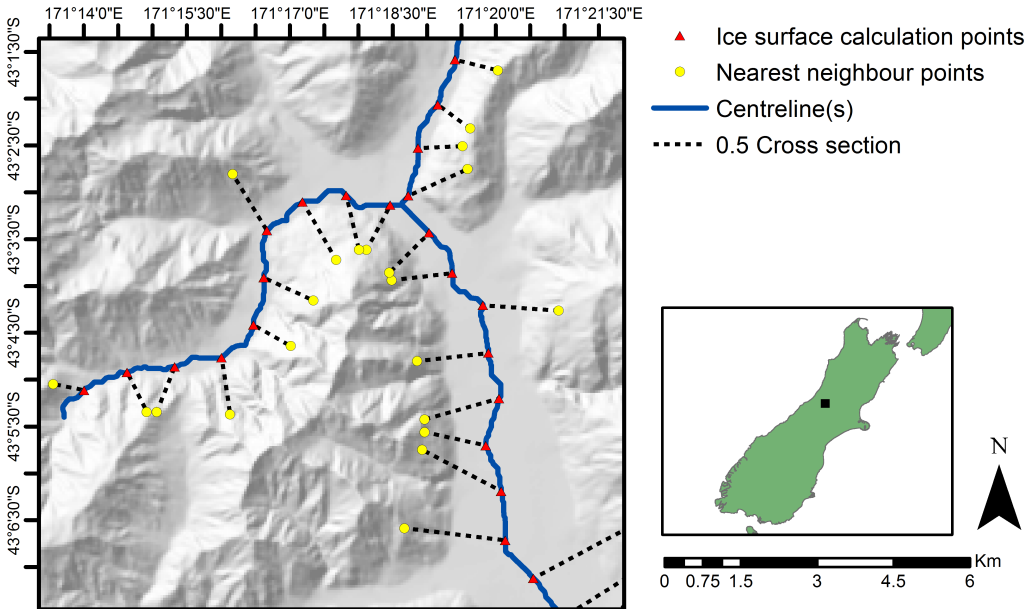

Figure 4.5 Example of the 'nearest neighbour' routine for automated calculation of cross-section profiles

During REVOLTA development, multiple nearest neighbour searching of this form was found to be a computationally intensive and slow task, with prototype modelling concluding the standard ArcGIS tools were unable to cope with the large data requirements. A bespoke Python coded solution was therefore developed, with the DEM converted to a Numpy Array and a KD-tree (De Berg, 2010) approach used to locate the nearest neighbour. Whilst producing the same output as the standard ArcGIS tools, this method is much more computationally efficient, allowing REVOLTA to run on a standard desktop PC.

4.2.1.6 Creation of a 3D surface

REVOLTA initially estimates ice surface elevations along a set of central flowlines in a 2D fashion. Although this provides a reconstruction of the former surface profile, it does not estimate distributed thickness or volume. To achieve this, a 'nearest neighbour' approach is combined with a 'glaciologically correct' interpolation routine to generate a 3D surface.

For each point at which the ice surface elevation is estimated along the centreline, the 'nearest neighbour' approach (section 4.2.1.5) is used again to find the closest point along each of the valley sides which is of equal or greater elevation (Figure 4.6). Here, the procedure is executed twice for each point (once for each valley side). The resultant points effectively mark the lateral extent of glaciation (zero ice thickness) and are used in the subsequent interpolation routine (Figure 4.6). Once the nearest neighbour points have been located on each of the valley sides, the ANUDEM 5.3 interpolation routine (Hutchinson, 1989) is used to generate a fully distributed surface. This interpolation routine is an iterative finite difference technique designed for the creation of hydrologically correct DEMs and is widely used for glaciological applications (e.g. Farinotti *et al.*, 2009; Li *et al.*, 2012; Linsbauer *et al.*, 2012). ANUDEM is implemented via the 'TopoToRaster' tool in ArcGIS, using the initial centreline elevations and nearest neighbour point elevations as 'spot elevation' inputs (zero ice thickness), with an example output shown in Figure 4.6.

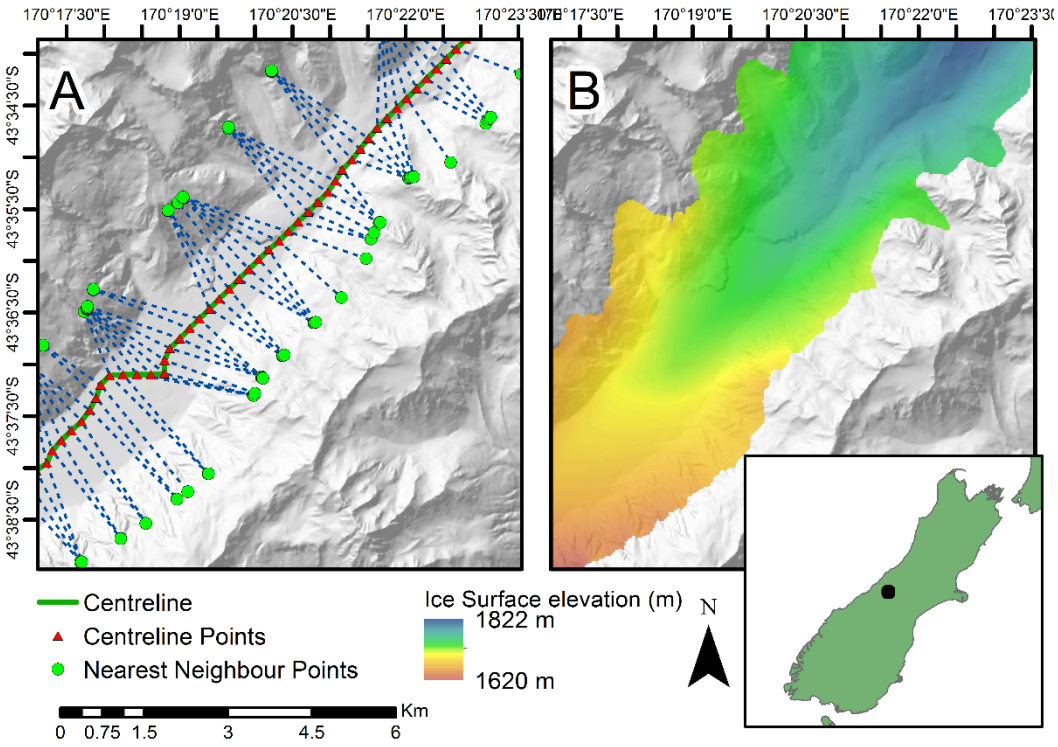

Figure 4.6 Example of 3D ice surface generation procedure. a) Centreline with point ice thickness estimates and nearest neighbour points b) Interpolated ice surface

4.2.1.7 Transverse glacier profiles

For a glacier in steady state, flow will converge towards the centreline in the accumulation zone and diverge towards the margins in the ablation zone, commonly resulting in a concave transverse profile above the ELA and a convex profile below (Nesje, 1992). Using the nearest neighbour approach shown in Figure 4.6, REVOLTA generates generally 'flat' transverse ice surface profiles, which are perhaps not indicative of the typical convex-concave profiles.

Some reconstruction studies use the contemporary ice surface profile to inform the degree of curvature (e.g. Carrivick *et al.*, 2015; Porter, 1975; Carrivick *et al.*, 2012), whilst Glasser *et al.* (2011) allowed an offset of 50 m between the ice surface on the centreline and at the margin. It is possible to prescribe such curvature into the REVOLTA model by applying an offset during the nearest neighbour search, with Figure 4.7 demonstrating the influence of an offset on the output surface. However, it is difficult to estimate the magnitude of offset required and its variation along the profile for palaeoglaciers, especially in studies comprising of multiple glaciers. With the offset unlikely to be more than 50 m for mountain valley glaciers (Glasser *et al.*, 2011), the impact on reconstructed ice thickness distributions is likely to negligible.

Furthermore, volume over-prediction in the ablation zone will be counterbalanced by volume under-prediction in the accumulation zone, reducing the overall impact of transverse profile curvature error. For these reasons, whilst it is acknowledged that the standard model may not reproduce the typical convex-concave transverse profiles, REVOLTA does not take into account such curvature by default, although this can be optionally included if the degree of curvature is known.

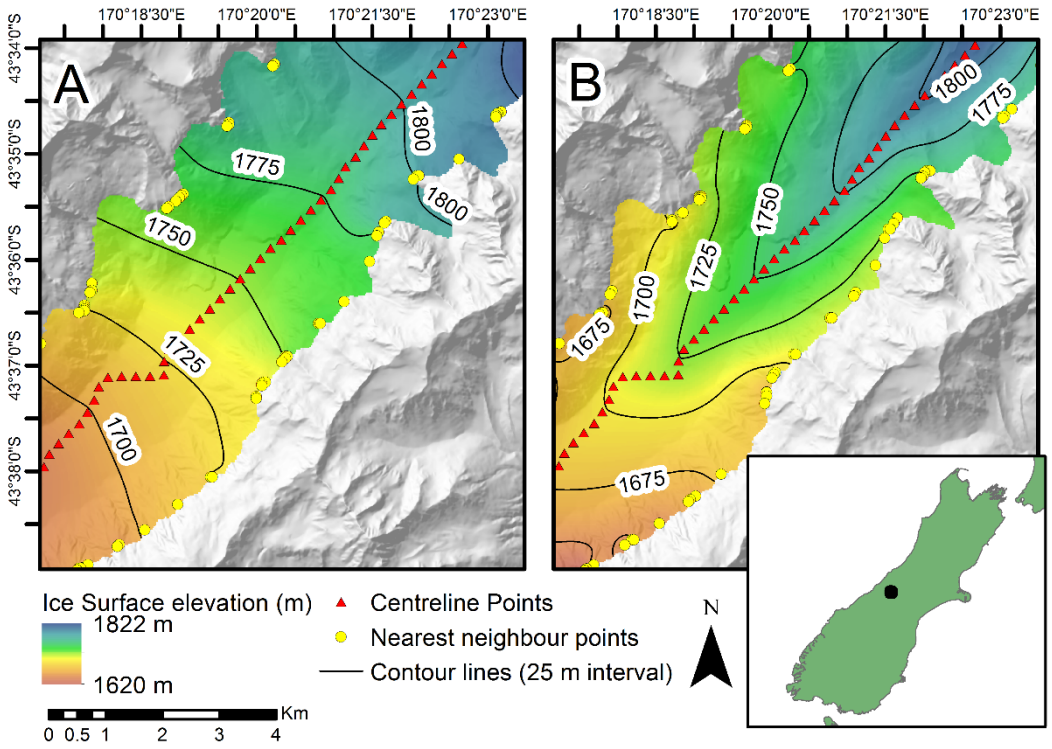

Figure 4.7 a) Standard REVOLTA derived ice surface (no transverse curvature) b) Ice surface with convex curvature enforced

4.2.1.8 Automated palaeo-ELA estimation

The equilibrium line altitude (ELA) of former glaciers is of great interest for glaciological and paleoclimate study (Benn & Ballantyne, 2005). There are a number of methods available for estimating the ELAs of palaeoglaciers, based on either landform evidence of reconstructed glacier geometry (Table 4.1) although many are laborious and time consuming, especially when considering multiple glaciers. With REVOLTA permitting the output of high resolution palaeoglacier reconstructions at a regional scale, there is scope to automate the ELA estimation procedure for multiple glaciers, improving calculation time and reliability.

Table 4.1 Methods for estimating the ELA of palaeoglaciers. Adapted from Pellitero *et al.* (2015) and Carrivick and Brewer (2004).

Name of method	Type	Description
Cirque floor	Landform	ELA inferred to lie above the elevation of the cirque floor. (Péwé & Reger, 1972)
Maximum elevation of lateral moraines	Landform	ELA approximated by up glaciers limit of lateral moraines (from glaciation being studied)
Ice surface contours	Geometry	ELA approximated where ice surface contours transition from convex (ablation zone) to concave (accumulation zone).
Altitude ratio – median altitude	Geometry	ELA approximated to be halfway between the altitude of the glacier head and glacier terminus
Altitude ratio – terminus head altitude (THAR)	Geometry	Assumes the ELA lies at some fixed proportion of the altitudinal range of the glacier.
Accumulation-Area Ratio (AAR)	Geometry	Most widely used method, assumes a constant ratio between the accumulation area and ablation area. Empirical studies suggest the ratio of the accumulation area to the total area is approximately 0.65 (Hubbard & Glasser, 2005)
Median Glacier elevation (MGE)	Geometry	Assumes the ELA lies at the median glacier elevation.
Area-altitude balance ratio (AABR)	Geometry	The second most widely used ELA estimation technique, although recognised to be more robust than the AAR and MGE methods as it takes into account mass balance gradients and glacier hypsometry (Pellitero *et al.*, 2015).

Recently, Pellitero *et al.* (2015) developed an ArcGIS based Python toolbox for the automated estimation of ELAs using either the Accumulation Area Ration (AAR), Area-Altitude Balance Ratio (AABR), Area Altitude or Median Glacier elevation (MGE) methods (Table 4.1), requiring just the reconstructed surface topography of the glacier as an initial input. Whilst the original tool presented by Pellitero *et al.* (2015) can only estimate the ELA of a single glacier per model run, it provides a promising method for automated ELA estimation at a regional scale. As such, the initial code has subsequently been modified in this thesis to allow the iterative ELA calculation for multiple glaciers and has consequently been applied to LGM palaeoglaciers of the New Zealand Southern Alps.

This thesis uses the Accumulation Area Ratio (AAR) method (Table 4.1) for estimating former ELAs of the Southern Alps. That method was deemed the most appropriate firstly because it is the most widely used method for estimating former ELAs (Pellitero *et al.*, 2015) with numerous examples of its application in the literature (e.g. Benn & Ballantyne, 2005; Kerschner *et al.*, 2000), including in New Zealand (Porter, 1975). Secondly, whilst the alternative Area-Altitude Balance Ratio (AABR) may sometimes be considered more robust (Pellitero *et al.*, 2015), it incorporates a

number of assumptions which may not be indicative of LGM glaciers in the New Zealand Southern Alps. For example, the AABR method is best suited to clean, snow fed glaciers and should technically not be applied to glaciers with extensive debris cover or inputs from avalanching. Whilst debris cover at the LGM in New Zealand is likely to be lower than present due to glaciers extending into regions of lower uplift and erosion, combined with covering a larger proportion of the catchment reducing the source area (McKinnon *et al.*, 2012), the steep topography and high precipitation of the Southern Alps is likely to have resulted in avalanche inputs. Furthermore, the AABR method assumes that a glacier is constrained by topography, with a change in climate reflected in a change in terminus elevation. This is not the case for piedmont style glaciers which extend into lowland plains (Pellitero *et al.*, 2015), such as those known to have occurred in some locations across the Southern Alps of New Zealand during the LGM (see section 3.4).

The initial script developed by Pellitero *et al.* (2015) uses the ArcGIS 'SurfaceVolume_3D' tool, which is part of the standard 3D analyst package. The tool iteratively calculates the area above and below a given altitude in response to the altitudinal extent of the glacier. Besides the reconstructed topography, the only additional requirement of the AAR method is the specification of the ratio between the accumulation area and total area of the reconstructed glacier. Empirical studies suggest that a value of 0.65 is appropriate for glaciers in steady state (e.g. Hubbard & Glasser, 2005). This value is also consistent with Porter (1975) who suggested an AAR ratio of 0.6 ± 0.05 for Quaternary glaciers in the New Zealand Southern Alps. As such, with REVOLTA reconstructing glaciers with equilibrium profiles, 0.65 was therefore deemed appropriate, with the associated uncertainty explored in section 4.3.7.

4.2.2 Palaeoclimatic reconstruction

Former ELAs are of great interest for palaeoclimatic study as they offer a valuable tool for estimating palaeo-precipitation or palaeo-temperature. Relationships have been developed between temperature and precipitation at the ELA (e.g. Ohmura *et al.*, 1992; Braithwaite, 1984), allowing for one of the parameters to be estimated provided an independent estimate of the other is available (e.g. Benn & Ballantyne,

2005). For modelling purposes, a scaled version of contemporary temperature or precipitation may be used as the independent estimate, thereby providing a method for exploring the influence of a specified temperature change on palaeo-precipitation or vice-versa.

Relationships between precipitation and temperature are possible to derive as annual accumulation will exactly equal annual ablation at the ELA. With ablation correlated with summer temperatures and accumulation correlated with precipitation (Benn & Ballantyne, 2005), a positive correlation also exists between summer temperatures and precipitation at the ELA (Ohmura *et al.*, 1992). Precipitation - temperature relationships have been developed for specific regions such as Russia / Asia (Kotlyakov & Krenke, 1982), North America (Leonard, 1989) and Europe (Sutherland, 1984) amongst others. These region-specific examples differ in form due to the varying interplay between surface energy balance and air temperature at each location (Benn & Ballantyne, 2005), although such a relationship has never been derived for the Southern Alps of New Zealand. This issue is negated by Ohmura *et al.* (1992) who compiled a global dataset of 70 glaciers spanning both hemispheres (including the Tasman glacier, New Zealand Southern Alps), smoothing out regional variations in energy balance. The globally averaged relationship between summer temperature and precipitation at the ELA derived by Ohmura *et al.* (1992) is defined as:

$$P_a = 645 + 296T_3 + 9T_3^2$$

Equation 13

Where P_a is the water equivalent annual precipitation (mm yr^{-1}) and T_3 is the 3-month mean summer temperature in °C (December, January, February in the Southern Hemisphere). Whilst the standard error of the relationship described by Equation 13 is quite large (± 200 mm), it is nevertheless a powerful tool for estimating palaeo-precipitation.

Furthermore, Equation 13 can also be rearranged to solve for summer temperature (T_3) if an independent measure of precipitation is available:

$$T_3 = \frac{1}{9}\sqrt{9P_a + 16009} - 148$$

Equation 14

In this thesis, reconstructed LGM ELAs of the New Zealand Southern Alps are combined with estimates of palaeo-precipitation and palaeo-temperature using Equation 13 and Equation 14 to assess the likely climatic conditions required to generate the ELAs and glacier geometry in question. A similar approach was employed by Benn and Ballantyne (2005) to estimate former precipitation during the Loch Lomond re-advance for glaciers of the West Drumochter Hills, Scotland, but it has never been applied on a broader scale. Palaeoclimatic reconstruction of this nature allows the spatial pattern of precipitation / temperature change to be considered, which contrasts with the findings of 'top down' glaciological (ice dynamics driven by climate reconstruction) models which assume a homogenous change in temperature and precipitation across the entire model domain (e.g. Golledge *et al.*, 2012; de Boer *et al.*, 2015).

Figure 4.8 shows the contemporary temperature and precipitation datasets used in the modelling of this thesis. The precipitation dataset (Figure 4.8a) was provided by NIWA and is based upon data from 2002 irregularly-spaced precipitation gauges, spanning the time period 1981 to 2010, generating a 500 m resolution dataset. The orographic effect of the Southern Alps is clearly visible, with precipitation totals reaching 13,000 mm yr^{-1} close to the main divide before rapidly diminishing to < 500 mm yr^{-1} over the eastern ranges.

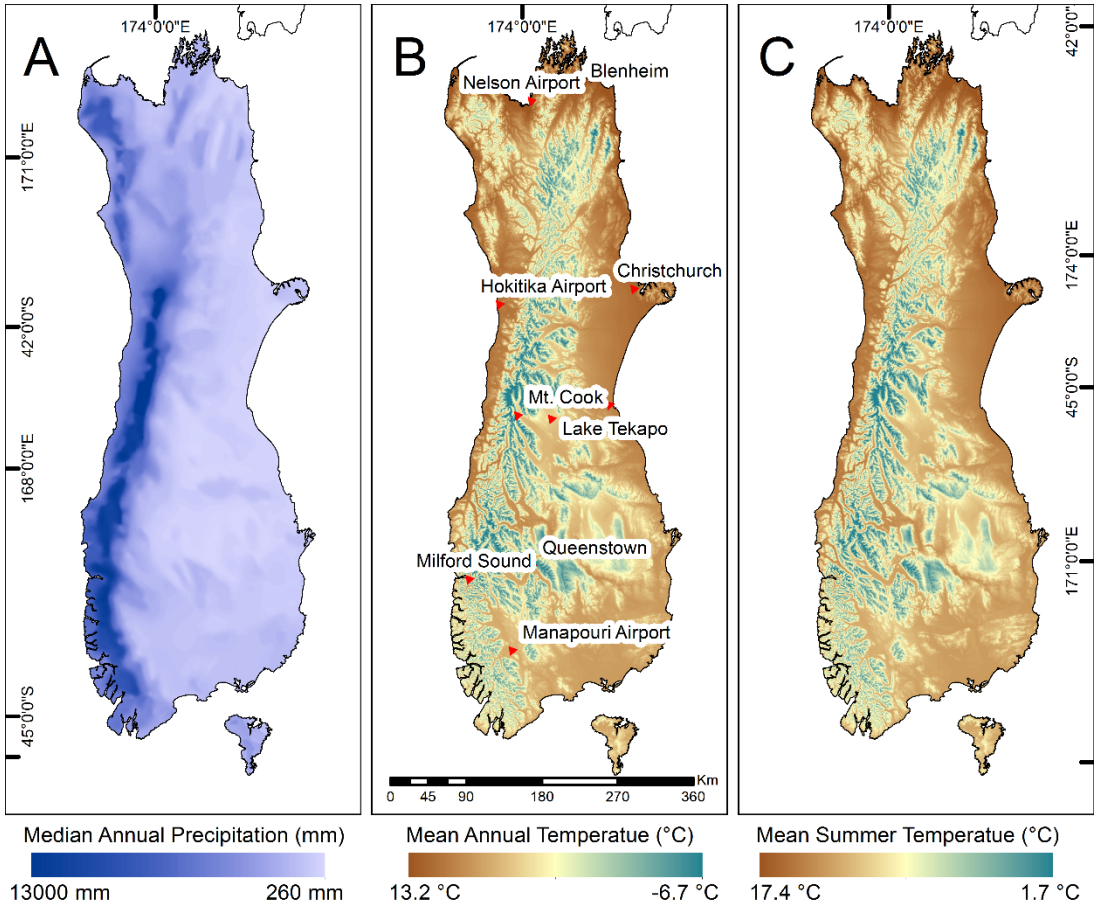

Figure 4.8 Contemporary climatic data for New Zealand South Island. a) Median annual precipitation (NIWA data). b) Mean annual temperature (Landcare data) c) Mean summer temperature (derived from Figure 4.8b using Equation 15)

The contemporary air temperature distribution (Figure 4.8b) was sourced from New Zealand Landcare Research, downloaded from https://lris.scinfo.org.nz/. This 25 m resolution dataset shows the mean annual temperature across the entire South Island for the years 1950 to 1980 and was originally created by coupling a DEM to consider lapse rates with air temperature data from 300 weather stations (Leathwick & Stephens, 1998). The altitudinal effect of the Southern Alps is clearly defined, with mean annual temperatures as low as minus 6.7 °C in the heavily glaciated Mt. Cook region. A latitudinal gradient is also evident, with temperatures gradually increasing further north.

Both the original precipitation and temperature distributions were originally created using a trivariate interpolation routine from a thin plate smoothing spline. Further details of the datasets and interpolation can be found in Wratt *et al.* (2006). Analysis of earlier versions of the same datasets by Leathwick and Stephens (1998) notes the

annual average uncertainties for the interpolated surfaces are ± 0.37 °C for the temperature dataset and ± 148.5 mm for the precipitation dataset. These uncertainties refer only to the interpolation process and do not take into account additional errors such as precipitation under-catch due to snowfall (Golledge *et al.*, 2012). Despite the limitations, it can be considered that the climatic datasets presented in Figure 4.8 adequately represent the long-term average contemporary conditions, smoothing out high frequency variability (e.g. due to ENSO/SAM cyclicity).

Equation 13 and Equation 14 define the temperature parameter as mean summer temperature (T_3), whilst the contemporary temperature dataset (Figure 4.8b) is expressed as annual mean temperature. This difference therefore needs to be taken into account when using the contemporary temperature dataset as the input or for comparison with the output. This can be achieved by converting annual temperatures to summer mean temperatures and vice-versa by using an empirical relationship in a similar manner to Benn and Ballantyne (2005). In this thesis, a relationship between mean summer temperature (T_3) and mean annual temperature (T_a) was derived for the New Zealand Southern Alps based on monthly mean temperatures (1981-2010) recorded from 10 meteorological stations spanning the extent of the Southern Alps (downloaded from https://www.niwa.co.nz/educationandtraining/schools/resources/climate/meanairtemp), with the location of each site shown on Figure 4.8b. The resultant relationship (R^2 = 0.8373) was derived, allowing the estimation of T_a from T_3 or vice versa:

$$T_a = 1.0577\, T_3 - 5.6331$$

Equation 15

Using Equation 15, Figure 4.8c shows the resultant temperature distribution for summer months based on the original annual dataset (Figure 4.8b). As expected, whilst the overall pattern of mean summer temperatures is consistent with that of annual temperatures, their magnitude is higher, ranging from 1.7 °C to 17.4 °C.

4.3 Results

4.3.1 Parameterising shear stress values for the Southern Alps at the LGM

In a select number of catchments within the New Zealand Southern Alps, the vertical extent of LGM glaciation is extremely well constrained, where fine-detail geomorphological mapping (e.g. Porter, 1975; Barrell *et al.*, 2011) combined with datasets of dated landforms provides age control (Table 4.2). Such information allows the estimation of T_b via manual model parameterisation to best-fit the known ice surface limits, in the manner as described by Benn and Hulton (2010). The Pukaki valley is perhaps the best example in the Southern Alps, where over 50 dated samples from a 40 km long series of lateral moraines provides an excellent constraint of LGM vertical ice limits. Table 4.2 summarises the various sites within the Southern Alps where vertical LGM ice limits are well constrained (both from dated landforms and alternative models), permitting the manual parameterisation of T_b. The location of each site is indicated in Figure 3.8 showing their distribution across the Southern Alps, on each side of the main divide and at a range of latitudes.

Table 4.2 Locations used for manually parameterising shear stress value for use in REVOLTA

Location	Description	Reference(s)
Pukaki valley	Clearly defined 40 km lateral moraine sequence constrained to LGM period (18 – 30 ka) by over 50 SED samples from various studies	Doughty *et al.* (2015) Kelley *et al.* (2014) Putnam *et al.* (2010) Schaefer *et al.* (2006) Schaefer *et al.* (2015)
	Glaciological model (PISM)	McKinnon *et al.* (2012)
Ohau valley	Series of SED samples constraining lateral moraines to LGM period (18 to 30 ka).	Putnam *et al.* (2013b)
	Glaciological model	Putnam *et al.* (2013a)
Milford Sound	Series of SED samples between 8 – 238 m.a.s.l within LGM period (18 to 30 ka)	Dykstra (2012)
Waimakariri Valley	SED samples constraining various geological features to LGM period (18 to 30 ka)	Rother *et al.* (2015)
Cascade valley	Clearly defined 13 km long lateral moraine dated to LGM (~21.85 ka) by a series of cosmogenic samples.	Sutherland *et al.* (2007)

Whilst these sites provide good evidence for specific catchments, LGM ice surface elevation limits are poorly defined for the majority of the Southern Alps, with not enough evidence to generate a regional distribution of shear stress values. Whilst glacial landforms have been dated in additional catchments (section 3.4) many of these are related to the terminus position only or apply to non-LGM events (e.g.

Kelley *et al.*, 2014; Putnam *et al.*, 2013a), thus providing little scope for directly determining LGM vertical extent in these catchments.

With insufficient evidence for individual catchment parameterisation, a single shear stress value for the entire Southern Alps was derived in this thesis to best-fit all of the available evidence indicated in Table 4.2. This approach is more reliable than simply using a globally-averaged value (e.g. Rea & Evans, 2007; Locke, 1995) because it encapsulates the climate and nature of glaciation in the Southern Alps (e.g. by implicitly considering styles of glacier motion including basal sliding). Whilst this regionally-averaged approach may not accommodate some inter-catchment variability, it can be considered appropriate for modelling that is mostly interested in volumetric and geometric details, rather than local ice dynamics or local thermal regime, for example.

The generally concave-convex transverse profiles above and below the ELA (Nesje, 1992) is considered in this thesis during the parameterisation process. With the majority of landform evidence pertaining to ice surface vertical extent being situated in former ablation zones, it is very likely that centreline elevations will be higher than corresponding evidence on valley sides. The exact offset is difficult to determine, although Glasser *et al.* (2011) suggests 50 m as a good initial approximation. Therefore, a value was sought to generate a central ice surface profile approximately 50 m above the valley-side landform evidence.

The exact age of samples within the LGM window (18 to 30 ka) was also considered as it acknowledged that glacial decline may have begun to occur in some catchments by the end of this period (e.g. McKinnon *et al.*, 2012). Whilst the parameterisation is based mainly on the geomorphological evidence (see section 3.4), palaeo ice surface profiles generated by other modelling studies were also considered (Table 4.2), thereby providing additional estimates of vertical extent.

The results of parameterisation are shown for each catchment (selected due to their geographical spread and excellent independent record of LGM vertical extents) in Figure 4.9. It was found that a T_b value of 30 kPa best fitted the available evidence, providing an acceptable fit to all of the locations parameterised. Since these catchments are situated both to the east and west of the main divide and with good

latitudinal coverage too, it seems as if a single value of T_b is appropriate for the entire Southern Alps, thus negating the need to vary T_b on a catchment by catchment basis. The sensitivity of model results to changes in T_b is further explored in section 4.3.4.2 with various permutations of T_b tested.

It should be noted that the geomorphological technique employed here to parameterise T_b effectively includes basal sliding as a component (as discussed in section 4.2.1.4), resulting in T_b becoming a 'lumped parameter'. As such, the T_b value here is lower than may be expected for a 'true' basal shear stress value and those employed in modelling of contemporary glaciers in Chapter 2.

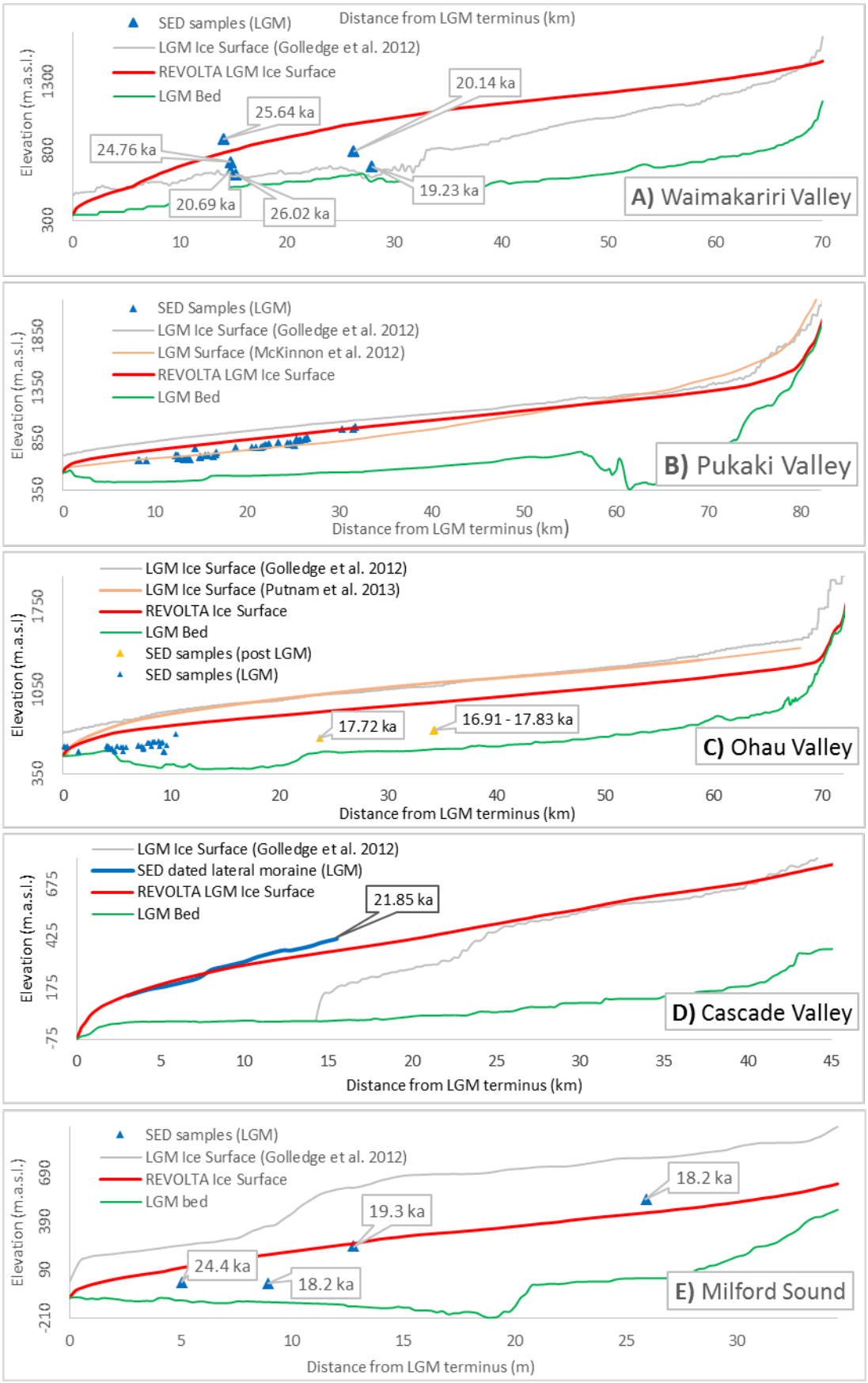

Figure 4.9 Optimal surface profiles (30 kPa) for each parameterisation site with independent evidence indicated.

4.3.2 Distributed ice thickness

The REVOLTA modelled ice thickness distribution of the entire Southern Alps is shown in Figure 4.10a, alongside 3D visualisations of specific regions of interest. The model clearly demonstrates the large, predominantly valley-constrained glaciers flowing to the east of the main divide (e.g. Pukaki Glacier, Figure 4.10b) and the piedmont style glaciers coalescing on the west coast (e.g. Haast Glacier, Figure 4.10c). A large number of nunataks are present, especially around the high peaks of the Mt. Cook region whilst fewer are present south of the Lake Wakatipu region where mountain peaks are lower in elevation, with a localised icefield is modelled in the Fiordland region (Figure 4.10e). A small number of the outlet glaciers on the west coast reach the LGM shoreline, with a very small proportion of the total ice volume occurring beyond. A maximum ice thickness of 1108 m is located at the Wakatipu glacier.

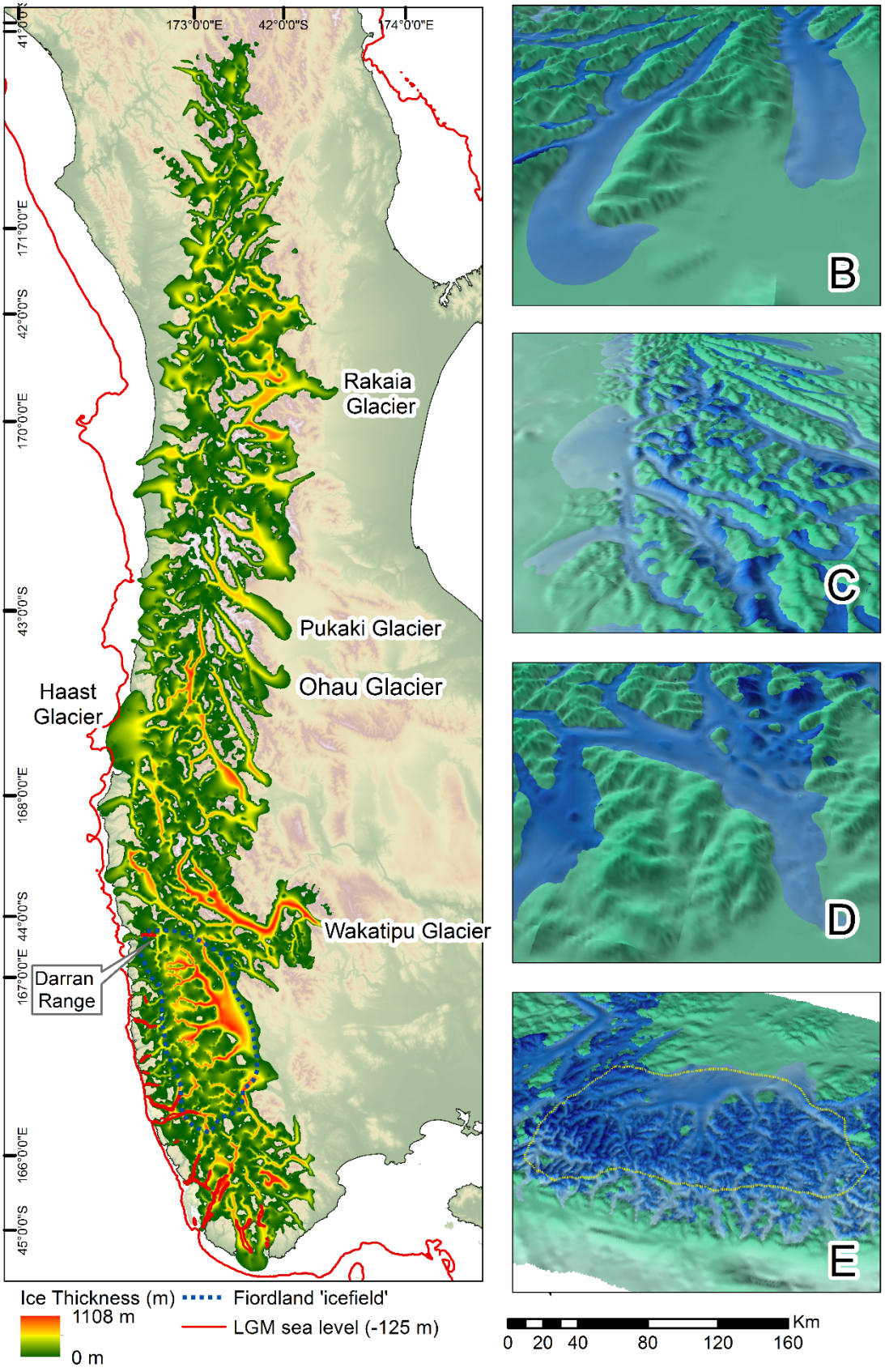

Figure 4.10 a) REVOLTA derived 100 m resolution simulation of LGM ice thickness for the Southern Alps domain using optimal parameters (30 kPa). 3D simulations of: b) Pukaki / Ohau glaciers, c) Haast glacier / west coast, d) Rakaia glacier and e) Fiordland

4.3.3 Total volume and sea level equivalent

The REVOLTA model estimates a total LGM ice volume of 6771.9 km^3 for the entire Southern Alps model domain (Table 4.3). That volume is consistent with calculations of Golledge *et al.* (2012) who estimated a volume of 6355.1 km^3 (adjusted herein for the same domain). Initial volumes were calculated by multiplying the thickness of each cell by its area, with subsequent water equivalent estimated using an assumed ice density of 900 kg m^{-3} (Haeberli & Linsbauer, 2013). The contribution to sea level rise was calculated by deducting the volume of contemporary ice from the LGM volume (50.67 km^3, see Chapter 2), whilst the small volume of ice below the LGM sea level (0.28 km^3) was also deducted.

Table 4.3 REVOLTA derived volumetric and sea level rise equivalent results for the Southern Alps. Corresponding volume calculation from Golledge et al. (2012) shown for comparison.

	LGM Volume (km^3)	LGM Sea Level Equivalent (mm)	Contemporary Volume (km^3)	Volume Below LGM sea level (km^3)	Sea Level Rise (mm)
REVOLTA	6771.9	17.15	50.67	0.28	17.02
Golledge *et al.* (2012)	6355.1				

4.3.4 Sensitivity analysis: distributed ice thickness

4.3.4.1 Influence of post LGM valley infill

As discussed in section 3.5.5, the major valley systems of the New Zealand Southern Alps have substantial sediment accumulation. Whilst the latest literature suggests the majority of sediment was deposited pre-LGM and later overridden by LGM glaciers, some accumulation has nonetheless occurred post-LGM. Thickness estimates of post-LGM sediment are sparse, with approximately 30 m inferred for the Hope valley (Rother *et al.*, 2007), 34 m to 97 m in the Franz Josef valley (Alexander *et al.*, 2014) and up to 300 m in the Pukaki valley (McKinnon *et al.*, 2012).

To assess the sensitivity of REVOLTA to post-LGM sediment infill, additional modelling was performed for the lower Pukaki valley, using the DEM with post-LGM sediment removed generated in section 3.5.5.1 as the input surface. Located at the former terminus of one of the largest glacial systems of the Southern Alps, this region is likely to contain some of the thickest sediments in the Southern Alps, thus providing a maximum estimate for sensitivity. The same parameters were used as

for the full model (T_b of 30 kPa), with the resultant differences in calculated ice volume used to assess model sensitivity. Figure 4.11 shows the original REVOLTA profile and of that generated using the 'sediment removed' DEM. Figure 4.12 shows the fully distributed ice thickness results for each profile, allowing a volumetric comparison.

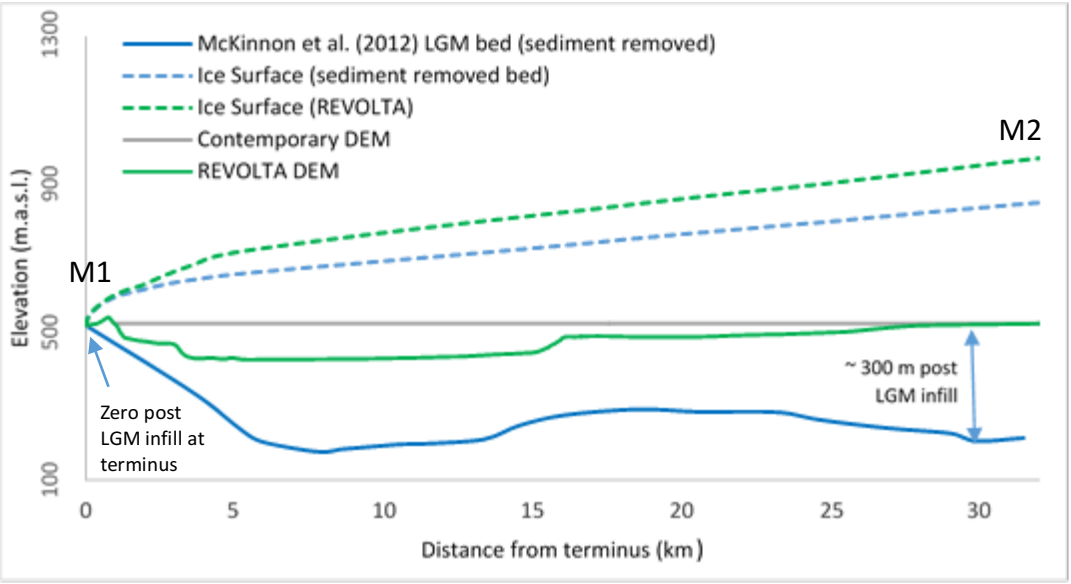

Figure 4.11 REVOLTA derived ice surface profiles for the lower Pukaki valley using standard (lake removed) DEM and 'sediment removed' DEM.

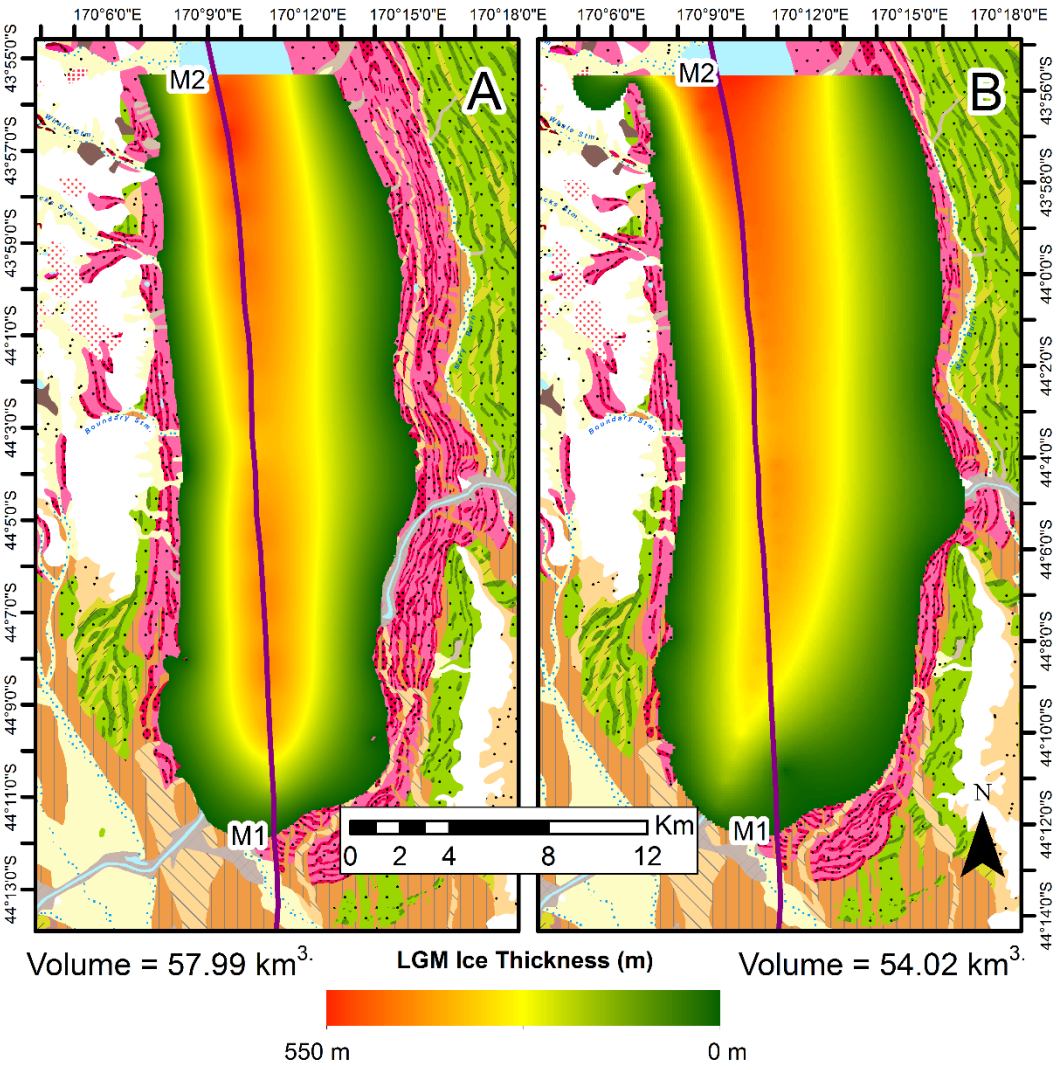

Figure 4.12 REVOLTA derived ice thickness distributions and volumetric calculations for the lower Pukaki valley. a) Standard (lake removed) DEM as input. b) 'Sediment removed' DEM as input.

Modelling with the 'sediment removed' profile results in an ice profile with a lower surface elevation than when using the standard REVOLTA DEM derived bed (Figure 4.11), as may be expected due to the reduced base level. However, with zero post LGM infill at the terminus resulting in the same initial elevation (M1 in Figure 4.11), differences between the ice surface profiles are relatively minor compared to the sediment thickness further up valley. For example, whilst post-LGM sediment thickness exceeds 300 m at 30 km along the transect (Figure 4.11), the difference between the ice elevation profiles is 120 m. When considering overall ice volumes, the models produce similar results, with the original DEM predicting a volume 3.97 km^3 (7.3 %) lower that that with the sediment removed. This analysis demonstrates that whilst post-LGM valley infill does need to be acknowledged when using REVOLTA, it is likely to result in a relatively minor change in volumetric output. With

the above-described analysis being performed in the Pukaki region, which has some of the thickest sediments in the Southern Alps, the influence of sediment infill is expected to be far less important for ice thickness reconstructions in other valleys.

4.3.4.2 Shear stress

To ascertain the sensitivity of REVOLTA to the shear stress (T_b) parameter, modelling was conducted using a variety of T_b values, encapsulating the potential range which could be reasonably parameterised from landform evidence. This approach generates a maximum and minimum estimate of glacier volume, allowing the effect of varying T_b to be observed. Analysis was performed for the Pukaki glacier, which is one of the prime sites for T_b parameterisation by this thesis in the Southern Alps. As noted in section 4.3.1, the 'best fit' shear stress value used for regional modelling (30 kPa) was purposely parameterised to generate a profile slightly above the dated landform evidence. This is due to the fact that the general convex profile of glaciers in the ablation zone (Nesje, 1992) results in the centreline ice elevation being higher than the valley wall evidence, with a differential of approximately 50 m deemed appropriate (Glasser *et al.*, 2011). Considering such a convex profile, a 'low' T_b estimate (15 kPa) was parameterised to approximate the lowest elevation landform evidence whilst a 'high' T_b estimate (40 kPa) was parameterised to exceed the elevation of the geomorphological evidence by over 50 m. Figure 4.14 shows that altering T_b within the bounds described has a relatively minor impact on glaciated area simulated by REVOLTA, with the 'low' T_b scenario predicting an area 17.5 % less than the 'best fit' scenario whilst the 'high' scenario predicts an area 9.5 % greater. However, the steep valley sides of the Pukaki valley result in a larger volumetric differential, with an underestimate of 47.4 % (low scenario) and an overestimate of 30.5 % (high scenario). These differences in volume estimates depending on T_b will be reduced if more high-precision independent estimates of vertical ice thickness become available, as is likely due to ongoing surface exposure dating campaigns.

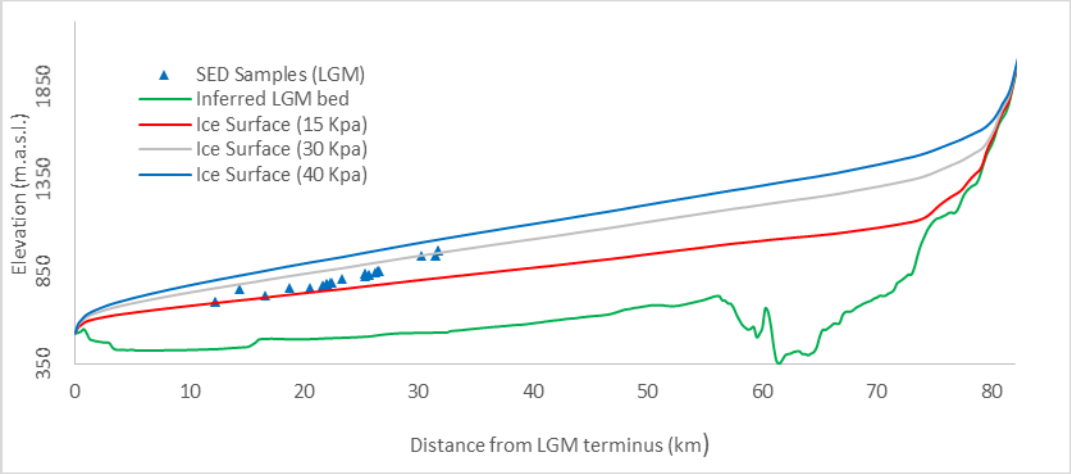

Figure 4.13 REVOLTA derived ice surface profiles for the Pukaki glacier using a 'low' T_b estimate of 15 kPa (red line), 'best fit' estimate of 30 kPa (grey line) and 'high' estimate of 40 kPa (blue line).

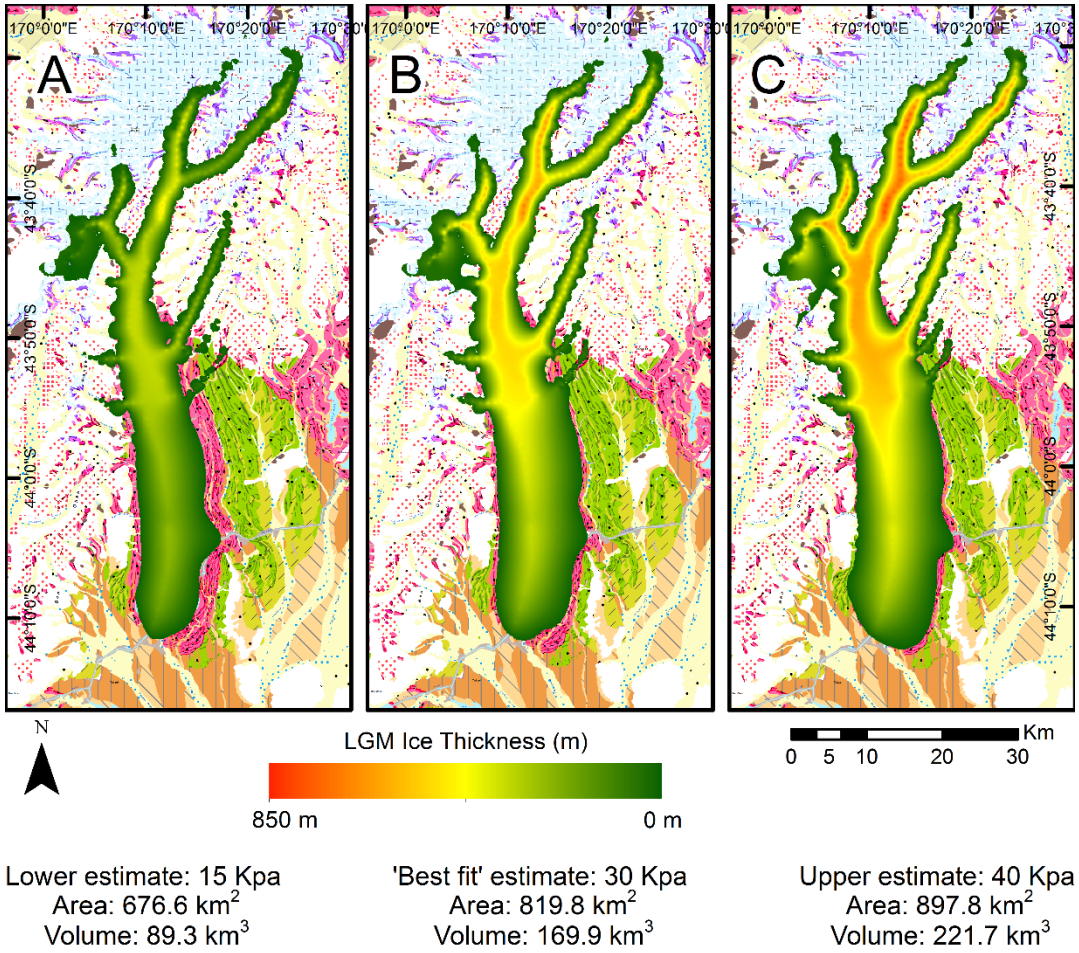

Figure 4.14 REVOLTA derived distributed ice thickness estimates for the Pukaki glacier: a) 'low' basal shear stress estimate (15 kPa), b) 'best fit' estimate (30 kPa) and c) 'high' estimate (40 kPa).

4.3.5 Palaeo Equilibrium Line Altitudes (ELAs) of the New Zealand Southern Alps

Using the REVOLTA reconstructed ice surface as depicted in Figure 4.10a, former LGM ELAs were estimated using the Accumulation Area Ratio (AAR) method outlined in section 4.2.1.8. Results are shown in Figure 4.15a and Table 4.4, with individual glacier ELAs ranging between 276 and 1458 m. There is large spatial variability, with glaciers flowing to the west coast exhibiting relatively low ELAs (median 595.5 m) whilst those to the east are at a higher elevation (median 1056.5 m). Superimposed upon the general east-west pattern is complex variability along the length of the main divide, with localised ELA low points found where additional mountain masses are parallel and offset to the west of the main divide (e.g. Solution Range) whilst higher ELAs are found where low passes penetrate the main divide (e.g. Hollyford Pass).

Figure 4.15b demonstrates the ELA depression from present, using the trend surface generated by Chinn and Whitehouse (1980) as the contemporary baseline (see section 2.3). ELAs were depressed by between 748 m to 1368 m (median 1074 m) at the LGM with the largest depressions found in the north-west region of contemporary glaciation (Figure 4.15b). Chinn & Whitehouse (1980) calculated contemporary ELA gradients normal to the main divide of 25 to 40 km^{-1}, whilst LGM gradients of between 12 to 26 km^{-1} were found in this study using the REVOLTA derived ELAs.

Table 4.4 Median and contemporary LGM ELAs for glaciers to the east and west of the main divide. Contemporary ELA data derived from Willsman *et al.* (2014).

	Entire S. Alps	East of Main divide	West of Main divide	East – West ELA gradient
LGM ELA (REVOLTA)	746.5 m	1056.5 m	595.5 m	12 – 26 m km^{-1}
Contemporary ELA Willsman *et al.* (2014)	1820.5 m	1954.9 m	1687.3 m	25 – 40 m km^{-1} (Chinn & Whitehouse, 1980)
ELA lowering from present	1074 m	898.4 m	1091.8 m	

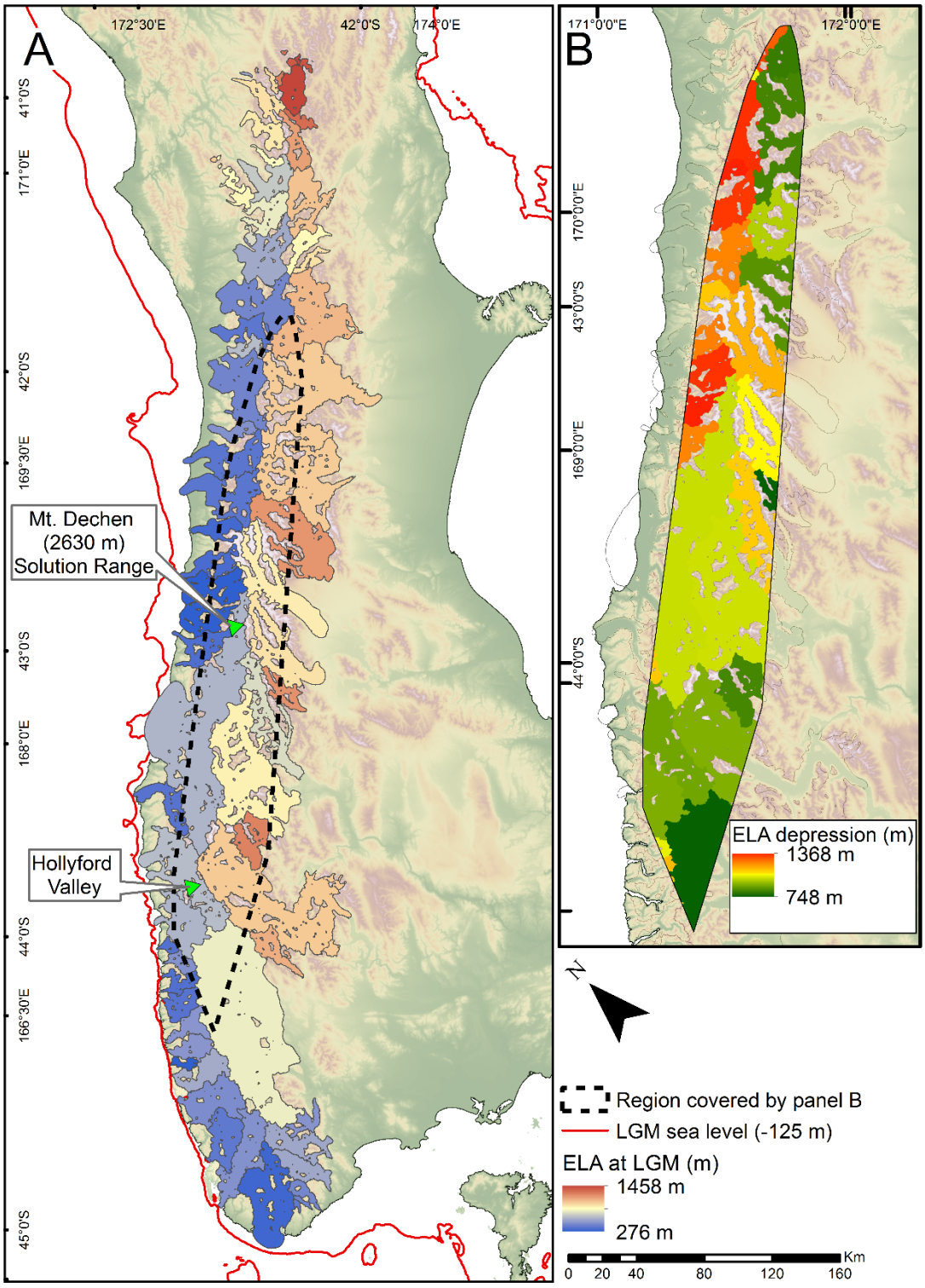

Figure 4.15 a) LGM equilibrium line altitudes (ELA's) estimated using the AAR method for REVOLTA reconstructed LGM glaciers of the Southern Alps. b) LGM ELA depression from present

4.3.6 Climatic implications

4.3.6.1 Estimates of palaeo-precipitation

Using the reconstructed LGM ELAs (Figure 4.15a), estimates of palaeo precipitation were generated under four different cooling scenarios. These scenarios were designed to encapsulate the range of potential LGM temperature reductions indicated from the literature (see section 3.3.1.1). For each cooling scenario, corresponding precipitation for each glacier (at the ELA) was estimated using the methods outlined in section 4.2.2. Cooling scenarios are based on the contemporary mean annual temperature dataset (Figure 4.8b) modified to approximate average summer temperatures using the empirical relationship developed for the Southern Alps (Equation 15), with a homogenous reduction across the model domain. Cooling scenarios were defined as 'minimal' (temperature reduction of 1 °C), 'intermediate' (2.5 °C and 6.5 °C cooling) and 'extreme' (8 °C cooling). Figure 4.16 shows the results of each scenario, with the spatial pattern of precipitation change at the ELA demonstrated. Precipitation change values were found to be non-normally distributed and as such the median value is used to describe the overall change.

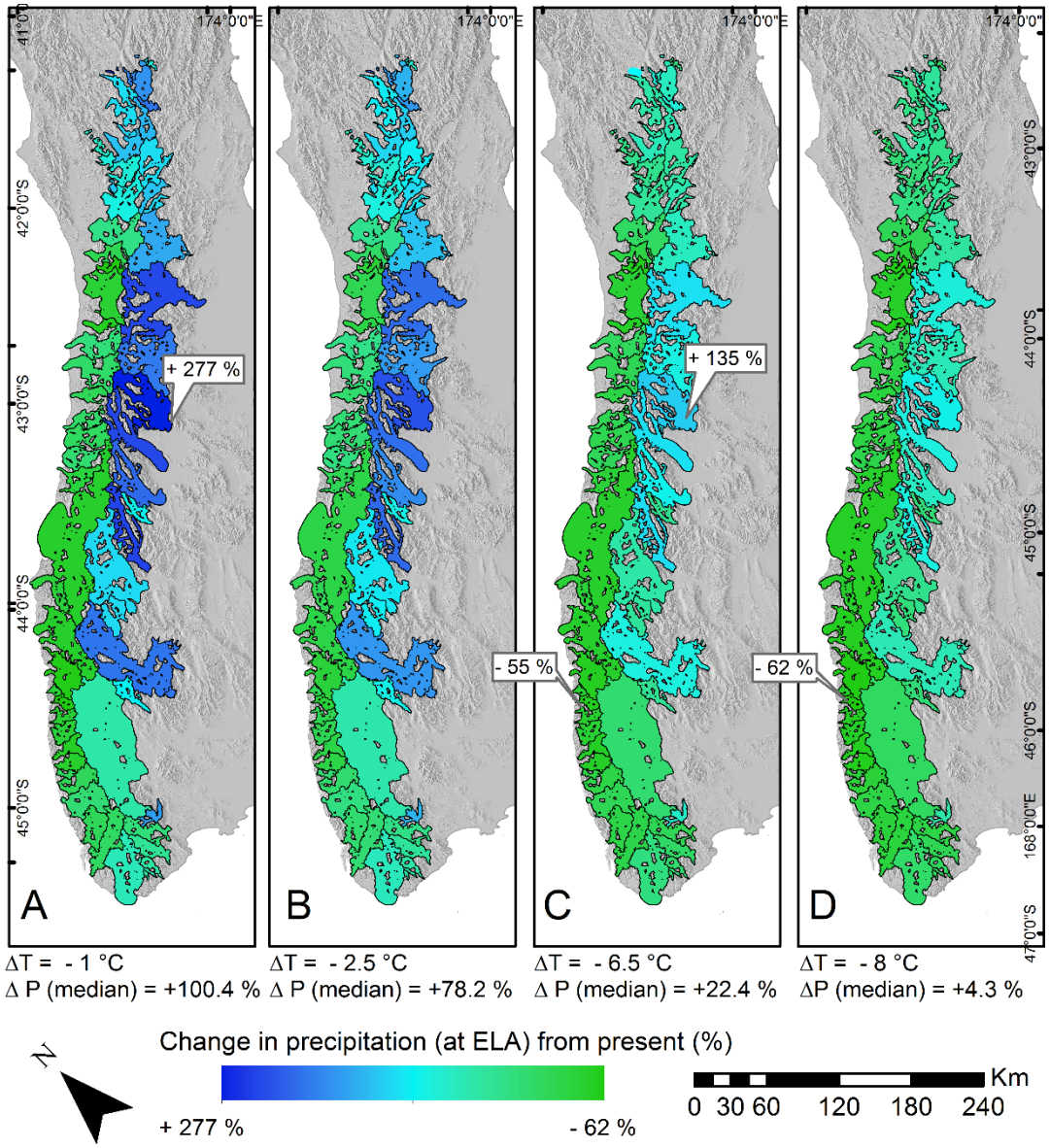

Figure 4.16 Simulated precipitation change (at ELA) for the LGM based upon a temperature decrease of: a) 1 °C, b) 2.5 °C, c) 6.5 °C and d) 8 °C.

All cooling scenarios estimate an overall (median) increase in precipitation, ranging from an approximate doubling (+ 100.4 %) of present values under the minimal cooling scenario of - 1 °C (Figure 4.16a) to a negligible increase of +4.3 % (extreme cooling scenario of - 8 °C, Figure 4.16d). Intermediate cooling scenarios (Figure 4.16b, Figure 4.16c) result in moderate precipitation increases of +78.2% and +22.4% respectively. However, these single median values do not capture the inter-catchment variability, with all scenarios displaying large spatial variability. Maximum precipitation increase for an individual glacier was found under the minimal cooling scenario (-1 °C), with a precipitation change of + 277 % for the Tekapo glacier (Figure

4.16a) whilst the greatest reduction was found under the extreme cooling scenario (- 8 °C), with a simulated decrease of - 62 % in South-west Fiordland (Figure 4.16d).

Under all scenarios there is a clear spatial pattern to the inter-catchment variability, with glaciers to the east of the main divide appearing to show a greater increase (or less decrease) in precipitation than their western counterparts. Table 4.5 numerically explores this spatial variability by splitting each scenario into glaciers to the east and west of the main divide and testing for statistical significance between the samples. With datasets non-normally distributed, the Mann-Whitney test was employed, with resultant p-values < 0.01 under all scenarios. This confirms a statistically significant difference between the precipitation change predicted for glaciers to the east and west of the main divide.

Table 4.5 Simulated precipitation change (at the ELA) for glaciers to the east and west of the main divide under each cooling scenario. Results of Mann-Whitney statistical test shown to test for statistically significant response between east and west flowing glaciers.

Cooling Scenario	-1 °C WEST	-1 °C EAST	- 2.5 °C WEST	- 2.5 °C EAST	- 6.5 °C WEST	- 6.5 °C EAST	- 8 °C WEST	- 8 °C EAST
Δ Precipitation Median	+26.0 %	+153.5 %	+13.9 %	+126.8 %	-16.1 %	+60.6 %	-26.4	+36.0 %
Mann-Whitney P-value	< 0.01		< 0.01		< 0.01		< 0.01	

4.3.6.2 Estimates of palaeo-temperature

In a similar approach to estimating palaeo-precipitation, palaeo-temperatures were estimated under four separate precipitation scenarios chosen to capture the range of potential precipitation change at the LGM as indicated by the literature (section 0). All scenarios were based upon the contemporary precipitation dataset (Figure 4.8a), with a uniform scaling factor applied. Precipitation scenarios were defined as ‘slight increase’ (+ 10 % from present levels), ‘No change’ (present values), ‘moderate decrease’ (-25 %) and ‘significant decrease’ (-50 %). Figure 4.17 shows the results of each scenario, with the spatial pattern of annual temperature change at the ELA demonstrated. As with precipitation modelling the temperature change values were found to be non-normally distributed and as such the median value is used to describe the overall change.

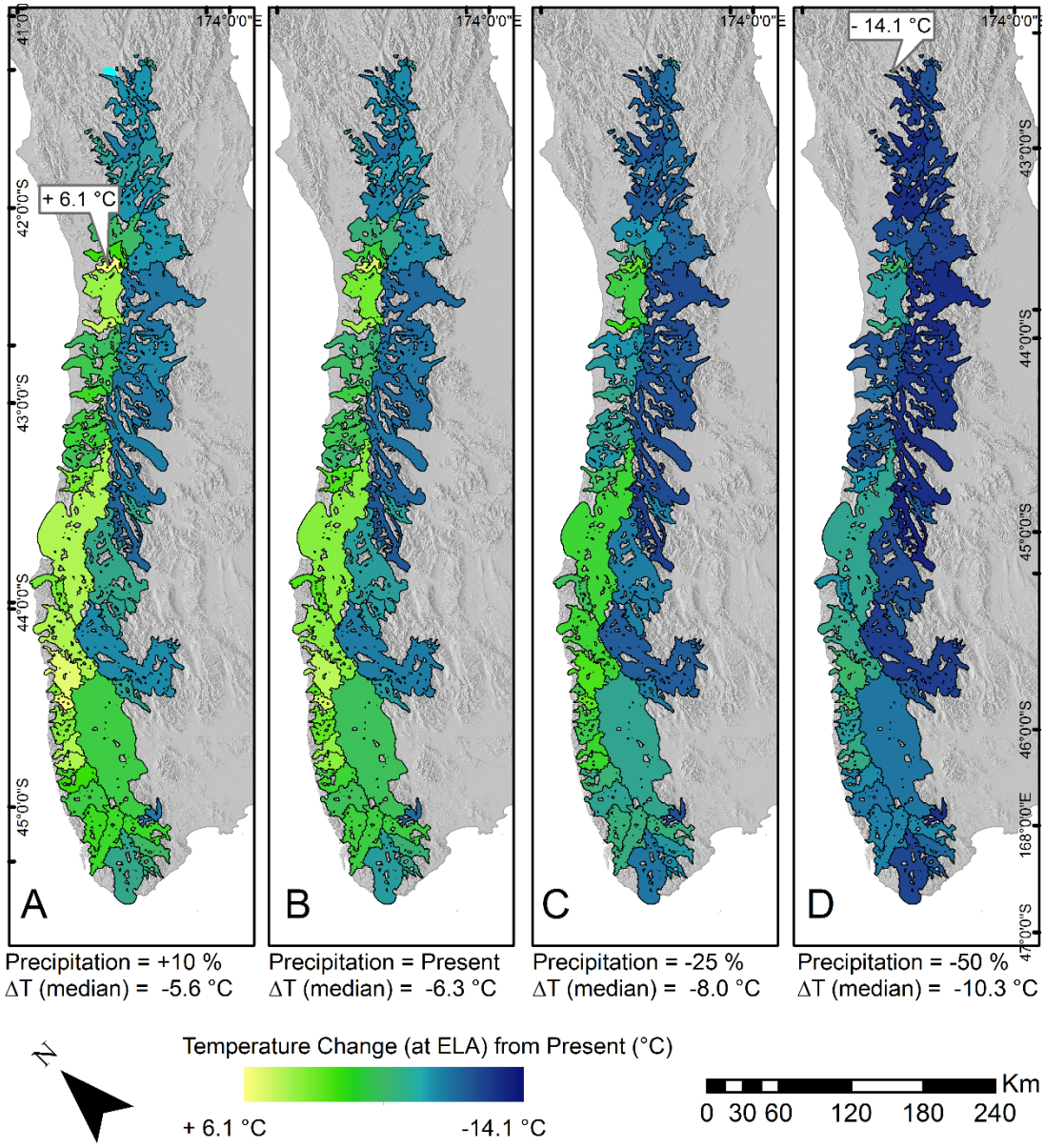

Figure 4.17. Simulated temperature change (at ELA) for the LGM based upon a precipitation regime change of: a) + 10 %, b) no change, c) -25 % and d) -50 %.

All scenarios predict a decrease in temperature at the LGM as compared with the modern state, with regional median temperature lowering (from present) ranging from 5.6 °C (slight precipitation increase scenario, + 10 %, Figure 4.17a) to 10.3°C (significant precipitation decrease scenario, - 50 %, Figure 4.17d). The intermediate scenarios of present precipitation levels and 25% decrease predict median temperature reductions of 6.3°C and 8°C respectively. On an individual glacier basis, differences in air temperature between the LGM and the present day ranged between -14.1 °C (Nelson region, - 50 % precipitation scenario, Figure 4.17d) to + 6.1

°C increase (Lake Brunner region, + 10 % precipitation scenario, Figure 4.17a). As with the precipitation modelling, there is substantial spatial variability within each scenario, with a clear east-west divide. Glaciers flowing to the east of the main divide demonstrate the greatest cooling of air temperature at the LGM compared to the present day, whereas glaciers to the west display significantly less cooling. Table 4.6 explores this spatial variability by splitting each scenario into glaciers to the east and west of the main divide, clearly showing greater cooling for eastern glaciers under all scenarios. With datasets non-normally distributed, the Mann-Whitney test was employed to test for statistical difference between samples, with resultant p-values < 0.01 under all scenarios. This shows a statistically significant difference between the temperature change predicted for glaciers to the east and west of the main divide.

Table 4.6 Simulated temperature change (at the ELA) for glaciers to the east and west of the main divide under each precipitation scenario. Results of Mann-Whitney statistical test shown to test for statistically significant response between east and west flowing glaciers.

Precipitation Scenario	+ 10 % WEST	+ 10 % EAST	+ 0 % WEST	+ 0 % EAST	- 25 % WEST	-25 % EAST	-50 % WEST	-50 % EAST
Δ Temperature Median	-2.3 °C	-7.2 °C	-3.4 °C	-7.8 °C	-6.1 °C	-9.1 °C	-9.5 °C	-10.7 °C
Mann-Whitney P-value	< 0.01		< 0.01		< 0.01		< 0.01	

4.3.7 Sensitivity analysis: AAR ratio and climatic estimates

As discussed in section 4.2.1.8, REVOLTA utilises the Accumulation Area Ratio (AAR) method for estimating the ELA of LGM glaciers, using a ratio of 0.65 as determined from previous empirical studies (Hubbard & Glasser, 2005; Porter, 1975). However, it is known that there is some uncertainty in the estimation of ELA ratios, with Porter (1975b) suggesting an uncertainty of $\pm$ 0.05 for glaciers in the New Zealand Southern Alps. As such, error propagation to final climatic estimates were explored by comparing the initial climatic reconstruction (precipitation and temperature) of the Pukaki LGM glacier (AAR ratio of 0.65) with that of using AAR ratios of 0.6 and 0.7, with results shown in Table 4.7. Boundary condition scenarios of current precipitation levels and a cooling of 6.5 °C were used for temperature and precipitation estimates respectively.

Table 4.7 Simulated precipitation and temperature change (at LGM ELA) for the Pukaki LGM glacier using a range of AAR ratios for ELA estimation.

AAR Ratio	ELA (m)	LGM annual precipitation estimate (6.5 °C cooling scenario)	LGM ELA temperature estimate (present precipitation scenario)
0.7 (+ 0.05)	925.5 m	3222 mm yr^{-1} (+ 52 % from present)	-1.0 °C (9.4 °C cooler than present)
0.65 (standard)	975.5 m	3167 mm yr^{-1} (+ 31 % from present)	-0.18 °C (8.5 °C cooler than present)
0.6 (-0.05)	1025.5 m	3086 mm yr^{-1} (+ 12.5 % from present)	0.68 °C (7.4 °C cooler than present)

As expected, reducing the AAR ratio to 0.6 increases the ELA estimate from 975.5 m to 1025.5 m whilst an increased ratio of 0.7 decreases the ELA to 925.5 m. This has a corresponding impact on simulated climatic variables, with precipitation estimates ranging from +12.5 % (AAR ratio 0.6) to +52% (AAR ratio 0.7) whilst temperature estimates ranged from 7.4 °C cooling from present (AAR ratio 0.6) to 9.4 °C cooling (AAR 0.7).

4.4 Discussion

4.4.1 A note on the time-frame under question

In order to generate a regional scale reconstruction, this thesis simulates the LGM glaciers of the New Zealand Southern Alps as if at a single timeframe, even though the dates pertain to 18 to 30 ka for the entire region (see section 3.2.2). Inevitably this means that some of the subtleties of individual catchment response to glaciation are omitted. There is growing recognition in the literature of catchment specific responses to glaciation (e.g. Rother *et al.*, 2014), highlighting that care must be taken when using an individual catchment to infer regional trends or assuming a single modelling scenario is appropriate for the entire region. Furthermore, a study of fossil beetle data by Marra *et al.* (2006) found that air temperature oscillated during the LGM in New Zealand, partially explaining the large variation of temperature estimates in the literature (Table 3.3). Although there is growing recognition that LGM glaciers of the Southern Alps may not have reached their maximum extents simultaneously (e.g. Rother *et al.*, 2014), analysis of dated landforms from catchments spanning the Southern Alps (Figure 4.9) shows overall coherence between sites, suggesting a single timeframe and modelling scenario is appropriate for the scale and scope of this investigation. This is in common with previous studies of distributed ice thickness (Golledge *et al.*, 2012) and lateral extent (e.g. Barrell, 2011; Suggate, 1990).

4.4.2 Reconstructed LGM ice volume and distributed thickness

Distributed ice thickness modelling for the Southern Alps (Figure 4.10a) shows that REVOLTA offers a viable method for palaeoglacier reconstruction. The REVOLTA total ice volume estimate for the entire Southern Alps domain of 6771.9 km^3 is in good correspondence with the earlier estimate by Golledge *et al.* (2012) of 6355.1 km^3. The comparability of the total ice volume is interesting as Golledge (2012) took climate proxy data to drive an ice dynamics model, whereas this thesis took geomorphological evidence of glacier extent and used it to derive distributed glacier ice thickness and is thus independent of climate estimates. Consequently, this thesis has been able to consider what climate parameters would have likely been associated with such a LGM ice geometry, and since those simulated climatic

conditions (especially temperature) are in good agreement with previous research (e.g. section 3.3.1.1), the reconstructed glacier geometries of this thesis can be said to be both climatically plausible as well as geomorphologically constrained.

REVOLTA simulation of LGM palaeoglaciers combined with modelling of contemporary glaciers by VOLTA (Chapter 2) has helped to refine estimates of ice volume loss across the Southern Alps since the LGM. The results show that the Southern Alps has lost the vast majority of ice present at the LGM, with only 0.75 % of the former LGM volume remaining today. Despite the large proportion of ice lost, the former glaciers of New Zealand have been a minor contributor to global sea level rise, accounting for just 17.02 mm (0.0136 %) of the 125 m rise since the LGM (Milne *et al.*, 2005; Barrell, 2011), although it is acknowledged this figure does not take into account ocean thermal expansion or isostatic rebound. Modelling by Bintanja *et al.* (2002) shows that this almost complete loss of ice volume since the LGM is consistent with other mid-latitude mountainous regions of the world, whilst the great ice sheets of Greenland and Antarctica have retained a far greater proportion (Table 4.8). Although the coarse resolution and precision of the study by Bintanja *et al.* (2002) is not sufficient to explore the intricacies of post LGM volume loss compared to other mountain glacier regions, further literature suggests that New Zealand is especially sensitive to climatic variability with Hoelzle *et al.* (2007) calculating that the Southern Alps have lost 49 % of their glaciated area since the Little Ice Age whilst the European Alps has lost 35 %. This apparent high sensitivity of New Zealand's glaciers is in agreement with literature suggesting that climate sensitivity (to both temperature and precipitation change) is greatest in maritime areas with high precipitation (De Woul & Hock, 2005; Oerlemans, 2001) due to:

- Changes in the snowfall/rainfall ratio having a larger effect where precipitation is higher (this is explored further in section 4.4.4.3)
- Increases in the length of the ablation season having the greatest impact on glaciers which extend into temperate climatic regions
- Amplifications of the initial climate forcing due to feedbacks between melting and albedo

Table 4.8 Estimated contemporary and LGM ice volume for various regions of the world. Adapted from Bintanja *et al.* (2002). *See Bintanja *et al.* (2002) for a full description of locations covered by each region.

Region*	Contemporary Volume (msle)	LGM Volume (msle)	Volume reduction (%)
Eurasia	0.0	64.6	100
North America	0.0	41.6	100
South-American Andes	0.0	4.6	100
Greenland	8.2	12.8	35.94
Antarctica	63.3	68.2	7.18
New Zealand (this thesis)	0.000128	0.01715	99.25

Even though New Zealand glaciation itself does not play a major role in terms of sea level rise (Table 4.3), its unique location means that it is a crucial site for understanding global climatic variability, glacier sensitivity to climate, and the role of the Southern Hemisphere in the global climate system. Understanding past and future glacier variability is also important on a local scale, with issues such as water resource management (e.g. Anderton, 1973), ecology (e.g. Fitzharris *et al.*, 1999) and the economy (e.g. Purdie, 2013) key issues in New Zealand. Glacial ice still constitutes a significant water resource, with fluctuations directly affecting downstream hydrology and associated hydro-electric industry (Chinn, 2001).

4.4.3 Style of glaciation at the LGM

The optimal ice thickness distribution generated by REVOLTA shown in Figure 4.10a simulates a large number of nunataks and exposed ridges, especially in central and northern regions of the Southern Alps. Sensitivity analysis shown in Figure 4.14 demonstrates that even when parameterising the model with a high T_b value, many ridges and nunataks will still be present, further adding confidence of their occurrence during the LGM. This is consistent with the view of Anderson and Mackintosh (2006a), suggesting the contemporary jagged topography is evidence of largely ice-free peaks during glacial phases. Whilst the presence of nunataks and exposed ridges is clearly modelled in the Mt. Cook region, the Fiordland area exhibits a largely 'ice field' style of glaciation (Figure 4.10e). This mode of glaciation is suggested by Rother and Shulmeister (2006) who postulates that reduced sea level during the LGM increased the relative height of the Southern Alps as a barrier for moist air masses, resulting in increased precipitation. In summary, modelling by REVOLTA supports the notion of a mostly valley-constrained style of glaciation

during the LGM with a localised ice field occurring in the Fiordland region. This is in excellent correspondence with (Chinn *et al.*, 2014) who postulates that the Darran Range (adjacent to Milford Sound) marks the approximate boundary between a southern ice cap free of central nunataks and more northern regions where peaks and ridges penetrated the ice. It is envisaged that our understanding of vertical ice extents will further be refined with independent age controlled samples at high altitude in the future.

4.4.4 Equilibrium Line Altitudes (ELAs) and climatic conditions

Figure 4.15a demonstrates the potential of automated ELA reconstruction in a GIS environment, offering a rapid method for palaeo-ELA estimation at a regional scale. ELAs reconstructed in this thesis for the New Zealand Southern Alps range from 276 m to 1458 m (median 746.5 m). This is consistent with estimates by Golledge *et al.* (2012) who found an ELA range of between approximately 300 m to 1500 m. Reconstructed ELAs of individual glaciers also show a good correspondence to findings of other catchment specific studies. For example, the LGM ELA of the Pukaki glacier is estimated by REVOLTA at 975 m, which is comparable with the values derived by Porter (1975) of 955 m and 1080 m for the Mt. John (late LGM) and Tekapo (early-mid LGM) stages respectively.

As expected during glacial phases, estimated LGM ELAs were lower than at present. By comparing the REVOLTA derived LGM ELAs to those of contemporary glaciers (Chinn & Whitehouse, 1980; Willsman *et al.*, 2014), an average lowering (from present) of 1074 m was calculated (Table 4.4). This is in good agreement with the globally averaged estimate of 1000 m by Broecker and Denton (1989). With the ELA very closely linked to local climate (Benn & Evans, 2010), it is therefore inferred that, on average, New Zealand experienced climatic change of a similar magnitude to that of the rest of the world. This assertion is shared by Seltzer *et al.* (2015), the latest study to estimate mean temperature reduction at the LGM in New Zealand using groundwater noble gas palaeothermometry. This study estimated a cooling of 4.6 ± 0.5 °C, noting its 'striking similarity' to the ~5 °C cooling found by similar studies in the Northern Hemisphere (Ma *et al.*, 2004; Beyerle *et al.*, 1998).

Using the REVOLTA derived ELAs, it is estimated that temperatures were depressed by between 5.6°C to 10.3°C at the LGM, with the 'intermediate' scenarios predicting depressions of 6.3 °C and 8°C (Figure 4.17). This is in good correspondence with published literature (Table 3.3), with previous investigations inferring temperature reductions of up to 9°C at some individual locations (Barrows & Juggins, 2005) and studies encompassing the entire Southern Alps reporting average temperature reductions of 6.5 °C (Golledge *et al.*, 2012) and 4.6°C (Seltzer *et al.*, 2015). It is therefore considered that the estimates presented in this thesis are plausible and thus reconstructing climatic conditions using this approach is suitable for the Southern Alps. All the precipitation scenarios are meteorologically possible, with corresponding absolute values of 4075 mm yr^{-1} (+4.3 %, extreme cooling scenario of 8°C) and 7831 mm yr^{-1} (+100.4 %, minimal cooling scenario of 1°C) well within observed values in contemporary mountainous environments (e.g. Henderson & Thompson, 1999).

4.4.4.1 An improved estimate of LGM temperature suppression

By combining the critically evaluated estimates of LGM temperature suppression and precipitation in previously published literature (section 3.3.1.1) with the REVOLTA climatic estimates (section 4.3.6), it is possible to refine an estimate of most likely LGM cooling. Under the minimal cooling scenarios of 1 °C and 2.5 °C (Figure 4.16a and 4.16b), predicted precipitation increased by 100.4 % and 78.2 % respectively, much greater than maximum increases suggested in the literature: +2.5 % (Drost *et al.*, 2007) and +25 % (Golledge *et al.*, 2012). Therefore, these minimal cooling scenarios are deemed unlikely. The enhanced cooling scenarios of 6.5 °C and 8 °C indeed both result in precipitation levels within that of the published literature and are thus deemed credible. As such, a most likely cooling of 6.5 °C to 8 °C is inferred, with cooling of more than 8 °C thought unlikely when considering and evaluating alternative proxy evidence presented in section 3.3.1.1.

4.4.4.2 Regional Variations

A major advantage of the climatic reconstruction approach used in this thesis (see section 4.3.6) is the production of spatially-distributed outputs of precipitation or temperature at a catchment scale. Whilst Drost *et al.* (2007) used the United

Kingdom Met Office HadRM3H model to investigate New Zealand's climate during the LGM at a catchment scale, this thesis is thought to be the first to use reconstructed ice thickness distribution for this purpose. Whereas previous studies have estimated climatic conditions in terms of a single (average) temperature and precipitation change across the entire Southern Alps (e.g. Golledge *et al.*, 2012) or for a single location (e.g. McKinnon *et al.*, 2012), REVOLTA has permitted the individual modelling of precipitation and temperature for 72 separate catchments spanning the entirety of the Southern Alps.

As shown in Table 4.4, contemporary ELAs display a 'fundamental' east-west differential driven by the precipitation gradient, evidenced by the extremely steep ELA gradients of 25 to 40 m km^{-1} (Chinn & Whitehouse, 1980). For comparison, gradients for arctic and sub-arctic regions have been estimated at approximately 4 m km^{-1} (Miller, 1973). Glacier reconstruction using the REVOLTA model suggests that a strong ELA gradient was maintained at the LGM, although reducing from present, ranging between 12 and 26 m $km^{-1.}$ This is consistent with (Porter, 1975) who calculated LGM gradients of 13.5 and 22 m km-1 for two separate transects normal to the main divide. The maintained presence of a strong east-west ELA gradient during the LGM suggests that regional flow of moist westerly air masses was a major feature of New Zealand's weather patterns at the LGM. Climatic modelling by Drost *et al.* (2007) also supports the prominence of westerly circulation during the LGM, finding an increased intensity over the northern parts of the South Island and similar conditions to present over southern regions.

Superimposed upon the east-west differential of LGM ELAs are many local variations along the length of the Southern Alps in regards to both absolute LGM ELA elevation (Figure 4.15a) and lowering from the contemporary ELA (Figure 4.15b). Local variations are also present in the contemporary ELA trend surface, here attributed to local topographic features such as additional mountain ranges offset from the main divide (e.g. Solution Range, Figure 4.15a) and topographic low points (e.g. Hollyford Pass, Figure 4.15a) (Chinn & Whitehouse, 1980). The LGM ice thickness distribution depicted in Figure 4.10a shows that these topographic features will be altered at the LGM, specifically with the 'filling' of topographic low points (e.g. Hollyford Pass) due to thick ice in valley floors. As such, the spatial pattern of LGM

ELAs will be altered, contributing to the localised variations in ELA lowering shown in Figure 4.15b.

A major finding of this thesis is that there is substantial spatial variability between catchments, with a statistically significant difference between the climatic change experienced to the east and west of the main divide. This assertion assumes that LGM glaciers were at (or near) equilibrium with the climate, which is thought to be likely due to the relatively stable LGM climatic conditions (Mix *et al.*, 2001) allowing glaciers to reach near steady state conditions (Benn & Evans, 2010). Estimation of palaeo-temperatures shows greater cooling in eastern regions compared to the west (Table 4.6). This is consistent with the study of ocean proxy records by (Barrows *et al.*, 2000) who found maximum sea surface temperature cooling (reductions of 6 °C to 10 °C) occurred to the southeast of New Zealand as a consequence of the equatorward shift of the Antarctic Circumpolar Current (ACC). Enhanced cooling of the eastern South Island was also found by Drost *et al.* (2007) with modelling suggesting a strong increase in the number of southerlies, bringing cold polar air up the east coast. Furthermore, changes in the position and intensity of southern westerly circulation is suggested as a mechanism for glacier advance during the Younger Dryas in Patagonia (Ackert *et al.*, 2008), further showing the potential of circulation pattern change as a driver of glacial advance and retreat in the Southern Hemisphere.

Estimation of palaeo-precipitation in this thesis shows LGM ELAs to the east of the main divide experienced greater precipitation increases (or less decrease) than their western counterparts (Table 4.5). With results in this thesis reported in terms of percentage change from contemporary values (at the altitude of the LGM ELA), some of the variability observed may be explained by a shift in the local precipitation pattern and distribution (e.g. location of maximum/minimum precipitation). Changes in the orographic influence of the Southern Alps due to sea level reduction as noted by Rother and Shulmeister (2006) is a potential mechanism for changes in the precipitation distribution, with air parcels effectively beginning to rise further west (Figure 4.18) due to a shift in shoreline position. Furthermore, Drost (2006) suggests that LGM glaciation itself may further shift the initial 'barrier' of the Southern Alps westwards, with the additional ice mass contributing to the

orographic barrier (Figure 4.18). Considering the extremely high precipitation gradients of contemporary precipitation (Figure 4.8a), a small shift in the location of orographic enhancement may have the potential to explain the changes in precipitation simulated in this thesis, especially the relatively drier conditions simulated on the western side of the Southern Alps.

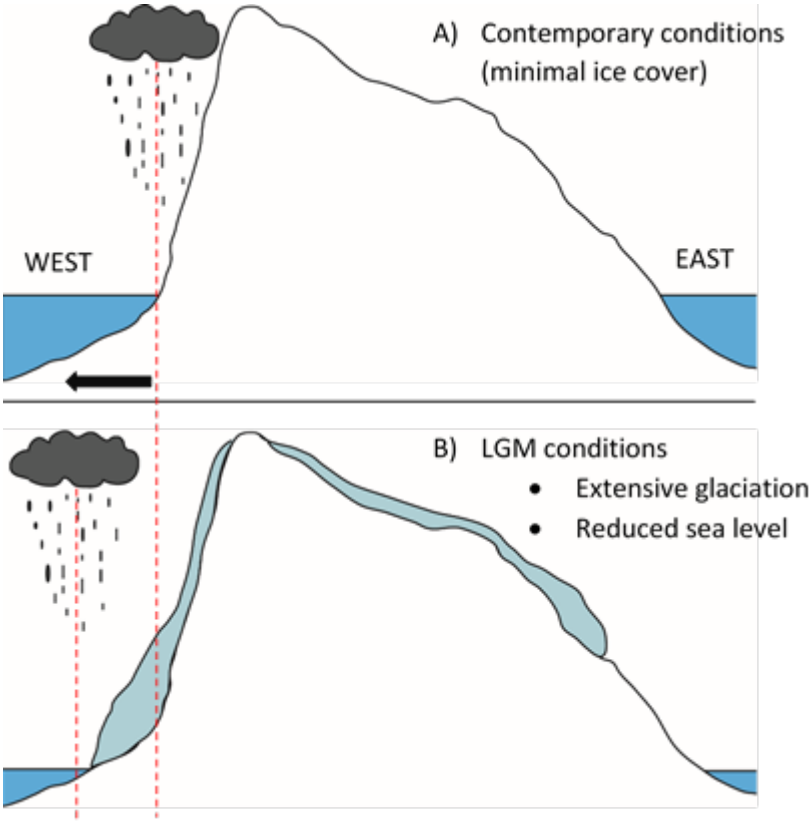

Figure 4.18 Diagram illustrating the potential westward shift in band of maximum precipitation at the LGM due to reduced sea level and addition of glacial ice (not to scale).

It should be noted here that the nature of the climatic reconstruction approach outlined in section 4.2.2 and the available input datasets (scaled versions of contemporary temperature or precipitation) permit the estimation of only one climate variable at a time. Although it has been shown that all of the climatic scenarios in this thesis are glaciologically and meteorologically plausible and broadly consistent with previous estimates (section 4.4.4), in reality it is likely that there was simultaneous regional variation in both temperature and precipitation change, as suggested by previous authors (e.g. Drost *et al.*, 2007). Capturing the spatial variability of only one parameter may also partly explain the relatively large differences estimated between the east and west regions (Table 4.5 and Table 4.6), with simultaneous changes in precipitation and temperature distributions

potentially offsetting each other and thus reducing the overall differential between them. There is scope to explore this interplay between temperature and precipitation change further if independent high resolution estimates of the spatial distribution of either variable at the LGM can be derived.

4.4.4.3 Rainfall-snowfall partitioning at the LGM

An interesting assertion of the results presented in section 4.3.6 is that reciprocal modelling of ELA precipitation and temperature does not appear to generate the reverse result as may be expected. For illustration, if a scenario of 10 % reduction in ELA precipitation (from contemporary values) simulated a 5 °C temperature reduction output, reverse modelling with 5 °C cooling applied as an input would be expected to result in a 10 % precipitation reduction. This does not appear to be the case for the climatic estimates in section 4.3.6 – for example, the 6.5 °C cooling scenario (Figure 4.16c) simulates an average precipitation increase of 22.4 % whilst in reverse modelling a similar cooling (6.3 °C) is achieved under contemporary precipitation levels (Figure 4.17b). This apparent discrepancy may partly be explained by the error and uncertainty related to:

- The initial palaeoglacier reconstruction and associated ELAs.
- The contemporary temperature/precipitation datasets.
- Conversion from annual mean temperatures to summer mean temperatures.
- The empirical relationship used for temperature / precipitation estimation.

However, the climatic conditions of the New Zealand Southern Alps and variations in the snowfall / rainfall ratio also provides a potential mechanism for the observed discrepancy. New Zealand glaciers are unique in that the hyper-humidity of the Southern Alps results in a strong depression of the ELA (Chinn & Whitehouse, 1980), generally around 1000 m lower than the European Alps (Rother & Shulmeister, 2006) with an average elevation of just 1820.5 m (section 4.3.5). Critically, at this altitude, atmospheric temperatures remain above freezing for much of the year, resulting in over half of the precipitation falling as rain at the present ELA. This is in contrast to the European Alps where approximately 83 % of precipitation at the contemporary ELA falls as snow (Rother & Shulmeister, 2006). Using the empirical relationship between mean monthly temperature and snow-rain ratio developed by Sevruk

(1992), Figure 4.19 explores the implications of this factor in regards to the LGM climatic simulations presented in section 4.3.6, with results showing that the Southern Alps received up to 50% of its precipitation as rainfall at the LGM ELA, with all scenarios predicting at least some rainfall input at the LGM. This is in contrast to the European Alps where the higher ELAs remain too cold for rain to form a significant portion of precipitation (Rother & Shulmeister, 2006). This assertion of potentially significant rainfall input at the LGM ELA in the Southern Alps is of interest in its own right regarding glacier dynamics, further adding confidence to the notion that glaciers were wet based and sliding at the LGM (Mager & Fitzsimons, 2007; Golledge *et al.*, 2012).

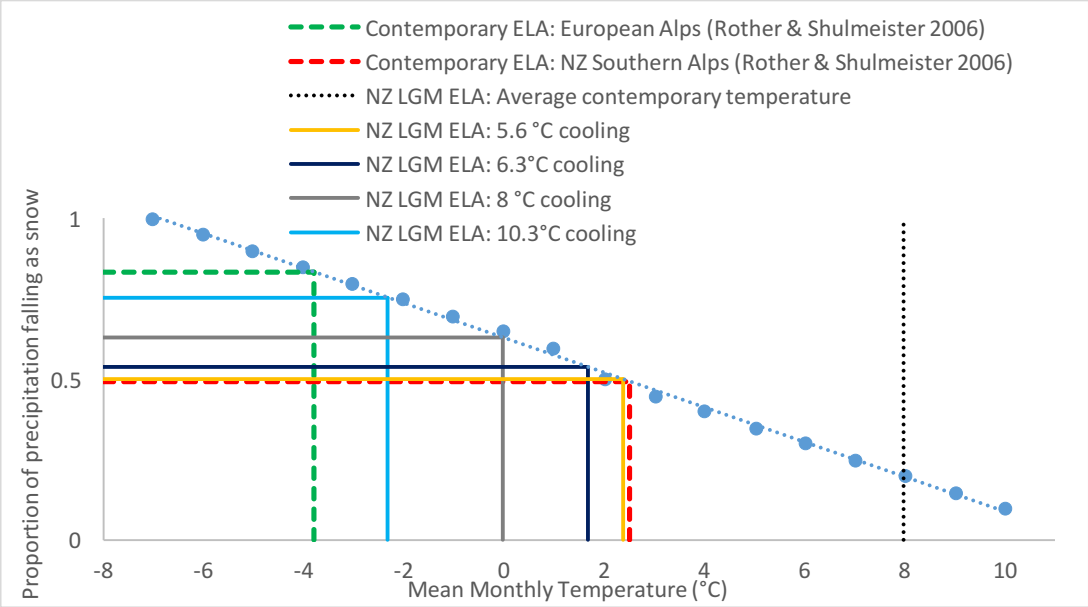

Figure 4.19 Empirical relationship between mean monthly temperature and snow-rain ratio (Sevruk, 1992). Average temperature at contemporary ELA shown for the New Zealand and European Alps. Scenarios from this thesis also shown. Adapted from Rother and Shulmeister (2006).

Despite the climatic estimates presented in section 4.3.6 being based upon the empirical relationship constructed by Ohmura *et al.* (1992) from glaciers across the world (including the Tasman glacier, New Zealand), the sample is still biased towards glaciers with a high snowfall-rainfall ratio at the ELA (such as the European Alps) due to their prominence in regions of intense glacial research. As such, whilst the estimates reported in section 4.3.6 represent total precipitation, much of this may not be available for glacier accumulation as up to 50 % may have been falling as rain at the LGM ELA. Critically, any temperature reduction applied to New Zealand

glaciers will also result in an increase in the proportion of precipitation falling as snow (Figure 4.19) thus increasing accumulation further. This feedback is not likely to be the case in other glaciated regions such as the European Alps where snowfall already constitutes the majority of precipitation at the ELA. This mechanism may therefore partly explain the apparent discrepancy between the reciprocal models as the results presented here are in respect to total precipitation without accounting for changes in the proportion of rainfall and snowfall.

Furthermore, using the empirical relationship between mean monthly temperature and snowfall-rainfall ratio described by Sevruk (1992), it is possible to produce an estimate of the percentage of precipitation falling as snow at the LGM ELA for each individual glacier, allowing for regional variations to be assessed. Whilst it is acknowledged there is some uncertainty in using the empirical relationship derived from contemporary glaciers in the Swiss Alps (Sevruk, 1992), this is the first attempt to quantify the regional distribution of the snowfall-rainfall ratio in the Southern Alps at the LGM. Figure 4.20 shows the results of this modelling, using the predicted cooling results reported in section 4.3.6.2.

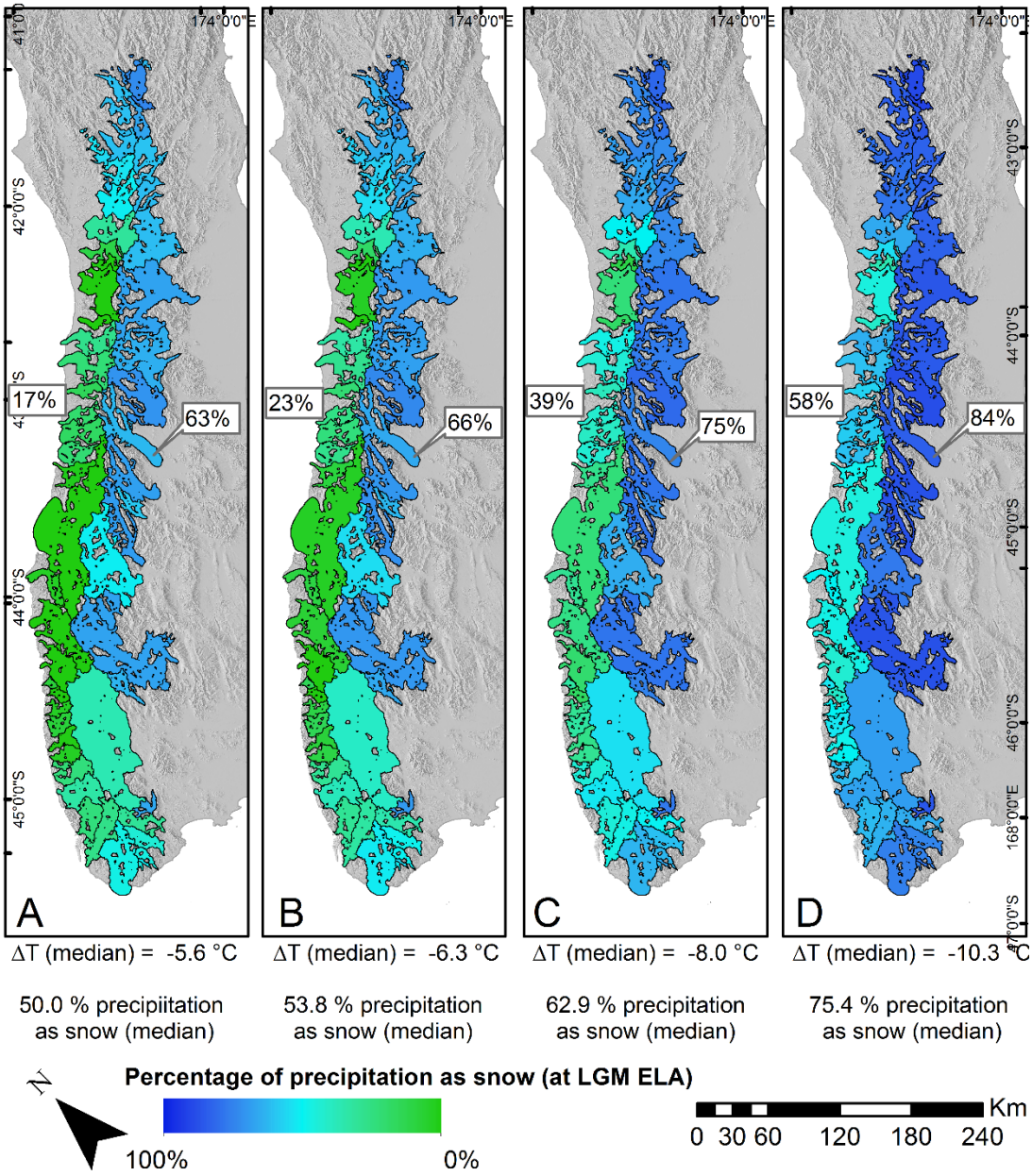

Figure 4.20 Estimated proportion of precipitation falling as snow at the LGM ELA. a) Cooling of 5.6 °C from present, b) 6.3 °C cooling, c) 8 °C cooling and d) 10.3 °C cooling.

As expected, Figure 4.20 shows that greater cooling results in an overall increase in the proportion of precipitation as snowfall, ranging from 50% under the lowest predicted cooling of 5.6 °C (Figure 4.20a) to 75.4% under the greatest cooling of 10.3 °C (Figure 4.20d). The intermediate scenarios of 6.3 °C (Figure 4.20b) and 8 °C (Figure 4.20c) result in 53.8% and 62.9% snowfall respectively. However, it is the distribution which is of most interest here, showing a clear east-west partition under all scenarios. For example, under the 6.3 °C cooling scenario, the Pukaki glacier received an estimated 66% of its precipitation as snowfall whilst the Fox glacier flowing to the west of the main divide received just 23% as snow (Figure 4.20b). A similar

differential is evident under all the cooling scenarios, with associated snowfall proportions indicated in Figure 4.20. It should be noted that the magnitude of the differential reduces under increased cooling (e.g. under the 5.6 °C cooling scenario the difference between the Pukaki and Fox catchment is 46% (Figure 4.20a) whilst under the 10.3 °C scenario (Figure 4.20d) it is just 26%).

This differential is explained via the lower (and consequently warmer) ELAs on the west coast (section 4.3.5), driven by the precipitation regime. Therefore, glaciers to the west of the main divide may be more sensitive to temperature variability as they have a substantial 'extra' snow resource if cooling occurs whilst this feedback will not be as pronounced for glaciers flowing to the east where a greater proportion already falls as snow due to the comparatively higher and consequently cooler ELAs. This hypothesis is similar to that of the regional scale study by Rother and Shulmeister (2006), comparing the relatively high and cool ELAs of the European Alps with the lower and warmer ELAs in the New Zealand Southern Alps.

The differential described here is a further potential cause for some of the difficulties encountered by the previous LGM reconstruction by Golledge *et al.* (2012) where the optimal scenario was in poor agreement with mapped extents at some locations on the east coast, underestimating terminus positions by up to 40km (see section 4.1.1.3). Golledge *et al.* (2012) applied a uniform temperature and precipitation change without accounting for the different feedbacks encountered by glaciers to the east and west coast discussed here. REVOLTA effectively circumvents this issue in the initial glacier reconstruction by using the geomorphological evidence to drive the model, with its influence becoming clear during the palaeoclimatic reconstruction.

4.5 Conclusions

This chapter presents the REVOLTA model, which is an alternative method for simulating regional ice volume and distributed thickness of palaeoglaciers. The REVOLTA model employs a perfect plasticity approach, requiring just a DEM and downstream limits of glaciation to model fully distributed ice thickness. Coded in Python and applied in ArcGIS^{TM}, it can be run on any standard desktop PC or laptop, allowing rapid modelling at a regional scale. Subsequent automated ELA estimation in a GIS environment allows for the reconstruction of former climatic conditions, providing a powerful new tool for palaeoclimatic study.

REVOLTA simulation of the New Zealand Southern Alps during the LGM estimates a total ice volume of 6771.9 km^3, in very good correspondence with the previous estimate of Golledge *et al.* (2012). Combined with the estimate of contemporary ice volume (50.67 km^3) by the VOLTA model (Chapter 2), this result reinforces the notion that New Zealand has lost almost the entirety of its glacial ice since the LGM, although this volume has played a minor role in global sea level rise.

Analysis of the distributed thickness generated by REVLOTA reveals a valley constrained style of glaciation with many exposed ridges and nunataks, even when parameterised to fit the maximum vertical extent of geomorphological evidence. This reconstructed style of glaciation is in agreement with studies suggesting the contemporary jagged topography is an indication of a valley-constrained style of glaciation (Anderson & Mackintosh, 2006a), further casting doubt on the notion of a complete ice-field style of glaciation during the LGM, although a localised icefield is simulated in the Fiordland region of lower relief.

Equilibrium Line Altitude (ELA) estimates for the LGM range between 1458 m and 276 m, in good correspondence with previous regional scale studies (e.g. Golledge *et al.*, 2012) and those concerning individual catchments (e.g. Porter, 1975). Subsequent palaeoclimatic estimates suggests LGM temperature reductions of between 5.6°C – 10.3°C from present, in good agreement with the published literature. Precipitation change estimates of +4.3 % to +100.4% are also deemed to be meteorologically and glaciologically plausible, in agreement with studies suggesting stronger westerly circulation and enhanced orographic enhancement

(Rother & Shulmeister, 2006). Analysis also suggests that rainfall contributed a portion of the precipitation at the LGM ELA, further reinforcing the hypothesis of wet based and sliding glaciers at the LGM.

A major output of this thesis is the refinement of the spatial variability in terms of ELA change, precipitation and temperature change. The ELA differential at the LGM was enhanced from present, with an average elevation of 1056.5 m to the east of the main divide compared to 595.5 m to the west. To accommodate the LGM glacier geometries, substantial changes in precipitation and temperature also occurred, with eastern regions experiencing significantly greater cooling and greater precipitation increases (or less decrease) than their western counterparts. Increased westerly circulation combined with an effective westward shift of the orographic barrier of the Southern Alps due to reduced sea level and the presence of glacial ice is a suggested potential mechanism for precipitation changes. Increased southerly flow bringing cool polar air up the east coast as suggested by other studies (e.g. Drost *et al.*, 2007) is a potential cause of the temperature differences.

Chapter 5. Synthesis and conclusions

5.1 Overall synthesis

Being one of the few locations in the Southern Hemisphere to experience multiple glacial-interglacial cycles, the New Zealand Southern Alps is a crucial site for the study of both contemporary and former glaciers, although historically has received relatively little research attention compared to counterparts in the Northern Hemisphere (Grove, 1988). Within the glacial record, the Last Glacial Maximum period is especially of interest as it represents a climatic state dramatically different to that of present (Mix *et al.*, 2001) whilst having well-constrained boundary conditions and an excellent geomorphological record (Barrell, 2011). Despite this, there is a large amount of uncertainty and debate in the literature surrounding the LGM, specifically related to climatic conditions, the 'style' of glaciation and regional variability.

To help address these debates, the primary aim of this thesis was to refine the understanding of distributed ice thickness and paleoclimate (specifically temperature and precipitation) of the New Zealand Southern Alps during the Last Glacial Maximum (LGM). In order to achieve this, the REVOLTA model was developed, allowing the regional reconstruction of former LGM glaciers solely from geomorphological evidence. This approach required two initial inputs: a DEM of LGM bed topography and an outline of former down-valley glacier extents. As such, initial research was conducted to generate these datasets, producing substantial standalone research outputs including the development of the VOLTA model for estimating contemporary ice thickness distribution (James & Carrivick, 2016) and the synthesis and analysis of data to produce a refined consideration of (lateral) ice extent during the Last Glacial Maximum (section 3.4) from the latest research.

With the generated input datasets, the LGM distributed ice thickness was successfully simulated using the REVOLTA model, revealing a largely valley constrained style of glaciation with exposed ridgelines and nunataks, with a localised icefield in the Fiordland region. The total ice volume was estimated at 6771.9 km^3, in good agreement with the only previous such estimate by Golledge *et al.* (2012) who simulated a volume of 6355.1 km^3. The close correspondence of these two studies is interesting as (Golledge *et al.*, 2012) used climate proxy data to drive an

ice dynamics model in a 'top down' approach whilst REVOLTA used a 'bottom up' methodology, using geomorphological evidence of glacier extent as the input.

The unique method of palaeoglacier reconstruction of the Southern Alps by REVOLTA allowed the simulation of former climatic conditions based upon reconstructed Equilibrium Line Altitudes. Simulated median temperature change for the entire Southern Alps (reduction of 5.6°C to 10.3°C from present) is in general agreement with previously published estimates whilst simulated precipitation estimates (+ 4.3 % to +110.4 % from present) are both meteorologically and glaciologically plausible, providing a valuable further estimate to the previously poorly constrained literature.

Although the overall (median) changes in precipitation and temperature mentioned above are of great interest for regional scale assessment and for comparison with previous literature, a major advantage of this thesis is the ability to output a distributed (glacier specific) estimate of precipitation or temperature change. This reveals a strong east-west partition in simulated ELA temperature and precipitation changes, with a statistically significant difference in response between glaciers to the east and west of the main divide. Specifically, glaciers to the east of the main divide show a greater increase (or less decrease) in precipitation than their western counterparts whilst temperature simulations predict greatest cooling for glaciers to the east of the main divide compared to their western counterparts. This east-west differential observed is potentially attributed to changes in atmospheric and ocean circulation patterns noted by other authors, with an equatorward shift of the Antarctic Circumpolar Current (ACC) (Barrows *et al.*, 2000) and associated increase in the number of southerlies bringing cold polar air up the east coast (Drost *et al.*, 2007). Furthermore, enhanced regional flow of moist westerly air masses as postulated by Rother and Shulmeister (2006) is a potential mechanism for the overall increases in precipitation predicted, whilst reduced sea level and addition of glacial ice effectively 'shifts' the position of the initial orographic barrier, resulting in the simulated differential in precipitation change. These mechanisms are believed to be plausible explanations for the observed changes as the climate of New Zealand has been proven to be extremely sensitive to circulation changes in the southwest pacific, with analysis of historical meteorological records by Salinger and Mullan

(1999) finding that national average temperatures increased by 0.58 °C during a period of enhanced airflow from the northeast around 1950 to 1975. Furthermore, changes in the position and intensity of southern westerly circulation is a suggested mechanism for glacier advance during the Younger Dryas in Patagonia (Ackert *et al.*, 2008), further showing the potential of circulation pattern change as a driver of glacial advance and retreat in the Southern Hemisphere.

An interesting assertion of this thesis is that rainfall probably contributed a significant proportion (up to 50%) of the total precipitation at the LGM ELA. This is in contrast to heavily studied northern hemisphere glaciers where the elevated ELAs and associated cooler temperatures result in negligible rainfall input both at present and at the LGM ELA (Rother & Shulmeister, 2006). This has implications regarding former glacier dynamics, further adding confidence to the notion that glaciers of the Southern Alps were wet based and sliding at the LGM (Mager & Fitzsimons, 2007; Golledge *et al.*, 2012). Further analysis suggests that glaciers flowing to the west coast experienced a greater proportion of their precipitation as rainfall at the LGM compared to the east, an additional factor which needs to be considered when studying palaeoglacier and paleoclimate in the Southern Alps which has perhaps previously been overlooked. Furthermore, it is thought that the relatively low altitude of the ELA in New Zealand (especially on the west coast) will result in the glaciers of New Zealand reacting more sensitively to any future warming due to a higher percentage of rain rather than snow (Hoelzle *et al.*, 2007).

5.2 The complex and dynamic nature of glaciation in the Southern Alps

This thesis has focussed on the spatial and temporal variability of both contemporary and former glaciers, associated climatic conditions and processes. An overarching finding of the research presented here is the large variability found, which has perhaps not been captured by previous studies concentrating on ‘average’ conditions or on a broader scale.

Previous research has shown that contemporary glaciation in New Zealand is highly complex, with features and processes such as debris cover (e.g. Kirkbride, 1989) and

the development of proglacial lakes (e.g. Hochstein *et al.*, 1995) resulting in spatial variability in terms of glacier response to climatic change. For example, a study by (Purdie & Fitzharris, 1999) found that the average rate of non-lake terminating glaciers was 12 m yr^{-1} whilst those with a lake calving termini retreated at 50 m yr^{-1}. The complex spatial and temporal variability of contemporary processes is also highlighted by the in depth analysis of glacier outline inventories in this thesis (see section 2.6.2.2) and of historical glacier length records (e.g. Purdie *et al.*, 2014), showing broad scale retreat since the Little Ice Age maximum has been punctuated by short-term re-advances of certain glaciers.

Whilst this complex and highly variable nature of contemporary glaciation is relatively well understood and documented in the literature, there has recently been an appreciation that similar processes may have also occurred during former glacial and interglacial phases, a fact which may have been previously overlooked. For example, research into the New Zealand Little Ice Age, has revealed a complex glacial record containing a number of re-advances and stillstands (Winkler, 2000) whilst a recent study by Rother *et al.* (2014) suggests that proglacial lakes played an important role in post-LGM deglaciation, with climate decoupling occurring in a similar manner as presently observed.

In common with all previous studies concentrating on the regional LGM in New Zealand (e.g. Golledge *et al.*, 2012; Barrell, 2011; Suggate, 1990) this thesis reconstructs glaciers as if at a single timeframe (effectively at maximum extent for each catchment), with the LGM defined as 18 to 30 ka according to the latest literature (see section 3.2.2). Although the LGM is conventionally described as a period of 'equilibrium state' climate where short term variability was smaller than other phases (Mix *et al.*, 2001), this thesis is in agreement with a growing body of evidence suggesting that the New Zealand LGM was a dynamic and complex period, with glaciers and climate experiencing spatial and temporal variability. The comprehensive synthesis and analysis of the latest data pertaining to the lateral extent of LGM glaciation in the Southern Alps (section 3.4) shows that individual glaciers reached their maximum extents at slightly different times within the LGM window. As such, it is acknowledged that reconstructing the LGM glaciers as if at a single timeframe means that some of the subtleties of individual catchment

response to glaciation are omitted. However, with reconstructed profiles of individual former glaciers across the Southern Alps showing overall coherence between sites when considering the vertical extents (Figure 4.9), the approach used here is deemed fully appropriate for the scale and scope of the investigation.

Within New Zealand, there are a large range of estimated LGM temperatures in the existing literature, ranging from 9°C of cooling from present (Barrows & Juggins, 2005) to little change from current conditions (Marra *et al.*, 2006). Climatic estimates of this thesis show that this range may be partly due to large spatial variability across the Southern Alps. For example, simulated climatic conditions under a contemporary precipitation regime (Figure 4.17b) found individual glacier simulations ranging from -11.3 to + 4.6 °C from present. Much of this variation is driven by changes in the circulation patterns and the interaction of air masses with the Southern Alps, with a distinctive east-west divide. Therefore, when considering estimates of climatic change since the LGM, the specific location of the study should be considered.

By combining the results of REVOLTA climatic simulations with critically evaluated previously published estimates, it has been possible to improve and refine an estimate of LGM temperature suppression. Modelling shows that the lower cooling scenarios presented in the previous literature produce very high precipitation levels much above that of alternative studies and are therefore discounted. Average cooling scenarios of 6.5 °C and 8 °C produce precipitation estimates in line with previous research and this narrower range of values is thus considered credible. Cooling of more than 8 °C is thought to be unlikely once considering critically evaluating alternative proxy evidence.

This research supports emerging evidence that the LGM in New Zealand was a complex and dynamic period (e.g. Rother *et al.*, 2014), with substantial spatial and temporal variability. As such, care should be taken when using an individual catchment to infer overall glacial or climatic trends as they may not be representative of the entire region. Although studies which report a single temperature and precipitation change value for the whole LGM period across the entire of the Southern Alps (e.g. Golledge *et al.*, 2012; Seltzer *et al.*, 2015) are useful

for assessing overall trends for global comparison, these average values need to be placed in the context of temporal and spatial variability within the Southern Alps.

5.3 Beyond the LGM

As discussed in section 3.3, this thesis concentrates almost entirely on the LGM due to its excellent geomorphological record and debate in the literature surrounding glaciological and climatic conditions. However, the LGM is just one of the glacial phases known to have occurred in New Zealand, with at least eight advances recognised and formerly named (Table 3.1). Whilst this thesis has achieved the aim of refining our understanding of distributed ice thickness and paleoclimate at the LGM, there is growing evidence to suggest that conditions at the LGM were unique and perhaps not applicable to earlier glaciations. As such, this research needs to be placed within the context of multiple glacial-interglacial phases, with the LGM representing just the most recent advance.

It has long been recognised that LGM glaciers were not the most extensive in the Southern Alps, with landform evidence of earlier glaciations further down-valley (e.g. Soons, 1963). This notion of sequential glaciations has been affirmed more recently by the advent of absolute dating techniques (e.g. Shulmeister *et al.*, 2010). However, there is virtually no research regarding the vertical extent and relative volume of former (pre-LGM) glaciations, with it unclear if any particular glaciation was more 'powerful' than others.

Through the review of previous studies investigating valley infill and postglacial sediment thickness (section3.5.5), it is clear that LGM glaciers were not powerful enough to excavate previously deposited sediments, overriding them instead. This thesis is the first study to amalgamate this research, revealing that the overriding of pre-LGM sediments is a regional occurrence, with examples to both the east (Rother *et al.*, 2010) and west (Alexander *et al.*, 2014) of the main divide and evident in both field measurements and modelling scenarios (McKinnon *et al.*, 2012). This suggests that the LGM glaciation was substantially less powerful than at least one of the previous episodes, with implications for landscape evolution and morphology.

With the evidence suggesting that previous glaciations were more extensive and more powerful than that at the LGM, climatic conditions were likely to have been even more extreme. Furthermore, the geomorphological evidence suggests that it was these earlier glaciations which fundamentally shaped the landscape of the New Zealand Southern Alps with LGM glaciers playing a relatively small part in landscape modification.

In conclusion, whilst this thesis has successfully refined our knowledge of LGM glaciation and climatic conditions, earlier (pre-LGM) glacial episodes are likely to represent substantially different conditions again, warranting further research. However, the study of pre-LGM glaciation presents a number of major challenges including a poorly preserved geomorphological record, the influence of tectonic uplift and denudation and thus great uncertainty surrounding boundary conditions. Despite this, New Zealand represents a crucial site for understanding Southern Hemisphere (and worldwide) glaciation and for the study of both former and future climatic conditions.

Reference List

Ackert RP, Becker RA, Singer BS, Kurz MD, Caffee MW, Mickelson DM. 2008. Patagonian glacier response during the Late Glacial–Holocene transition. *Science* **321**: 392-395.

Adams J. 1980. Contemporary uplift and erosion of the Southern Alps, New Zealand. *Geological Society of America Bulletin* **91**: 1-114.

Agassiz L. 1840. Glaciers, and the evidence of their having once existed in Scotland, Ireland, and England. *Proceedings of the Geological Society of London* **3**: 327-32.

Alexander D, Davies T, Shulmeister J. 2014. Formation of the Waiho Loop terminal moraine, New Zealand. *Journal of Quaternary Science* **29**: 361-369.

Alloway BV, Lowe DJ, Barrell DJ, Newnham RM, Almond PC, Augustinus PC, Bertler NA, Carter L, Litchfield NJ, Mcglone MS. 2007. Towards a climate event stratigraphy for New Zealand over the past 30 000 years (NZ-INTIMATE project). *Journal of Quaternary Science* **22**: 9-35.

Anderson B, Lawson W, Owens I. 2008. Response of Franz Josef Glacier to climate change. *Global and Planetary Change* **63**: 23-30.

Anderson B, Mackintosh A. 2006a. Interactive comment on "Synoptic climate change as a driver of late Quaternary glaciations in the mid-latitudes of the Southern Hemisphere" by H. Rother and J. Shulmeister. *Climate of the past discussions* **1**: S161-S167.

Anderson B, Mackintosh A. 2006b. Temperature change is the major driver of late-glacial and Holocene glacier fluctuations in New Zealand. *Geology* **34**: 121-124.

Anderson B, Mackintosh A. 2012. Controls on mass balance sensitivity of maritime glaciers in the Southern Alps, New Zealand: The role of debris cover. *Journal of Geophysical Research* **117**.

Anderson B, Mackintosh A, Stumm D, George L, Kerr T, Winter-Billington A, Fitzsimons S. 2010. Climate sensitivity of a high-precipitation glacier in New Zealand. *Journal of Glaciology* **56**: 114-128.

Anderton P. 1973. The significance of perennial snow and ice to the water resources of the South Island, New Zealand. *Journal of Hydrology (New Zealand)* **12**: 6-18.

Anderton P. 1975. *Tasman Glacier 1971-73*. Hydrological Research Annual Reoprt No 33, Ministry of Works and Development for the National Water and Soil Conservation Organisation.

Anderton P, Chinn T. 1978. Ivory Glacier, New Zealand, an IHD representative basin study. *Journal of Glaciology* **20**: 67-84.

Applegate PJ, Lowell TV, Alley RB. 2008. Comment on "Absence of cooling in New Zealand and the adjacent ocean during the Younger Dryas chronozone". *Science* **320**: 746d-746d.

Arendt A, A. Bliss, T. Bolch, J.G. Cogley, A.S. Gardner, J.-O. Hagen, R. Hock, M. Huss, G. Kaser, C. Kienholz, W.T. Pfeffer, G. Moholdt, F. Paul, V. Radić, L. Andreassen, S. Bajracharya, N.E. Barrand, M. Beedle, E. Berthier, R. Bhambri, I. Brown, E. Burgess, D. Burgess, F. Cawkwell, T. Chinn, L. Copland, B. Davies, H. De Angelis, E. Dolgova, L. Earl, K. Filbert, R. Forester, A.G. Fountain, H. Frey, B. Giffen, N. Glasser, W.Q. Guo, S. Gurney, W. Hagg, D. Hall, U.K. Haritashya, G. Hartmann, C. Helm, S. Herreid, I. Howat, G. Kapustin, T. Khromova, M. König, J. Kohler, D. Kriegel, S. Kutuzov, I. Lavrentiev, R. Lebris, S.Y. Liu, J. Lund, W. Manley, R. Marti, C. Mayer, E.S. Miles, X. Li BM, A. Mercer, N. Mölg, P. Mool, G. Nosenko, A. Negrete, T. Nuimura, C. Nuth, R. Pettersson, A. Racoviteanu, R. Ranzi, P. Rastner, F. Rau, B. Raup, J. Rich, H. Rott, A. Sakai, C. Schneider, Y. Seliverstov, M. Sharp, O. Sigurðsson, C. Stokes, R.G. Way, R. Wheate, S. Winsvold, G. Wolken, F. Wyatt, Zheltyhina N. 2015. *Randolph Glacier Inventory – A Dataset of Global Glacier Outlines: Version 5.0*. GLIMS Technical Report.

Bahr DB, Meier MF, Peckham SD. 1997. The physical basis of glacier volume-area scaling. *Journal of Geophysical Research-Solid Earth* **102**: 20355-20362.

Bahr DB, Pfeffer WT, Kaser G. 2015. A review of volume-area scaling of glaciers. *Reviews of Geophysics* **53**: 95-140.

Barnes PM. 2009. Postglacial (after 20 ka) dextral slip rate of the offshore Alpine fault, New Zealand. *Geology* **37**: 3-6.

Barrell D, Andersen B, Denton G. 2011. Glacial geomorphology of the central South Island, New Zealand. *GNS Science monograph* **27**.

Barrell DJ, Read SA. 2014. The deglaciation of Lake Pukaki, South Island, New Zealand—a review. *New Zealand Journal of Geology and Geophysics* **57**: 86-101.

Barrell DJA. 2011. Quaternary Glaciers of New Zealand. *In:* Ehlers, J, Gibbard, P and Hughes, P, eds. *Developments in Quaternary Science.* Amsterdam, Elsevier, pp.

Barrell DJA, Andersen BG, Denton GH, Smith Lyttle B. 2013. Glacial geomorphology of the central South Island, New Zealand – digital data. *GNS Science monograph* **27a**.

Barrows T, Juggins S, De Deckker P, Thiede J, Martinez J. 2000. Sea-surface temperatures of the southwest Pacific Ocean during the Last Glacial Maximum. *Paleoceanography* **15**: 95-109.

Barrows TT, Juggins S. 2005. Sea-surface temperatures around the Australian margin and Indian Ocean during the Last Glacial Maximum. *Quaternary Science Reviews* **24**: 1017-1047.

Barrows TT, Lehman SJ, Fifield LK, De Deckker P. 2007. Absence of cooling in New Zealand and the adjacent ocean during the Younger Dryas chronozone. *Science* **318**: 86-89.

Bauder A, Funk M, Gudmundsson GH. 2003. The ice-thickness distribution of Unteraargletscher, Switzerland. *Annals of Glaciology* **37**: 331-336.

Beavan J, Ellis S, Wallace L, Denys P. 2007. *Kinematic constraints from GPS on oblique convergence of the Pacific and Australian plates, central South Island, New Zealand*. A Continental Plate Boundary: Tectonics at South Island, New Zealand, (1118666143).

Beer J, Mende W, Stellmacher R. 2000. The role of the sun in climate forcing. *Quaternary Science Reviews* **19**: 403-415.

Benn DI, Ballantyne CK. 2005. Palaeoclimatic reconstruction from Loch Lomond Readvance glaciers in the West Drumochter Hills, Scotland. *Journal of Quaternary Science* **20**: 577-592.

Benn DI, Evans DJA. 2010. *Glaciers & glaciation.* 2nd ed. London, Hodder Education, xiv, 802 p.pp.

Benn DI, Hulton NRJ. 2010. An Excel (TM) spreadsheet program for reconstructing the surface profile of former mountain glaciers and ice caps. *Computers & Geosciences* **36**: 605-610.

Beyerle U, Purtschert R, Aeschbach-Hertig W, Imboden DM, Loosli HH, Wieler R, Kipfer R. 1998. Climate and groundwater recharge during the last glaciation in an ice-covered region. *Science* **282**: 731-734.

Bintanja R, Van De Wal R, Oerlemans J. 2002. Global ice volume variations through the last glacial cycle simulated by a 3-D ice-dynamical model. *Quaternary International* **95**: 11-23.

Björnsson H. 1981. Radio-echo sounding maps of Storglaciären, Isfallsglaciären and Rabots Glaciär, northern Sweden. *Geografiska Annaler. Series A. Physical Geography* **63**: 225-231.

Braithwaite RJ. 1984. Calculation of degree-days for glacier-climate research. *Zeitschrift für Gletscherkunde und Glazialgeologie* **20**: 1-8.

Broadbent M. 1974. *Seismic and gravity surveys on the Tasman Glacier: 1971-2.* Geophysics Division Department of Scientific and Industrial Research,

Brodrick T. 1894. Ice motion of the Canterbury glaciers. *New Zealand Alpine Journal* **1**: 307-315.

Broecker WS, Denton GH. 1989. The role of ocean-atmosphere reorganizations in glacial cycles. *Geochimica et Cosmochimica Acta* **53**: 2465-2501.

Brook MS. 2009. Glaciation of Mt Allen, Stewart Island (Rakiura): the southern margin of LGM glaciation in New Zealand. *Geografiska Annaler: Series A, Physical Geography* **91**: 71-81.

Burdis AJ. 2014. *Denudation rates derived from spatially-averaged cosmogenic nuclide analysis in Nelson/Tasman catchments, South Island, New Zealand*. thesis, University of Wellington.

Burrows CJ. 1990. *Processes of vegetation change.* Unwin Hyman London,

Carrivick J, Davies B, James W, Glasser N, Cook A. IN REVIEW-a. Spatial distribution of potential sea-level rise contributions from the Antarctic Peninsula and outlying islands. *Scientific Reports*.

Carrivick J, Davies B, James W, Quincey D, Glasser N. IN REVIEW-b. Distributed ice thickness and glacier volume in southern South America. *Global and Planetary Change*.

Carrivick JL. 2007. Modelling coupled hydraulics and sediment transport of a high-magnitude flood and associated landscape change. *Annals of Glaciology* **45**: 143-154.

Carrivick JL, Brewer TR. 2004. Improving local estimations and regional trends of glacier equilibrium line altitudes. *Geografiska Annaler: Series A, Physical Geography* **86**: 67-79.

Carrivick JL, Davies BJ, Glasser NF, Nývlt D, Hambrey MJ. 2012. Late-Holocene changes in character and behaviour of land-terminating glaciers on James Ross Island, Antarctica. *Journal of Glaciology* **58**: 1176-1190.

Carrivick JL, Geilhausen M, Warburton J, Dickson NE, Carver SJ, Evans AJ, Brown LE. 2013. Contemporary geomorphological activity throughout the proglacial area of an alpine catchment. *Geomorphology* **188**: 83-95.

Carrivick JL, James WH, Berry K, Geilhausen M, Williams C, Brown LE, Rippin DM, Carver SJ. 2015. Decadal Scale Changes Of The Ödenwinkelkees, Central Austria, Suggest Increasing Control of Topography and Evolution Towards Steady State. *Geografiska Annaler: Series A, Physical Geography*.

Carryer S. 1967. The glacial deposits along the northern flank of the Mount Hutt Range. *New Zealand Journal of Geology and Geophysics* **10**: 1136-1144.

Chen J, Ohmura A. 1990. Estimation of Alpine glacier water resources and their change since the 1870s. *In: Hydrology in Mountainous Regions. I - Hydrological Measurements; the Water.,* Lausanne. pp.127-135.

Chinn T. 1978. *Glacier inventory of New Zealand*. Wellington: Institute of Geological and Nuclear Sciences.

Chinn T. 1989. Glaciers of New Zealand. *In:* Williams, R, ed. *Satellite image atlas of glaciers of the world: Irian Jaya, Indonesia, and New Zealand.* U.S. Geological Survey professional paper 1386-H pp.

Chinn T. 2001. Distribution of the glacial water resources of New Zealand. *Journal of Hydrology (New Zealand)* **40**: 139-187.

Chinn T, Fitzharris BB, Willsman A, Salinger MJ. 2012. Annual ice volume changes 1976–2008 for the New Zealand Southern Alps. *Global and Planetary Change* **92–93**: 105-118.

Chinn T, Kargel J, Leonard G, Haritashya U, Pleasants M. 2014. New Zealand's glaciers. *In:* Js, K, Leonard, G, Bishop, M, Kaab, A and Raup, B, eds. *Global Land Ice Measurements from Space.* Chichester, Praxxis pp.

Chinn T, Whitehouse I. 1980. Glacier snow line variations in the Southern Alps, New Zealand. *World Glacier Inventory. International Association of Hydrological Sciences Publication* **126**: 219-228.

Chinn TJH. 1996. New Zealand glacier responses to climate change of the past century. *New Zealand Journal of Geology and Geophysics* **39**: 415 - 428.

Claridge DJE. 1983. *A geophysical study of the termini of the Mount Cook National Park glaciers*. MSc thesis, University of Auckland.

Clark PU, Alley RB, Pollard D. 1999. Northern Hemisphere ice-sheet influences on global climate change. *Science* **286**: 1104-1111.

Clark PU, Dyke AS, Shakun JD, Carlson AE, Clark J, Wohlfarth B, Mitrovica JX, Hostetler SW, Mccabe AM. 2009. The last glacial maximum. *Science* **325**: 710-714.

Clayton L. 1968. Late Pleistocene glaciations of the Waiau valleys, North Canterbury. *New Zealand Journal of Geology and Geophysics* **11**: 753-767.

Coates G. 2002. *The rise and fall of the Southern Alps.* Christchurch, Canterbury University Press, 80pp.

Cowan H. 1990. Late Quaternary displacements on the Hope Fault at Glynn Wye, North Canterbury. *New Zealand Journal of Geology and Geophysics* **33**: 285-293.

Davies B, Glasser N. 2012. Accelerating shrinkage of Patagonian glaciers from the Little Ice Age (~ AD 1870) to 2011. *Journal of Glaciology* **58**: 1063-1084.

De Berg M. 2010. *Computational geometry: algorithms and applications* 3ed. Berlin, Springer,

De Boer B, Dolan A, Bernales J, Gasson E, Golledge N, Sutter J, Huybrechts P, Lohmann G, Rogozhina I, Abe-Ouchi A. 2015. Simulating the Antarctic ice sheet in the late-Pliocene warm period: PLISMIP-ANT, an ice-sheet model intercomparison project. *The Cryosphere* **9**: 881-903.

De Woul M, Hock R. 2005. Static mass-balance sensitivity of Arctic glaciers and ice caps using a degree-day approach. *Annals of Glaciology* **42**: 217-224.

Denton G, Hendy C. 1994. Younger Dryas age advance of Franz Josef glacier in the southern Alps of New Zealand. *Science* **264**: 1434-1437.

Deynoux M, Miller J, Domack E. 2004. *Earth's glacial record.* Cambridge University Press,

Donnadieu Y, Goddéris Y, Ramstein G, Nédélec A, Meert J. 2004. A 'snowball Earth'climate triggered by continental break-up through changes in runoff. *Nature* **428**: 303-306.

Doughty AM, Anderson BM, Mackintosh AN, Kaplan MR, Vandergoes MJ, Barrell DJ, Denton GH, Schaefer JM, Chinn TJ, Putnam AE. 2012. Evaluation of Lateglacial temperatures in the Southern Alps of New Zealand based on glacier modelling at Irishman Stream, Ben Ohau Range. *Quaternary Science Reviews* **74**: 160-169.

Doughty AM, Schaefer JM, Putnam AE, Denton GH, Kaplan MR, Barrell DJ, Andersen BG, Kelley SE, Finkel RC, Schwartz R. 2015. Mismatch of glacier extent and summer insolation in Southern Hemisphere mid-latitudes. *Geology* **43**: 407-410.

Driedger C, Kennard P. 1986a. Glacier volume estimation on Cascade volcanoes: an analysis and comparison with other methods. *Annals of Glaciology* **8**: 59-64.

Driedger CL, Kennard PM. 1986b. *Ice volumes on Cascade volcanoes: Mount Rainier, Mount Hood, Three Sisters, and Mount Shasta*. Washington: U.S. Geological Survey Professional Paper 1365

Drost F. 2006. *An investigation into New Zealand's climate during the Last Glacial Maximum: A climate modelling approach*. PhD thesis, Victoria University of Wellington.

Drost F, Renwick J, Bhaskaran B, Oliver H, Mcgregor J. 2007. A simulation of New Zealand's climate during the Last Glacial Maximum. *Quaternary Science Reviews* **26**: 2505-2525.

Dunai TJ. 2010. *Cosmogenic Nuclides: Principles, concepts and applications in the Earth surface sciences.* Cambridge University Press,

Dykes RC, Brook MS, Winkler S. 2010. The contemporary retreat of Tasman Glacier, Southern Alps, New Zealand, and the evolution of Tasman proglacial lake since AD 2000. *Erdkunde* **64**: 141-154.

Dykstra J. 2012. *The role of mass wasting and ice retreat in the post-LGM evolution of Milford Sound, Fiordland, New Zealand*. PhD thesis, University of Canterbury, New Zealand.

Eden DN, Hammond AP. 2003. Dust accumulation in the New Zealand region since the last glacial maximum. *Quaternary Science Reviews* **22**: 2037-2052.

Evans DJ. 2008. Geomorphology: Avalanches and moraines. *Nature Geoscience* **1**: 493-494.

Farinotti D, Corr H, Gudmundsson GH. 2013. The ice thickness distribution of Flask Glacier, Antarctic Peninsula, determined by combining radio-echo soundings, surface velocity data and flow modelling. *Annals of Glaciology* **54**: 18-24.

Farinotti D, Huss M. 2013. An upper-bound estimate for the accuracy of glacier volume–area scaling. *The Cryosphere* **7**: 1707-1720.

Farinotti D, Huss M, Bauder A, Funk M, Truffer M. 2009. A method to estimate the ice volume and ice-thickness distribution of alpine glaciers. *Journal of Glaciology* **55**: 422-430.

Finlayson A. 2013. Digital surface models are not always representative of former glacier beds: Palaeoglaciological and geomorphological implications. *Geomorphology* **194**: 25-33.

Fischer A, Kuhn M. 2013. Ground-penetrating radar measurements of 64 Austrian glaciers between 1995 and 2010. *Annals of Glaciology* **54**: 179-188.

Fitzharris B, Lawson W, Owens I. 1999. Research on glaciers and snow in New Zealand. *Progress in Physical Geography* **23**: 469-500.

Flain M. 1970. *Lake Coleridge Bathymetry*. *In:* Institute, NO (Ed.).

Fountain AG, Jacobel IRW. 1997. Advances in ice radar studies of a temperate alpine glacier, South Cascade Glacier, Washington, USA. *Annals of Glaciology* **24**: 303 - 308.

Fretwell P, Pritchard HD, Vaughan DG, Bamber J, Barrand N, Bell R, Bianchi C, Bingham R, Blankenship D, Casassa G. 2013. Bedmap2: improved ice bed, surface and thickness datasets for Antarctica. *The Cryosphere* **7**.

Frey H, Haeberli W, Linsbauer A, Huggel C, Paul F. 2010. A multi-level strategy for anticipating future glacier lake formation and associated hazard potentials. *Natural Hazards and Earth System Science* **10**: 339-352.

Geographix. 2012. *NZ 8m Digital Elevation Model* Wellington.

Gjermundsen E, Mathieu R, Kääb A, Chinn T, Fitzharris B, Hagen J. 2011. Assessment of multispectral glacier mapping methods and derivation of glacier area changes, 1978–2002, in the central Southern Alps, New Zealand, from ASTER satellite data, field survey and existing inventory data. *Journal of Glaciology* **57**: 667-683.

Glasser NF, Harrison S, Jansson KN, Anderson K, Cowley A. 2011. Global sea-level contribution from the Patagonian Icefields since the Little Ice Age maximum. *Nature Geoscience* **4**: 303-307.

Glims. 2014. *GLIMS Glacier Database.* Boulder, Colorado USA.

Golledge NR. 2015. *Email correspondance with Nick Golledge.* 1/8/2015.

Golledge NR, Mackintosh AN, Anderson BM, Buckley KM, Doughty AM, Barrell DJA, Denton GH, Vandergoes MJ, Andersen BG, Schaefer JM. 2012. Last Glacial Maximum climate in New Zealand inferred from a modelled Southern Alps icefield. *Quaternary Science Reviews* **46**: 30-45.

Google Earth. 2013. *Tasman Glacier, 43°35'53.93"S, 170°13'0.24"E*. *In:* 2012, D (Ed.).

Gosse JC, Phillips FM. 2001. Terrestrial in situ cosmogenic nuclides: theory and application. *Quaternary Science Reviews* **20**: 1475-1560.

Grant-Taylor T, Rafter T. 1971. New Zealand radiocarbon age measurements—6. *New Zealand Journal of Geology and Geophysics* **14**: 364-402.

Grinsted A. 2013a. An estimate of global glacier volume. *The Cryosphere* **7**: 141-151.

Grinsted A. 2013b. *Estimating global glacier volume* [online]. [Accessed]. Available from: http://www.glaciology.net/Home/MiscellaneousDebris/estimatingglobalglaciervolume.

Grove JM. 1988. *The Little Ice Age.* London, Methuen,

Haeberli W, Hoelzle M. 1995. Application of inventory data for estimating characteristics of and regional climate-change effects on mountain glaciers: A pilot study with the European Alps. *Annals of Glaciology* **21**: 206-212.

Haeberli W, Linsbauer A. 2013. Brief communication" Global glacier volumes and sea level–small but systematic effects of ice below the surface of the ocean and of new local lakes on land". *The Cryosphere* **7**: 817-821.

Hambrey M, A J. 2004. *Glaciers.* 2nd ed. ed. Cambridge, Cambridge University Press,

Harbor JM, Wheeler DA. 1992. On the mathematical description of glaciated valley cross sections. *Earth Surface Processes and Landforms* **17**: 477-485.

Harper A. 1893. Exploration and character of the principal New Zealand glaciers. *The Geographical Journal* **1**: 32-42.

Hart R. 2014. *The ice thickness distribution of a debris-covered glacier: Tasman Glacier, New Zealand.* thesis, Victoria University of Wellington.

Henderson R, Thompson S. 1999. Extreme rainfalls in the Southern Alps of New Zealand. *Journal of Hydrology (New Zealand)* **38**: 309-330.

Heron DW. 2014. *Geological Map of New Zealand 1:250 000*. Lower Hutt, New Zealand: GNS Science.

Hinderer M. 2001. Late Quaternary denudation of the Alps, valley and lake fillings and modern river loads. *Geodinamica Acta* **14**: 231-263.

Hochstein MP, Claridge D, Henrys SA, Pyne A, Nobes DC, Leary SF. 1995. Downwasting of the Tasman Glacier, South Island, New Zealand: changes in the terminus region between 1971 and 1993. *New Zealand Journal of Geology and Geophysics* **38**: 1-16.

Hochstein MP, Watson MI, Malengreau B, Nobes DC, Owens I. 1998. Rapid melting of the terminal section of the Hooker Glacier (Mt Cook National Park, New Zealand). *New Zealand Journal of Geology and Geophysics* **41**: 203-218.

Hoelzle M, Chinn T, Stumm D, Paul F, Zemp M, Haeberli W. 2007. The application of glacier inventory data for estimating past climate change effects on mountain glaciers: A comparison between the European Alps and the Southern Alps of New Zealand. *Global and Planetary Change* **56**: 69-82.

Hubbard B, Glasser N. 2005. *Field techniques in glaciology and glacial geomorphology.* Chichester, John Wiley,

Hughes PD, Braithwaite RJ. 2008. Application of a degree-day model to reconstruct Pleistocene glacial climates. *Quaternary research* **69**: 110-116.

Huss M, Farinotti D. 2012. Distributed ice thickness and volume of all glaciers around the globe. *Journal of Geophysical Research* **117**.

Huss M, Farinotti D, Bauder A, Funk M. 2008. Modelling runoff from highly glacierized alpine drainage basins in a changing climate. *Hydrological Processes* **22**: 3888-3902.

Huss M, Hock R. 2015. A new model for global glacier change and sea-level rise. *Frontiers in Earth Science* **3**.

Hutchinson M. 1989. A new procedure for gridding elevation and stream line data with automatic removal of spurious pits. *Journal of Hydrology* **106**: 211-232.

Imbrie J, Boyle E, Clemens S, Duffy A, Howard W, Kukla G, Kutzbach J, Martinson D, Mcintyre A, Mix A. 1992. On the structure and origin of major glaciation cycles 1. Linear responses to Milankovitch forcing. *Paleoceanography* **7**: 701-738.

Irwin J. 1969. *Lake Manapouri provisional bathymetry*. *Department of Scientific and Industrial Research.*

Irwin J. 1970a. *Lake Ohau provisional bathymetry NZ Oceanographic Institute.*

Irwin J. 1970b. *Lake Pukaki provisional bathymetry 1:31680*. *NZ Oceanographic Institute.*

Irwin J. 1971. *Lake Te Anau provisional bathymetry 1:63360*. *NZ Oceanographic Institute.*

Irwin J. 1972. *Lake Wakatipu provisional bathymetry*. *NZ Oceanographic Institute.*

Irwin J. 1975. *Lake Hawea provisional bathymetry NZ Oceanographic Institute.*

Irwin J. 1976. *Lake Wanaka provisional bathymetry NZ Oceanographic Institute.*

Irwin J. 1979. *Lake Sumner, Katrine, Mason and Marion provisional bathymetry NZ Oceanographic Institute.*

Irwin J. 1980. *Lake Hauroko provisional bathymetry 1:30000*. *NZ Oceanographic Institute.*

Irwin J. 1981a. *Lake Benmore provisional bathymetry NZ Oceanographic Institute.*

Irwin J. 1981b. *Lake Brunner provisional bathymetry NZ Oceanographic Institute.*

Irwin J. 1981c. *Lake Monowai provisional bathymetry*. *NZ Oceanographic Institute.*

Irwin J. 1982a. *Lake Kaniere provisional bathymetry*. *NZ Oceanographic Institute.*

Irwin J. 1982b. *Lake Rotoroa provisional bathymetry*. *NZ Oceanographic Institute.*

Irwin J. 1983. *Lake McKerrow and Lake Alabaster provisional bathymetry*. *NZ Oceanographic Institute.*

Irwin J. 1987. *Lake Aviemore provisional bathymetry 1:10000*. *NZ Oceanographic Institute.*

Ivy-Ochs S, Schlüchter C, Kubik PW, Denton GH. 1999. Moraine exposure dates imply synchronous Younger Dryas glacier advances in the European Alps and in the Southern Alps of New Zealand. *Geografiska Annaler: Series A, Physical Geography* **81**: 313-323.

Jaboyedoff M, Derron M-H. 2005. A new method to estimate the infilling of alluvial sediment of glacial valleys using a sloping local base level. *Geografia Fisica e Dinamica Quaternaria* **28**: 37-46.

James WH, Carrivick JL. 2016. Automated modelling of distributed glacier ice thickness and volume. *Computers & Geosciences* **92**: 90 - 103.

Jarvis A, Reuter HI, Nelson A, Guevara E. 2008. *Hole-filled SRTM for the globe Version 4*. *In:* Cgiar-Csi (Ed.).

Kamp PJ, Green PF, White SH. 1989. Fission track analysis reveals character of collisional tectonics in New Zealand. *Tectonics* **8**: 169-195.

Kaplan MR, Schaefer JM, Denton GH, Barrell DJA, Chinn TJH, Putnam AE, Andersen BG, Finkel RC, Schwartz R, Doughty AM. 2010. Glacier retreat in New Zealand during the Younger Dryas stadial. *Nature* **467**: 194-197.

Kaser G, Großhauser M, Marzeion B. 2010. Contribution potential of glaciers to water availability in different climate regimes. *Proceedings of the National Academy of Sciences* **107**: 20223-20227.

Kayastha RB, Takeuchi Y, Nakawo M, Ageta Y. 2000. Practical prediction of ice melting beneath various thickness of debris cover on Khumbu Glacier, Nepal, using a positive degree-day factor. *In: Debris covered glaciers, Seattle, USA*. IAHS, pp.71-82.

Kelley SE, Kaplan MR, Schaefer JM, Andersen BG, Barrell DJ, Putnam AE, Denton GH, Schwartz R, Finkel RC, Doughty AM. 2014. High-precision ^{10}Be chronology of moraines in the Southern Alps indicates synchronous cooling in Antarctica and New Zealand 42,000 years ago. *Earth and Planetary Science Letters* **405**: 194-206.

Kerschner H, Kaser G, Sailer R. 2000. Alpine Younger Dryas glaciers as palaeo-precipitation gauges. *Annals of Glaciology* **31**: 80-84.

Kienholz C, Rich J, Arendt A, Hock R. 2014. A new method for deriving glacier centerlines applied to glaciers in Alaska and northwest Canada. *The Cryosphere* **8**: 503-519.

Kirkbride M. 1989. *The influence of sediment budget on geomorphic activity of the Tasman Glacier, Mount Cook National Park, New Zealand*. PhD thesis, University of Canterbury.

Kirkbride M. 1995. Ice flow vectors on the debris-mantled Tasman Glacier, 1957-1986. *Geografiska Annaler. Series A. Physical Geography* **77**: 147-157.

Kirkbride MP. 1993. The temporal significance of transitions from melting to calving termini at glaciers in the central Southern Alps of New Zealand. *The Holocene* **3**: 232-240.

Kirkbride MP. 2000. Ice-marginal geomorphology and Holocene expansion of debris-covered Tasman Glacier, New Zealand. *IAHS PUBLICATION* 211-218.

Kirkbride MP, Warren CR. 1999. Tasman Glacier, New Zealand: 20th-century thinning and predicted calving retreat. *Global and Planetary Change* **22**: 11-28.

Koerner R. 1977. Ice thickness measurements and their implications with respect to past and present ice volumes in the Canadian High Arctic ice caps. *Canadian Journal of Earth Sciences* **14**: 2697-2705.

Kotlyakov M, Krenke AN. 1982. Investigations of the hydrological conditions of alpine regions by glaciological methods. *In: Hydrological Aspects of Alpine and High Mountain Areas, Exeter*. IAHS.

Lawrence DB. 1965. Glacier studies in New Zealand. *Mazama.* **47**, pp.17-27.

Le Bris R, Paul F. 2013. An automatic method to create flow lines for determination of glacier length: A pilot study with Alaskan glaciers. *Computers & Geosciences* **53**: 234 - 245.

Leathwick J, Stephens R. 1998. *Climate surfaces for New Zealand*. Landcare Research Contract Report LC9798.

Leonard EM. 1989. Climatic change in the Colorado Rocky Mountains: estimates based on modern climate at late pleistocene equilibrium lines. *Arctic and Alpine Research* **21**: 245-255.

Li H, Ng F, Li Z, Qin D, Cheng G. 2012. An extended 'perfect-plasticity' method for estimating ice thickness along the flow line of mountain glaciers. *Journal of Geophysical Research-Earth Surface* **117**.

Linsbauer A, Paul F, Haeberli W. 2012. Modeling glacier thickness distribution and bed topography over entire mountain ranges with GlabTop: Application of a fast and robust approach. *Journal of Geophysical Research* **117**.

Linsbauer A, Paul F, Hoelzle M, Frey H, Haeberli W. 2009. The Swiss Alps without glaciers – a GIS-based modelling approach for reconstruction of glacier beds. *In: Proceedings of Geomorphometry, Zurich, Switzerland*.

Locke WW. 1995. Modelling of icecap glaciation of the northern Rocky Mountains of Montana. *Geomorphology* **14**: 123-130.

Ma L, Castro MC, Hall CM. 2004. A late Pleistocene–Holocene noble gas paleotemperature record in southern Michigan. *Geophysical Research Letters* **31**.

Machguth H, Huss M. 2014. The length of the glaciers in the world: a straightforward method for the automated calculation of glacier center lines. *The Cryosphere Discussions* **8**: 2491-2528.

Mager S, Fitzsimons S. 2007. Formation of glaciolacustrine Late Pleistocene end moraines in the Tasman Valley, New Zealand. *Quaternary Science Reviews* **26**: 743-758.

Marra M, Shulmeister J, Smith E. 2006. Reconstructing temperature during the Last Glacial Maximum from Lyndon Stream, South Island, New Zealand using beetle fossils and maximum likelihood envelopes. *Quaternary Science Reviews* **25**: 1841-1849.

Mathews W. 1967. Profiles of late Pleistocene glaciers in New Zealand. *New Zealand Journal of Geology and Geophysics* **10**: 146-163.

Mccarthy A, Mackintosh A, Rieser U, Fink D. 2008. Mountain glacier chronology from Boulder Lake, New Zealand, indicates MIS 4 and MIS 2 ice advances of similar extent. *Arctic, Antarctic, and Alpine Research* **40**: 695-708.

Mcglone MS, Salinger MJ, Moar NT. 1993. Paleovegetation studies of New Zealand's climate since the Last Glacial Maximum. *In:* Wright, HE, Kutzbach, JE, Webb, T, Ruddimann, WF, Street-Perrott, F.A. and Bartlein, PJ, eds. *Global Climates since the LGM.* University of Minnesota, 294–316pp.

Mckellar I. 1960. Pleistocene deposits of the upper Clutha valley, Otago, New Zealand. *New Zealand Journal of Geology and Geophysics* **3**: 432-460.

Mckinnon KA, Mackintosh AN, Anderson BM, Barrell DJ. 2012. The influence of sub-glacial bed evolution on ice extent: a model-based evaluation of the Last Glacial Maximum Pukaki glacier, New Zealand. *Quaternary Science Reviews* **57**: 46-57.

Mckinzey KM, Lawson W, Kelly D, Hubbard A. 2004. A revised Little Ice Age chronology of the Franz Josef Glacier, Westland, New Zealand. *Journal of the Royal Society of New Zealand* **34**: 381-394.

Michel L, Picasso M, Farinotti D, Bauder A, Funk M, Blatter H. 2013. Estimating the ice thickness of mountain glaciers with an inverse approach using surface topography and mass-balance. *Inverse Problems* **29**.

Miller GH. 1973. Late Quaternary glacial and climatic history of northern Cumberland Peninsula, Baffin Island, NWT, Canada. *Quaternary Research* **3**: 561-583.

Milne GA, Long AJ, Bassett SE. 2005. Modelling Holocene relative sea-level observations from the Caribbean and South America. *Quaternary Science Reviews* **24**: 1183-1202.

Mitchell J, Mackay K, Neil H, Mackay E, Pallentin A, P N. 2012. *Undersea New Zealand, 1:5,000,000*. *In:* Niwa (Ed.) *Miscellaneous Series No. 92.*

Mix AC, Bard E, Schneider R. 2001. Environmental processes of the ice age: land, oceans, glaciers (EPILOG). *Quaternary Science Reviews* **20**: 627-657.

Murray DR, Locke WW. 1989. Dynamics of the late pleistocene Big Timber Glacier, Crazy Mountains, Montana, USA. *Journal of Glaciology* **35**: 183-190.

Nesje A. 1992. Topographical effects on the equilibrium-line altitude on glaciers. *GeoJournal* **27**: 383-391.

New Zealand Geological Survey. 1973. *Quaternary Geology-South Island, 1: 1000000*. Department of Scientific and Industrial Research Wellington.

Norris RJ, Cooper AF. 2001. Late Quaternary slip rates and slip partitioning on the Alpine Fault, New Zealand. *Journal of Structural Geology* **23**: 507-520.

Nye J. 1951. The flow of glaciers and ice-sheets as a problem in plasticity. *Proceedings of the Royal Society of London. Series A. Mathematical and Physical Sciences* **207**: 554-572.

Nye J. 1965. The flow of a glacier in a channel of rectangular, elliptic or parabolic cross-section. *Journal of Glaciology* **5**: 661-690.

Nye JF. 1952. A method of calculating the thicknesses of the ice-sheets. *Nature* **169**: 529-530.

Oerlemans J. 1997. Climate sensitivity of Franz Josef Glacier, New Zealand, as revealed by numerical modeling. *Arctic and Alpine Research* **29**: 233-239.

Oerlemans J. 2001. *Glaciers and climate change.* CRC Press,

Oerlemans J. 2005. Extracting a climate signal from 169 glacier records. *Science* **308**: 675-677.

Oerlemans J, Anderson B, Hubbard A, Huybrechts P, Johannesson T, Knap W, Schmeits M, Stroeven A, Van De Wal R, Wallinga J. 1998. Modelling the response of glaciers to climate warming. *Climate Dynamics* **14**: 267-274.

Ohmura A, Kasser P, Funk M. 1992. Climate at the equilibrium line of glaciers. *Journal of Glaciology* **38**: 397-411.

Otto JC, Schrott L, Jaboyedoff M, Dikau R. 2009. Quantifying sediment storage in a high alpine valley (Turtmanntal, Switzerland). *Earth Surface Processes and Landforms* **34**: 1726-1742.

Paterson WSB. 1994. *The physics of glaciers.* 3rd ed. Oxford, Pergamon,

Pearson PN, Palmer MR. 2000. Atmospheric carbon dioxide concentrations over the past 60 million years. *Nature* **406**: 695-699.

Pellikka P, Rees WG. 2009. *Remote sensing of glaciers: techniques for topographic, spatial and thematic mapping of glaciers.* CRC Press,

Pellitero R, Rea BR, Spagnolo M, Bakke J, Ivy-Ochs S, Hughes P, Lukas S, Ribolini A. 2015. A GIS tool for automatic calculation of glacier equilibrium-line altitudes. *Computers & Geosciences* **82**: 55-62.

Péwé T, Reger R. 1972. Modern and Wisconsinan snowlines in Alaska. *In: 24th International Geological Congress,* Montréal. pp.187-197.

Pickrill RA, Fenner JM, Mcglone MS. 1992. Late Quaternary evolution of a fjord environment in Preservation Inlet, New Zealand. *Quaternary research* **38**: 331-346.

Porter SC. 1975. Equilibrium-line altitudes of late Quaternary glaciers in the Southern Alps, New Zealand. *Quaternary research* **5**: 27-47.

Pugh JM. 2008. *The late quaternary environmental history of the Lake Heron Basin, Mid Canterbury, New Zealand*. MSc thesis, University of Canterbury.

Purdie H. 2013. Glacier Retreat and Tourism: Insights from New Zealand. *Mountain Research and Development* **33**: 463-472.

Purdie H, Anderson B, Chinn T, Owens I, Mackintosh A, Lawson W. 2014. Franz Josef and Fox Glaciers, New Zealand: Historic length records. *Global and Planetary Change* **121**: 41-52.

Purdie J, Fitzharris B. 1999. Processes and rates of ice loss at the terminus of Tasman Glacier, New Zealand. *Global and Planetary Change* **22**: 79-91.

Putnam A, Schaefer J, Barrell D, Vandergoes M, Denton G, Kaplan M, Finkel R, Schwartz R, Goehring B, Kelley S. 2010. In situ cosmogenic ^{10}Be production-rate calibration from the Southern Alps, New Zealand. *Quaternary Geochronology* **5**: 392-409.

Putnam AE, Schaefer JM, Denton GH, Barrell DJ, Andersen BG, Koffman TN, Rowan AV, Finkel RC, Rood DH, Schwartz R. 2013a. Warming and glacier recession in the Rakaia valley, Southern Alps of New Zealand, during Heinrich Stadial 1. *Earth and Planetary Science Letters* **382**: 98-110.

Putnam AE, Schaefer JM, Denton GH, Barrell DJ, Birkel SD, Andersen BG, Kaplan MR, Finkel RC, Schwartz R, Doughty AM. 2013b. The Last Glacial Maximum at 44° S documented by a ^{10}Be moraine chronology at Lake Ohau, Southern Alps of New Zealand. *Quaternary Science Reviews* **62**: 114-141.

Quincey DJ, Glasser NF. 2009. Morphological and ice-dynamical changes on the Tasman Glacier, New Zealand, 1990–2007. *Global and Planetary Change* **68**: 185-197.

Radić V, Hock R. 2010. Regional and global volumes of glaciers derived from statistical upscaling of glacier inventory data. *Journal of Geophysical Research* **115**.

Rea BR, Evans DJ. 2007. Quantifying climate and glacier mass balance in north Norway during the Younger Dryas. *Palaeogeography, Palaeoclimatology, Palaeoecology* **246**: 307-330.

Reznichenko NV, Davies TR, Winkler S. 2016. Revised palaeoclimatic significance of Mueller Glacier moraines, Southern Alps, New Zealand. *Earth Surface Processes and Landforms* **41**: 196-207.

Robertson CM. 2012. *Temporal evolution of the termini and subaqueous morphologies of lake-calving glaciers in Aoraki/Mount Cook National Park, New Zealand.* PhD thesis, Massey University.

Robertson CM, Benn DI, Brook MS, Fuller IC, Holt KA. 2012. Subaqueous calving margin morphology at Mueller, Hooker and Tasman glaciers in Aoraki/Mount Cook National Park, New Zealand. *Journal of Glaciology* **58**: 1037-1046.

Rother H. 2006. *Late Pleistocene Glacial Geology of the Hope-Waiau Valley System in North Canterbury, New Zealand*. PhD thesis, University of Canterbury.

Rother H, Fink D, Shulmeister J, Mifsud C, Evans M, Pugh J. 2014. The early rise and late demise of New Zealand's last glacial maximum. *Proceedings of the National Academy of Sciences* **111**: 11630-11635.

Rother H, Jol HM, Shulmeister J. 2007. Stratigraphy and tectonic implications of late Pleistocene valley fill in the Hope Valley, Canterbury, South Island, New Zealand. *Geological Society of America Special Papers* **432**: 155-167.

Rother H, Shulmeister J. 2006. Synoptic climate change as a driver of late Quaternary glaciations in the mid-latitudes of the Southern Hemisphere. *Climate of the Past* **2**: 11-19.

Rother H, Shulmeister J, Fink D, Alexander D, Bell D. 2015. Surface exposure chronology of the Waimakariri glacial sequence in the Southern Alps of New Zealand: Implications for MIS-2 ice extent and LGM glacial mass balance. *Earth and Planetary Science Letters* **429**: 69-81.

Rother H, Shulmeister J, Rieser U. 2010. Stratigraphy, optical dating chronology (IRSL) and depositional model of pre-LGM glacial deposits in the Hope Valley, New Zealand. *Quaternary Science Reviews* **29**: 576-592.

Rowan AV, Plummer MA, Brocklehurst SH, Jones MA, Schultz DM. 2013. Drainage capture and discharge variations driven by glaciation in the Southern Alps, New Zealand. *Geology* **41**: 199-202.

Rowan AV, Roberts HM, Jones MA, Duller GA, Covey-Crump SJ, Brocklehurst SH. 2012. Optically stimulated luminescence dating of glaciofluvial sediments on the Canterbury Plains, South Island, New Zealand. *Quaternary Geochronology* **8**: 10-22.

Salinger M, Mullan A. 1999. New Zealand climate: temperature and precipitation variations and their links with atmospheric circulation 1930–1994. *International Journal of Climatology* **19**: 1049-1071.

Samson CR, Sikes EL, Howard WR. 2005. Deglacial paleoceanographic history of the Bay of Plenty, New Zealand. *Paleoceanography* **20**.

Sandiford A, Newnham R, Alloway B, Ogden J. 2003. A 28 000–7600 cal yr BP pollen record of vegetation and climate change from Pukaki Crater, northern New Zealand. *Palaeogeography, Palaeoclimatology, Palaeoecology* **201**: 235-247.

Schaefer JM, Denton GH, Barrell DJ, Ivy-Ochs S, Kubik PW, Andersen BG, Phillips FM, Lowell TV, Schlüchter C. 2006. Near-synchronous interhemispheric termination of the last glacial maximum in mid-latitudes. *Science* **312**: 1510-1513.

Schaefer JM, Putnam AE, Denton GH, Kaplan MR, Birkel S, Doughty AM, Kelley S, Barrell DJ, Finkel RC, Winckler G. 2015. The Southern Glacial Maximum 65,000 years ago and its Unfinished Termination. *Quaternary Science Reviews* **114**: 52-60.

Schiefer E, Menounos B, Wheate R. 2008. An inventory and morphometric analysis of British Columbia glaciers, Canada. *Journal of Glaciology* **54**: 551-560.

Schilling D, Hollin J. 1981. Numerical reconstructions of valley glaciers and small ice caps. *In:* Hughes, P and Gh, D, eds. *The Last Great Ice Sheets.* New York, John Wiley and Sons, 207-221pp.

Schrott L, Hufschmidt G, Hankammer M, Hoffmann T, Dikau R. 2003. Spatial distribution of sediment storage types and quantification of valley fill deposits in an alpine basin, Reintal, Bavarian Alps, Germany. *Geomorphology* **55**: 45-63.

Seltzer A, Stute M, Morgenstern U, Stewart M, Schaefer J. 2015. Mean annual temperature in New Zealand during the last glacial maximum derived from dissolved noble gases in groundwater. *Earth and Planetary Science Letters* **431**: 206-216.

Sevruk B. 1992. *Snow cover measurements and areal assessment of precipitation and soil moisture*. WMO Operational Hydrology Report no. 36, Geneva.

Shean DE, Head JW, Marchant DR. 2007. Shallow seismic surveys and ice thickness estimates of the Mullins Valley debris-covered glacier, McMurdo Dry Valleys, Antarctica. *Antarctic Science* **19**: 485-496.

Shulmeister J, Davies TR, Evans DJ, Hyatt OM, Tovar DS. 2009. Catastrophic landslides, glacier behaviour and moraine formation–A view from an active plate margin. *Quaternary Science Reviews* **28**: 1085-1096.

Shulmeister J, Fink D, Augustinus PC. 2005. A cosmogenic nuclide chronology of the last glacial transition in North-West Nelson, New Zealand—new insights in Southern Hemisphere climate forcing during the last deglaciation. *Earth and Planetary Science Letters* **233**: 455-466.

Shulmeister J, Fink D, Hyatt OM, Thackray GD, Rother H. 2010. Cosmogenic exposure ages of moraines in the Rakaia Valley, New Zealand and the nature of the last termination in New Zealand glacial systems. *Earth and Planetary Science Letters* **297**: 558-566.

Shulmeister J, Goodwin I, Renwick J, Harle K, Armand L, Mcglone M, Cook E, Dodson J, Hesse P, Mayewski P. 2004. The Southern Hemisphere westerlies in the Australasian sector over the last glacial cycle: a synthesis. *Quaternary International* **118**: 23-53.

Shulmeister J, Shane P, Lian OB, Okuda M, Carter JA, Harper M, Dickinson W, Augustinus P, Heijnis H. 2001. A long late-Quaternary record from lake Poukawa, Hawke's Bay, New Zealand. *Palaeogeography, Palaeoclimatology, Palaeoecology* **176**: 81-107.

Sikes E, Howard W, Neil H, Volkman J. 2002. Glacial-interglacial sea surface temperature changes across the subtropical front east of New Zealand based on alkenone unsaturation ratios and foraminiferal assemblages. *Paleoceanography* **17**.

Singer C, Shulmeister J, Mclea B. 1998. Evidence against a significant Younger Dryas cooling event in New Zealand. *Science* **281**: 812-814.

Singh S, Rathore B, Bahuguna I, Ramnathan A. 2012. Estimation of glacier ice thickness using Ground Penetrating Radar in the Himalayan region. *Current Science (Bangalore)* **103**: 68-73.

Sirguey P. 2010. *GLIMS Glacier Database Analysis IDs 97043-97358*. *National Snow and Ice Data Center.* http://dx.doi.org/10.7265/N5V98602. Boulder, CO.

Soons JM. 1963. The glacial sequence in part of the Rakaia Valley, Canterbury, New Zealand. *New Zealand Journal of Geology and Geophysics* **6**: 735-756.

Soons JM, Gullentops F. 1973. Glacial advances in the Rakaia valley, New Zealand. *New Zealand Journal of Geology and Geophysics* **16**: 425-348.

Span N, Fischer A, Kuhn M. 2005. *Radarmessungen der Eisdicke österreichischer Gletscher [1995-1998]: Messungen 1995 bis 1998.* Zentralanstalt für Meteorologie und Geodynamik,

Speight R. 1914. Recent changes in the position of the terminal face of the Franz Josef Glacier. *Transactions of the New Zealand Institute* **47**: 353-354.

Speight R. 1934. The Rakaia Valley. *Transactions of the New Zealand Institute* **63**.

Staines KE, Carrivick JL. 2015. Geomorphological impact and morphodynamic effects on flow conveyance of the 1999 jökulhlaup at Sólheimajökull, Iceland. *Earth Surface Processes and Landforms* **40**: 1401–1416.

Stone JO. 2000. Air pressure and cosmogenic isotope production. *Journal of Geophysical Research: Solid Earth* **105**: 23753-23759.

Straumann RK, Korup O. 2009. Quantifying postglacial sediment storage at the mountain-belt scale. *Geology* **37**: 1079-1082.

Straumann RK, Purves RS. 2008. Delineation of valleys and valley floors. *Geographic Information Science.* Springer, 320-336pp.

Suggate R. 1990. Late Pliocene and quaternary glaciations of New Zealand. *Quaternary Science Reviews* **9**: 175-197.

Suggate R. 2004. South Island, New Zealand; ice advances and marine shorelines. *Developments in Quaternary Sciences* **2**: 285-291.

Suggate RP. 1965. *Late Pleistocene geology of the northern part of the South Island, New Zealand*. (76-77). New Zealand Dept. of Scientific and Industrial Research.

Suggate RP, Almond PC. 2005. The Last Glacial Maximum (LGM) in western South Island, New Zealand: implications for the global LGM and MIS 2. *Quaternary Science Reviews* **24**: 1923-1940.

Sutherland DG. 1984. Modern glacier characteristics as a basis for inferring former climates with particular reference to the Loch Lomond Stadial. *Quaternary Science Reviews* **3**: 291-309.

Sutherland R, Kim K, Zondervan A, Mcsaveney M. 2007. Orbital forcing of mid-latitude Southern Hemisphere glaciation since 100 ka inferred from cosmogenic nuclide ages of moraine boulders from the Cascade Plateau, southwest New Zealand. *Geological Society of America Bulletin* **119**: 443-451.

Tippett JM, Kamp PJ. 1993. Fission track analysis of the late Cenozoic vertical kinematics of continental Pacific crust, South Island, New Zealand. *Journal of Geophysical Research: Solid Earth* **98**: 16119-16148.

Tovar DS, Shulmeister J, Davies T. 2008. Evidence for a landslide origin of New Zealand's Waiho Loop moraine. *Nature Geoscience* **1**: 524-526.

Trommelen M, Ross M. 2010. Subglacial landforms in northern Manitoba, Canada, based on remote sensing data. *Journal of Maps* **6**: 618-638.

Usgs. 2014. *ASTER Level 1 Precision Terrain Corrected Registered At-Sensor Radiance*. 3 ed. Sioux Falls: USGS Earth Resources Observation and Science (EROS) Center.

Vandergoes MJ, Newnham RM, Preusser F, Hendy CH, Lowell TV, Fitzsimons SJ, Hogg AG, Kasper HU, Schlüchter C. 2005. Regional insolation forcing of late Quaternary climate change in the Southern Hemisphere. *Nature* **436**: 242-245.

Veen CJ. 2013. *Fundamentals of glacier dynamics.* 2 ed. Rotterdam, Balkema,

Ward C. 1988. Marine terraces of the Waitutu district and their relation to the late Cenozoic tectonics of the southern Fiordland region, New Zealand. *Journal of the Royal Society of New Zealand* **18**: 1-28.

Warren CR, Kirkbride MP. 1998. Temperature and bathymetry of ice-contact lakes in Mount Cook National Park, New Zealand. *New Zealand Journal of Geology and Geophysics* **41**: 133-143.

Warren CR, Kirkbride MP. 2003. Calving speed and climatic sensitivity of New Zealand lake-calving glaciers. *Annals of Glaciology* **36**: 173-178.

Weaver PP, Carter L, Neil HL. 1998. Response of surface water masses and circulation to late Quaternary climate change east of New Zealand. *Paleoceanography* **13**: 70-83.

Whittaker TE, Hendy CH, Hellstrom JC. 2011. Abrupt millennial-scale changes in intensity of Southern Hemisphere westerly winds during marine isotope stages 2–4. *Geology* **39**: 455-458.

Willsman A. 2011. *Annual Glacier Volumes in New Zealand 1995-2010*. Christchurch: NIWA.

Willsman A, Chinn T, Lorrey A. 2014. *New Zealand Glacier Monitoring: End of summer snowline survey 2013*. Christchurch: NIWA.

Wilmshurst JM, Mcglone MS, Leathwick JR, Newnham RM. 2007. A pre-deforestation pollen-climate calibration model for New Zealand and quantitative temperature reconstructions for the past 18 000 years BP. *Journal of Quaternary Science* **22**: 535-547.

Winkler S. 2000. The 'Little Ice Age' maximum in the Southern Alps, New Zealand: preliminary results at Mueller Glacier. *The Holocene* **10**: 643-647.

Winkler S. 2004. Lichenometric dating of the 'Little Ice Age' maximum in Mt Cook National Park, Southern Alps, New Zealand. *The Holocene* **14**: 911-920.

Wratt D, Tait A, Griffiths G, Espie P, Jessen M, Keys J, Ladd M, Lew D, Lowther W, Mitchell N. 2006. Climate for crops: integrating climate data with information about soils and crop requirements to reduce risks in agricultural decision-making. *Meteorological applications* **13**: 305-315.

Wyshnytzky. 2013. *Constraining ice advance and linkages to palaeoclimate of two glacial systems in the Olympic Mountains, Washington and the Southern Alps, New Zealand*. MSc thesis, Utah State University.